EUROPEAN COMMISSION

European Research Area

Recently the technological evolution in structural steels, particularly in the area of off-shore and marine applications, points towards an increasing use of high-strength welda-ble steels with the aim of guaranteeing high-quality/high-strength welded joints for light-weight structures, reducing both weight and cost.

The need to develop specific knowledge on the fatigue behaviour of high-grade steel-welded joints, considering the consistent improvement in mechanical properties of con-sumables and in welding technologies, is becoming a more crucial issue.

The FATHOMS project was aimed at improving the knowledge on this matter, contribut-ing to potential upgrades of the design criteria.

The activity carried out highlights the conservativeness of the current design standards in force in the offshore area in predicting the fatigue performances of welded joints when high-steel grades, together with improved and innovative welding techniques, are used, in particular for the girth welds on pipes made from one side usually penalised by the codes.

The conservativeness of the standards was highlighted both in terms of S-N design curves and in terms of limit values for the accumulated fatigue damage in conditions similar to the in-service ones.

The beneficial effect in fatigue performances of the use of high-strength steels, new welding technologies and post-welding treatments was outlined.

In particular promising behaviour was shown in terms of fatigue strength of laser hybrid welding technology when applied in the root pass in single-side welds, which allows fatigue performances to be reached that are comparable with double-side good quality welds.

Price (excluding VAT) in Luxembourg: EUR 8

ISBN 978-92-79-14544-5

Publications Office

EC

KI-NA-24214-EN-C

Fatigue behaviour of high-strength steel-welded joints in offshore and marine systems (FATHOMS)

EUR 24214

Fatigue behaviour of high-strength steel-welded joints in offshore and marine systems (FATHOMS)

Research Fund for Coal & Steel

Interested in European research?

RTD info is our quarterly magazine keeping you in touch with main developments (results, programmes, events, etc.). It is available in English, French and German. A free sample copy or free subscription can be obtained from:

Directorate-General for Research
Information and Communication Unit
European Commission
B-1049 Brussels
Fax (32-2) 29-58220
E-mail: research@ec.europa.eu
Internet: http://ec.europa.eu/research/rtdinfo/index_en.html

European Commission

Research Fund for Coal and Steel

Fatigue behaviour of high-strength steel-welded joints in offshore and marine systems (FATHOMS)

E. Mecozzi, M. Lecca, S. Sorrentino
Centro Sviluppo Materiali SpA
Via di Castel Romano 100/102, 00128 Rome, ITALY

M. Large, C. Davies
CORUS UK Limited
30 Millbank, London SW1P 4WY, UNITED KINGDOM

H. Gouveia, C. Maia
Instituto de Soldadura e Qualidade
Av. Prof. Cavaco Silva N° 33, Talaide, 2780 920 Porto Salvo-Oeiras, PORTUGAL

M. Erdelen-Peppler
Salzgitter Mannesmann Forschung GmbH
Eisenhüttenstraße, 99, 38239 Salzgitter, GERMANY

S. Karamanos, P. Perdikaris
University of Thessaly
Argonafton & Filellinon, 38221 Volos, GREECE

Final report

Directorate-General for Research

Table of content

1 Final summary

Recently the technological evolution in structural steels, particularly in the area of offshore and marine applications, seems to point towards an increasing use of high strength weldable steels.

Main advantages could be summarized as follows:

→ Structural weight reduction, and therefore lower problems/costs during transport and installation (e.g. deepwater application).

→ Increasing the steel grade the wall thickness can be lowered reducing, therefore, welding time which would impact on line laying productivity and time for construction of structures that are main concerns for the offshore installations.

→ Safety against occasional special events leading to high stress ranges.

In parallel with this trend a consistent improvement, both in the mechanical properties of consumables and in welding technologies, has been achieved in order to guarantee high-quality/high-strength steel welded joints for lightweight structures.

Accordingly, the need to develop specific knowledge about the fatigue behaviour of high grade steel welded joints is becoming a more crucial issue.

Several design curves are available in the Standards in force to the offshore area considering fatigue, referring to many types of welding details.

In the last years new materials became available, together with new welding technologies, therefore the curves given by the Standards could be over conservative or not fully representative of the actual weld geometry.

As an example could be mentioned, for offshore girth welded pipes, the case of one-sided welds, the most practicable and economical solution compared with double-groove, two-sided butt welds, especially where field welding is required. The major fatigue design codes penalize butt welds made from one side, in some cases equating them to fillet welds, even if design rules for one-sided girth welds, made without permanent backing, are not based on experimental data but on the assumption that they are likely to have poor weld root conditions and to be misaligned [1].

In this context was born the FATHOMS project aimed at achieving an improvement in knowledge on the fatigue behaviour of welded joints in high strength steels (specified minimum yield strength ≥ 420 MPa), contributing to improve design criteria for welded structures and components for offshore applications, in terms of reductions both in weight and cost. The final goal of the current project was to produce and collect valuable information to extend the applicability of design standards to the use of high strength steels for high performance welded structures. In order to achieve this goal the work has been focused on the evaluation of:

→ the eventual conservativeness of both the selected design S-N curves and the fatigue damage tolerances recommended in the Standards when high steel grades are used;

→ the influence of loading conditions similar to those encountered in service (e.g. high R or σ mean values and selected load spectra), together with various external environments (such as cathodic protection in sea water), in conjunction with the use of new welding technologies and post-weld treatments.

The results of the projects are described task by task in the following.

1.1 WP 1: Review on fatigue problems on offshore components/structures, selection of materials and welded joints geometry.

With the main aim of investigating the possible employ of high strength steels in conjunction also with promising welding technologies, were selected two different products, connected with the offshore and marine systems, for which fatigue is one of the primary design criterion and the weld is a detail of particular concern:

→ Offshore renewable energy devices.
→ Pipes for oil and gas recovery as risers and trunk-lines.

At the beginning of the work a detailed study about materials and welding techniques currently employed was performed with reference to the present and future offshore projects.
After reviewing the current scenario, the common practice and the future trends of the offshore and marine industry, the following materials for the experimental activity were chosen:

→ RQT 701 plate related to renewable applications;
→ X70 seamless pipe, OD 273.1 mm and 14.2mm WT representative of offshore risers;
→ X100 TMCP pipe, OD 914.4 mm and 16 mm WT with size representative of trunk-lines applications, with high steel grade.

The geometry of the welded connections, T joints for plates and girth weld for pipes, was selected and the corresponding S-N design curves were chosen after the review of the current standards.
The loading sequences for fatigue tests under variable amplitude loading were set up for both renewable applications and oil &gas field. Both sequences are representative of the relative fields of applications.
For girth welded pipes an approach based on procedures and tools adopted in fatigue design was used to find out the load sequence. In particular the load sequence set up is representative of the real case of a girth welded riser connected to a semi submersible platform located in Gulf of Mexico.

Main conclusions at the end of WP1 are as follows:
→ The materials of interest for the project were selected according to the review of the offshore scenarios.
→ After the review of standards accounting for fatigue the S-N design curves to be used as reference were outlined.
→ The loading sequences for the variable amplitude small scale fatigue tests were set up.
→ The specimens geometry for small scale fatigue tests was defined.

1.2 WP2: Welding technologies, manufacturing of welded joints and geometrical and mechanical characterisation

The selection of the welding technologies for the manufacturing of the joints for the project was based on the state of the art both in offshore and marine applications, with particular regards to the field of interest, and the need to obtain high performance welds increasing the productivity and reducing the welding time.

According to these considerations the following welding techniques were selected:

→ Submerged Arc Welding technology (SAW) to manufacture the "T" joints from plates.

→ Flux Cored Arc Welding (FCAW) and Laser-GMA hybrid/GMAW named LH in the following to perform girth welded pipes.

FCAW was selected as a quick and easy welding technique which main advantages are an arc more stable, low defect rate and less passes to fill the joint. This technology was considered promising as in field girth welding technique by oil and gas companies which recognised that the cycle time reduction was so positive that further studies were claimed.

HYBRID LASER/GMAW: The proposed welding technology consists in Laser Hybrid weld for the root pass and GMAW for the other passes filling the joint. It was selected as promising technique in the offshore field allowing to obtain a good quality in the root pass enhancing welding productivity as the overall productivity in pipeline construction is governed by root pass welding speed. Furthermore laser welds have peculiar morphology and mechanical behaviour; in particular fatigue resistance of welds may be favourably influenced by the limited weld reinforcement size often found in laser welds, as well from the probably lower residual stress level.

In the frame of this work package the WPS to manufacture the welded joints for the project were set up.

In particular for the two pipe materials included in the project, welding was aimed to simulate real activity in offshore linepipe fabrication/prefabrication, as following reported.

The FCAW welded pipes, both X70 and X100 pipes, simulated the prefabrication of double joints at barge/land base and were welded in 1G/PA position.
The HYBRID LASER/GMAW welded pipes were welded as follows: :
→ for X70 pipes linepipe/riser the fabrication at the lay barge (J-lay) was simulated. Joints were welded in 2G/PC position;
→ for X100 pipes the prefabrication of double joints at barge/land base was simulated. Joints were welded in 1G/PA position.

The welded joints were manufactured and characterized in terms of macro features, microstructure, mechanical properties and residual stress field.
After a state of the art review on the possible post welding treatments available to enhance fatigue performances, ultrasonic peening was selected and applied on FCAW welded joints.

1.3   WP3: Basic fatigue assessment of the selected welded joints.

The basic fatigue assessment of the selected joints was carried out. Small-scale endurance tests in air on full thickness specimens containing the weld were performed, under constant amplitude load with a stress ratio R = 0.1, in order to qualify welds with respect to the main standards in force in the welded structures and offshore area. A limited number of tests were performed in sea water with a standard level of cathodic protection (<-900 mV), in order to study the environment effect on fatigue performances.

The influence on fatigue performances of loading conditions similar to the in-service ones was investigated. In particular small-scale endurance tests in air were performed under constant amplitude load with a stress ratio R=0.5. A limited number of tests was performed in sea water with a standard level of cathodic protection (<-900 mV) with a frequency of about 0.3 Hz, in order to study the environment effect on fatigue. For SAW welds on T butt plates, also the influence of cathodic overprotection was investigated (<-1300 mV).

In addition some tests in order to measure fatigue crack growth rates using fracture mechanics specimens were performed.

At the end of the work package a consistent number of fatigue tests was performed.

First point to be highlighted is that the tests results put in evidence the conservativeness of the S-N design curves proposed in the reference standards generally for all the welded joints investigated in the project.

This is more evident when high grades are welded by innovative welding technique that is LH performed at the weld root. In fact it is remarkable that this welding technique allows to improve significantly the fatigue behavior for both the steel grades employed. In particular X100 LH shows very good performances.

Fatigue performances at higher stress ratio, that is a higher mean stress applied, seem to be slightly worst for all the joints typologies tested.

Joints in seawater show, as expected, lower performances than in air but the general behavior is still good if compared with the design standard. Again in seawater, Laser Hybrid technique, with its improvement in the root geometry, showed good performances.

According to the number of tests performed in the frame of the current project it seems that in some cases the use of ultrasonic peening leads to better fatigue performance than the Laser Hybrid welding technique applied in the root pass. Nevertheless it should be underlined that the performance of the post welding treatment requires additional time before laying the joint in the sea bed and this should be taken into account when considering the potential benefits achievable.

1.4 WP4: Influence on fatigue behaviour of typical loading and environmental in-service conditions.

The effect of variable amplitude loads on fatigue behavior of the selected high strength welded joints was evaluated, by means of the load sequences selected in WP1.

Small-scale endurance tests in air were performed and the results were compared to the ones under constant amplitude load. A limited number of tests on T joints from plates was performed in seawater + cathodic protection.

The work performed in the present work package highlighted that the conservativeness evidenced for the S-N design curves is still remarkable when loads similar to the in service conditions are applied.
In particular it was put in evidence that in the design of structures or components employing high strength steel welded joints their real performance could be underestimated. In fact adopting the S- N design curves suggested in the current standards damage values can be much more higher than the limit values usually recommended.

1.5 WP5: Full-scale fatigue tests program

In this work package, fatigue behavior of welded joints was investigated by means of full-scale fatigue tests, in order to estimate the difference between full and small scale test results.

Full-scale rotating four-point-bending fatigue tests were carried out with constant amplitude loads on X70 FCAW welded pipes.

The obtained results evidenced that despite welding standards could allow some types of defect, difference in the weld quality are of fundamental importance in fatigue behavior.

Strategies for achieving high fatigue strength in welded steel structures include good design practice (e.g. using joints with low stress concentration factors, or avoiding the placing of welds in regions of high stress range) but above all high quality welding.

From the comparison between full scale and small scale fatigue tests results it is detectable that all small scale test results are well above the relevant design curves and in line with the mean curves, whereas the full scale test results lie below these design curves. Generally, the fact that small scale tests yield a better fatigue performance is expected. It was highlighted by some

authors, that strip specimens could give higher fatigue lives than full-scale pipes, especially in the high-cycle regime.

Two main factors have been evidenced as possible explanation for this difference:

→ the greater likelihood of finding a large defect in an entire girth weld with respect to a portion of it in the strip specimen;

→ the cutting out of the strip specimens, expected to relax residual stresses due to girth welds and thus leave lower residual stresses in the strips.

No single factor could completely and especially quantitatively explain the difference and the debate on the reliability of tests on strip specimens in reproducing the full scale behavior is still ongoing.

1.6   WP6: Analysis of experimental results and elaboration by a local approach methodology (Hot Spot)

Hot Spot Method was applied both at T joints from plates and at girth welds from pipes.

It was highlighted that for T joints from plates the Hot Spot Stress coincides with the nominal stress.

As regards pipes main outcome is that for FCAW joints a SCF = 1.16 was calculated while for LH joints the SCF results close to 1. This is a further confirmation that Laser Hybrid performed at the root pass improves the geometry at the weld root increasing fatigue performances of the welds.

As further attempts for girth welded pipes local approach was applied on the basis of the results collected in the activity of geometrical characterisation of the weld profile.

As expected after the results obtained in the previous work packages, the results highlighted that LH welds are characterised by a lower value of Kt than FCAW joints.

On the basis of the results obtained tentative S- N design curve in terms of both Hot Spot stress and local stress were drawn for the joints object of the hereby presented work.

1.7   WP7: Proposal for design criteria of light welded structures or components for offshore applications

The experimental results obtained in the present work were analyzed in order to supply information to be taken into account in future Standards proposal or upgrades, to properly include the high strength/high quality steel welded joints in the fatigue design Standards.

In particular the BS7608 was considered as reference.

Main aims of the analysis were the followings:

→ To verify and when possible quantify the conservativeness of the design S-N curves recommended by the main Standards accounting for fatigue in the offshore field when high grade steels are intended to be used.

→ To assess the effect of different loading conditions (e.g. high R or σ average values) and of environment (sea water and cathodic protection) which are representative of real in-service behavior for the high grade welded joints considered.

→ To assess the correspondence and the eventual conservativeness of the cumulative fatigue damage limit values recommended in fatigue design codes for the high strength welded joints under investigation.

The first outcome that should be highlighted is that the design curve recommended by the BS code results conservative generally for all the selected joints. This is a clear input to reconsider the design curves in the standards when high steel grades together with improved and innovative welding techniques are planned to be used.

Laser Hybrid welding technologies when employed in the root pass results very promising in improving the fatigue performances of the selected joints. In fact the fatigue performances of LH welded joints are particularly good so that the fatigue strength is close to the one of a particularly good weld that is weld made from both sides with overfill dressed flush, corresponding to the curve C reported in the BS rule.

The fatigue performances of the selected welded joints are still good in comparison with the reference curve suggested by BS standard when loading condition similar to in service ones are applied, also if a slight decrease in fatigue strength is noticeable. It is remarkable that also in this case the LH joints show an improved behavior.

Generally it is noticeable that the high steel grades joints maintain a good fatigue behavior also in seawater + cathodic protection that is in an environment with high H_2 content and the risk of hydrogen embrittlement is present. It should be noticed that also in seawater LH welds show a very promising behavior.

The case study about the design of a girth welded riser connected to a semi submersible platform located in Gulf of Mexico put in evidence that the Standards in force to the offshore area can results conservative also as concerns the limit value of the accumulated fatigue damage when loading conditions similar to the in service ones are applied.

Most of the welded joints tested were welded in horizontal position with the pipe rotating simulating the prefabrication of double joints at barge/land base, except than the X70 laser hybrid pipes simulating the fabrication at the lay barge (J-lay) that were welded in 2G/PC position.

In order to extend the obtained results to other welding situations (e.g. orbital welding) it should be considered that in a welded joint the main factor affecting fatigue performances is the weld profile and the related stress concentration factor in the expected region of failure, that is the weld root for the selected applications.

According to CSM experience, for the Laser Hybrid joints no significant variations are expected in the weld root, moving from 1G welding position to orbital welding. Therefore the results obtained can be considered representative also of the orbital welding solution.

For the FCAW welds moving from horizontal to orbital welding position a less promising profile in the root pass could be expected, giving a lower fatigue performance but affecting the welded joints geometry with a weight not higher than other welding parameters. Anyway, as first step, it is assumable that the difference expected in fatigue performances could be compatible with the scatter typical of fatigue phenomenon and that the results obtained in the project could be extended also to the orbital welding case. This assumption is supported also by the consideration that the S-N curves proposed in the fatigue design recommendations/standards are obtained from a big amount of experimental data from tests on the same welding detail but disregarding the welding position that falls in the scatter band.

1.8   *Conclusions and main results*
At the end of this project the following conclusions can be drawn.

→   The activity carried out put in evidence the conservativeness of the current standards in force in the offshore area in predicting the fatigue performances of welded joints when high steel grades together with improved and innovative welding techniques are used, in particular for the girth welds on pipes made from one side usually penalized by the codes.

→   The conservativeness of the standards was highlighted both in terms of S-N design curves proposed and in terms of limit values for the accumulated fatigue damage when variable loading conditions similar to the in service ones are applied. In this respect the case study simulating the design of a girth welded riser connected to a semi submersible platform located in Gulf of Mexico, showed that the limit damage values recommended in the standards

correspond to a number of cycles significantly lower than the number of cycles to failure in experimental tests leading to an excessive penalization of the joints when high strength steel together with new welding technologies are used. Nevertheless a "good quality" of welds is a basic condition to get a notable improvement of fatigue behavior of high steel grades welded joints.

→   The beneficial effect in fatigue performances of the employ of high strength steel, new welding technologies and post-welding treatments was outlined.

In particular it was highlighted what follows:

Laser Hybrid welding technology: It was noticed the promising behavior in terms of fatigue strength of Laser Hybrid welding technology when applied in the root pass. In fact nevertheless this is a single side weld the fatigue performances are comparable with the ones of a double side good quality weld. This is related to the fine geometry achievable in the weld root, the most critical site for fatigue failures as put in evidence in full scale fatigue tests that showed that a careful check of the quality of the weld in the inner of the pipe is mandatory for fatigue applications. The fine geometry of the weld root in Laser Hybrid welds was confirmed by both geometrical measurements and Hot spot analysis. Finally it should be underlined that Laser Hybrid welding is a technology currently feasible in field on the lay barge as the laser beam (either from Nd:YAG or Yb:fibre laser systems) can be delivered to the work pipes easily by a flexible optical fiber.

Ultrasonic peening: According to the number of tests performed in the frame of the current project it seems that the use of ultrasonic peening, applied on as welded FCAW joints, leads in some cases to fatigue performance even better than the Laser Hybrid welding technique applied in the root pass. As regards ultrasonic peening at the time being the technology to apply this treatment to the weld root of girth welded pipes is not available on the market, but it could be set up and developed in a short time and become feasible if required by offshore contractors.

In the comparison between the two "techniques", it should be considered also that the post welding treatment requires additional time before laying the joint in the sea bed and this should be taken into account when considering the potential benefits achievable.

→   The high strength welded joints investigated in the project maintain a generally good performance also in conditions similar to the in service ones that is when a high mean stress is applied and in seawater + cathodic protection that is in an environment with high H_2 content and the risk of hydrogen embrittlement is present. It should be noticed that also in seawater LH welds show a very promising behavior.

→   S-N curves both in terms of Hot Spot stress and local stress for the joints object of the current research were outlined.

2   Scientific and technical description of the results

In the following main aims, activities and results of the project are described. Additional details are reported in the enclosed appendixes.

2.1   *Objectives of the project*

Recently the technological evolution in structural steels, particularly in the area of offshore and marine applications, seems to point to a trend towards an increasing use of high strength weldable steels. Accordingly, the need to develop specific knowledge about the fatigue behaviour of high grade steel welded joints is becoming a more crucial issue. In parallel with these developments a consistent improvement, both in the mechanical properties of consumables and in welding technologies, has been achieved in order to guarantee high-quality/high-strength steel welded joints for lightweight structures.

In this context was born the FATHOMS project aimed at an improvement in knowledge on the fatigue behaviour of welded joints in high strength steels (specified minimum yield strength ≥ 420 MPa), contributing to improve design criteria for welded structures and components for offshore applications, in terms of reductions both in weight and cost. The final goal of the proposed project is to produce and collect valuable information to extend the applicability of design standards to the use of high strength steels in welded structures.

In particular in order to achieve the above mentioned goal the work was mainly focused on the evaluation of:

→ the eventual conservativeness of both the selected design S-N curves and the fatigue damage tolerances recommended in the Standards when high steel grades are used;
→ the influence of loading conditions similar to those encountered in service (e.g. high R or σ mean values and selected load spectra), together with various external environments (such as cathodic protection in sea water), in conjunction with the use of new welding technologies and post-weld treatments.

2.2 *Comparison of initially planned activities and work accomplished*

The aims and objectives of the project have been accomplished without any substantial changes from the initial plan.
Agreed that a considerable number of tests have been performed allowing to cover the main aims of the project, it was not possible to perform all the hoped tests. In fact it would be interesting to perform, as well as done for the plates, a limited number of tests in condition similar to the in service ones (i.e variable amplitude loading in seawater conditions) on the most promising welded joint that is on samples from the X100 LH girth welded pipes.
These tests are very challenging and few labs in Europe are endowed of testing devices suited for this purpose.
Tests were in charge to CSM but unfortunately during the first test a structural failure of the testing equipment occurred and it was not possible to complete the testing activity as the repairing time was not compatible with the deadline of the project.
Currently repairing is still in progress but the device will be restored as soon as possible.

2.3 *Description of activities and discussion*
In the following the activities performed in each Work Package are reported, together with the main results and conclusions achieved.

2.3.1 *WP 1: Review on fatigue problems on offshore components/structures, selection of materials and welded joints geometry.*
Main aim of this work package were as follows:

→ Selection and provision of the materials of interest.
→ Literature survey of the main design Standards and of and in-service loading conditions in offshore components/structures.
→ Selection of the loading conditions to be applied in variable amplitude fatigue testing activity.
→ Detailed definition of the welded joints and specimen geometry for the small-scale fatigue tests.

In particular, with the main aim of investigating the possible employ of high strength steels in conjunction also with promising welding technologies, were selected two different products connected with the offshore and marine systems for which fatigue is one of the primary design criterion and a detail of particular concern is the weld:

→ Offshore renewable energy devices.
→ Pipes for oil and gas recovery as risers and trunk-lines.

At the beginning of the work a detailed study about materials and welding techniques currently employed was performed with reference to the present and future projects. Main highlights are herein reported.

2.3.1.1 <u>Fatigue on renewable energy field</u>

Climate change concerns coupled with changeability of oil price and uncertainties about hydrocarbon supply and reserves, recently boosted the development of technologies for the exploitation of renewable energy.

Renewable energy sources can be used to provide:

→ Renewable energy source electricity ("RES-E"),
→ Fuels (including gaseous fuels for various applications and liquid fuels for road vehicles, rail vehicles, aircraft and marine vessels)
→ Renewable energy source heat ("RES-H"): typically used for space heating, domestic hot water (DHW) and industrial process heat.

Targets for increased use of energy from renewable sources have been set at national and international level. The setting of these targets has been motivated by:

→ Concern over the climate-change effects of CO_2 emissions,
→ The perceived need to improve the security of energy supply through a reduction in the dependence on energy imports,
→ A desire to ensure a foundation for the development of indigenous industries in the renewable energy sector,
→ In the particular case of the use of biomass in the EU, the opportunity to redirect agriculture away from the subsidised production of surplus foods.

A wide variety of renewable energy technologies can be considered for supplying the requirements for RES-E, RES-H and fuels for transport. From Figure 1 to Figure 3 are reported examples of renewable technologies, well-established as wind turbines, and the newer ones like marine waves energy devices and tidal stream turbines. More examples and details can be found in Appendix A.

Figure 1 – Offshore wind turbines

Figure 2 - Pelamis P1A, wave energy device

Figure 3 - The SeaGen, tidal stream turbine

A number of materials issues are common to all of the renewable applications. These include:

→ Installation costs – high transport cost, weight restrictions, etc.
→ Formability and weldability of the steel.
→ Fabrication time/cost issues, e.g. welding of thick sections, etc.
→ Toughness of both base metal and welded joints.

→ Erosion/wear – for subsurface structural components.
→ Fatigue critical designs – structures subject to fatigue and corrosion fatigue.

Fatigue of offshore renewable energy devices is due to the action of environmental loading as wind, waves and marine currents, combined with the dynamics of the devices. A deepening is reported in Appendix B.

Life extension issues are of particular importance. This may be achieved in a number of ways:

→ Reclassification of current welds if 'better' than their historical classification.
→ Increase compressive residual stresses
→ Control/reduce tensile residual stresses (e.g. by welding modelling)
→ Weld improvement techniques and the use of novel welding techniques

The investigation of these aspects is within the scopes of the present report.

2.3.1.2 Fatigue on Steel Catenary Risers

Steel Catenary Risers (SCR) are proven and cost-effective riser system solutions that have been adopted for many offshore fields since 1994. This concept of production riser boosted the development of deepwater and ultradeepwater systems involving the use of production floaters. In particular its compliant feature makes it suitable in many offshore sites and for every type of production vessel, as show the field developments from Figure 4 to Figure 7.
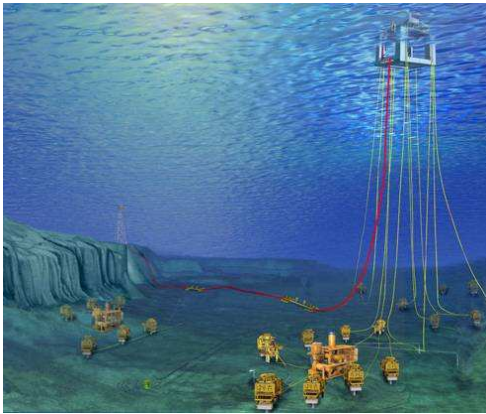

Figure 4 - Semisubmersible vessel for Independence Hub development, actual world's deepest project, 2439 m water depth in Gulf of Mexico. [1]
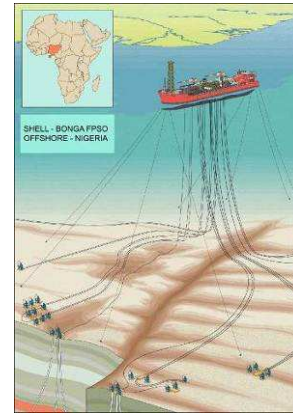

Figure 5 – Floating Production, Storage and Offloading (FPSO) vessel for Bonga development, 1245 m in West of Africa. [3]
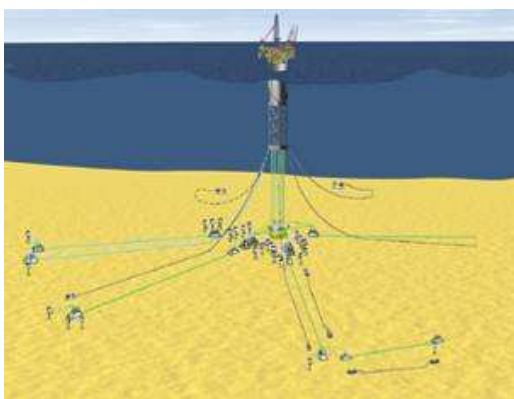

Figure 6 - SPAR vessel for Perdido project, 2380 m of water in Gulf of Mexico. First production is expected by the end of 2010. Water depth record using SPAR [4]
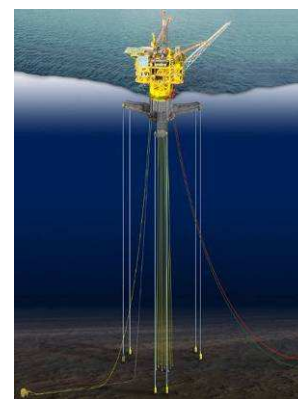

Figure 7 – Tension Leg Platform (TLP) for Matterhorn field, 850 m of water in Gulf of Mexico. [5]

The use of production floaters allows environmental loads to act over the whole structure and to put it in motion, generating fatigue loading. Main sources of fatigue loading are:

→ First order wave frequency (WF) and second order low frequency (LF) vessel motions, due to waves and wind;
→ Vortex Induced Vibration (VIV) of the riser, due to currents;
→ Vortex Induced Vibration of the riser, due to vessel heave (HVIV);
→ Vortex Induced Motion (VIM) of the vessel, due to currents;
→ Installation.

Fatigue affects particularly two main critical areas of the SCR, the Hang Off point (HOP), near the connecting point with the floater, and the Touch Down Point (TDP), where the riser touches the seabed.

More details about fatigue loading on Steel Catenary Risers can be found in Appendix C.

2.3.1.3 <u>Fatigue on trunklines</u>

Trunklines (or export lines), connect offshore fields to onshore, as shown in the scheme of Figure 8.

Offshore pipelines frequently pass over areas with uneven seafloor. In such cases the pipeline may have free spans, as shown in Figure 9. Fatigue can affect pipeline welded joint if dynamic loads act over the free span generating stress cycles. A major source for dynamic stresses in deep water free span pipelines is vortex induced vibrations (VIV) caused by current. VIV causes both cross and in-line oscillation with respect to the flow direction (see Figure 10).
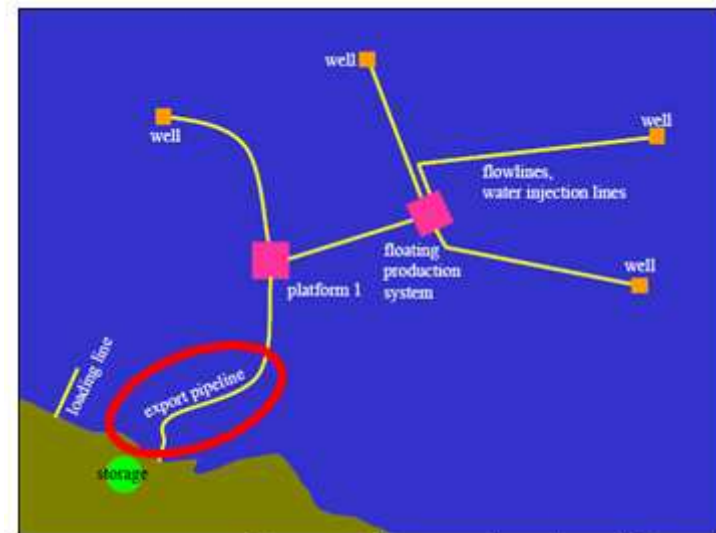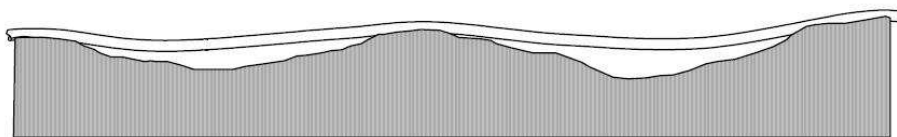

Figure 8 – A scheme of export line/trunkline

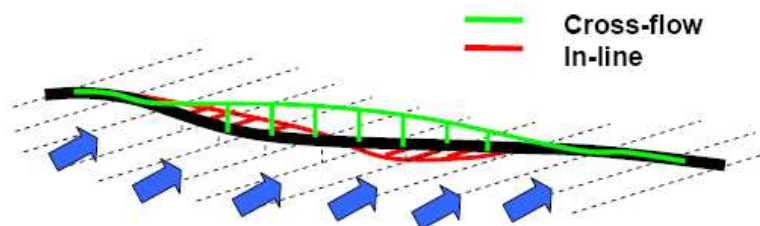**Figure 9 –** Free spanning pipeline [6]

Figure 10 – Static shape and VIV of free span pipeline [7]

14

Another source of fatigue damage is, where applicable, direct wave loading acting over the free span.

More details about offshore pipelines can be found in Appendix D.

2.3.1.4 <u>Materials and welds for offshore applications – Present scenario and future trends</u>

As concerns the renewable energy devices several welding details recommended are reported in the reference standards. For offshore wind turbines, as an example, welds recommended in the DNV-OS-J101 [8] are shown in Figure 11.
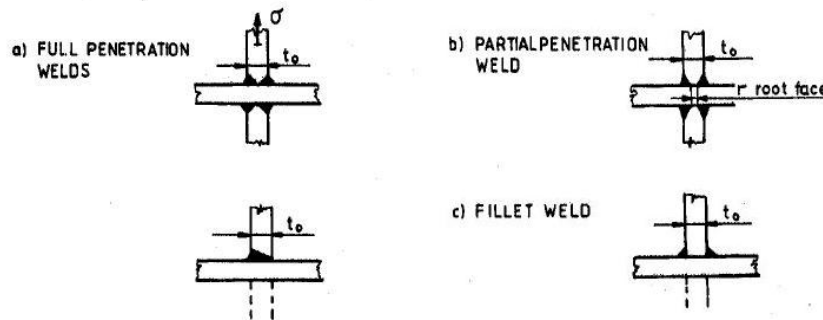

Figure 11 – Tee and cross joints for offshore wind turbines [8]

As concerns the steel grades in Table 1 are reported some types of steel used in maritime applications, together with the reference standards about the material properties and delivery conditions.

Type of steel	Steel grade	Standard	Yield strength ReH [N/mm²] min.
Structural steel	A36	ASTM	250
high-strength normalised structural steel	A 537	ASTM	345
	S355 J2G3	EN 10025	345
	P 355 N	EN 10028-3	345
	50 D	BS 4360 (1986)	345
	A 572	ASTM	380
	55 E	BS 4360 (1986)	430
	P 460 N	EN 10028-3	450
high-strenth, quenched and tempered structural steel	A 678-B	ASTM	415
	55 F	BS 4360 (1986)	430
	S 690 QL1	EN 10137-2	690

Table 1 - Steel for maritime applications, notations and standards [9]

As regards pipes for oil and gas recovery, in particular for risers and trunklines, in Table 2 are summarized pipe grades and pipe sizes commonly used for such applications.

Pipe application	Pipe grade	Size Range
<u>Steel Catenary Riser</u>	API 5L Gr X52, X60, X65 X70*	OD from 6" to 24"
Export pipelines (Trunklines)	API 5L Gr X52, X60, X65,X70**	OD from 12" to 55", typical 30"

* X70 has been recently used in the most challenging applications in deepwater
** X70 has limited applications

Table 2 – Common pipe grades and size ranges for the pipe applications selected

In Table 3 are reported relevant SCR projects. From Figure 12 to Figure 14 a view of the developments is shown.

Oil&GasCompany	Project Name	Location	Water depth	Steel grade	OD
Petrobras	P-18	Brazil	910 m	APIX60	10 3/4"
Anadarko	Independence Hub	Gulf of Mexico	2400 m	APIX65	20"
BP	Thunder Horse	Gulf of Mexico	1850 m	APIX65/X70	8 5/8", 10 3/4" 12 3/4"

Table 3 – Relevant SCR projects
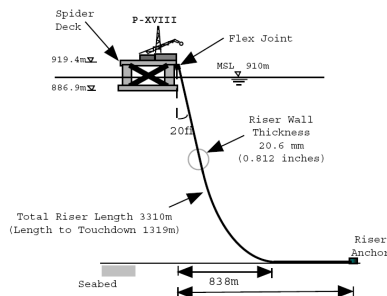
Figure 12 –P-18 [10]
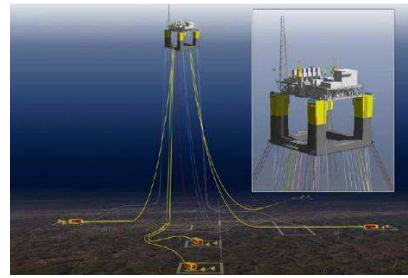
Figure 13 – Independence Hub [11]
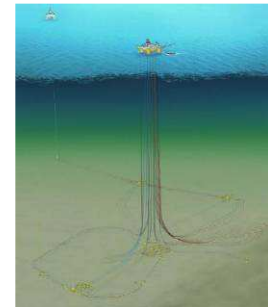
Figure 14 – Thunder Horse[12]

In Table 4 are reported relevant export pipelines.

Oil&GasCompany	Project Name	Location	Line length	Steel grade	OD
Conoco and Chevron	Britannia	North Sea	186 km	APIX70	27"
Anadarko	Independence Hub	Gulf of Mexico	217 km	APIX65	24"
Woodside	North Rankin	Western Australia	130 km	APIX65	42"

Table 4 – Relevant export pipelines

As detectable from the above mentioned projects, the higher grade used up to now is X70. In the industry there is now the need to move toward high strength steels, for several reasons:

→ Structural weight reduction, and therefore lower problems/costs during transport and installation (e.g. deepwater application).
→ Increasing the steel grade the wall thickness can be lowered reducing, therefore, welding time which would impact on line laying productivity, main concern for the offshore installation.
→ Safety against occasional special events leading to high stress ranges.

As regards welds, the state of the art techniques for offshore risers and pipelines are:

→ Gas Tungsten Arc Welding (GTAW).
→ Gas Metal Arc Welding (GMAW).
→ Flux Cored Arc Welding (FCAW).
→ Submerged Arc Welding (SAW).

Welding is usually performed using the following positions, illustrated in Figure 15.

→   1G for out of firing line welds (double/quad joints)
→   2G for firing line welds in J lay configurations
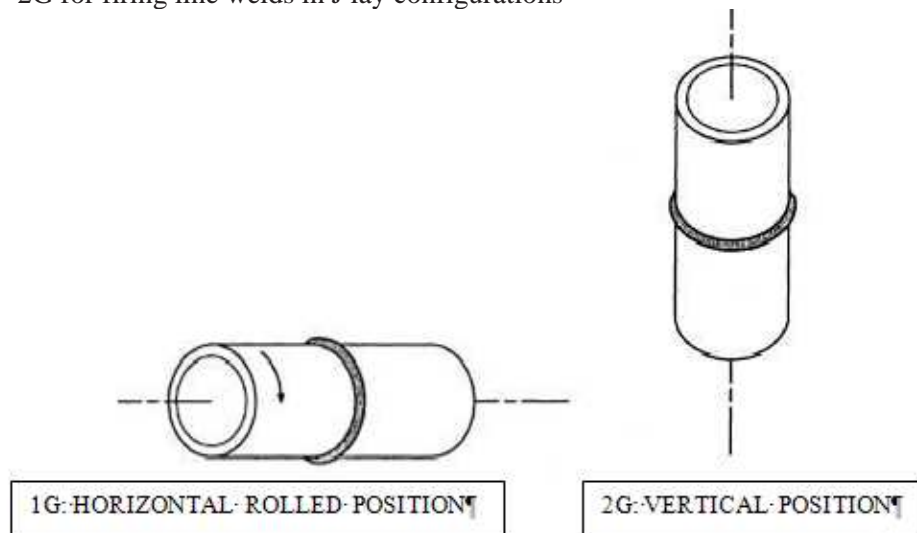

Figure 15 – Welding positions for offshore risers and pipelines

2.3.1.5 Materials chosen for the project

Pipes and plates for the experimental activity were selected on the basis of the current use and the future trends of the offshore and marine industry.
After reviewing the current scenario, the common practice and the future trends, the following materials for the experimental activity were chosen:

→   RQT 701 plate (15 mm wall thickness), related to renewable applications;
→   X70 seamless pipe, OD 273.1 mm and 14.2mm WT representative of offshore risers;
→   X100 TMCP pipe, OD 914.4 mm and 16 mm WT with size representative of trunk-lines applications, with high steel grade.

2.3.1.6 Offshore Standards

A considerable number of fatigue design standards or recommendations for the fatigue design of welded connections are available from different areas of interest (e.g. bridges structures, offshore platforms, pipelines and risers) covering different application fields. The most popular are stated in the following:

→   EN 1993-1-9, Eurocode 3: Design of steel structures, part 1.9: "Fatigue strength of steel structures", EN 1993-1-9, CEN TC250, Brussels, February 2006.
→   BS 7608 (1993), "Code of practice for fatigue design and assessment of steel structures", British Standards Institute, London, UK.
→   BS 7910 (1999), "Guide on methods for assessing the acceptability of flaws in metallic structures" British Standards Institution, London.
→   International Institute of Welding, "Recommendations for fatigue design of welded joints and components", IIW document XIII-1965r14-03 / XV-1127r14-03, 2006.
→   DNV Offshore Standard OS-F101 "Submarine Pipeline Systems", 2000.
→   DNV Recommended Practice RP – C203 "Fatigue Design of Offshore Steel Structures" – 2005.
→   API RP2A-LRFD: "Recommended practice for planning, designing and constructing fixed offshore platforms – load and resistance factor design", American Petroleum Institute, 1993, 20th edition.

→ API RP2RD: "Design of risers for Floating Production Systems (FPSs) and Tension-Leg platforms (TLPs)", American Petroleum Institute, 1998, 1st edition.

→ ISO 13628-7 "Petroleum and natural gas industries – Design and operation of subsea production systems – Part 7: Completion/workover riser system" 2005, equivalent to API RP 17G for riser design.

Eurocode 3 is a general design code for steel structures (buildings and bridges, but not offshore structures or offshore pipelines.) and in part 1-9 there are specific rules for fatigue design of steel structures.

BS 7608 is a general specification for fatigue design and assessment of parts of steel structures that are subject to repeated fluctuations of stress. It is restricted to structural steel with specified minimum yield strength less than 700 MPa. It should be noted that most of the welding contractors refers to this standard when qualifying girth welded pipes for fatigue.

BS 7910 focuses on structures containing flaws, and is suitable for "fitness-for-purpose" fatigue assessments.

IIW document is another fatigue document referring to welded components. The document is not a code of practice or a standard but presents recommendations for the fatigue design of welded joints and components.

DNV OS-F101 is used in all over the world in pipeline design applications. For fatigue design, DNV OS-F101 refers to the DNV RP – C203. This DNV Recommended Practice (RP) covers fatigue of both offshore structures and pipeline systems.

API RP2A-LRFD is a widely used specification for fixed offshore platforms, and has been widely used in the Gulf of Mexico, in the North Sea and elsewhere.

API RP2RD is a relatively new standard that covers the design of risers for Floating Production and Storage (FPSs) and Tension Leg Platform (TLPs), and contains provisions for fatigue design.

ISO 13628-7 as concerns fatigue design refers to the DNV RP C203 recommendations.

It is important to note that in the above specifications, the applicability of the specifications/standards is limited by the material strength; for instance the API RP2A-LRFD can be applied up to API X60 steels (420 MPa) and the ISO/DIS 13628-7 up to API X70 (490 MPa) steels in seawater with cathodic protection or free corrosion and up to API X100 (690 MPa) steel grades for steels in air. Therefore, those standards may not be applied to high-strength steels and this limitation constitutes one of the major motivations for conducting the present work.

It is worth noting that no significant differences are remarkable in the different Standards as concerns the design S - N curves proposed for the corresponding welding details.

The design approach followed by the above Standards and Recommendations for fatigue design or assessment is quite similar. The first step is the determination of the long term distribution of stress range applied to the structural component under consideration, followed by the selection of the suitable S-N design curves depending on the joint class selected. Subsequently, after replacing the long term distribution of stress range with a stress histogram consisting of a number of constant amplitude stress range blocks (σ_i) and the corresponding number of cycles (n_i), the accumulated damage (D) should be determined.

In all the above Standards, the accumulated damage evaluation follows the well-known Miner Rule:

$$D = \sum_{i=1}^{k} \frac{n_i}{N_i}$$

where n_i is the number of occurrences at a fixed stress range drawn from the load spectrum and N_i is number of cycles to failure at a fixed stress range drawn from the S-N curve. It is commonly believed that fatigue damage occurs when the accumulated damage factor is equal to 1. In practice, a critical value of this factor is specified (less than unity). Different critical values of D are recommended in various Standards. For instance both British Standards and API RP2A-LRFD recommend $D=1$. On the other hand, DNV Standards consider different limit damage values with respect to the consequence of failure, through an appropriate factor of safety, which may range from 3 to 10. It should be noted that above striking differences in critical D values do not necessarily represent such significant differences in fatigue design. To compare fatigue design procedures from different specifications/recommendations, the entire procedure has to be examined, including load factors and load spectra, as well as the application range of the specification/recommendation under consideration. More details about design procedure and fatigue analysis can be found in Appendix E.

At the end of this review three standards were outlined as particularly relevant for the project: BS 7608, Eurocode 3 (the S-N curves recommended coincide with the ones reported in the IIW recommendation on fatigue) and DNV RP C203.

2.3.1.7 <u>Selection of the loading conditions for variable amplitude fatigue testing activity</u>

Two different variable amplitude sequences were defined and set up for the applications considered in the project. Main characteristics are described in the following and further details can be found into Appendix F, and Appendix G.

2.3.1.7.1 <u>*Variable amplitude sequence for renewable applications*</u>

For the variable amplitude fatigue loading tests, connected to the renewable application field, a pre-existing spectrum was modified on purpose considering the offshore loading conditions for renewable devices.

The spectrum was first simplified by reducing the numbers of pairs of stress range and cycle values. Then was abridged by removing stress ranges with the lower contribute to overall damage.

Moreover, as in the original spectrum a fatigue load ratio R=0 was used, a further elaboration has been carried out. Indeed for the specimen design and loading arrangement to be used in the fatigue tests on welded plates, it is desirable to employ a positive minimum load. Therefore a mean stress and minimum stress cut-off have been imposed, giving a truncated spectrum. The truncated spectrum and the abridged spectrum are compared in Figure 16 and Figure 17 below.

For practical use in fatigue testing, the truncated spectrum was scaled, i.e. converted to a basic loading history with turning points expressed as fractions of the maximum value of maximum stress.
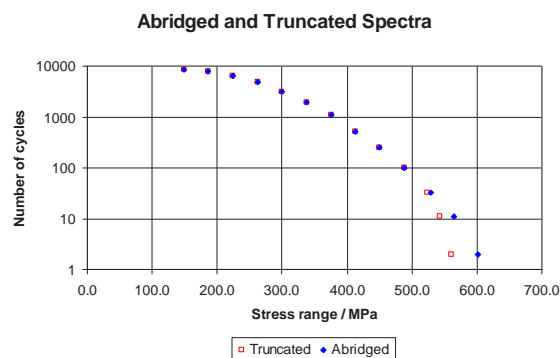
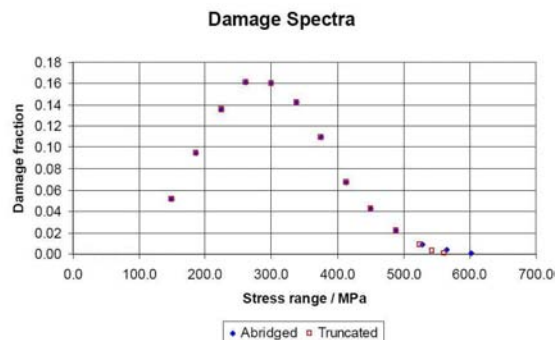

Figure 16 – Composition of truncated and abridged spectra

Figure 17 – Damage contributions in the truncated and abridged spectra

19

2.3.1.7.2 *Variable amplitude sequence for Steel Catenary Risers*

Environmental loads acting on riser systems generate complex loading histories. In particular the random motion of sea waves generates a loading that translates into variable amplitude stress on the riser. This load originates from vessel motions due to waves that are transferred to the entire riser through the connecting section.

Welds connecting the riser joints are the most critical points for fatigue.

Therefore riser fatigue design is based on welds fatigue resistance, i.e fatigue calculations are performed using SN curves related to the welding detail.

Regarding fatigue testing of riser welds, common practice is to test full-scale girth welded pipes, through the application of a rotating bending moment by a resonance machine. This type of testing has the advantage to allow testing frequency up to 30 Hz. On the other side, it applies a constant amplitude load.

Therefore arises the need to understand welded joint performances under a loading spectrum representative of the actual in-service conditions.

In literature several works and projects, aimed to obtain standardized loading histories representative of offshore loading conditions, are reported, but such sequences were developed for welded joints of fixed offshore structures.

There is now the need of representative loading spectra suitable for testing welds under variable amplitude loading, with time histories similar to the in service ones.

Two ways can be followed to know the actual loading conditions of risers:

→   Real measurements through strain gauges, but this could be expensive and difficult in deepwater locations.
→   Simulating and analyzing riser behaviour through Finite Element Analysis.

According to the latter way, an approach for the determination of a variable amplitude sequence for fatigue testing of girth welded pipes was developed and applied. Main steps are summarized in the following and depicted in Figure 18.

1.   Simulation of an offshore system under real environmental conditions.

2.   Tracing of the time histories of stress in a selected riser section (preferably a critical section, in the Hang Off or in the Touch Down Point).

3.   Composition of the time histories of stress into a global sequence representative of riser stress in a long period.

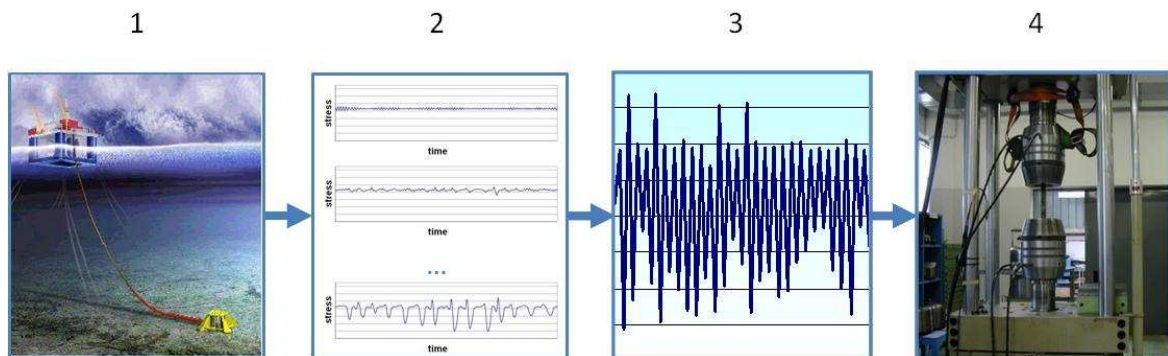4.   Testing on a machine suitable for variable amplitude loading.

Figure 18 – Scheme for the determination of a variable amplitude sequence for fatigue testing of welds

20

In particular it was decided to simulate the case of a girth welded riser connected to a semi submersible platform located in Gulf of Mexico. In Figure 19 and Figure 20are reported respectively the composition and the damage contribution of the spectrum obtained for steel catenary risers.
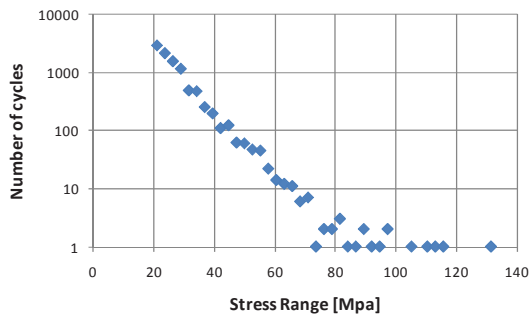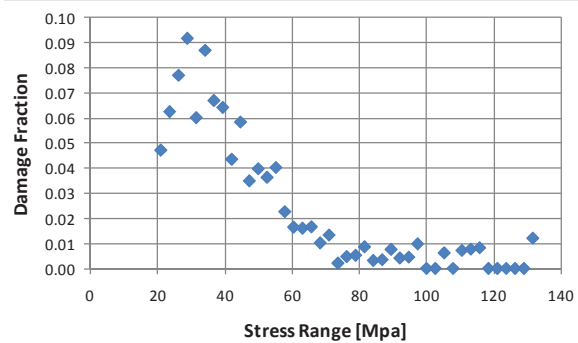

Figure 19 - Composition of the spectra

Figure 20 - Damage contributions in the spectra

2.3.1.8 Definition of specimens for small scale fatigue tests

After defining the welds details, T joints for plates and girth welds from pipes, the aim was to find out samples that could be considered representative of the full scale behaviour of the selected components.
For plates T joints full thickness samples were selected as reported in Figure 21.
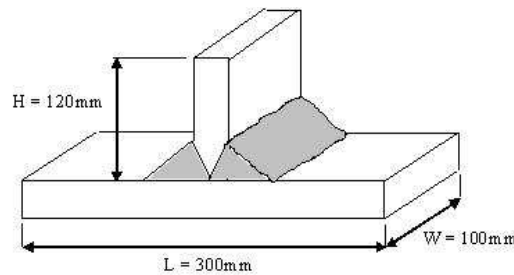
Figure 21 – Fatigue specimen - SAW full penetration fillet welded 'T' joint

For pipes, the full thickness specimen shown in Figure 22 was designed in order to obtain samples for fatigue tests as much as possible representative of the behavior of the whole pipe.
The internal and external surface of the welded pipes were preserved in order to maintain the actual notch and weld reinforcement stress concentration factors as in the full-scale girth weld joint.
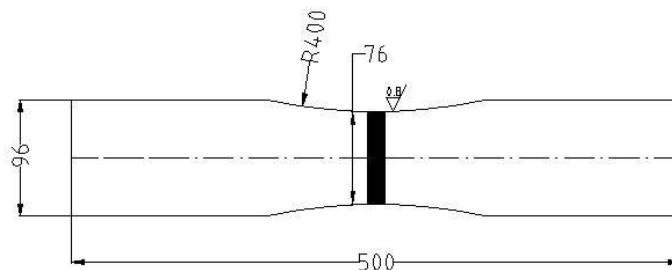
Figure 22 - "Large" scale fatigue tests specimen geometry (full thickness)

2.3.1.9 <u>Conclusion of WP 1</u>

Main conclusions at the end of WP1 are as follows:
  → Selection of the materials of interest for the project.
  → The Standards accounting for fatigue to which refer to were outlined together with the S-N design curves.
  → Set up of the loading sequence for the variable amplitude small scale fatigue tests .
  → Definition of the specimens geometry.

2.3.2 WP2: Welding technologies, manufacturing of welded joints and geometrical and mechanical characterisation

The selection of the welding technologies for the manufacturing of the joints for the project was based both on the state of the art in offshore and marine applications, with particular regards to the field of interest, and the need to obtain high performance welds increasing the productivity.

In particular for pipes in the choice of the welding techniques it was also considered that, to reduce the costs related to the welding activity, for large offshore projects it is current practice to use extensively prefabrication of double/quadruple joints, to be realized either at the lay barge or at the land base, and then join such trunks at the lay barge while laying the pipeline onto the seabed. Whether the laying system used (S-lay, J-lay, reeling), prefabrication as well onboard joining activity for girth welding rely heavily on automated GMA systems; SAW is also extensively employed for prefabrication purpose only.

As well as these consideration the attempt was also to find solutions to obtain high performance girth welds increasing the productivity and reducing the welding time.

According to these considerations the following welding techniques were selected:

  → To manufacture the "T" joints from plates Submerged Arc Welding technology (SAW) was selected.
  → To perform girth butt welds from pipes were selected Flux Cored Arc Welding (FCAW) and Laser-GMA hybrid/GMAW named LH in the following.

FCAW was selected as a quick and easy welding technique which main advantages are an arc more stable, low defect rate and less passes to fill the joint. This technology was considered promising as in field girth welding technique by Oil and Gas Companies which recognised that the cycle time reduction was so positive that further studies were claimed.

HYBRID LASER/GMAW: The proposed welding technology consists in Laser Hybrid weld for the root pass and GMAW for the other passes filling the joint It was selected as promising technique in the offshore field allowing to obtain a good quality in the root pass enhancing welding productivity as the overall productivity in pipeline construction is governed by root pass welding speed. Furthermore laser welds have peculiar morphology and mechanical behaviour, in particular fatigue resistance of welds may be favourably influenced by the limited weld reinforcement size often found in laser welds, as well from the probably lower residual stress level.

Weld improvement techniques have been reviewed and classified by the marine structures industry [13] according to the scheme represented in Table 5 below. Details are given in Appendix H.

Weld geometry improvement methods	Machining methods		Burr grinding
			Disc grinding
			Water jet gouging
	Remelting methods		TIG dressing
			Plasma dressing
			Laser dressing
	Special welding techniques		Weld profile control
			Special electrodes
Residual stress methods	Mechanical methods	Peening methods	Hammer peening
			Needle peening
			Shot peening
			Ultrasonic peening
		Overloading methods	Initial overloading
			Local compression
	Thermal methods		Thermal stress relief
			Spot heating
			Gunnert's method
			Low temperature transformation electrodes

Table 5 – Classification of weld improvement techniques for marine structures

Among the techniques developed to increase the fatigue life of welded components currently available, ultrasonic peening was selected for the current project as post welding treatment to be employed on FCAW pipes.

In particular for the two pipe materials included in the project, welding was aimed to simulate real activity in offshore linepipe fabrication/prefabrication, as following reported.

The FCAW welded pipes, both X70 and X100 pipes, simulated the prefabrication of double joints at barge/land base and were welded in 1G/PA position.
The HYBRID LASER/GMAW welded pipes were welded as follows: :
  − for X70 pipes linepipe/riser the fabrication at the lay barge (J-lay) was simulated. Joints were welded in 2G/PC position;
  − for X100 pipes the prefabrication of double joints at barge/land base was simulated. Joints were welded in 1G/PA position.

A detail description of the WPS and of the mechanical characterisation of the joints are reported in Appendix I, while the main mechanical properties are herein summarised.
Each partner in charge of welding activity selected the Standard commonly used in its welding lab.
In particular for SAW T joints from plates and for FCAW welds on pipes respectively the BS 4515 and the EN 15614 were used. The two Standards are equivalent as the BS 4515 refers to the EN 288 that is currently replaced by EN 15614-1:2004.
For LH welds, as the above mentioned Standards cover only arc welding processes, the DNV OS F 101 was adopted.
NdT inspections was performed according to the facilities available in each welding lab in observance to the Standard selected for the weld qualification. In particular visual inspection and radiographic testing were adopted.

2.3.2.1 <u>SAW welds on T plates – Main properties</u>

Microhardness measurements were performed according to the profiles shown in Figure 23, with a load of 2kgr on Vickers scale. The results in detail are presented in Figure 23. All measurements are within the range of 220-335 HV_2 in agreement with BS4515.
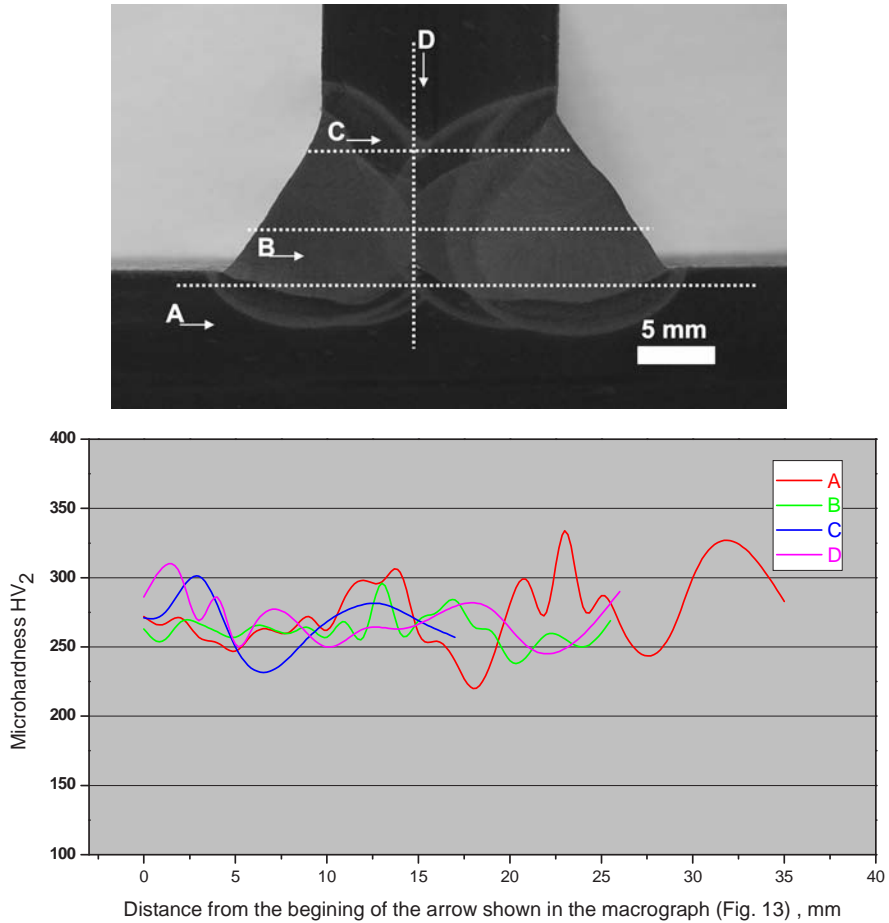

Figure 23 - Microhardness measurements

Tensile tests were carried out according to BS EN 10002 - part1 on round specimens taken from the parent plate in both longitudinal and transverse direction (in terms of the rolling direction) at RT and at T=-10°C. The results are shown in Figure 24.
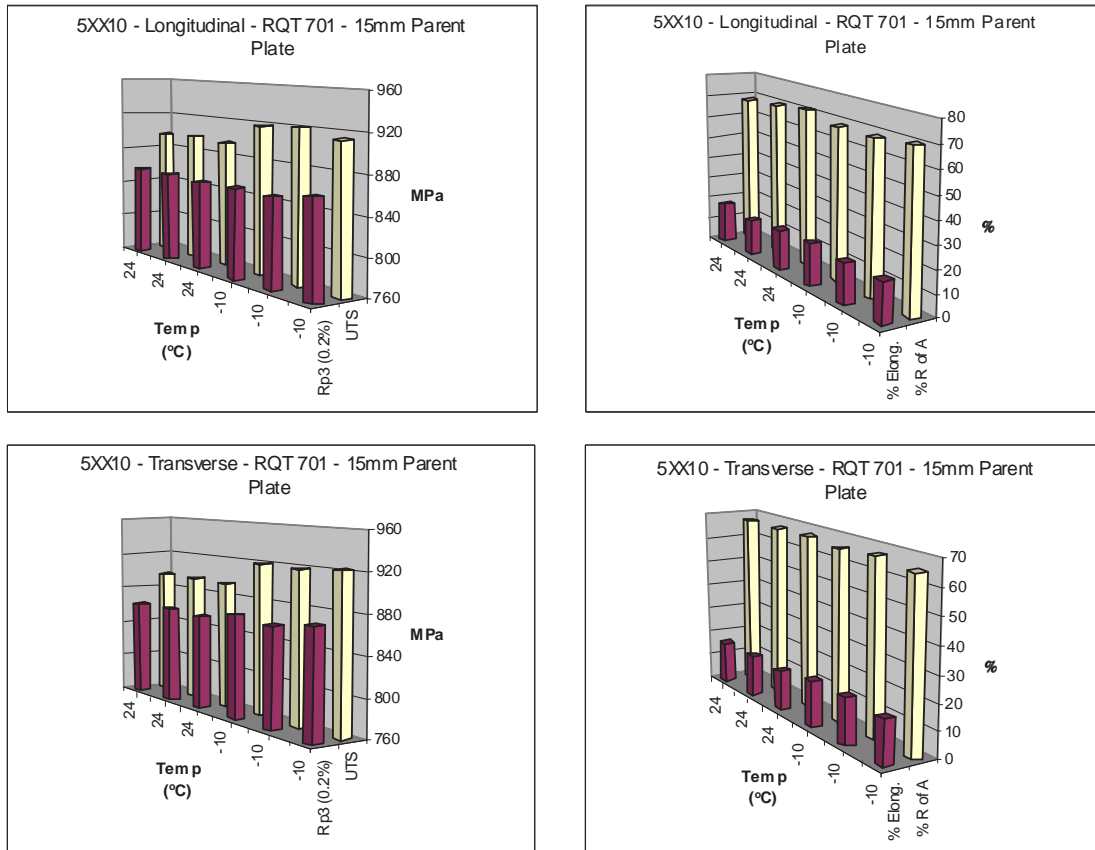
Figure 24 - Results of tensile tests on RQT 701 Parent Plate

Charpy impact tests to BS EN 10045 Part 1 [14] were conducted on specimens taken from the parent plate material and machined with the notch parallel to the plate rolling direction. A Ductile-Brittle Transition Temperature (DBTT) curve was generated as shown in Figure 25 giving a $T_{27J} = -62°C$.
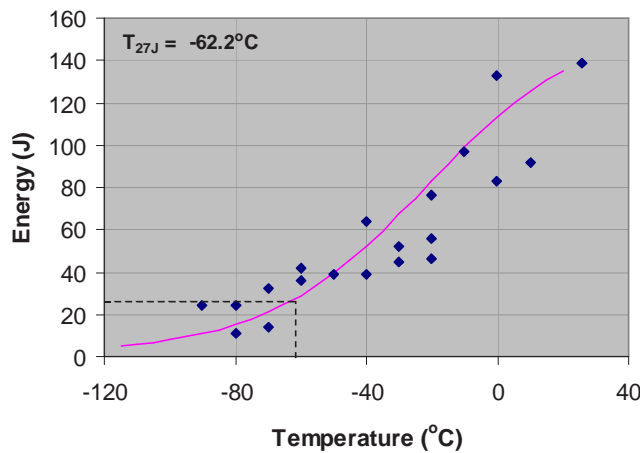
Figure 25 - Ductile-Brittle Transition Temperature Curve for Parent RQT 701 Plate Material

Fracture toughness (CTOD) tests were performed by SENB specimens machined from the parent plate with notch perpendicular (T) and parallel (L) to the plate rolling direction according to [15]. Tests were performed at RT and at T=-10°C and the results are reported in Table 6 showing that no relevant differences are remarkable.

Specimen ID	Orientation	Test Temp. (°C)	CTOD, δ (mm)	CTOD Fracture Type [1]
5XX10 -12	T		0.176	m
5XX10 -13	T		0.187	m
5XX10 -14	T		0.160	m
5XX10 -21	L	RT	0.128	m
5XX10 -22	L		0.146	m
5XX10 -23	L		0.141	m
5XX10 -24	L		0.126	m
5XX10 1a	T		0.164	m
5XX10 1b	T		0.239	m
5XX10 1c	T		0.177	m
5XX10 1d	T	-10	0.150	m
5XX10 2a	L		0.144	m
5XX10 2b	L		0.136	m
5XX10 2c	L		0.159	m
5XX10 2d	L		0.133	m

Notes: (1) m = maximum load

Table 6 – Fracture toughness test results for Parent RQT 701 Plate Material

Residual stresses were measured by X-ray diffraction in longitudinal and transverse directions, in the centre of weld seam, at the weld toe and at 10 mm and 100 mm away from the weld toe.

The measured stress values are presented in Figure 26 and Figure 27.
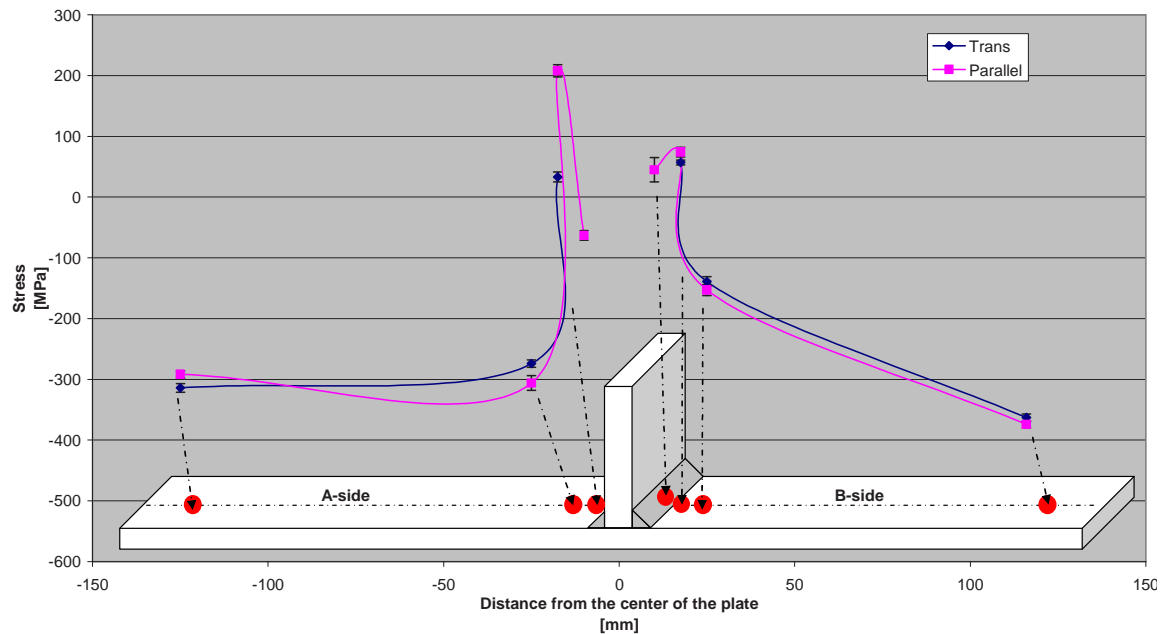
Figure 26 - Parallel and transverse stress profile along a line at the middle of the plate
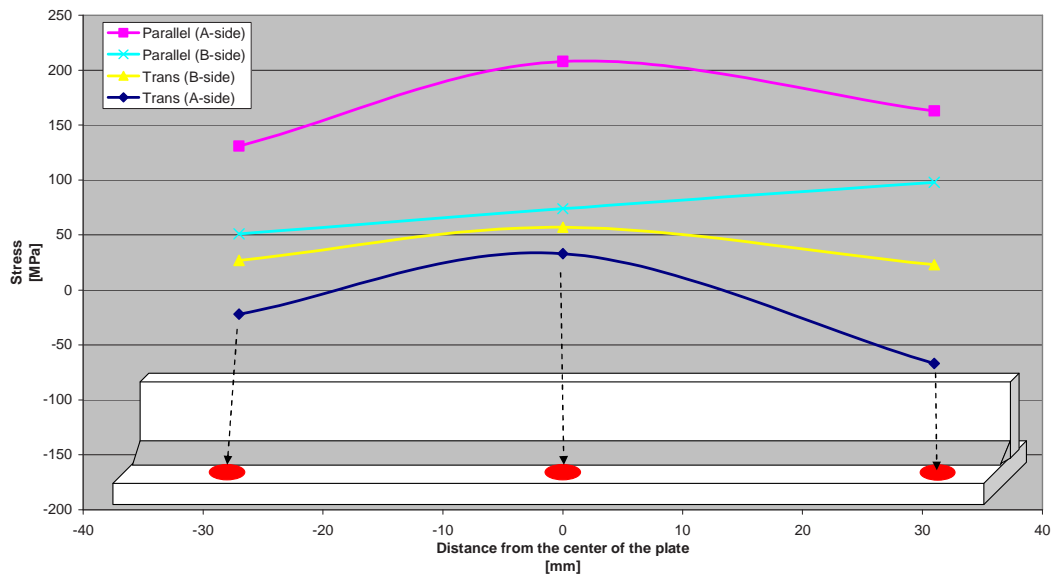
Figure 27 - Parallel and transverse stress profile at the weld toe in both sides of the plate

The following conclusions can be drawn:

→ Residual stresses are slightly tensile (0-100 MPa) in both transverse and parallel directions at the weld toe and weld seam and this can affect the fatigue performance of the joint.

→ Residual stresses are mainly compressive in both transverse and parallel directions at 10 mm and 110 mm away from the weld toe.

2.3.2.2 FCAW welds on pipes – Main properties

For X100 and X70 FCAW joints micro-hardness measurements were performed with a load of 2kgr on Vickers scale, according to the profiles shown in Figure 28 and Figure 29. The results are in agreement with the BS4515 requirements.
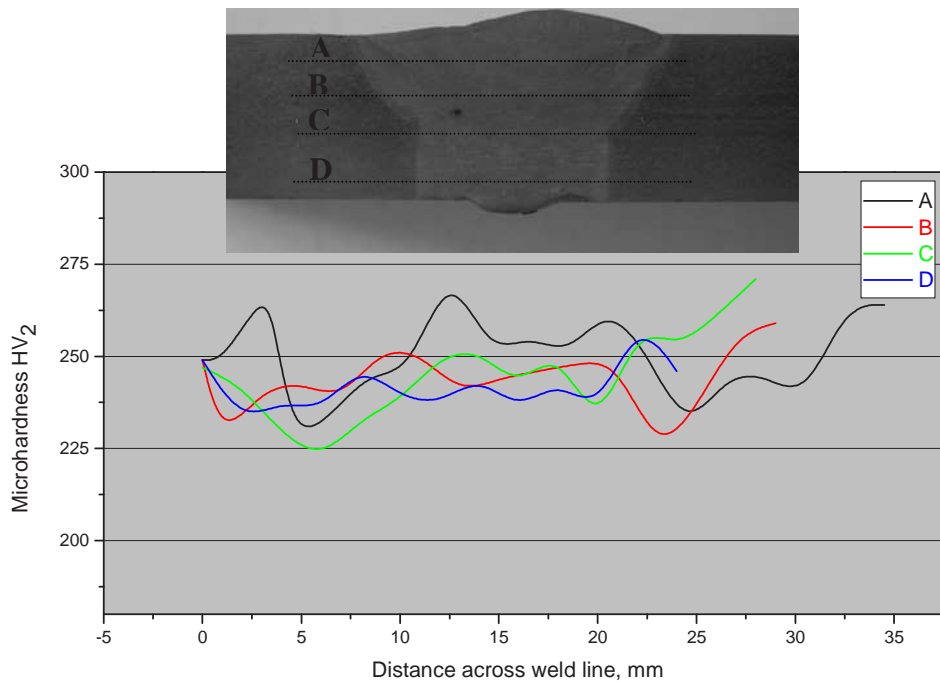
Figure 28 – X100 FCAW - Microhardness profile across the weld. - Measurements performed across the lines A,B,C,D shown in the embedded macrograph
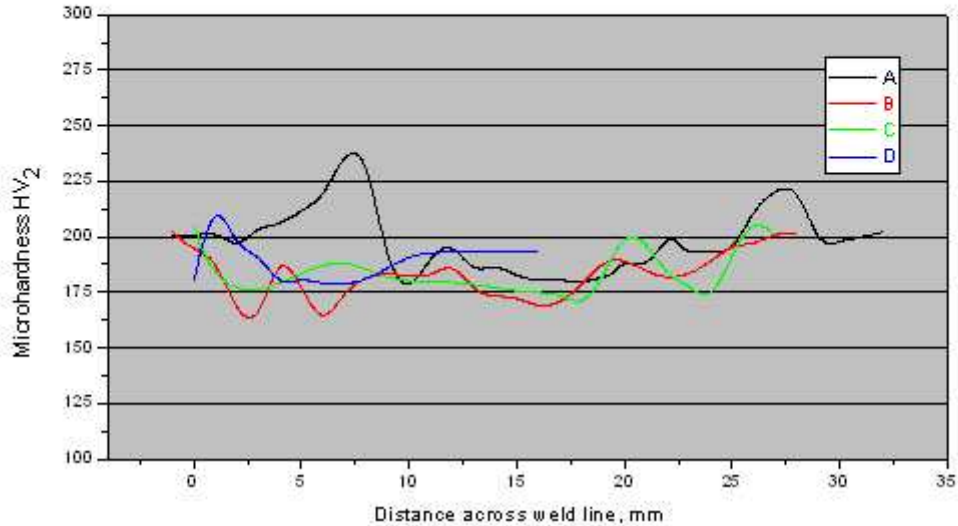
Figure 29 – X70 FCAW - Microhardness profile across the weld. - Measurements performed across the lines A,B,C,D shown in the embedded macrograph

Tensile tests have been performed at room temperature (RT) on prismatic specimens taken transverse to the weld, and the results are reported in Table 7 and Table 8.

Specimen label	Test temperature (°C)	Rm (MPa)	Notes
T1	23	775	Failure in base metal
T2	23	769	Failure in base metal

Table 7 – X100 FCAW pipes **-** Tensile tests results

Specimen label	Test temperature (°C)	Rm (MPa)	Notes
T1	23	613	Failure in weld metal
T2	23	602	Failure in weld metal

Table 8 – X70 FCAW pipes - Tensile tests results

The results are in agreement with the Standard as for X100 failure occurs in the base metal and for X70 the tensile strength of the specimens is higher than the specified minimum value for the parent metal (i.e 565 MPa according to API 5L).

Impact tests have been performed using Charpy V samples with notch located in the the Weld Metal (WM), Heat Affected Zone (HAZ) and base metal (BM), according to EN 875, as shown in Figure 30.
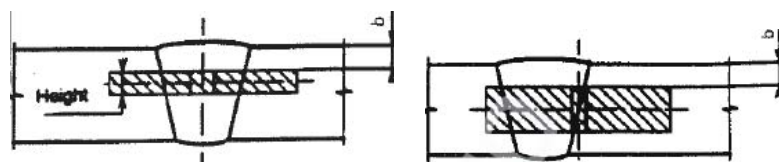
Figure 30 - Impact specimens in WM and HAZ

Tests have been performed at T=-10° C. The results are reported in Table 9 and Table 10.

Specimen label	Test temperature (°C)	Notch location	Absorbed Energy (J)	Average Absorbed Energy (J)
R1	-10		69	
R2	-10	WM	68	68
R3	-10		68	
R4	-10		129	
R5	-10	HAZ	134	134
R6	-10		139	
TL-2	-10	BM	246	246

Table 9 – X100 FCAW pipes **-** Impact tests results

Specimen label	Test Temperature (°C)	Notch location	Absorbed Energy (J)	Average Absorbed Energy (J)
R1	-10		124	
R2	-10	WM	124	128
R3	-10		136	
R1	-10		243	
R2	-10	HAZ	235	239
R3	-10		240	
R1	-10		266	
R2	-10	BM	268	267
R3	-10		268	

Table 10 –X70 FCAW pipes - Impact tests results

CTOD tests were carried out following the BS 7448 standard, with specimens B x 2B type, loaded in bending, with the maximum thickness allowed by the pipe wall. Test were performed at RT and at T=-10°C with specimens taken with transverse notch located in the Base Metal (BM), in the weld metal (WM) and in the Fusion Line (FL).

CTOD tests results shown in Table 11 and in Table 12 are in agreement with the standard requirements (0.15 mm) for all notch locations.

Weld	Notch position	T [°C]	CTOD (mean) [mm]	CTOD (range) [mm]	CTOD type
X100 FCAW	WM	RT	0.24	0.18 – 0.30	δ_m
	FL	RT	0.31	0.27 – 0.34	δ_m
	BM	-10	0.39	0.27 – 0.50	δ_m
	WM	-10	0.21	0.19 – 0.22	δ_m
	FL	-10	0.155	0.153 – 0.158	δ_u

Table 11 – X100 FCAW **-** CTOD testing results

Weld	Notch position	T [°C]	CTOD (mean) [mm]	CTOD (range) [mm]	CTOD type
X70 FCAW	WM	RT	0.61	0.59 – 0.65	δ_m
	FL	RT	0.72	0.66 – 0.77	δ_m
	BM	-10	0.99	0.99 – 1.00	δ_m
	WM	-10	0.55	0.45 – 0.62	δ_m
	FL	-10	0.75	0.52 – 0.86	δ_m

Table 12 – X70 FCAW **-** CTOD testing results

Residual stresses were measured by X ray diffraction.The attention was focused on the inner surface of the pipes that is expected to be the most critical location were usually failure occurs. Measurements were performed in longitudinal and hoop direction, on the inner surface of the pipe on strip specimens devoted to the testing program (see Figure 31).
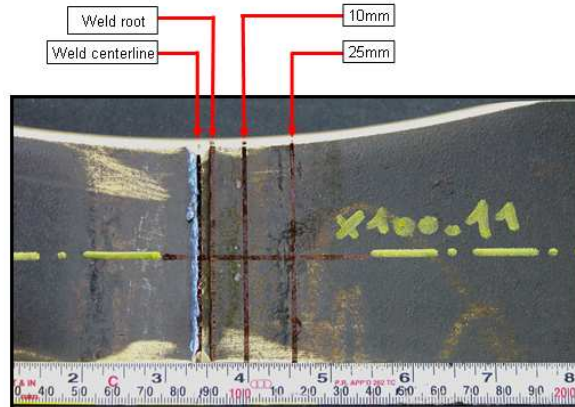
Figure 31 – FCAW girth joints– Residual stresses measurement points on inner surface

Here for the sake of brevity only the longitudinal residual stresses are reported as the most affecting the fatigue behaviour of the joint as they influence the load applied in service. The results are reported in Figure 32 and Figure 33 and highlight that residual stresses are around zero or slightly compressive.
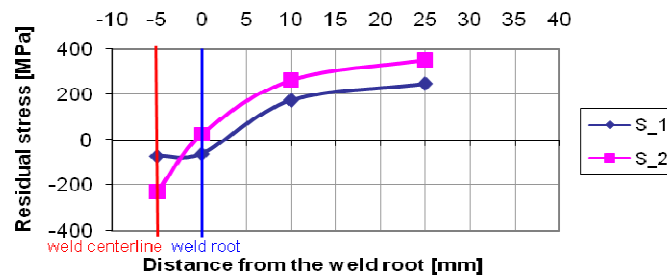
Figure 32 – X100 FCAW - Residual stresses on internal surface in longitudinal direction measured on two samples S_1, S_2.

Figure 33 – X70 FCAW - Residual stresses on internal surface in longitudinal direction measured on three samples S_1, S_2, S_3

2.3.2.3 <u>LH welds on pipes – Main properties</u>

Vickers hardness measurements (HV_{10}) were made on metallographic samples taken through the thickness of the welds. The results are shown in Table 13 Table 14. No values exceed DNV general requirements (max. 325 HV) even in the root area, despite to the hardening occurred from the severe laser thermal cycle.
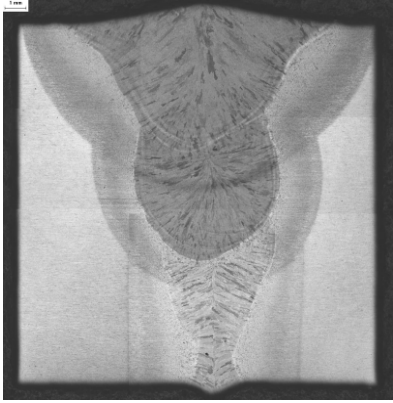
Location	HV (mean)	HV (range)
BM (outer surface)	292	290 ÷ 295
BM (mid thickness)	290	288 ÷ 291
BM (root)	283	280 ÷ 289
CGHAZ root	255	253 ÷ 256
CGHAZ cap	247	244 ÷ 249
FZ root	242	240 ÷ 244
FZ cap	249	247 ÷ 250

Table 13 – Hardness testing results on X100 pipes welded by Laser – GMAW
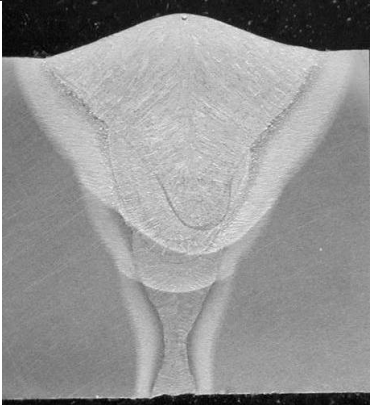
Location	HV(mean)	HV(range)
BM (root)	243	241 ÷ 244
CGHAZ root	297	291 ÷ 302
CGHAZ cap	275	273 ÷ 276
FZ root	313	309 ÷ 315
FZ cap	228	225 ÷ 231

Table 14 – Hardness testing results on X70 pipes welded by Laser – GMAW

Transverse tensile tests were carried out on two nominally identical specimens (rectangular, 25 mm wide at the gauge section) with full pipe wall thickness (see Figure 34).
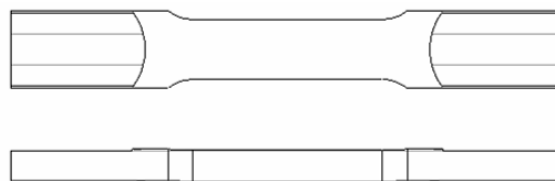
Figure 34 – Specimen geometry for transverse tensile testing of welds on X100 pipes

The results (see Table 15 and Table 16) are in agreement with the DNV OS F101 Standard as for X100 the tensile strength of the specimens is higher than the specified minimum value for the parent metal (i.e 760 MPa according to ISO 3183) and for X70 failure occurs in the base metal.

Specimen label	Test temperature (°C)	Rm (MPa)	Notes
T1	23	760	Failure in weld metal
T2	23	771	Failure in weld metal

Table 15 – X100 LH pipes **-** Tensile tests results

Specimen label	Test temperature (°C)	Rm (MPa)	Notes
T1	23	683	Failure in base metal
T2	23	666	Failure in base metal

Table 16 – X70 LH pipes **-** Tensile tests results

Full size Charpy – V specimens were extracted from weld samples 2 mm below the surface, with notch perpendicular to the surface. Charpy – V notch toughness test were performed at -20 °C (i.e. Tmin – 10 °C) and results are shown in Table 17 for X100 LH and in Table 18 for X70 LH.

Notch position	T [°C]	KVT (mean) [J]	KVT (range) [J]
WM	-20	104	70 ÷ 150
FL	-20	59	42 ÷ 79
FL+2 mm	-20	81	74 ÷ 91
FL+5 mm	-20	243	232 ÷ 253

Table 17 – Charpy – V testing results on X100 pipes welded by Laser – GMAW

Notch position	T [°C]	KVT (mean) [J]	KVT (range) [J]
WM	-20	158	148 ÷ 164
FL	-20	179	163 ÷ 187
FL+2 mm	-20	248	237 ÷ 265
FL+5 mm	-20	265	265 ÷ 266

Table 18 – Charpy – V testing results on X70 pipes welded by Laser – GMAW

CTOD testing was carried out following the well recognised BS 7448 standard, specimens being of the B x 2B type, loaded in bending, with the maximum thickness permitted by the pipe wall (actually 12 mm). CTOD specimens were extracted with notch perpendicular to the surface. The results are reported in Table 19 and Table 20.

Notch position	T	COD (mean)	COD (range)	CTOD type
	[°C]	[mm]	[mm]	
WM	-10	0.205	0.19 ÷ 0.22	δ_m, δ_u
FL	-10	0.15	0.15 ÷ 0.152	δ_c

Table 19 – CTOD testing results on X100 pipes welded by Laser – GMAW

Material	Notch position	T [°C]	COD (mean) [mm]	COD (range) [mm]	CTOD type
X70 Laser - GMAW	WM	-10	0.48	0.40 ÷ 0.56	δ_m
X70 Laser - GMAW	FL	-10	0.53	0.50 ÷ 0.54	δ_u, δ_m
BM	-	-10	0.97	0.95 ÷ 1.00	δ_m

Table 20 – CTOD testing results on X70 pipes welded by Laser – GMAW

Residual stress measurements have been carried out on a number of samples destined to fatigue testing program. Measurements have been performed in longitudinal and hoop directions, on internal surface (see Figure 35), considered the critical area for fatigue failure according to the in service loading conditions. In the following the results obtained are reported.

Figure 35 – Measurement points on internal surface

Results are reported in Figure 36 and Figure 37.
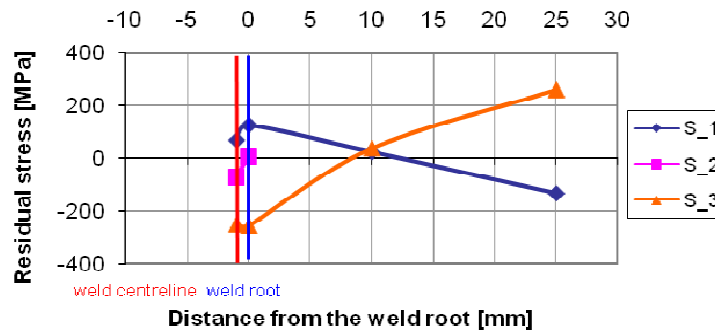
Figure 36 – X100 LH - Residual stresses on internal surface in longitudinal direction measured on three samples (S_1, S_2, S_3)
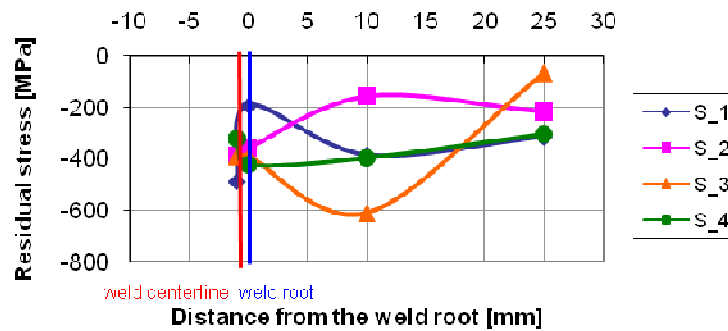
Figure 37 – X70 LH - Residual stresses on internal surface in longitudinal direction measured on three samples (S_1, S_2, S_3)

As concerns X100 LH longitudinal residual stresses are very scattered in the weld root with compressive, near zero and tensile values. For X70 LH residual stresses are compressive in both longitudinal and circumferential direction.

2.3.2.4 Post welding treatment

In WP1 the state of the art on post-welding treatments that could be applied to enhance the fatigue performances of the selected products, was investigated.

Ultrasonic peening, a mechanical method, was selected as a promising technique to increase the general fatigue strength of the structure. This technique consists in the application of ultrasonic- and mechanical-impulses to the high stressed locations in the weld; as a result of these ultrasonic- and mechanical-impulses the welded metal is modified at the atomic- and/or metallurgical-level.

The contractor selected to perform ultrasonic peening on the joints of interest was Lets Global, an engineering and consulting company based in the Netherlands, which main field of business is the life extension of welded structures and components. Lets Global specializes in the application of ultrasonic peening treatment on customer's installation in the offshore field.

Ultrasonic peening was applied on FCAW welded strips both X70 and X100 destined to the fatigue program. It was stated to apply the treatment only on FCAW welds as for LH welds the weld geometry at the root pass was sensibly of good quality.

Residual stresses on treated samples were measured by X-ray diffraction method. In Figure 38, as an example, the comparison between the residual stresses measured before and after UP on the inner surface of a X100 FCAW welds, is reported. As evident after the treatment residual stress field is strongly compressive.

The same situation is noticeable on X70 FCAW welds in Figure 39 where the residual stress field after applying ultrasonic peening is shown.
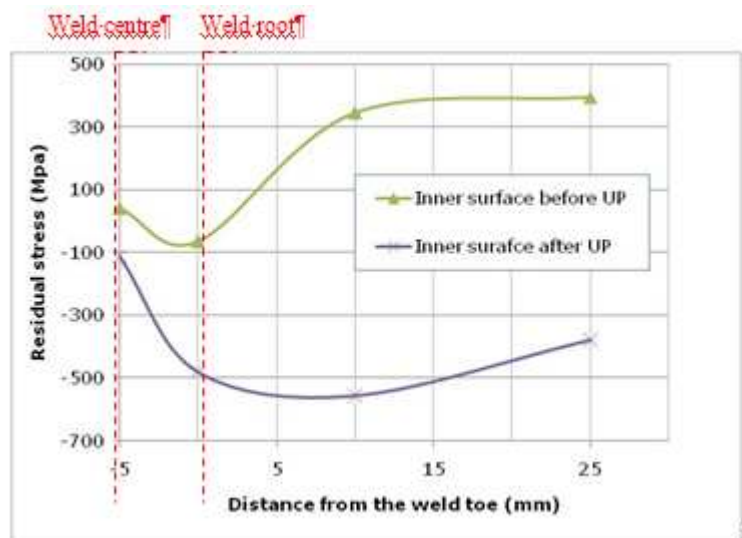
Figure 38 – X100 FCAW – Residual stresses before and after UP

34
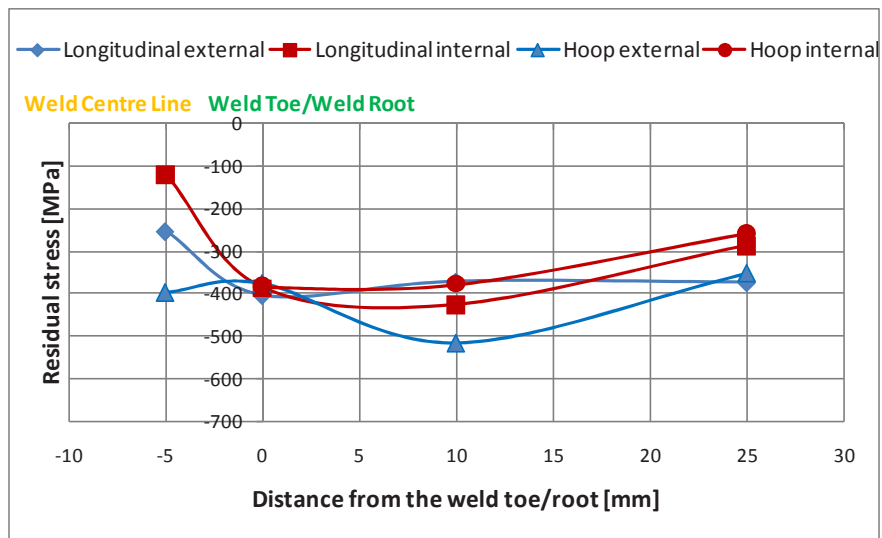
Figure 39 – X70 FCAW – Residual stresses after UP

2.3.2.5 Conclusion of WP 2
- → In the frame of this WP the WPS to manufacture the welded joints for the project have been set up.
- → The welded joints have been manufactured and characterized in terms of macro features, microstructure, mechanical properties and residual stress field.
- → After a state of the art review on the possible post welding treatments available to enhance fatigue performances, ultrasonic peening was selected and applied on FCAW welded joints.

2.3.3   WP3: Basic fatigue assessment of the selected welded joints.

In order to qualify welds with respect to the main Standards in force in the welded joints/offshore area, the basic fatigue assessment of the selected joints was carried out by means of small-scale endurance tests in air on full thickness specimens taken from welds, under constant amplitude load with a stress ratio R = 0.1.

The influence on fatigue performances of loading conditions similar to the in-service ones was investigated by means of small-scale endurance tests in air under constant amplitude load with a stress ratio R=0.5.

In both cases with the aim to study the environment effect on fatigue of the selected high strength steel welded joints, a limited number of tests was performed in sea water with a standard level of cathodic protection (<-900 mV) with a frequency of about 0.3 Hz, For SAW welds on T butt plates, also the influence of cathodic overprotection was investigated (<-1300 mV).

In addition some tests in order to measure fatigue crack growth rates using fracture mechanics specimens were performed.

2.3.3.1 SAW welds on T butt plates - Constant amplitude test results

Constant amplitude tests were carried out, on T-Joints specimens fabricated from plates, specified in WP1.

The load was applied in a four point bend load configuration, as shown in Figure 40.
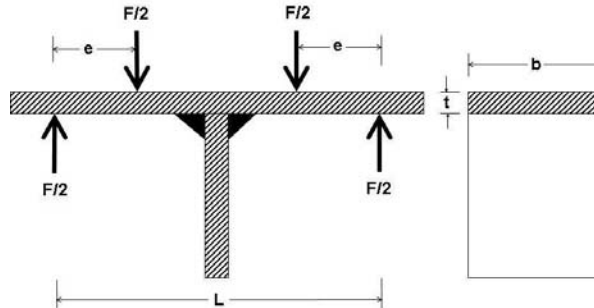
Figure 40 – Four point bend load configuration

Basic fatigue curves were obtained for the joints at R=0.1 both in air and in seawater with a standard level of cathodic protection (<-900 mV).

Loading conditions similar to the in service ones were investigated with test at R=0.5, both in air and seawater. Tests in seawater were carried out using synthetic seawater having the composition specified in ASTM D1141 and applying both a standard level of cathodic protection (<-900 mV) and under overcathodic protection (<-1300 mV).

Results are shown in Figure 43 and Figure 44, together with the reference curve selected for this welding detail.

Figure 41 presents a typical failed specimen and in Figure 42 the fracture surface appearance is shown.

Figure 41 – Typical failed specimens - Crack initiating at the weld toe

Figure 42 – Fracture surface appearance

As regards the results in air, reported in Figure 43 a generally good behavior is noticeable with respect to the S-N curve recommended by the Standards, as the experimental results are all above the mean line suggested by the BS standard and well above the S-N design curves (i.e. mean – 2 standard deviations). The effect of the stress ratio R on fatigue performances is not relevant and the difference in fatigue performances at R=0.1 and R=0.5 could be considered of the same order of the typical scatter intrinsic in fatigue phenomenon.
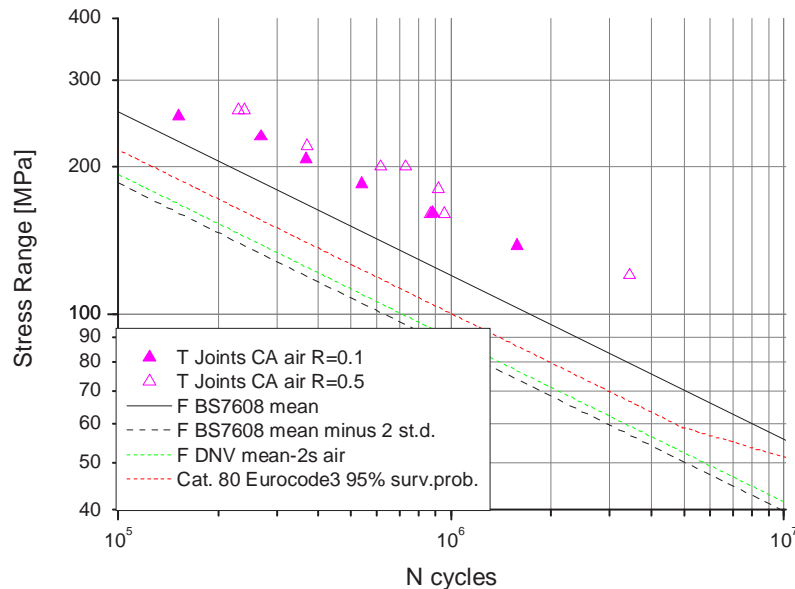
Figure 43 – T joints from plates – Experimental results in air under constant amplitude (CA)

In Figure 44 the results from fatigue tests in seawater with cathodic protection are reported in comparison with the reference curves from DNV and BS 7608 Standards. Note that BS recommends for fully protected joints the same S-N curve proposed in air.

The fatigue endurance data generated for the cathodically protected joints indicate a strong dependence of fatigue performances on applied stress range when compared to the Class F mean line. At stress ranges below 180 MPa and 140 MPa for R ratios of 0.1 and 0.5 respectively there appears to be a marked improvement in the fatigue life of the joints as shown by the data points above the Class F mean line for protected joints in seawater. Although there is a small amount of scatter in the results at the higher stress ranges there appears to be little deviation from the Class F mean line for air and fully protected joints. However, all the results in the low stress – long life regime showed significant improvements in fatigue life compared to the Class F mean line for air and fully protected joints.

The fatigue life enhancements from cathodic protection have been attributed by some authors to calcareous deposits (mainly CaCO3 and Mg (OH)2) within the nascent crack. This calcareous deposit is considered to form a wedge at the crack tip, reducing the effective stress range, thus the early stages of crack growth are significantly delayed. However, as shown by the data above, delayed initiation is not always accompanied by increased life at all stress ranges, particularly at the higher stress ranges for CP. This is because once a crack is established higher fatigue crack growth rates in the corrosive environment can negate the benefits obtained from delayed initiation. In terms of increased total life a balance exists between the extent to which an incipient crack can be delayed and the growth rate of an established crack.
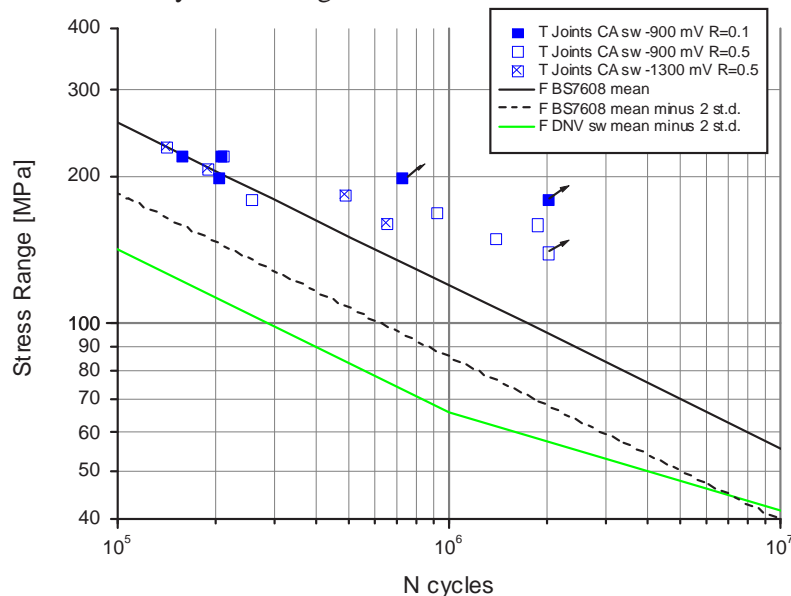
Figure 44 – T joints from plates **-** Experimental results in seawater under constant amplitude (CA)

2.3.3.2 <u>Welded joints from pipes - Constant amplitude test results</u>

Tensile constant amplitude tests were carried out on large scale specimens extracted from pipes specified in WP1.

Basic fatigue curves were obtained for all welded joints, in air at R=0.1.

For three typologies of welds, X100 FCAW, X70 FCAW and X70 LH, tests were performed at R=0.5, in order to investigate fatigue behavior in loading conditions similar to the in service ones.

Tests in seawater, with a standard level of cathodic protection (<-900 mV) with a stress ratio =0.1 and R=0.5 were performed on X100 FCAW and X70 LH joints, that is very high strength steel with traditional weld and high strength steel with innovative weld.

Additionally, a limited number of tests was performed on samples from girth FCAW welded joints after than the ultrasonic peening treatment, described in WP1 and WP2, was applied.

The experimental tests performed are listed in the following and all the results are resumed in Figure 46 and compared with the S-N design curves selected in the main Standards considered in the project.

→ X100 FCAW joints, air, R=0.1

→ X100 FCAW joints, air, R=0.5

→ X100 FCAW joints, seawater, R=0.1

→ X100 FCAW joints, seawater, R=0.5

- → X70 FCAW joints, air, R=0.1

- → X70 FCAW joints, air, R=0.5

- → X70 LH joints, air, R=0.1

- → X70 LH joints, air, R=0.5

- → X70 LH joints, seawater, R=0.1

- → X70 LH joints, seawater, R=0.5

- → X100 LH joints, air, R=0.1

- → X100 FCAW joints postwelding treated, air, R=0.1

- → X100 FCAW joints postwelding treated, air, R=0.5

- → X70 FCAW joints postwelding treated, air, R=0.5

Fatigue failures usually occurred in correspondence to the weld root and Figure 45 presents a typical failed specimen.

Figure 45 – Typical failed specimen and fracture surface appearance
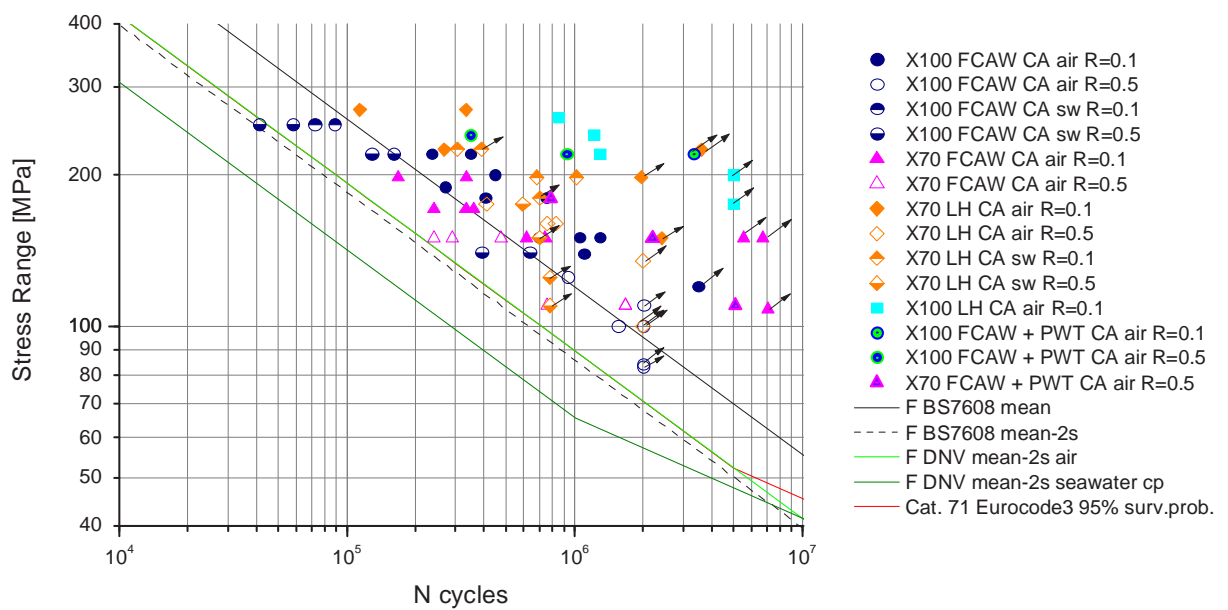
Figure 46 – Samples from girth welded pipes **-** Experimental results compared with the standard requirements

A general good behavior in comparison with the standards can be noticed. In the following the data have been grouped with different criteria in order to properly analyze the performance of the high strength steel joint typologies in the different loading/environmental conditions applied.

In Figure 47 are shown fatigue tests results performed in air with a stress ratio R=0.1 for all the joint typologies.

It is evident that all the results lie above the design standard fatigue curves proposed in the standards, highlighting that, as noticed for T joints from plates, the S-N curve recommended results conservative generally for all the selected joints.

This is more evident when high grades are welded by the innovative welding technique i.e LH performed at the weld root. In fact it is remarkable that Laser Hybrid in the root pass allows to improve significantly the fatigue behavior for both the steel grades employed. In particular X100 LH shows very good performances.

In Figure 48 are shown results from tests performed in air with stress ratios R=0.1 and R=0.5 for all the joint typologies. Fatigue performances at higher stress ratio (that is a higher mean stress applied) seem to be slightly worst for all the joints typologies tested.

In Figure 49 are reported the results from tests in artificial seawater with cathodic protection for X100 FCAW and X70 LH joints, at both the stress ratios considered, R=0.1 and R=0.5.
Joints in seawater show, as expected, lower performances than in air but the general behavior is still good if compared with the BS and DNV design standards selected. It is to be noted that the BS code recommends to use the same curves as in air for fully protected joints but the document states that this curve is not proven for steels with σ_y>400 MPa as for X100 joints that are closer to the design curve therein proposed, but well above the DNV requirements.

Looking at the stress ratio it is noticeable a certain detrimental effect due to the higher mean stresses applied. Again in seawater, Laser Hybrid Technique, with its improvement in the root geometry, showed good performances.
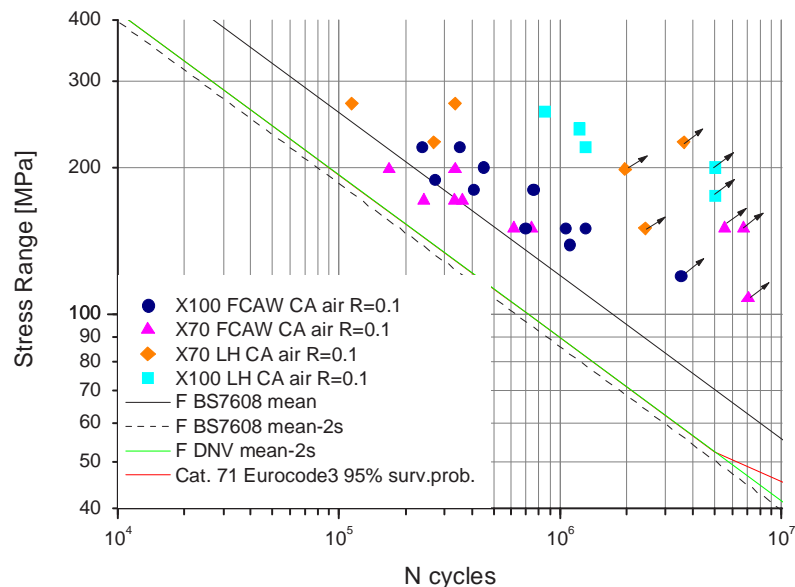
Figure 47 – Samples from girth welded pipes **-** Fatigue performances of the selected joints in air at R=0.1 - comparison with the standard requirements
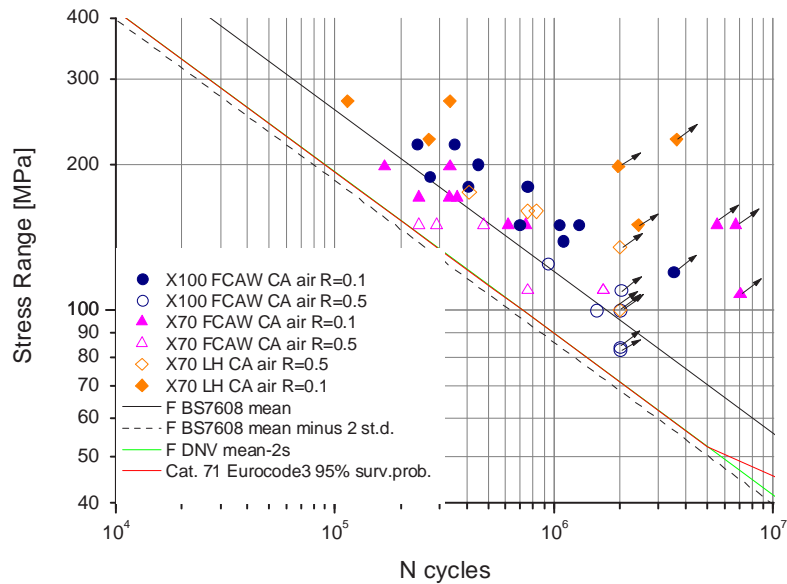
Figure 48 – Samples from girth welded pipes **-** Results in air R=0.1 and R=0.5
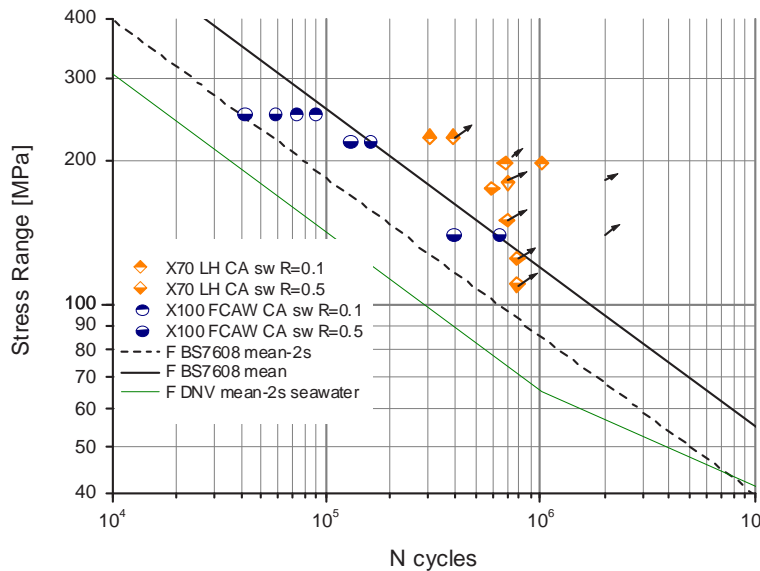
Figure 49 – Samples from girth welded pipes **-** Results in seawater with cathodic protection R=0.1 and R=0.5

In Figure 50 the effect of ultrasonic peening applied on FCAW welds is shown. Fatigue tests were performed mainly at high stress ratio, R=0.5, in order to investigate the beneficial effect of the postwelding treatment on fatigue performances in more strict conditions close to the in-service ones. It is noticeable that the treatment improves fatigue behavior for both X100 and X70 welds. This was expected, as the residual stresses after the treatment, as shown in WP2, results strongly compressive.

In Figure 51 the results in post-welded specimens are compared with the promising results obtained on LH joints. According to the number of tests performed in the frame of the current project it seems that the use of ultrasonic peening (UP) leads to better fatigue performance of the joints with respect to the Laser Hybrid welding technique applied in the root pass. Nevertheless it should be underlined that the performance of the post welding treatment requires additional time before laying the joint in the sea bed and this should be taken into account when considering the potential benefits achievable.

41
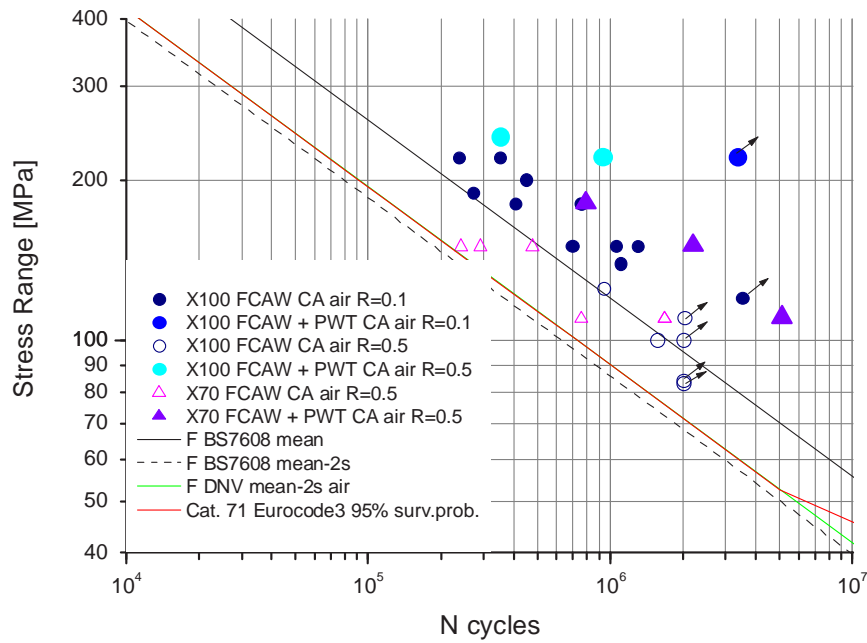
Figure 50 – Samples from girth welded pipes **-** Results from specimens treated by ultrasonic peening compared with as welded joints
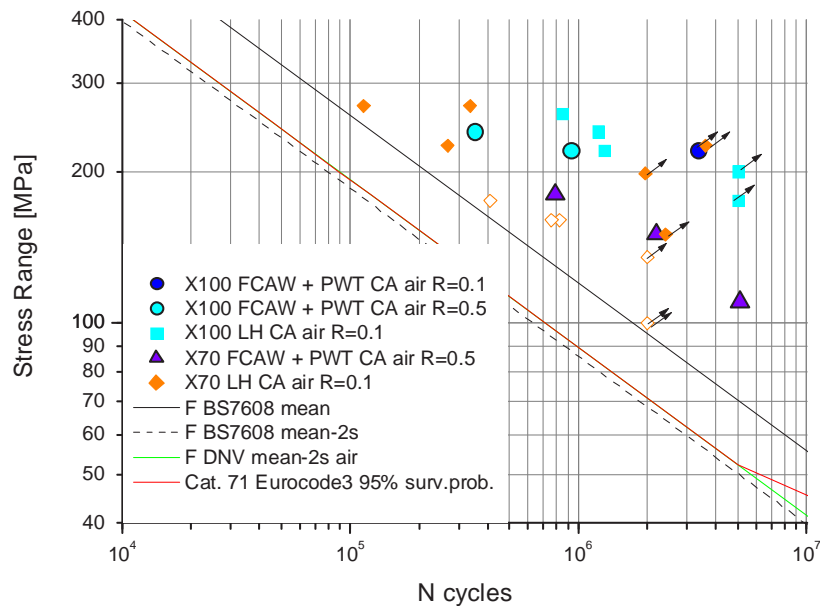
Figure 51 – Samples from girth welded pipes **-** Results from specimens treated by ultrasonic peening compared with LH welds

2.3.3.3 Fatigue crack growth tests on plates

In order to investigate the suitability of the available Standards accounting for fatigue when high strength steels are intended to be used, fatigue crack growth rate tests have been performed on T joints from plates RQT701. Compact tension (CT) specimens extracted from plates were used. Performances in air and seawater environments have been investigated, both for the parent metal and the Heat Affected Zone.

As well known the overall relationship between da/dN (m/cycle) and ΔK (MPa m^1/2) is normally a sigmoidal 'S' curve in a log da/dN versus log ΔK plot. The central portion of the curve is usually assumed to be linear and may be described using the Paris Law:

$$\frac{da}{dN} = C\Delta K^m$$

Where C and m are constants which depend on the material and the applied conditions, including environment and cyclic frequency. (It should be noted that these parameters are also dependent on the units of K and the growth rate). These constants, C and m govern the speed of fatigue crack growth and are thus critical inputs when, for example, defining safe inspection intervals for structures and components which are subjected to cyclic loading conditions in service. Reliable fatigue crack growth prediction is critically important for safe design and maintenance of engineering structures subjected to cyclic loading [16][17][18].

The results of the tests performed are summarized in Table 21 with the best fits to the straight line, while further details are available in Appendix K.

Material	Environment	R-ratio	C	m
Base metal	Air	0.1	4.6×10^{-11}	2.479
	Air	0.1	8.32×10^{-12}	2.863
	Seawater CP -900 mV	0.1	4.5×10^{-10}	1.808
	Seawater CP -900 mV	0.1	3.3×10^{-10}	1.886
	Air	0.7	1.1×10^{-11}	2.861
	Seawater CP -900 mV	0.7	8.6×10^{-11}	2.353
	Seawater CP -900 mV	0.7	5.1×10^{-10}	1.816
HAZ	Air	0.1	5.1×10^{-12}	2.79
	Air	0.1	2.5×10^{-11}	2.38

Table 21 - Summary of Paris Law constants obtained from FCGR conducted on RQT 701 parent material and HAZ

The Paris Law coefficients (C) and exponents (m) were determined from regression analyses of log (da/dN) – log (ΔK) data, where da/dN in m/cycle and ΔK in MPa √m.

In Figure 52 and Figure 53 the experimental results for the base metal are reported in comparison of the Paris curves proposed in BS7910, while in Figure 54 the experimental results on HAZ are reported in comparison with the BS7910 and the base metal.

While the slopes (m values) obtained for the tests undertaken in air at the two R-ratios of 0.1 and 0.7 are higher for the latter stress ratio (see Figure 52 and Figure 53), the fatigue crack growth rates are very similar. The theory explaining similar crack growth rates in air at two different R-ratios might be that the crack is fully open at both R = 0.1 and 0.7. As RQT 701 is a high strength steel, so one could argue that the residual strains (controlling the plasticity induced closure) in the wake of the growing crack are limited and this is the reason why the crack may be fully open and consequently have the same effective crack tip driving force (delta K effective) at R = 0.1 and the higher ratio 0.7.

In Figure 52 and Figure 53 the fatigue crack growth data have been compared to the recommended fatigue crack growth laws for steels in air and marine environment as stated in BS 7910.
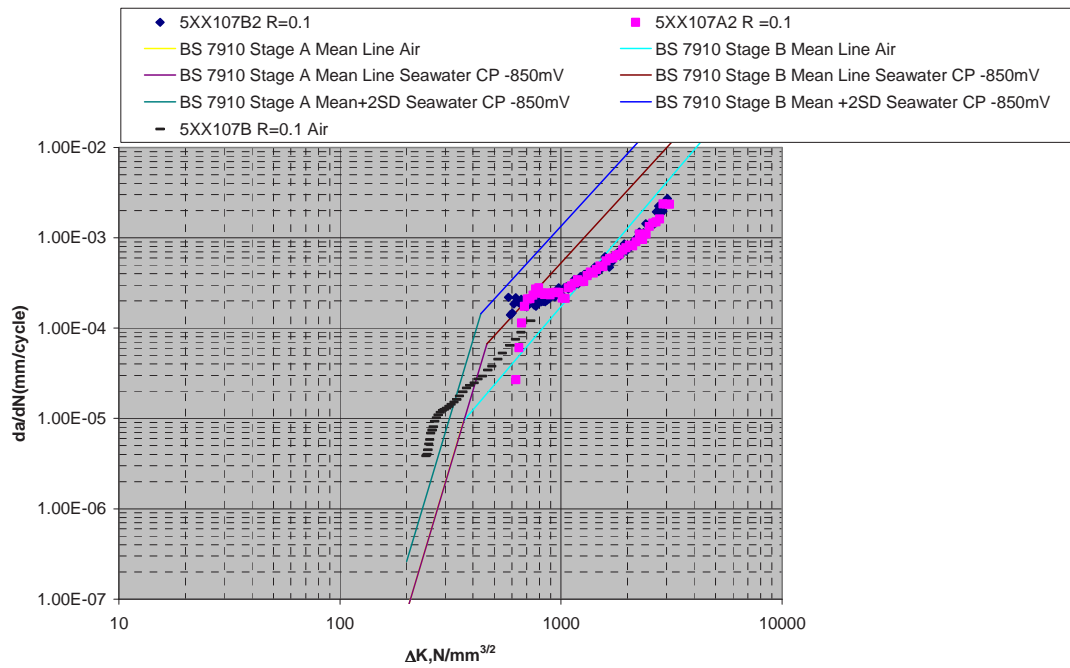
Figure 52 - Fatigue crack growth data in air and seawater at R = 0.1 versus fatigue crack growth laws in BS 7910
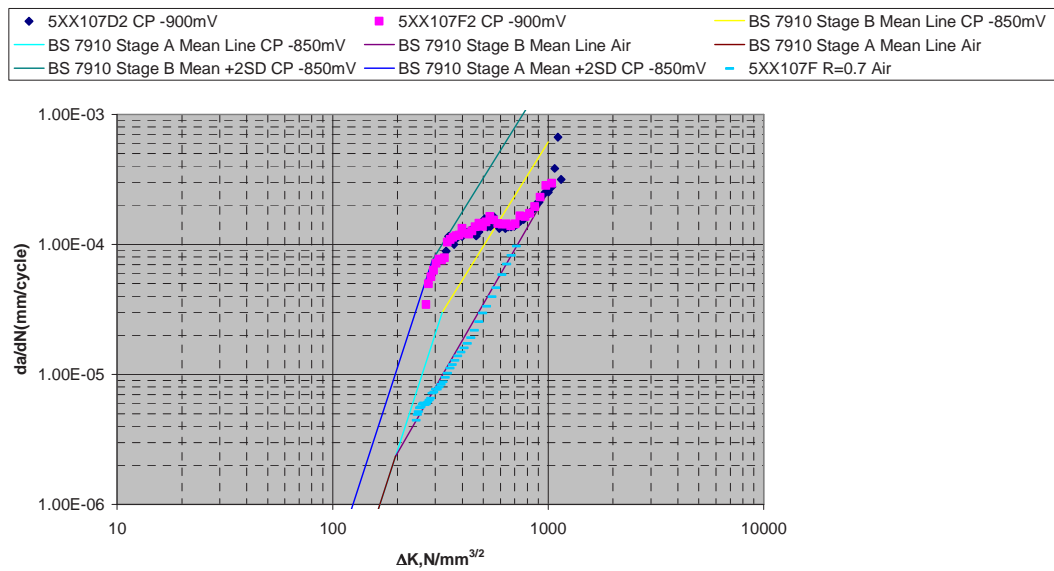
Figure 53 - Fatigue crack growth data in air and seawater at R = 0.7 versus fatigue crack growth laws in BS 7910
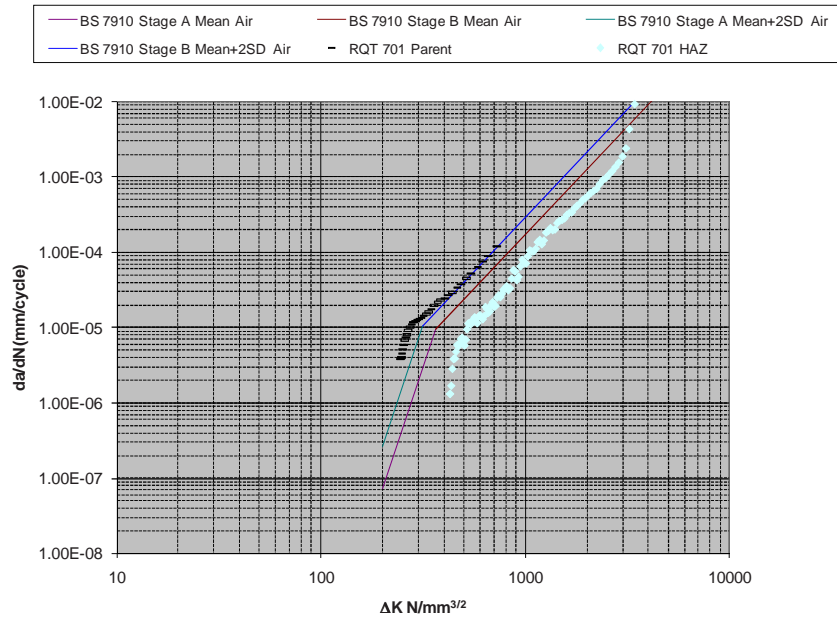
Figure 54 – HAZ and base metal - Fatigue crack growth data in air at R = 0.1 versus fatigue crack growth laws in BS 7910

While the generated FCGR data have been compared to the fatigue crack growth laws quoted in BS 7910 it should be recognised that the data in BS 7910 is for steels with yield strengths less than 700 MPa and therefore may not obey the same rules. The seawater data with R-ratio of 0.7 crosses both the mean and mean +2SD lines before tracking the mean line in air, suggesting this may well be the case. A possible explanation is that the real-time crack extension rate (da/dt) exceeds the rate at which the environment can influence the crack growth and the crack continues to grow as if it's in air, as shown in Figure 52 and Figure 53. The environmental influence decreases with increases in the real-time rate of crack extension (da/dt) because the faster the crack growth rate, the less time available for environmental interaction. The real-time rate of crack extension (da/dt) depends on the cyclic fatigue crack growth rate (da/dN), itself a function of the applied ΔK, stress ratio and test frequency. Finally, the environmental influence depends on the accessibility of the environment to the crack tip, which can be affected by crack length, specimen thickness, ΔK, Kmax, and stress ratio.

2.3.3.4 Conclusion of WP3

In this WP a consistent number of fatigue tests was performed.

→ First point to be highlighted is that the tests results put in evidence the conservativeness of the S-N design curves proposed in the reference Standards for large of the welded joints investigated.
→ The beneficial effect in fatigue performances of the employ of high steel grades together with the new welding technologies and post welding treatment investigated was outlined. In particular in this respect it is worth noting the excellent behavior of X100 LH welds.

2.3.4   WP4: Influence on fatigue behaviour of typical loading and environmental in-service conditions.

The effect of variable amplitude loads on fatigue behavior of the selected high strength welded joints has been evaluated, using the load sequences set up in WP1. Small-scale endurance tests were performed and the results were compared to the ones under constant amplitude.

2.3.4.1 SAW welds on T butt plates - Variable amplitude test results

T-joints were tested at variable amplitude loading given by the sequence properly modified to represent loading conditions typical of welds in renewable energy devices. The generated test data were analyzed according to the Gassner technique described in Appendix J.

The equivalent constant amplitude stress ranges were then assessed accordingly, in order to compare the variable amplitude results with the constant amplitude test data and relevant S-N curve design curves as illustrated by Figure 55 and Figure 56 where the tests results are summarized.
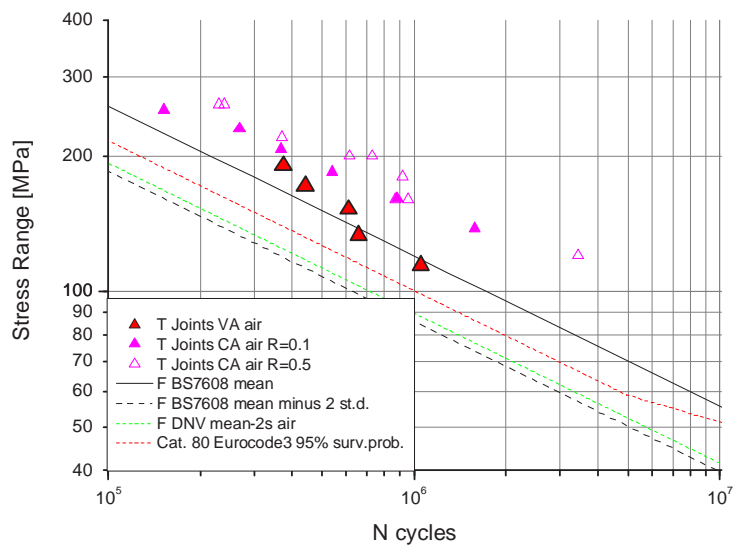
Figure 55 – T joints from plates - S-N plot combining the constant amplitude test results, and the variable amplitude results against the main standards selected
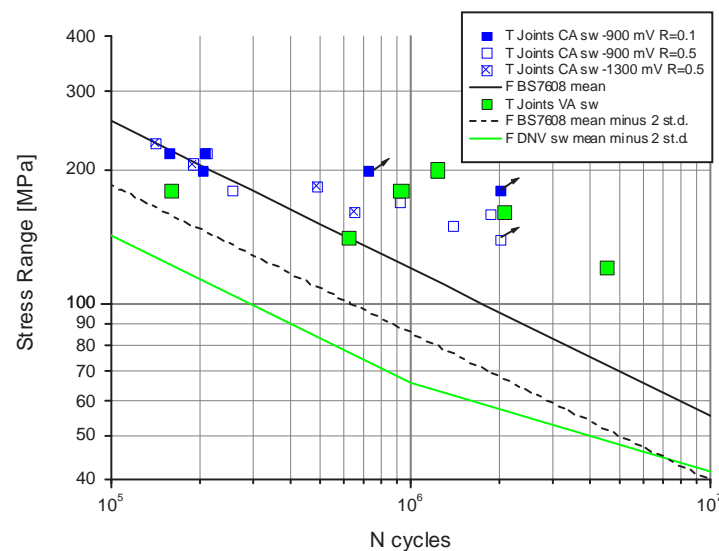
Figure 56 – T joints from plates - S-N plot combining the constant amplitude test results, and the variable amplitude results against the BS 7608 and the DNV F curve in seawater with cathodic protection

46

The results obtained in air are seen to match the class F mean curve very closely, whereas for seawater the results are well above the mean line, showing that the Palmgren-Miner Rule applied taken as reference the design S-N curve proposed in the standard can be non-conservative.

As regards results in seawater, they are in line with the ones obtained at constant amplitude.

2.3.4.2 Welded joints from pipes - Variable amplitude test results

Variable amplitude fatigue tests were conducted in air on full thickness strip specimens extracted from pipes with the loading sequence for risers developed in WP1 representing the real scenario of Gulf of Mexico.

As for T joints from plates, the generated test data were analysed according to the Gassner technique and the equivalent constant amplitude stress ranges were then recalculated accordingly, in order to make a comparison with the constant amplitude test data and relevant S-N curve design curves, as illustrated by Figure 57.
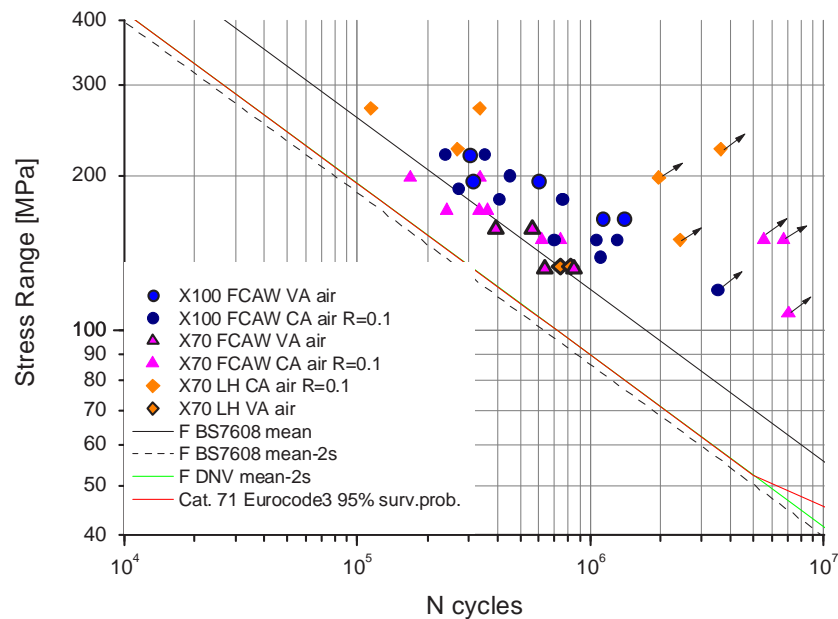
Figure 57 – Samples from girth welded pipes - Comparison with CA and VA tests and the standard curves

As regards X100 FCAW and X70 FCAW joints, results are in line with the ones performed at constant amplitude. X70 LH joints have slightly lower performances at variable amplitude with respect to the constant amplitude loading.

2.3.4.3 Conclusion of WP4

The present WP highlights that the conservativeness evidenced for the S-N design curves is still remarkable when loads similar to the in service conditions are applied.
In particular it was put in evidence that in the design of structures or components employing high strength steel welded joints their real performance could be underestimated. In fact adopting the S- N design curves suggested in the current Standards damage values can be much more higher than the limit values usually recommended.

2.3.5   WP5: Full-scale fatigue tests program

In this work package, fatigue behavior of welded joints was investigated by means of full-scale fatigue tests, in order to estimate the difference between full and small scale test results.

Full-scale rotating four-point-bending fatigue tests were carried out with constant amplitude loads on X70 FCAW welded pipes.

Due to the specific test set-up available within the project (see Figure 58) the tests were conducted with an R-value of -1, thus having a mean stress equal to 0 MPa.
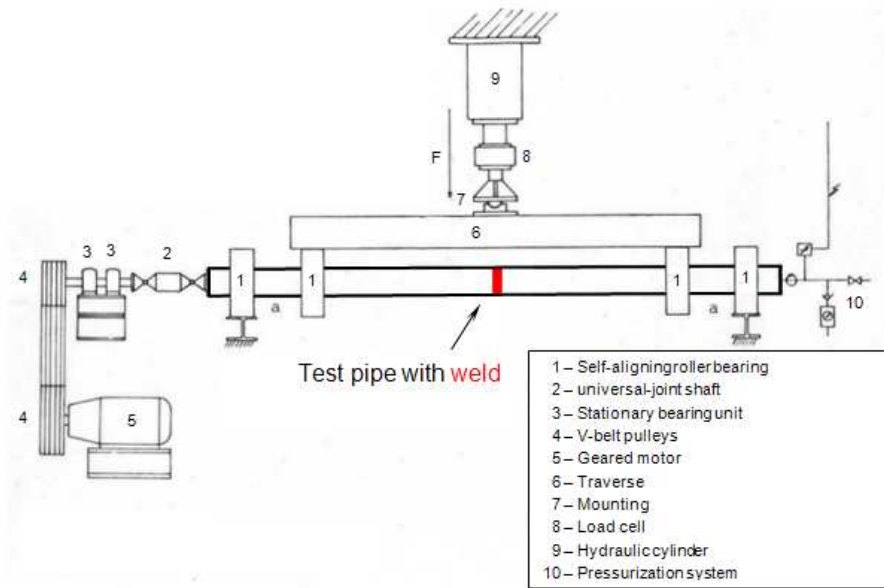
Figure 58 – Schematic drawing of the test setup for tests

In a next step the test rig was modified to allow full-scale rotating bending tests under seawater conditions. For this purpose a tub was installed beneath the inner section of the pipe that contained a supply and a drain pipe for the corrosive seawater environment. The welded pipe was rinsed with the seawater from the outer side using a submerged pump with one or more sprinkler pipes. A pH-control unit monitored the pH-value of the seawater.

In total, 6 full scale rotating bend tests were conducted, 4 of which in air and 2 of which in seawater solution. The load level was selected on basis of the results of small scale tests.

Tests in seawater solution were conducted at a frequency of 0.3 Hz. Cathodic protection (-900mV) was applied to the test pipes as it is representative for actual pipelines or pipe components exposed to seawater. Test results are shown in Figure 60.

After having tested the first specimens in air and having investigated the failure initiation site, it became evident that each one of the welds contained areas of non-penetration in the root, in the majority of cases in conjunction with the start-stop position, as shown in Figure 59. The welds that had been produced according to EN 15614 were inspected by X-ray. Each weld was considered acceptable when applying the stipulated criteria. Nevertheless, new welds were produced with the specific aim to avoid this kind of defect also if acceptable, to investigate the influence of such root defects on the fatigue performance.
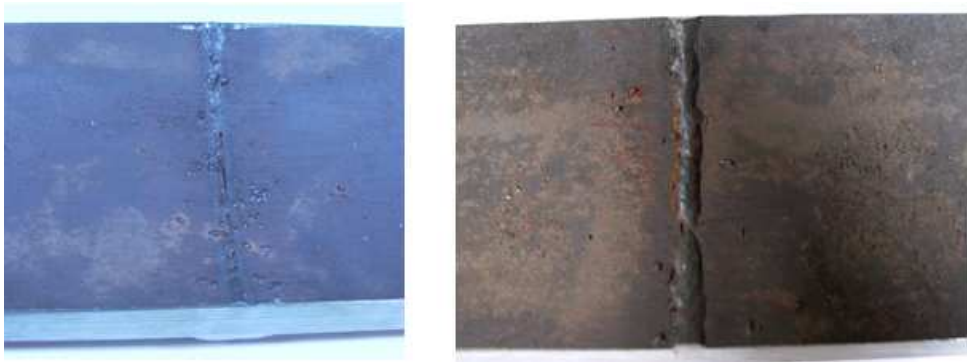
Figure 59 – Root pass appearance

Results of tests conducted in different environmental conditions are depicted in Figure 60. Except for one data point every result is within a relatively small scatter band independent of the environmental surrounding. The single data red point was generated in the test of the weld without lack of penetration.

In comparison to the design curves it can be stated that the results of the tests in air fall below the corresponding curve with the exception of the test result generated on the defect-free weld.
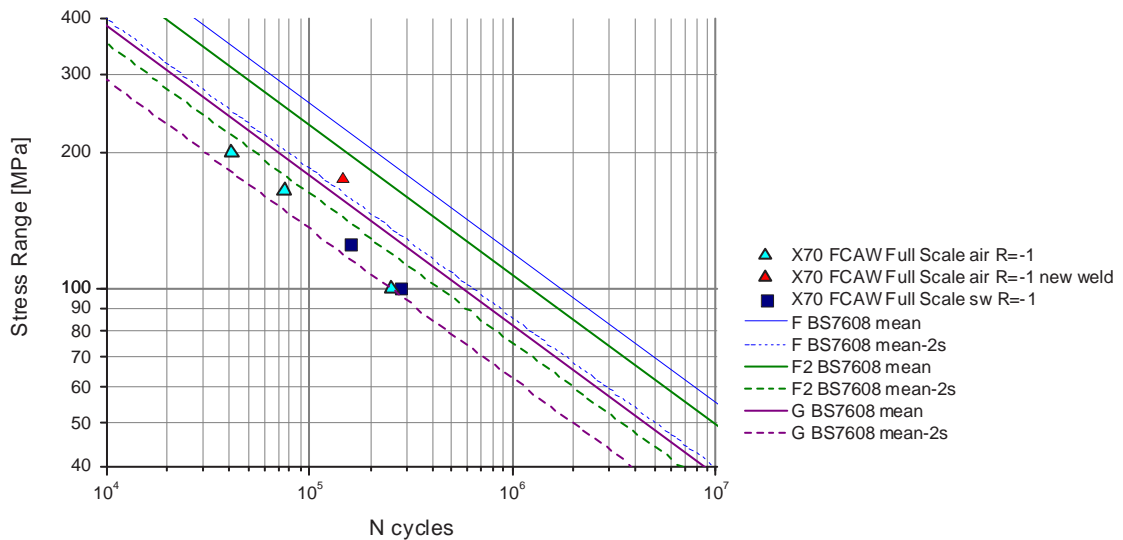
Figure 60 - S-N curve containing results of full scale rotating bend tests alongside applicable design curves

Figure 61 shows the full scale results compared with the small scale ones. All small scale test results are well above the relevant design curves and in line with the mean curves, whereas the full scale test results lie, as discussed above, below these design curves. Generally, the fact that small scale tests yield a better fatigue performance is expected. The debate on the reliability of tests on strip specimens in reproducing the full scale behavior is still ongoing. It was highlighted in some works (see Figure 62 and Figure 63), that strip specimens could give higher fatigue lives than full-scale pipes, especially in the high-cycle regime.

Two main factors have been evidenced as possible explanation for this difference:

→ the greater likelihood of finding a large defect in an entire girth weld with respect to a portion of it in the strip specimen;

→ the cutting out of the strip specimens, expected to relax residual stresses due to girth welds and thus leave lower residual stresses in the strips.

No single factor could completely and especially quantitatively explain the difference.

The obtained results evidenced that despite standards could allow some types of defect, difference in the weld quality are of fundamental importance in fatigue behavior.

Strategies for achieving high fatigue strength in welded steel structures include good design practice (e.g. using joints with low stress concentration factors, or avoiding the placing of welds in regions of high stress range) but above all high quality welding.
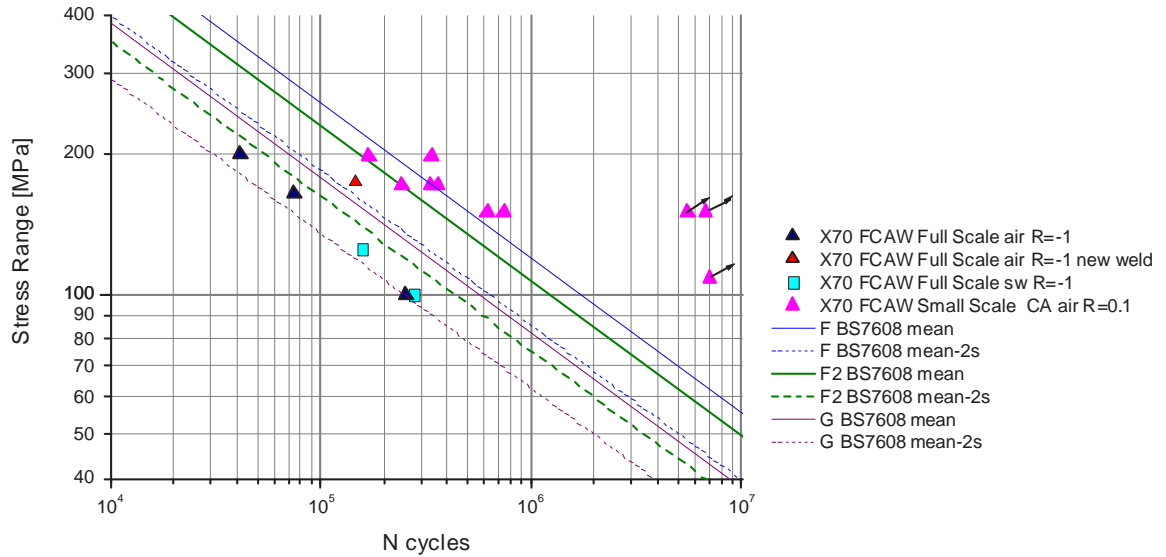
Figure 61 – Comparison between full scale and small scale results
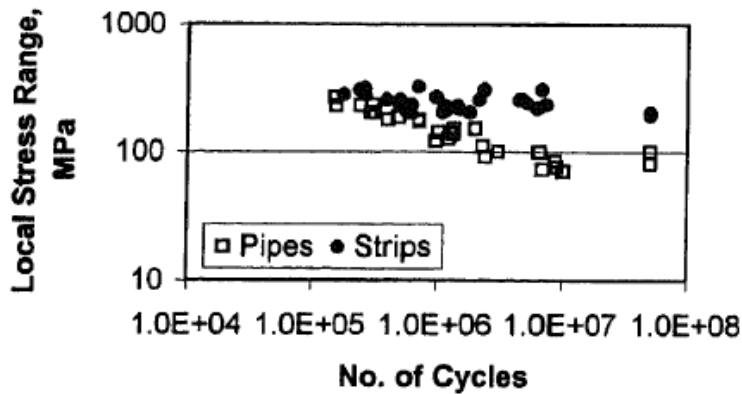
Figure 62 - Results from tests on full-scale pipes and strips [19]
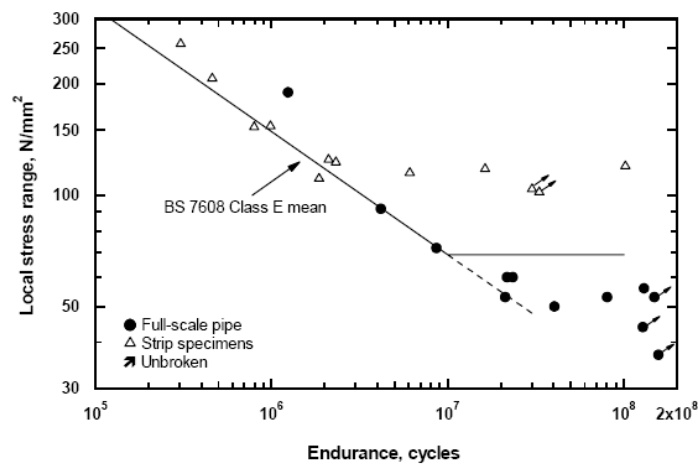
Figure 63 - Tests results [22]

2.3.5.1 Conclusion of WP5

It was remarked a difference in fatigue performance between full scale and small scale fatigue tests. Generally, the fact that small scale tests yield a better fatigue performance is expected. The debate on the reliability of tests on strip specimens in reproducing the full scale behavior is still ongoing

The obtained results evidenced that despite the welding standards could allow some types of defect, difference in the weld quality are of fundamental importance in fatigue behavior.

Strategies for achieving high fatigue strength in welded steel structures include good design practice (e.g. using joints with low stress concentration factors, or avoiding the placing of welds in regions of high stress range) but above all high quality welding. This is in line with the recent trend for welding contractor in the offshore field; in fact is a recent practice, in the stage of WPS definition, to perform full scale fatigue tests on the welded pipes at a very high number of cycles.

2.3.6 WP6: Analysis of experimental results and elaboration by a local approach methodology (Hot Spot)

In the classification method, structural joint details are classified, and a specific S-N fatigue curve is associated with each class, to be used with the nominal stress acting on the weld detail under consideration. This means that there exist quite a few S-N curves, covering a large number of classes of structural welded details. On the other hand, the hot spot stress adopts a different philosophy: due to the local nature of fatigue crack initiation and propagation, one has to determine the maximum local stress at the weld vicinity and, subsequently, using an appropriate S-N curve, calculate the fatigue design life. The main difference is that the hot spot stress approach uses a single fatigue S-N curve, but requires a reliable calculation of the maximum geometric or "hot spot stress", which is quite often more demanding than nominal stress calculation.

It has been recognized that the stress at the vicinity of the weld toe is responsible for fatigue cracks in welded structures. Therefore, the use of the hot spot stress approach is a more rational method compared with the "nominal stress" approach. The hot spot stress method for assessing the fatigue strength of welded connections is based on the important assumption that the local stress increases at the weld toe can be subdivided into two parts; one part is structural (i.e. macro-geometrical) and the other part is created by the localized notch effect, restricted to a region of 2-3 mm around the toe (see Figure 64). Furthermore, it is assumed that the fatigue assessment can be based on the first part, i.e. the structural stress at the "hot spot" location, together with an appropriate S-N fatigue curve, which considers the effects of localized notch in an implicit manner, and is valid for a certain class of weld shapes and materials.
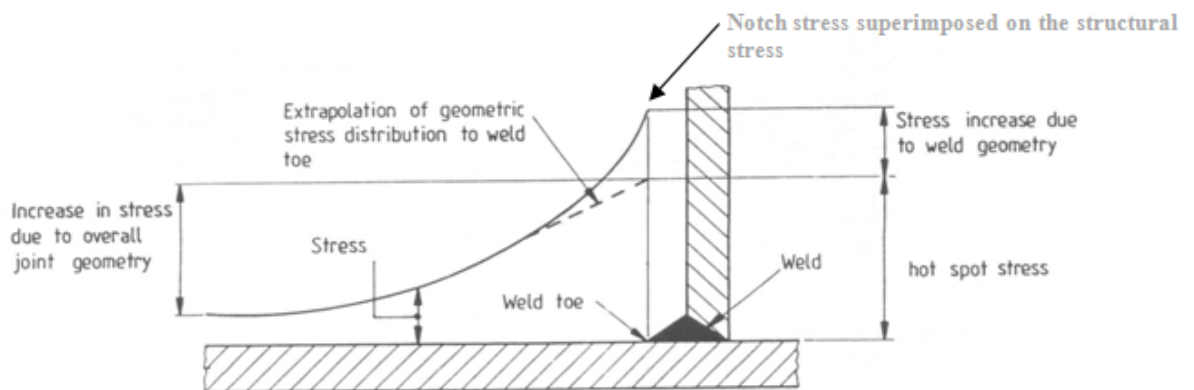
Figure 64: Example of Hot Spot stress in a nodal joint

2.3.6.1 <u>Hot spot stress method in welded plate connections</u>

The hot spot stress method has been initially proposed for the design of welded tubular connections, with emphasis in offshore platform tubular joints. In those tubular connections, the geometry is quite complex and, furthermore, loading of the joint results in local bending of the concurrent tubular members at the vicinity of the connection, resulting in a very high stress concentration at those locations. The hot-spot stress range, denoted as $\Delta\sigma_{Hot\ Spot}$ or S_{hs}, and the nominal stress range, denoted as $\Delta\sigma_{Nominal}$, are related through the following relationship:

$$S_{hs} = SCF \cdot \Delta\sigma_{nominal} \tag{1}$$

Where SCF is the Stress Concentration Factor.

In the case of welded tubular connections, a very large number of different cases exist, depending on the number of concurrent members, the inclination angle of the braces with respect to the chord, the possible eccentricities etc. Therefore, the classification method is difficult to be applied. Instead, the hot spot stress method has been widely used, considering a specific S-N curve, and appropriate stress concentration factors (SCFs) to multiply the nominal stress in the member. The SCFs for some specific and rather simple geometries are given in the literature in the form of parametric equations in terms of the geometric parameters of the connection (Kuang et al. 1977, Karamanos et al. 2000). In addition, the SCF value for a specific connection can be determined numerically, calculating the local stresses at the vicinity of the weld through an appropriate linear-elastic finite element simulation. Guidelines regarding this simulation have been published in the literature and the reader is referred to the work of Romeijn et al. (1993).

Traditionally, the stress analysis of plated structures, such as ships and other marine vessels, was conducted through an approximate estimate of "nominal stresses", to be used in fatigue assessment through a classification approach. The classification method has been adopted in all major specifications for the fatigue design of relevant structures. However, recently, there has been a serious attempt to extend the local stress concept in plated connections as well. The motivation of this attempt is the safe design of Floating Production Storage and Off-loading (FPSO) vessels, which are used for deep-offshore oil and gas production. Those structures are mainly composed by plates and the fatigue design of welded connections is a critical issue for the structural integrity (Maddox, 2001). Moreover, the advent of numerical methods (such as the finite element method) has allowed for an accurate calculation of local stress, towards an efficient local (hot-spot) stress fatigue design.

The use of local stress approach for assessing the fatigue strength of welded joint should employ the stress in the vicinity of the location of crack initiation, which can be obtained from stress measurement or numerical analysis like FE analysis. The philosophy of local stress approach and many research works are well surveyed in the book of Radaj and Sonsino (1998). In order to obtain a precise stress by numerical calculation, it is necessary to know the detail information of local structural geometry. It has been noted that the stress at cracked location is sometimes very sensitive against the local geometry, and that the structural modelling of local geometry itself includes sometimes very uncertainty. In such area, it needs an expertise in numerical modelling and calculations to obtain the precise stress in a reliable manner.

There are several advantages of the use of a design approach based on the local stress range instead of the nominal stress approach, which can be summarized as follows:

→ hot spot stress can be calculated from stresses in front of weld toe, which can be obtained from numerical stress analysis and also from stress measurement on site (if possible)

→ fatigue evaluation can be conducted for the welded joint whose (nominal stress base) fatigue strength category is unknown (i.e. unclassified details)

→ hot spot stress can be obtained from appropriate structural analysis, using a finite element analysis. It is noted that in various welded plated joint details, which are part of large structural system (e.g. an FPSO), it is sometimes quite difficult to define the nominal stress in a universal manner

→ in the case where hot spot stress can be obtained in field, a fatigue evaluation can be conducted for this particular detail, even after change of the structural detail due to repair and retrofit.

2.3.6.2 Finite element modeling for local stress calculations

Towards calculating the hot spot stress at the vicinity of the weld toe, two-dimensional simulations are considered, employing plane-strain continuum elements. In particular, the general-purpose finite element program ABAQUS is employed, with eight-node quadratic plane-strain continuum finite elements, with reduced integration (CPE8R). This type of finite element has been shown to perform very well in predicting the exact stress state in plated metal structures.

A main question in these simulations is the type of stress to be computed in the finite element calculations, and how to employ it in fatigue assessment. To be consistent with previous works, the local stress of interest is the weld toe is "geometric" part of the stress, which can be considered as "structural" (i.e. macro-geometrical), and does not include the influence created by the localized notch effect on the stress. The effects of localized notch in should be considered in an implicit manner, through the consideration of an appropriate S-N curve. The geometric stress is usually calculated through an extrapolation procedure, as followed in tubular welded connections (e.g. in marine/off-shore structures). However, this extrapolation is not unique; in various fatigue design specifications or recommendations, several extrapolation procedures to calculate the local (hot spot) stress have been proposed.

Most of methods propose the calculation of the local stress at weld toe through an appropriate extrapolation from stresses at two points in front of weld toe. Some extrapolation methods have been proposed in the past, considering two reference points. Recently, the International Institute of Welding (IIW) recommendations specify the extrapolation points of $0.4T$ and $1.0T$ far from weld toe, where T is base plate thickness. Other methods have also been proposed, such as one-point stress method where stress at one location at a certain distance far from weld toe is decided as hot spot stress (for example some researchers recommend the stress at $0.3T$).

Although the definition of the local geometric stress is a subjective matter, it is our opinion that this definition should be based on a standardized procedure which excludes most of the uncertainties of the numerical calculations, and lead to the reliable (and repeatable) calculation of the local stress. Therefore, extrapolation methods are usually more preferable than single-point methods. Furthermore, the minimum distance from the weld toe should be a certain fraction of the weld toe, to avoid any uncertainties in the results, due to the sensitivity of the numerical results near the weld toe because of singularity. In order to use this hot spot stress range for fatigue evaluation, an appropriate fatigue curve should be specified with hot spot stress range. Recently, Niemi and Marquis (2002) proposed the fatigue strength category of IIW-FAT100 or 90 specified with hot spot stress range for weld-attachment plated joints.

Initially, the case of welds on T butt plates was simulated. Pipe joints were also modeled through finite elements simulations. In all cases, the corresponding Stress Concentration Factors (SCF) are calculated.

2.3.6.3 Numerical simulation of plated welded T-joints

A typical weld profile with the relevant meshing is given below in Figure 65. The weld profile is based on the macroscopic weld evaluation of WP2. Based on this evaluation, the shape of the weld is considered with a "sharp" toe configuration, as shown in more detail in Figure 65.

According to IIW recommendations it is suggested to interpolate between 0.4 t and 1.0 t as reported in Figure 66.
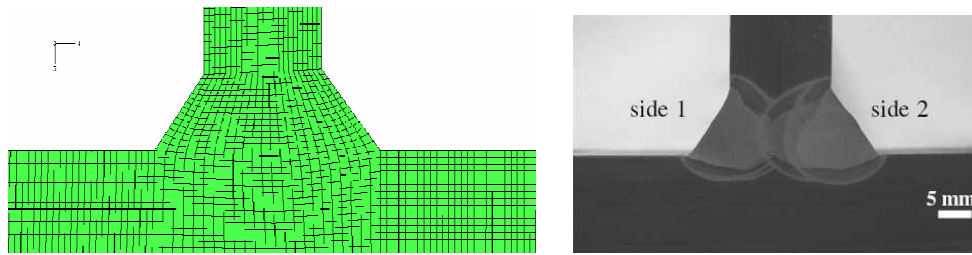
Figure 65 - Typical weld profile, modeled with plane strain finite elements, based on the weld profile.
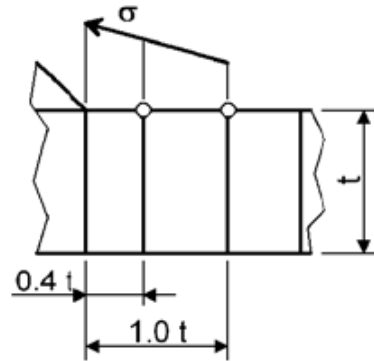
Figure 66 – Reference points for Hot Spot extrapolation

The numerical results of Figure 67 show the variation of the normal stress perpendicular to the weld toe with respect to the distance from the weld toe, for three different values of the weld toe angle (50°, 60°, 70°). As expected, the maximum stress concentration occurs at the weld toe vicinity, and this responsible for the development of fatigue cracking.

According to the obtained results for the selected structural detail the Hot Spot stress coincides with the nominal stress as shown in Figure 67.
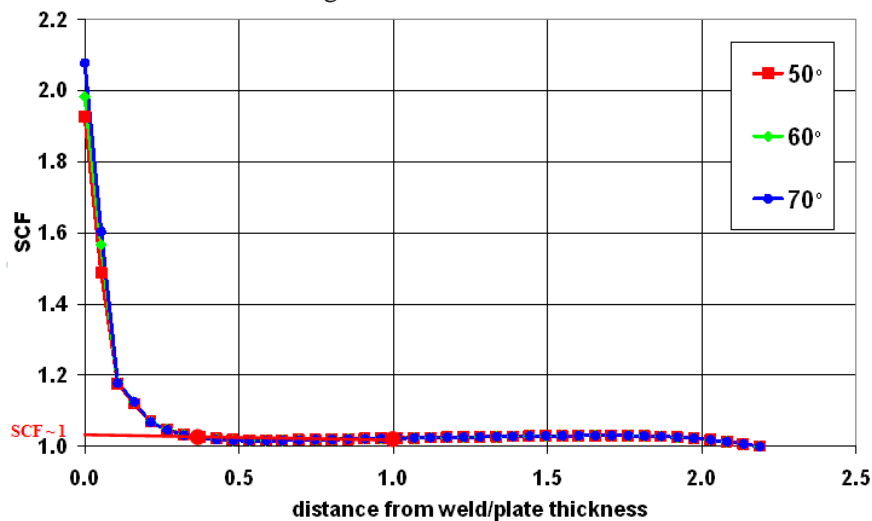
Figure 67 - Stress concentrations at the weld toe; variation of normal stress perpendicular to the weld toe with respect to the distance from the weld toe. Weld shape is extracted from the actual weld profile

There are several interesting observations from the numerical results:
- → The local stress is definitely higher than the nominal stress. The results show that the maximum local stress value at the immediate neighbourhood of the weld toe is about twice the nominal stress value (i.e. $SCF_{max} \sim 2$).
- → The sensitivity of the local stress on the value of the weld angle is not very important, for the range of values used in our parametric study (50°-70°).
- → The increase of local stress occurs in a relatively small area at the vicinity of the weld toe.

The last observation is important. It is reminded that, according to all extrapolation methodologies, the hot spot stress is calculated through extrapolation from stresses at two points in front of weld toe.

2.3.6.4 Girth welded pipe connections

In order to get the main geometrical characteristics of the weld profile affecting fatigue strength, this last one was measured by macroscopic evaluation on samples for FCAW joints and by mean of a 3D laser scan device for LH joints.

In the following details about geometrical characterization and Hot Spot analysis performed are reported.

2.3.6.4.1 *Geometrical characterization*

In order to get information about the weld profile an on the main geometrical features affecting fatigue performances, for girth welded pipes a number of samples devoted to fatigue program were measured.

According to the facilities available in each Company two different method were employed for FCAW joints and for LH ones.

In particular for FCAW joints the measurements have been performed by an analysis on macro photos of samples taken from longitudinal sections.

For LH joints the weld profile was measured on longitudinal full thickness strips obtained from the butt weld pipes, by means of a high precision 3D laser device (1mm x 1mm grid, vertical precision 0.01 mm). The output of the analysis is a scanned 3D surface available in *.dwg* format that allows to measure the geometrical features of interest.

Measurements have been performed on both the weld cap and root; only in the case of X70 LH welds the weld root pass performed by laser hybrid showed not a significant profile therefore measurements have been performed only on the weld cap.

The main characteristics of the weld profile measured are described in Figure 68.

Label	Explanation
A1 to A4	**A**ngles of attack, in the toe of the weld, in degrees
R1 to R4	**R**adius between weld and base metal
FR	**F**ace **R**einforcement of the weld, in mm
RR	**R**oot **R**einforcement of the weld, in mm
T	**T**hickness of base metal measured (in mm) on the magnified prints; it is used to determine the exact magnification for each macro and to correct the final real values
MISAL	**Misal**ignement of welded joint
FW	**F**ace **W**idth, in mm
RW	**R**oot **W**idth, in mm
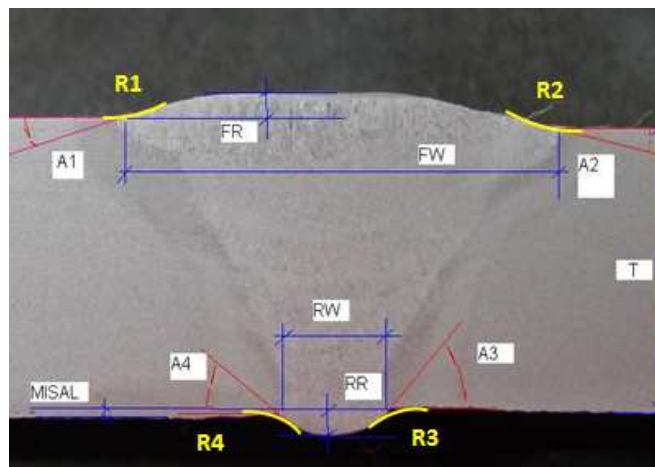
Figure 68 - Specification of measurements

In the following the main results obtained for the examined welded joints are reported.

In Table 22 and Table 23 the main results obtained for X100 and X70 FCAW welded joints are reported.

It is detectable that the weld profile in the weld cap is quite asymmetrical in particular as regards the radius between weld and base metal showing a high value of the standard deviation. It should be noted that the measurements performed highlighted that the weld cap seems not a critical point for fatigue of the selected joints as high values of the radius and limited values of the angles have been encountered.

The measurements put in evidence the worst features of the weld root characterised by higher angles and lower radius than the weld toe, meaning that the weld root is the real critical points of the whole welded joint.

	#1	#2	#3	#4	#5	#6	#7	#8	AVG.	ST.DEV.	AVG+2ST.DEV-
A1 [°]	21	26	31	22	25	33	30	28	27	4.3	35.6
A2 [°]	12	23	22	13	11	12	25	22	17.5	6.0	29.5
A3 [°]	32	35	33	33	41	20	26	27	30.9	6.4	43.7
A4 [°]	37	23	49	37	37	26	28	42	34.9	8.7	52.3
R1 [mm]	3.9	7.13	6.03	7.98	5.22	4.07	4.36	6.62	5.66	1.52	8.70
R2 [mm]	19.36	4.15	7.16	15.42	54.81	14.82	9.89	5.3	16.36	16.43	49.21
R3 [mm]	4.97	4.07	3.98	5.1	4.71	5.64	4.89	5.16	4.82	0.56	5.93
R4 [mm]	3.6	6.41	4.51	5.33	6.95	7.85	5.38	4.58	5.58	1.41	8.39
FW [mm]	31.4	27.9	29.7	28.1	28.2	29.6	31.1	28.4	29.3	1.4	32.1
FR [mm]	3.2	2.7	3.6	2.8	3.4	2.8	3.5	2.6	3.1	0.4	3.9
RW [mm]	8.8	9.5	6.6	7.4	6.8	7.3	6.6	7.6	7.6	1.0	9.6
RR [mm]	1.6	1.9	2.0	1.7	1.7	1.1	1.6	2.2	1.7	0.3	2.3
MISAL [mm]	0.0	0.0	0.0	0.3	0.3	0.0	0.0	0.8	0.2	0.3	0.8

Table 22 - Geometrical characterisation for X100 FCAW welded joints

	#1	#2	#3	#4	#5	#6	#7	#8	#9	#10	AVG	ST. DEV.	AVG +2ST DEV
A1 [°]	13	12	18	16	12	22	19	14	11	19	15.5	3.7	22.9
A2 [°]	4	6	11	10	4	8	13	3	4	9	7.2	3.5	14.2
A3 [°]	44	40	35	48	38	25	55	40	43	28	39.6	8.9	57.4
A4 [°]	45	38	33	32	30	17	38	48	49	28	35.8	9.9	55.6
R1 [mm]	15.63	20.77	15.02	28.41	14.52	15.67	5.64	23.14	10.82	7.7	15.63	6.94	29.61
R2 [mm]	15.31	42.33	10.75	29.99	33.85	3.68	16.35	28.08	64.7	21.98	26.70	17.62	61.95
R3 [mm]	4.51	5.25	5.5	4.25	4.52	4.00	2.76	3.32	4.33	4.01	4.25	0.81	5.87
R4 [mm]	4.05	5.75	2.95	4.31	4.56	3.57	3.48	4.27	4.12	3.86	4.09	0.75	5.59
FW [mm]	23.3	23.6	23.8	22.2	22.4	24.6	23.3	23.7	25.8	23.3	23.6	1.0	25.6
FR [mm]	1.5	1.6	2.2	1.4	1.5	1.9	2.7	1.5	1.6	2.0	1.8	0.4	2.6
RW [mm]	4.9	6.7	3.8	5.9	5.7	3.3	3.9	5.0	4.2	3.2	4.7	1.2	7.1
RR [mm]	2.0	2.7	0.8	1.2	1.5	0.8	1.0	1.5	1.2	0.7	1.3	0.6	2.5
MISAL [mm]	0.0	0.5	0.0	0.7	0.0	0.7	0.4	0.0	0.5	0.5	0.3	0.3	0.9

Table 23 - Geometrical characterisation for X70 FCAW welded joints

In Table 24 and Table 25 are reported the results from geometrical measurements on the LH welded joints respectively for X100 and X70. As above mentioned as regards X70 LH, the weld root pass showed not a significant profile therefore measurements have been performed only on the weld cap.

It should be noted that when laser Hybrid is applied in the root pass, the root geometry results more promising for fatigue performances and a favorable geometry is detectable in general with quite low values of the angles of attack to the weld root and for X70 no discontinuities are recorded in the weld root area as the profile is substantially flat (see Figure 69).

	#1	#2	#3	#4	#5	#6	#7	#8	#9	#10	AVG.	ST.DEV.	AVG+2 ST.DEV
A1 [°]	13.7	14.6	14.8	10.1	15.5	11.5	11.2	16.0	19.1	12.6	13.9	2.7	19.3
R1 [mm]	2.5	4.4	3.8	14.7	4.8	5.1	6.1	4.0	2.8	2.8	5.1	3.6	12.2
A2 [°]	15.7	11.2	16.8	12.1	13.6	15.2	10.0	9.9	15.1	13.5	13.3	2.4	18.2
R2 [mm]	3.9	6.9	6.3	8.2	4.6	9.1	18.4	3.9	4.7	3.5	7.0	4.5	15.9
A3 [°]	13.8	-	10.3	8.5	15.3	14.1	17.9	13.5	18.2	14.4	14.0	3.1	20.3
R3 [mm]	5.6	-	6.6	12.8	2.4	2.4	3.9	2.9	2.9	7.4	5.2	3.4	12.0
A4 [°]	11.1	23.8	27.2	18.7	13.5	11.3	13.1	9.1	23.4	16.4	16.8	6.2	29.3
R4 [mm]	6.7	2.9	2.4	3.5	2.7	6.2	3.7	7.4	1.8	2.6	4.0	2.0	8.0
FW [mm]	16.0	16.3	15.5	12.5	15.0	15.3	14.8	13.5	13.5	13.00	14.5	1.3	17.2
FR [mm]	1.9	1.8	2.0	1.1	1.6	1.3	1.2	1.1	1.5	1.3	1.5	0.3	2.1
RW [mm]	2.5	-	3.3	3.5	3.0	2.5	2.9	2.5	3.0	3.8	3.00	0.47	3.93
RR [mm]	0.3	-	0.4	0.3	0.3	0.2	0.4	0.3	0.4	0.4	0.33	0.07	0.47
MISAL [mm]	0.1	0.4	0.3	0.2	0.0	0.1	0.1	0.2	0.2	0.1	0.2	0.1	0.4

Table 24 – Geometrical factors for the LH welds on X100

	#1	#2	#3	#4	#5	#6	#7	#8	#9	#10	AVG.	ST.DEV.	AVG. +2 ST.DEV
A1 [°]	13.0	16.0	16.0	18.0	15.0	9.2	10.3	8.9	13.9	18.7	13.9	3.5	20.9
R1 [mm]	6.0	9.0	11.0	9.0	9.0	4.7	7.3	8.2	7.6	10.1	8.2	1.9	11.9
A2 [°]	16.0	14.0	16.0	14.0	17.0	13.1	6.4	7.9	11.5	11.9	12.8	3.5	19.7
R2 [mm]	6.0	6.0	5.0	7.0	5.0	3.7	6.5	12.8	5.6	6.1	6.4	2.4	11.2
FW [mm]	10.0	10.0	10.0	10.0	10.0	11.0	11.0	10.5	9.5	11.8	10.4	0.7	11.8
FR [mm]	0.9	1.0	1.2	1.1	1.0	1.1	1.2	1.1	1.1	1.6	1.1	0.2	1.5
MISAL [mm]	0	0.1	0.0	0.1	0.3	0.0	0.3	0.1	0.2	0.1	0.1	0.1	0.3

Table 25 – Geometrical factors for the LH welds on X70

X100 LH **-** 3D External surface – Weld cap	X100 LH **-** 3D Internal surface – Weld root
X70 LH - 3D External surface – Weld cap	X70 LH - 3D Internal surface – Weld root
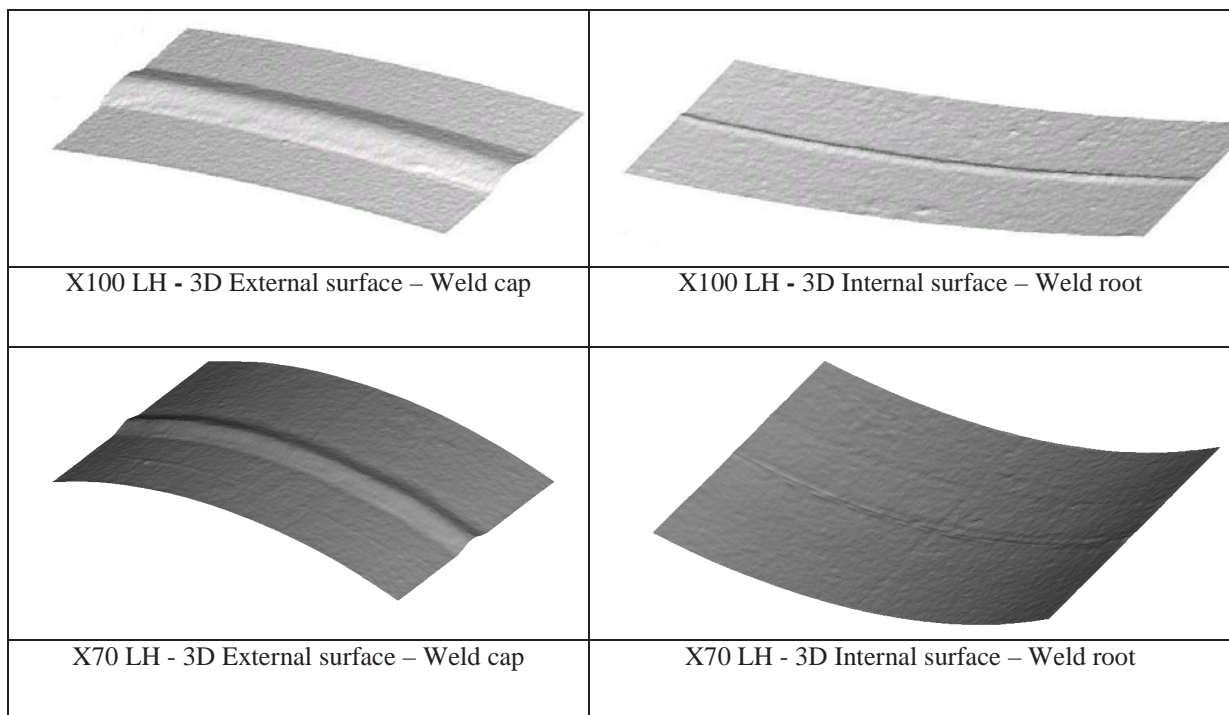
Figure 69 – Geometrical features for LH joints

2.3.6.4.2   Numerical simulations on pipes

The same numerical tools adopted for plates have been also employed to examine stress concentrations at the vicinity of pipe-to-pipe welds. A typical geometry with misalignment is shown schematically in Figure 70.
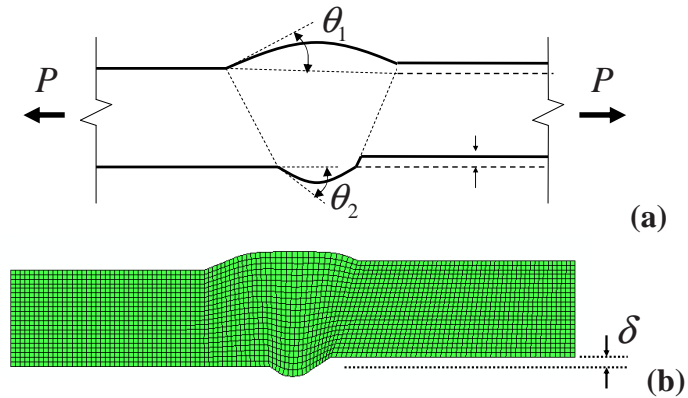
Figure 70 - Weld profile with misalignment discretized with plane strain finite elements.

The boundary conditions employed in the numerical procedure are analogous to the ones imposed in the experiments, so that pure axial tension conditions apply. For that reason, the load is applied uniformly in the one side of the specimen whereas the other side is fixed. The weld was simulated considering the typical geometry of FCAW joints. The results are reported in Figure 71 where it is detectable that the SCF is quite small and around 1.16.
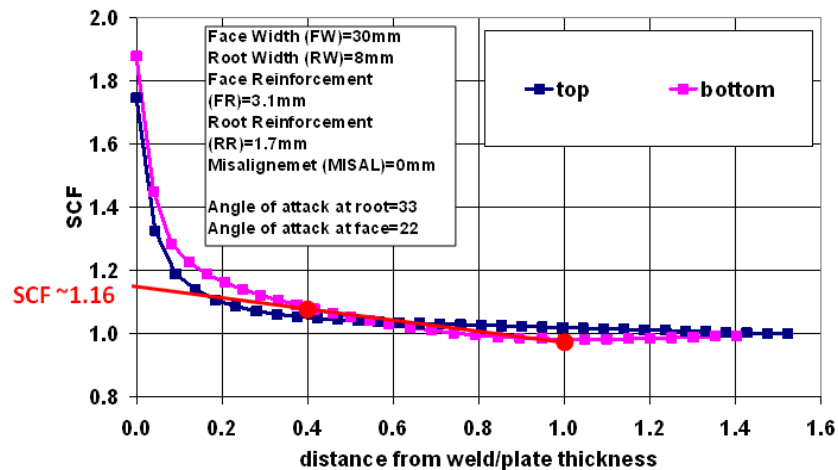
Figure 71 – FCAW welds - Values of stress concentration with respect to the distance from the weld;

Similar analysis was performed for LH welds and the results are shown in Figure 72. The SCF results no significantly above 1 meaning that the Hot Spot Stress is very close to the nominal stress.
This confirms the better fatigue performances of the LH joints.
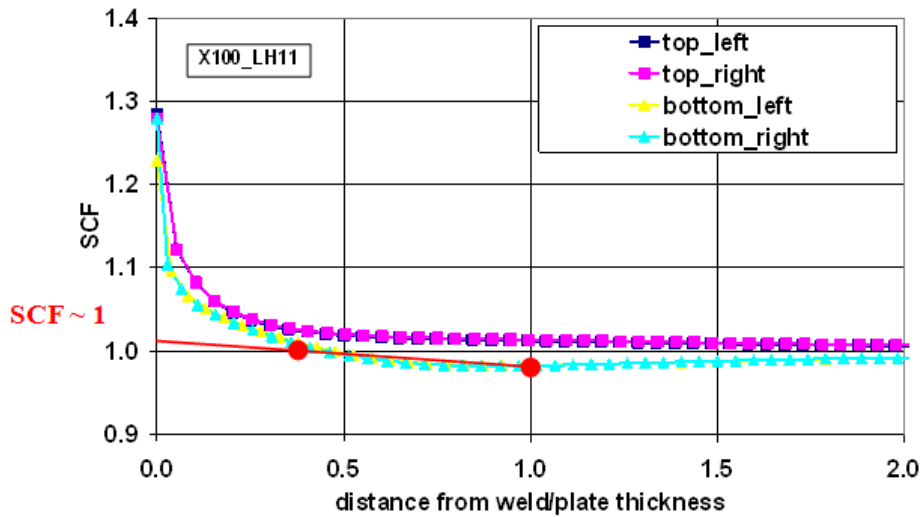
Figure 72 - Variation of local stress with respect to the distance from the weld toe.

The effect of misalignment in FCAW joints was investigated. For the purposes of this study misalignments typical of the welded joints employed was considered i.e 0.4 and 0.8 mm. The results are shown in Figure 73. As detectable the change in SCF value is not remarkable.
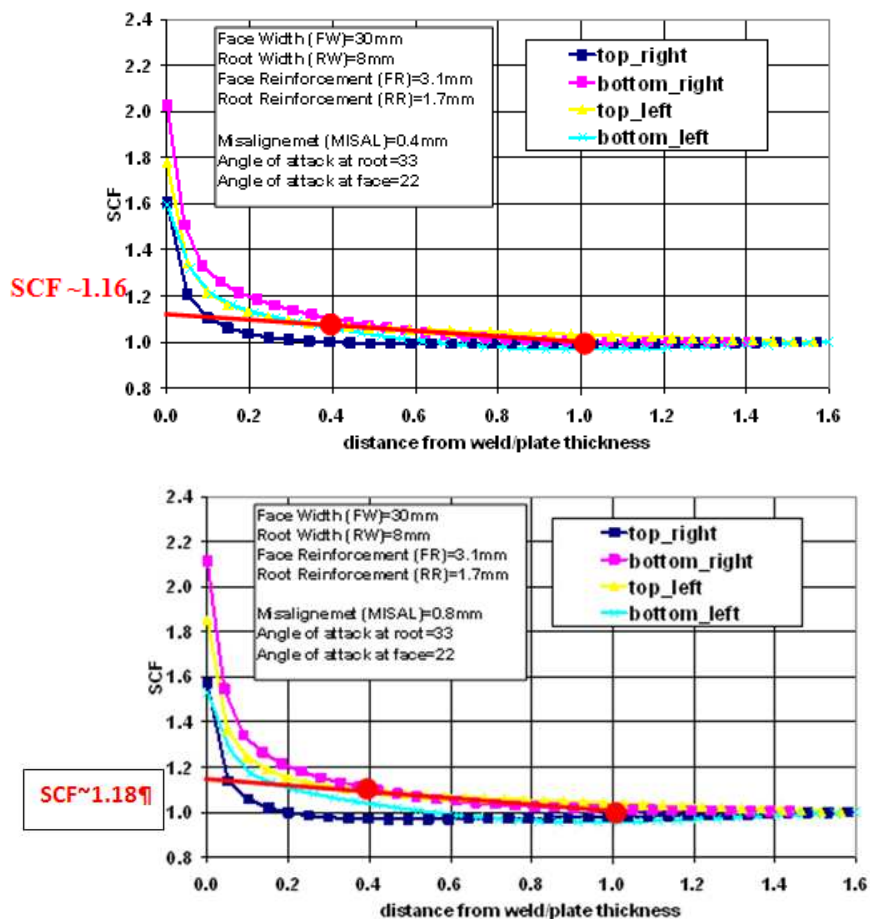
Figure 73 - Values of stress concentration with respect to the distance from the weld; misalignment equal to 0.4 mm and 0.8 mm.

According to the results of FEM analysis leading to the definition of the stress concentration factors the Hot Spot stress range has been calculated for the experimental results. In Figure 74 the results are shown together with a tentative Hot Spot S-N mean and design curve for the joints selected for the project.
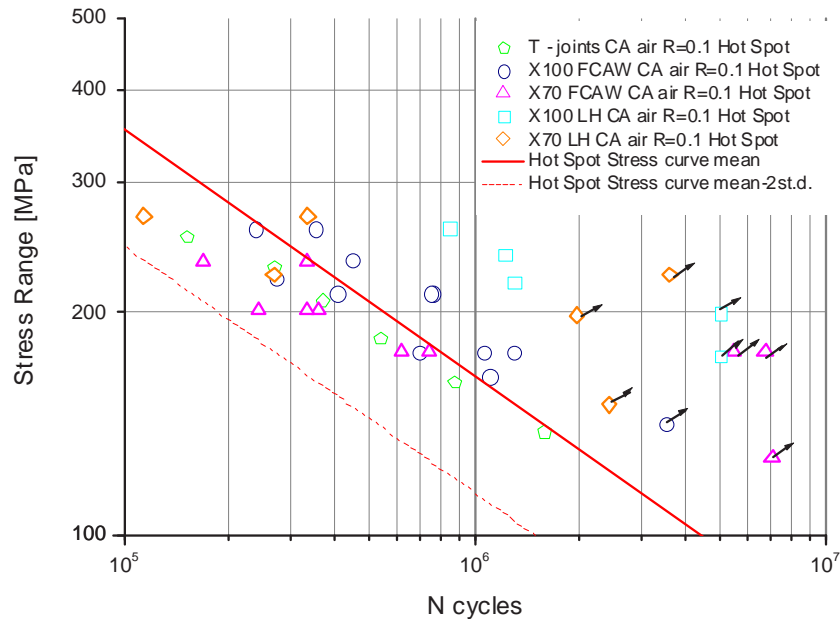
Figure 74 –Hot Spot stress vs N

The parameters for the local S- N mean curve are reported in Table 27.

K	3
Log C₀	12.65
Log σ	0.239

Table 26 - Parameters for the Hot Spot S- N mean curve

As further attempt, only for girth welded pipes, the local stress was calculated by the notch factor Kt.

$$K_t = \frac{\sigma_{local}}{\sigma_{nominal}}$$

The stress concentration factor was evaluated according the below reported equation starting from the geometrical measurements of the weld profile, in correspondence of the weld root where fatigue failure was expected.

$$K_t = \left(1 + b_1 \cdot \left(\frac{t}{\rho}\right)^{b_2}\right) \cdot \left(1 + \left(a_0 + a_1 \cdot \sin(\theta) + a_2 \cdot \sin^2(\theta) + a_3 \cdot \sin^3(\theta)\right) \cdot \left(\frac{t}{\rho}\right)^{l_1 + l_2 \cdot \sin(\theta + l_3)}\right)$$

The coefficient to be applied in the equation for the evaluation of Kt were derived from Table 27.

Coefficients / load	a₀	a₁	a₂	a₃	b₁	b₂	l₁	l₂	I₃
Normal load	0,169	1,503	-1,968	0,713	-0,138	0,2131	0,2491	0,3556	6,1937
Bending load	0,181	1,207	-1,737	0,689	-0,156	0,2070	0,2919	0,3491	3,2830

Table 27 - Coefficient to be used in Eq. 1

In particular for each class of girth welded joints the distribution of the Kt values was calculated. The critical Kt value corresponding to the mean + 2 standard deviations was considered as representative for each class of joints (i.e. the one for which there is the 97.7% of probability to find a lower value) as it is highly likely that fatigue crack initiates at the most unfavorable geometry. The results are reported in Table 28.

Weld class	Kt mean	Kt mean + 2 standard deviations
X100 FCAW	1.50	1.64
X70 FCAW	1.54	1.66
X100 LH	1.38	1.36

Table 28 – Notch factor values for the selected classes of joints

For X70 LH it was not possible to calculate the Kt as the root resulted almost flat, so that geometrical measurements of the profile were not possible.
It is evident that the FCAW joints, as expected, shows similar Kt values while a lower value is encountered for the LH joints due to the high quality of the root pass.
The resulting local stress was calculated as

$$\sigma_{local} = K_t * \sigma_{no\min al}$$

In Figure 75 the results are reported together with the proposed S-N local mean and design curve obtainable from the experimental results.
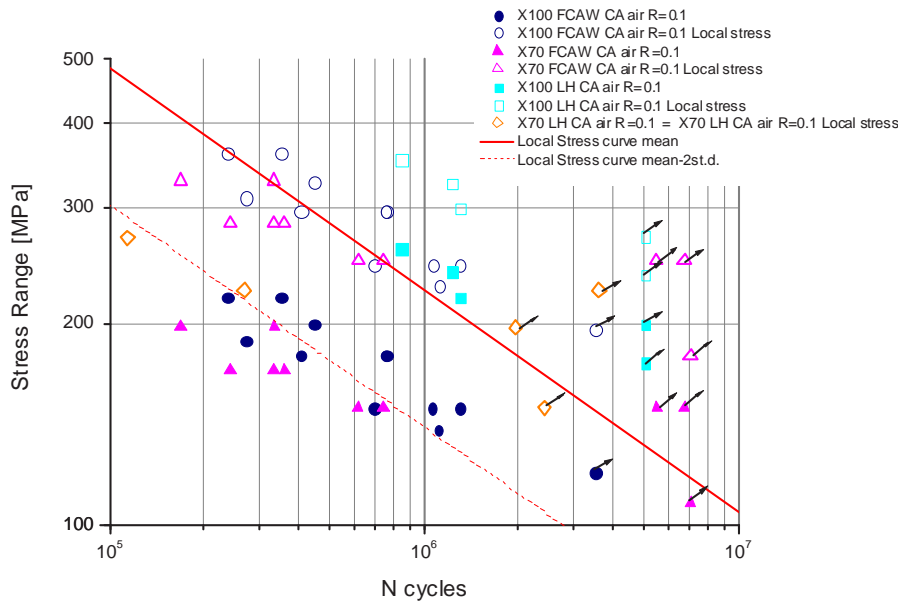
Figure 75 - Comparison between Nominal and Local stress vs N

The parameters for the local S- N mean curve are reported in Table 29

K	3
Log C$_0$	13.130
Log σ	0.272

Table 29 - Parameters for the local S- N mean curve

61

2.3.6.5 Conclusion of WP6

Hot Spot Method was applied both at T joints from plates and at girth welds from pipes.
It was highlighted that for plates the Hot Spot Stress coincides with the nominal stress.
As regards pipes main outcome is that for FCAW joints a SCF = 1.16 was calculated while for LH joints the SCF results close to 1. This is a further confirmation that Laser Hybrid performed at the root pass improves the geometry at the weld root increasing fatigue performances of the welds.
As further attempts for girth welded pipes local approach was applied on the basis of the results collected in the activity of geometrical characterisation of the weld profile.
As expected, the results highlighted that LH welds are characterised by a lower value of Kt than FCAW joints.
On the basis of these results a tentative mean S- N curve in terms of local stress was drawn.

2.3.7 WP7: Proposal for design criteria of light welded structures or components for offshore applications

The experimental results obtained in the present work were analyzed in order to supply information to be taken into account in future Standards proposal or upgrades, to properly include the high strength/high quality steel welded joints in the fatigue design Standards.

Main aims of the analysis were the followings:

→ To verify and when possible quantify the conservativeness of the design S-N curves recommended by the main Standards accounting for fatigue in the offshore field when high grade steels are intended to be used.

→ To assess the effect of different loading conditions (e.g. high R or σ average values) and of environment (sea water and cathodic protection) which are representative of real in-service behavior for the high grade welded joints considered.

→ To assess the correspondence and the eventual conservativeness of the cumulative fatigue damage limit values recommended in fatigue design codes for the high strength welded joints under investigation.

2.3.7.1 Fatigue performances with respect to the main standards

Among the three Standards selected in WP1, in this WP it was decided to make reference to the BS 7608. Even though it is a quite old Standard it is definitely in line with other codes available and reviewed in the current project as the design curves and main design criteria are very similar, but should be considered particularly valuable as it is the only Standard giving the mean curve and the standard deviations values related to the S-N design curves proposed, allowing a direct comparison with the experimental results and the information required for a designer to select an appropriate nominal probability of survival (i.e. standard deviations values).
This aspect is considered so relevant that this is the Standard commonly used by offshore contractors in fatigue assessment of the girth welded pipes.

As concerns design in seawater the BS7608 recommends to use the same curves as in air for fully protected joints but it states that this is not proven for steels with σ_y>400 MPa. Therefore, for the final analysis of results the curve suggested by DNV was considered.

As regards T joints from plates destined to the renewable applications field in Figure 76 the results obtained in WP3 are reported, highlighting that The S-N curve proposed by the BS Standard results quite conservative with respect to the experimental results that shows a good fatigue performance being all above the design and the mean curve.
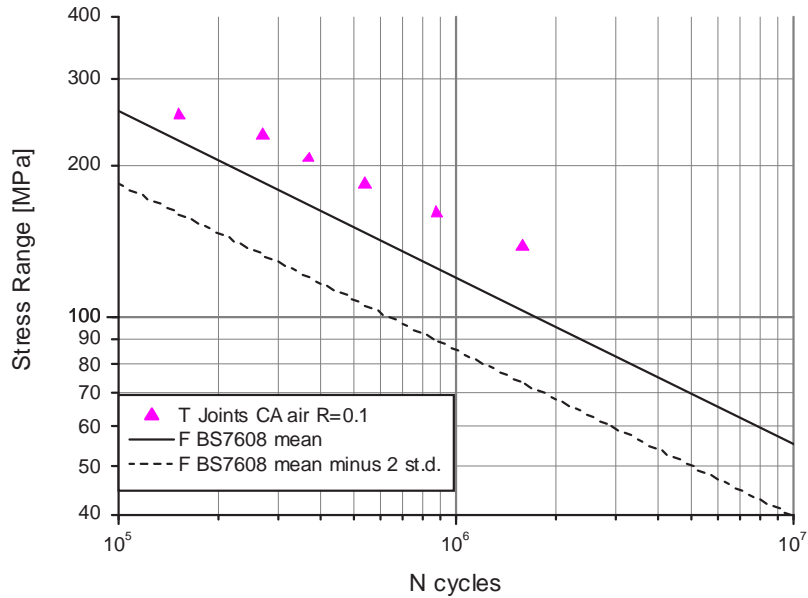
Figure 76 – T-Joints from plates **-** Fatigue performances in air compared with the SN curve proposed by the BS Standard

In Figure 77 the results obtained from the fatigue tests in air performed at R=0.1 on butt joints from girth welded pipes are summarized and compared with the S-N curve proposed in the BS Standard in terms of mean and design curve.
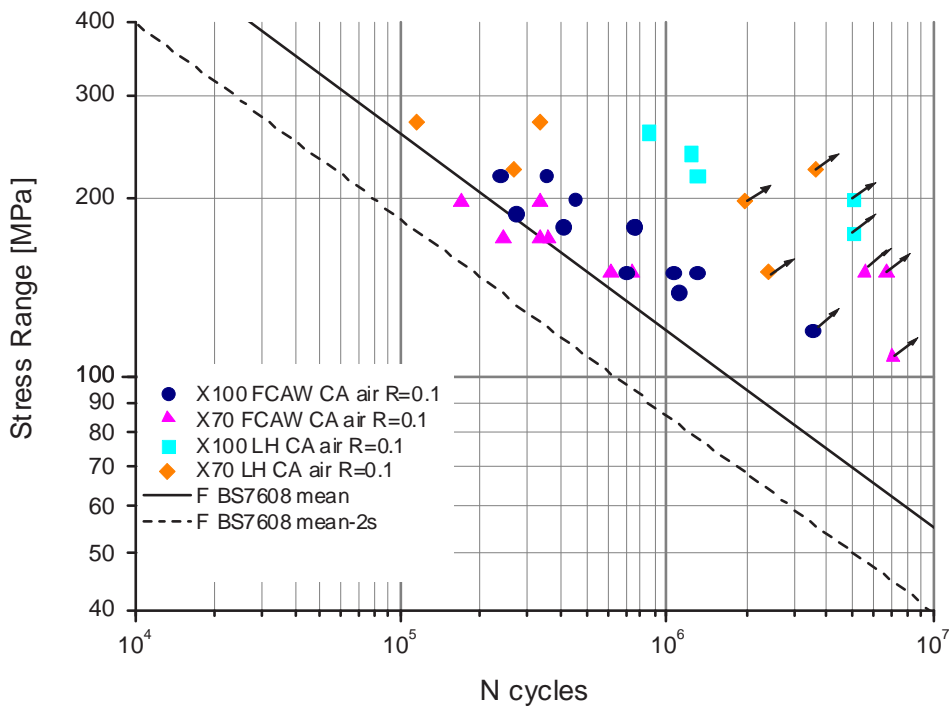
Figure 77 – -Samples from girth welded pipes **-** Fatigue performances in air compared with the "F" SN curve proposed by the BS Standard

As noticed for T joints from plates, the S-N curve recommended by BS results conservative generally for all the selected joints. This is more evident when high grades are welded by the innovative welding technique i.e LH performed at the weld root that shows very promising fatigue performances.

63

The experimental results were compared with the several S-N curves proposed in the BS standard for different quality of the weld (see Figure 78 where the mean curves are reported in order to allow the comparison with the tests results).
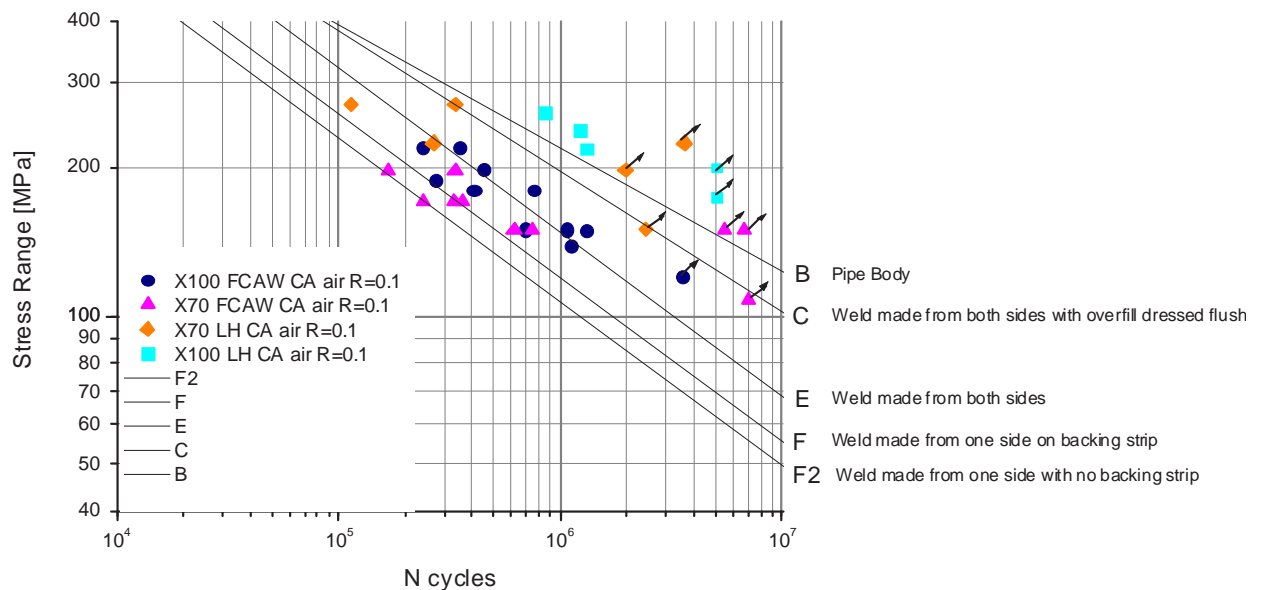
Figure 78 – Samples from girth welded pipes - Fatigue performances in air compared with the mean SN curves proposed by the BS Standard

Generally the results obtained from tests on FCAW joints are between the F and E curve meaning that if the quality of the welded joint is good there is a margin of improvement. It should be noticed that for LH welded joints the fatigue performances are particularly good so that the fatigue strength is close to the one of a particularly good weld that is weld made from both sides with overfill dressed flush, corresponding to the curve C.

2.3.7.2 Assessment of the influence of loading conditions and of the environment

The effect of different loading conditions (e.g. high R or σ average values) and of environment (sea water and cathodic protection) representative of real in-service behavior has been evaluated for the high grade welded joints considered.

In Figure 79 are shown the results of all the selected welded joints,(T joints from plates, X100 FCAW, X70 FCAW, X70 LH) tested in air at R=0.5, compared with the mean and the design curves recommended by BS code.

The fatigue performances of the selected welded joints are still good in comparison with the reference curve suggested by BS also when loading condition similar to in service ones are applied, also if a slight decrease in fatigue strength is noticeable. It is remarkable that also in this case the LH joints show an improved behavior.
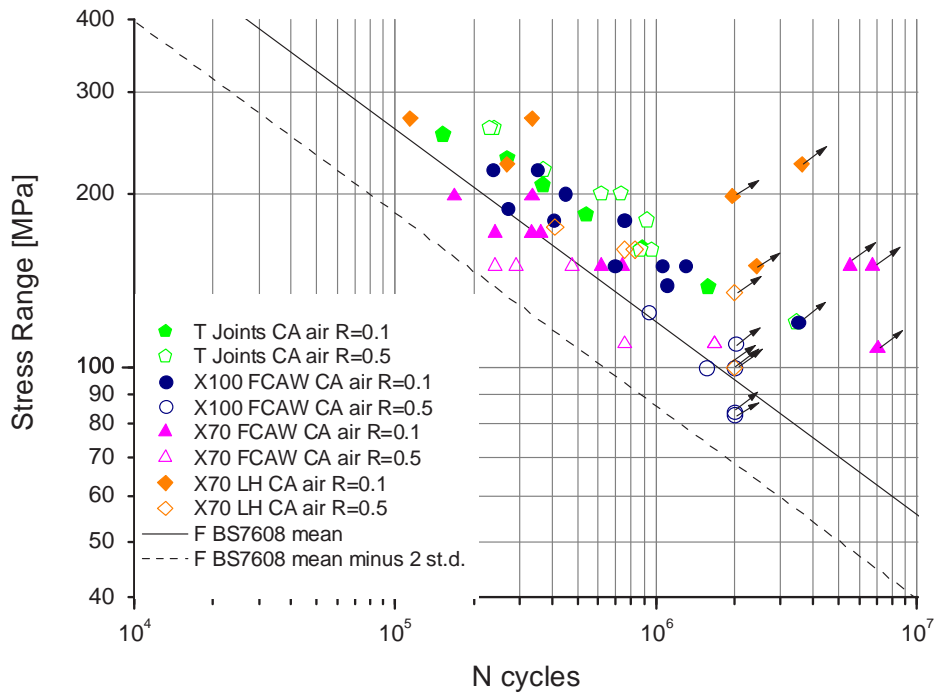
Figure 79 – Experimental results in air R=0.1 and R=0.5

In Figure 80 are shown the results from tests in seawater with cathodic protection compared with the relevant design curve from DNV RP C203.
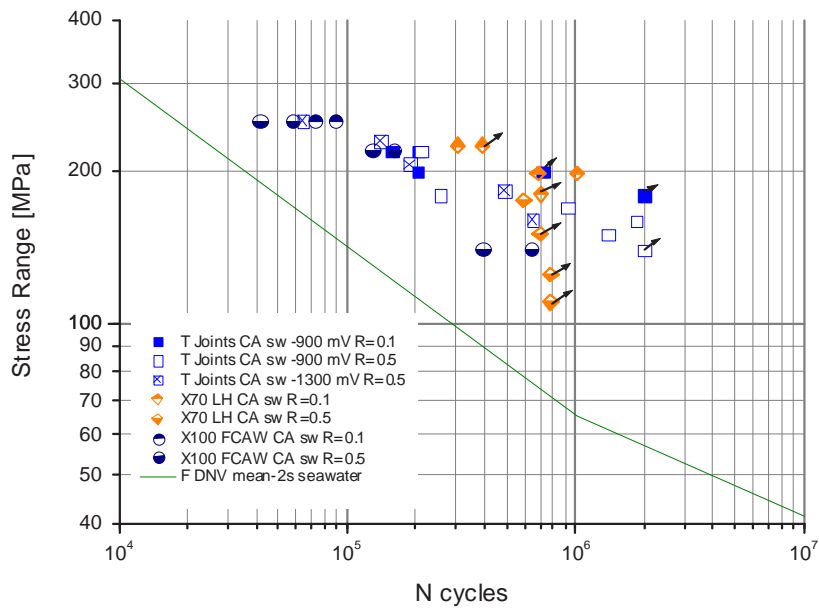
Figure 80 – Experimental results in seawater with cathodic protection R=0.1 and R=0.5

Generally it is noticeable that the high steel grades joints maintain a good fatigue behavior also in sweater + cathodic protection that is in an environment with high H_2 content and the risk of hydrogen embrittlement is present. It should be noticed that also in seawater LH welds show a very promising behavior.

2.3.7.3 Assessment of fatigue performances at variable amplitude loading

As noticed in Figure 81 also in this case all the obtained results are conservative with respect to the S-N design curves in the selected Standard.
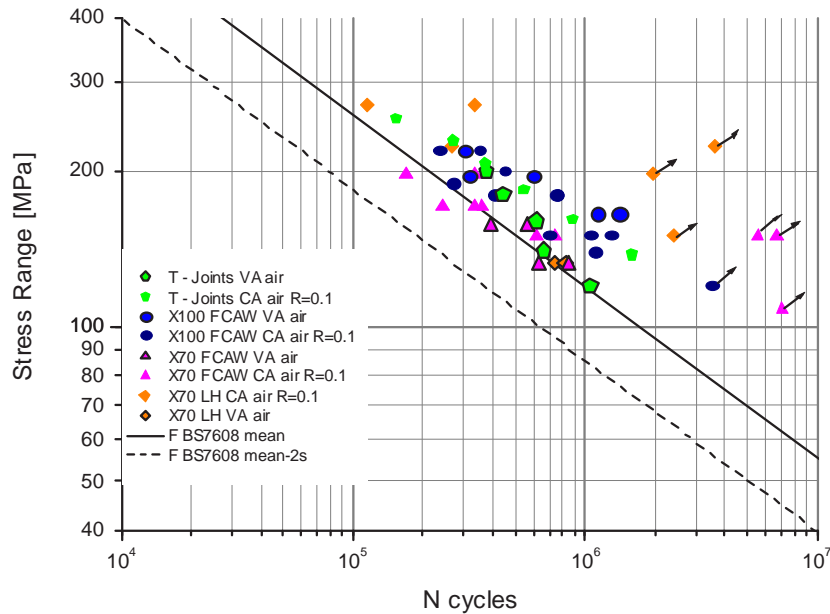
Figure 81 – Experimental results at variable amplitude loading

In order to verify and quantify the conservativeness of the standards, as case study, the real case of the design of a girth welded riser connected to a semi submersible platform located in Gulf of Mexico was studied.

Basing on the tests results obtained in WP4, the accumulated damage has been calculated as described in Figure 82.

$$D = \sum_{i=1}^{k} \frac{n_i}{N_i}$$

n_i = number of occurrences at a fixed stress range drawn from the load spectrum;

N_i = number of cycles to failure at a fixed stress range drawn from the S-N curve.
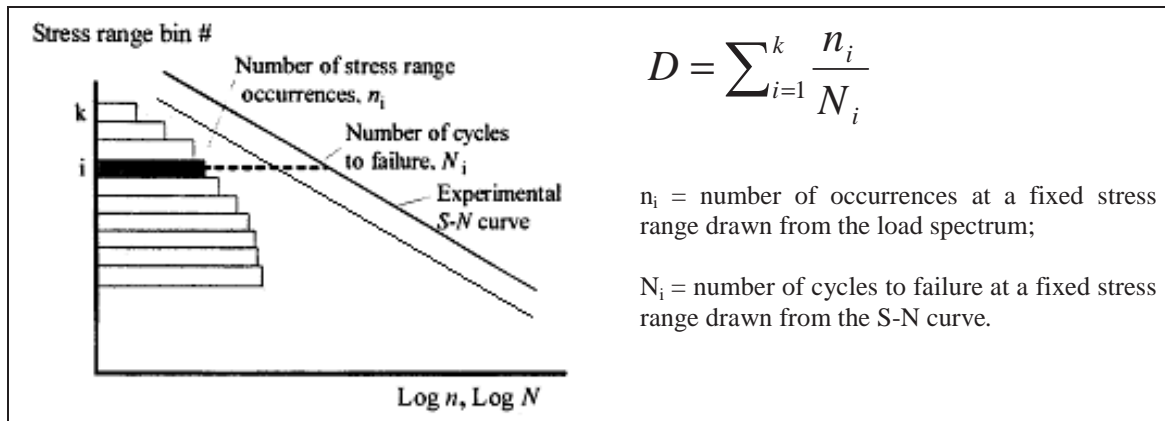
Figure 82 – Calculation of the accumulated fatigue damage

As reference for the critical damage values, the DNV OS-F201 and DNV RP-F204 [19], [20], specific for risers, were chosen.

During design the fatigue criterion to be satisfied is:

D_{fat}*DFF ≤ 1.0

where:

D_{fat} = Accumulated fatigue damage calculated according to Palmgren Miner rule
DFF = Design fatigue factor

Standards consider different Design Fatigue Factors, reported in Table 30 according to the safety class, based on potential failure consequences.

Safety class	Low	Normal	High
DFF	3.0	6.0	10.0

Table 30 - Design Fatigue Factors DFF

Fatigue damage should be calculated according to the appropriate mean minus two-standard deviations design S-N curve proposed in the DNV-RP-C203.

The damage caused to the selected welded joints during variable amplitude fatigue tests was evaluated and compared with the limit values given by:

$D_{fat} \leq 1.0/ DFF$

In Figure 83 the results are shown in comparison with the limit values; in particular are reported the highest value allowed by the DNV OS-F201 and DNV RP-F204 and the value D=1 taken as reference of the traditional Miner Rule.

All the results stay above the highest value of damage recommended by the selected codes (i. e. D=0.33) and even above D=1. This highlights that the Standards result to be excessively conservative in assessing the fatigue performance of a product in loading conditions close to the in service ones.
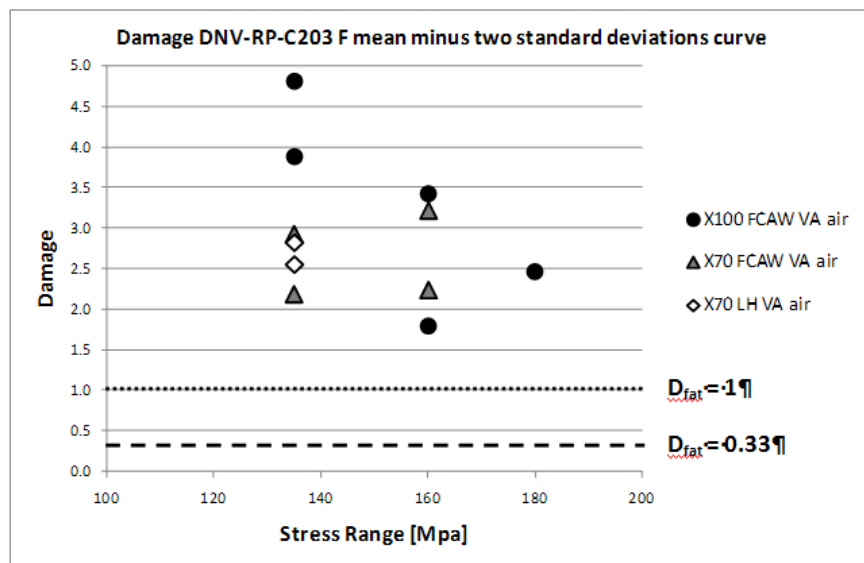
Figure 83 – Damage calculated according to DNV-RP-C203 F S-N design curve

Finally starting from the S-N design curve, and applying the selected load spectrum used in the testing activity, the number of cycles necessary to reach the limit D value suggested in the DNV standard was evaluated.

As detectable from Figure 84 to Figure 86 the limit damage values recommended in the Standards corresponds to a number of cycles significantly lower than the number of cycles leading to failure in experimental tests.
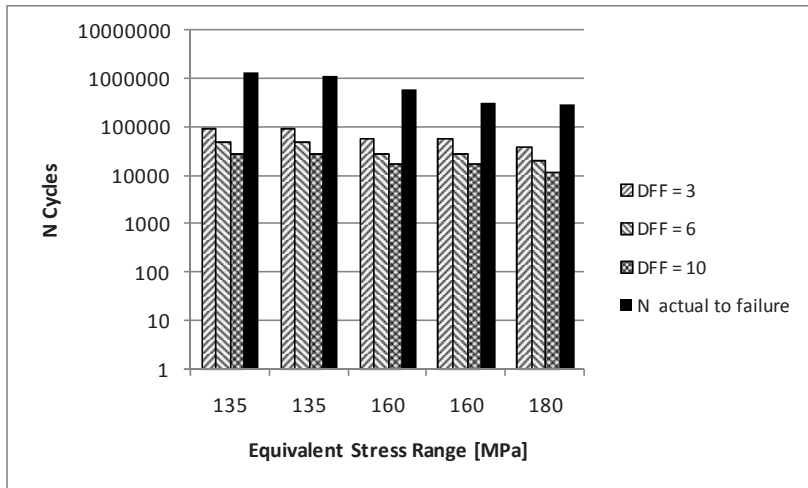
Figure 84 - Damage calculation results on X100 FCAW joints
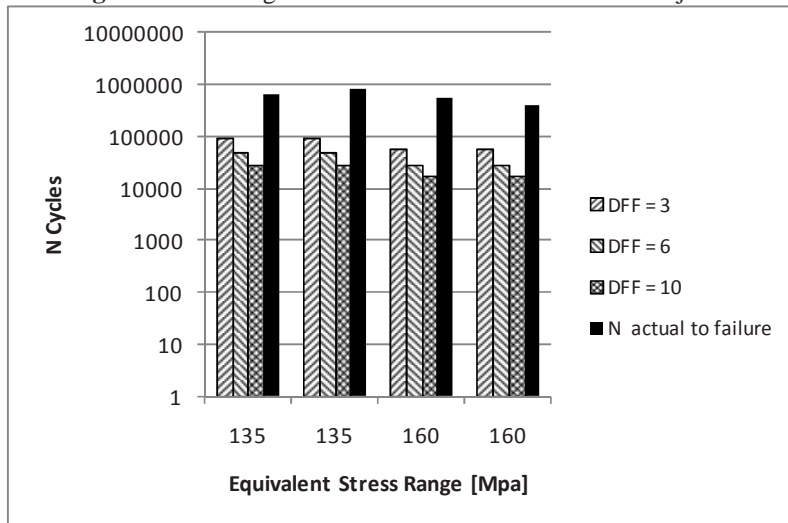
Figure 85 - Damage calculation results on X70 FCAW joints
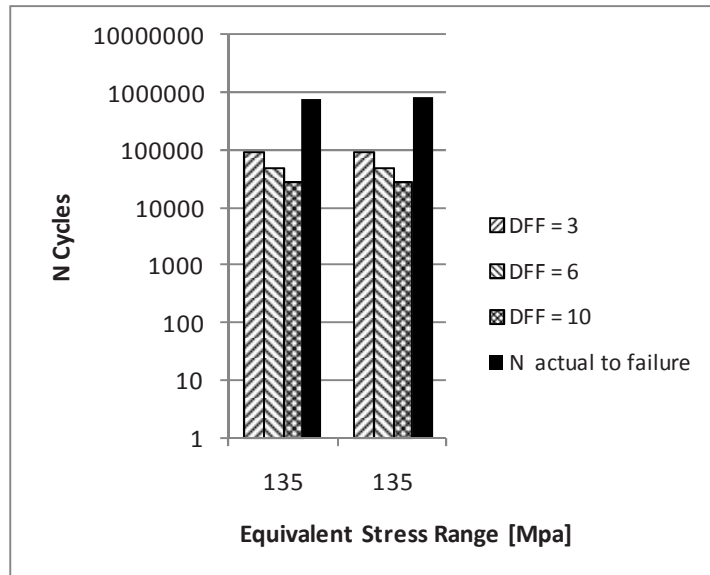
Figure 86 - Damage calculation results on X70 LH joints

2.3.7.4 Conclusion of WP7

All the obtained experimental results have been collected and critically analyzed.

The first outcome that should be highlighted is that the design curve recommended by the BS standard results conservative generally for all the selected joints. This is a clear input to reconsider the design curves in the standards when high steel grades together with improved and innovative welding techniques are planned to be used.

Laser Hybrid welding technologies when employed in the root pass results very promising in improving the fatigue performances of the selected joints. In fact the fatigue performances of LH welded joints are particularly good so that the fatigue strength is close to the one of a particularly good weld that is weld made from both sides with overfill dressed flush, corresponding to the curve C.

The fatigue performances of the selected welded joints are still good in comparison with the reference curve suggested by BS also when loading condition similar to in service ones are applied, also if a slight decrease in fatigue strength is noticeable. It is remarkable that also in this case the LH joints show an improved behavior.

Generally it is noticeable that the high steel grades joints maintain a good fatigue behavior also in seawater + cathodic protection that is in an environment with high H_2 content and the risk of hydrogen embrittlement is present. It should be noticed that also in seawater LH welds show a very promising behavior.

The case study about the design of a girth welded riser connected to a semi submersible platform located in Gulf of Mexico put in evidence that the Standards in force to the offshore area can results conservative also as concerns the limit value of the accumulated fatigue damage when loading conditions similar to the in service ones are applied.

2.4 Conclusions

At the end of this project the following conclusions can be derived.

→ The activity carried out in the present project demonstrates the conservativeness of the current Standards in force in the offshore area in predicting the fatigue performances of welded joints when high steel grades together with improved and innovative welding techniques are used, in particular for the girth welds on pipes made from one side usually penalized by the codes.

→ In particular the conservativeness of the Standards was highlighted both in terms of S-N design curves and in terms of limit values for the accumulated fatigue damage when variable loading conditions similar to the in service ones are applied. In this respect the case study simulating the design of a girth welded riser connected to a semi submersible platform located in Gulf of Mexico showed that the limit damage values recommended in the standards corresponds to a number of cycles significantly lower than the number of cycles leading to failure in experimental tests leading to an excessive penalization of the joints when high strength steel together with new welding technologies are used. Nevertheless a "good quality" of welds is a basic condition to get a notable improvement of fatigue behavior of high steel grades welded joints.

→ The beneficial effect in fatigue performances of the employ of high steel, new welding technologies and post-welding treatments has been outlined.

In particular it was highlighted what follows:

Laser Hybrid welding technology: The promising behavior in terms of fatigue strength of Laser Hybrid welding technology when applied in the root pass. In fact nevertheless this is a single side weld the fatigue performances are comparable with the ones of a double side good quality weld. This is related to the fine geometry achievable in the weld root, the most critical site for fatigue failures as put in evidence in full scale fatigue tests that showed that

a careful check of the quality of the weld in the inner of the pipe is mandatory for fatigue applications. The fine geometry of the weld root in Laser Hybrid welds was confirmed by both geometrical measurements and Hot spot analysis. Finally it should be underlined that Laser Hybrid welding is a technology currently feasible in field on the lay barge as the laser beam (either from Nd:YAG or Yb:fibre laser systems) can be delivered to the work pipes easily by a flexible optical fiber.

Ultrasonic peening: According to the number of tests performed in the frame of the current project it seems that the use of ultrasonic peening, applied on as welded FCAW joints, leads in some cases to fatigue performance even better than the Laser Hybrid welding technique applied in the root pass. As regards ultrasonic peening at the time being the technology to treat the weld root of welded pipes by this kind of treatment is not available on the market, but it could be set up and developed in a short time and become feasible if required by offshore contractors.

In the comparison between the two "techniques", it should be considered also that the post welding treatment requires additional time before laying the joint in the sea bed and this should be taken into account when considering the potential benefits achievable.

→ The welded joints investigated in the project maintain a generally good performance also in conditions similar to the in service ones that is when a high mean stress is applied and in seaweater + cathodic protection that is in an environment with high H_2 content and the risk of hydrogen embrittlement is present. It should be noticed that also in seawater LH welds show a very promising behavior.

→ S-N curves both in terms of Hot Spot stress and local stress for the joints object of the current research were outlined.

2.5   *Exploitation and impact of the research results*

The exploitation and impact of the results obtained in the present project can be summarized in the following points:

1.   *Upgrade the existing codes in order to properly use the high grade steel in the design of lighter steel structures achieving a good fatigue performance*. In fact, the fine fatigue performances of welded joints when higher steel grades together with improved and innovative welding (and post welding) techniques are used have been put in evidence. The results obtained highlighted the conservativeness of the S-N design curves recommended in the Standards in force to the offshore field. Information, suggestions and data have been collected in order to quantify this conservativeness for the joints considered in the project. These results can be helpful for a possible upgrade of the current Standards in order to use high strength steels for lighter structures, both for off-shore and on-shore structures.

2.   *Bring out recently available welding technique to build a steel welded structure with very good fatigue performance*. In fact, it was also highlighted the good performance of Laser Hybrid welding technology applied in the root pass, in particular when used in conjunction with very high steel grades. This aspect results very promising and also attractive not only for off-shore structures but also for the building field. In fact in a lot of applications single side welds are commonly applied but current design codes usually have a negative view of their fatigue performances for the potential poor root condition and place them in low categories in terms of S-N design curves; from here the need of designers to improve the design class of the weld by several methods as weld grinding in the root and other solutions. The laser hybrid technology could be a good solution to overcome this problem allowing to get very good fatigue performances without any additional action on the weld. Moreover Laser Hybrid, as single side weld, could be applied also in welding small diameter pipes leading to a possible employ not only for offshore and marine applications, but also in structural applications and building field.

Appendix A: Renewable applications

1 Renewable energy classification

Renewable energy technologies can be classified in many different ways. For the purpose of this report it is convenient to classify renewable energy sources according to the primary source of the energy and then according to the techniques used in capturing and handling the energy. The reviewed technologies are listed according to this classification scheme in Table 31.

1.1 Hydroelectric

Hydroelectric schemes rely upon rainfall on high ground. In large schemes water is stored behind a large dam and the water allowed to flow out of the reservoir through turbines to generate electricity. In small schemes water from a river is diverted through turbines.

1.2 Wind

Wind energy arises from variations in air pressure due to differential heating of the earth's surface by the sun. Electricity-generating turbines are generally mounted on tall towers. These towers may be based on land or on the seabed. Small turbines may be used for a variety of purposes; in particular, turbines rated at between 0.5 kW and 1.5 kW are suitable for direct mounting on residential properties. In some parts of the world it is common to use tower-mounted wind turbines to drive mechanical pumps for irrigation.

Primary source	Technique		†
Solar	Hydroelectric	Large (storage dam)	E
		Small (run-of-river)	E
	Wind	Onshore turbines	E
		Offshore turbines	E
	Wave	Surface-effect mechanisms	E
		Oscillating water column (OWC) devices	E
		Variable buoyancy devices	E
	Solar thermal	Direct heat (DHW, space heating and process heat)	H
		Passive solar design of buildings (HVAC)	H
		Solar thermal generation (including solar chimneys)	E
	Photovoltaic (PV)	Monocrystalline silicon	E
		Polycrystalline silicon	E
		Amorphous thin film	E
	Biomass	Solid fuels for direct combustion	F
		Fuels based on vegetable oil (e.g. biodiesel)	F
		Bioalcohols (biomethanol, bioethanol)	F
		Biogas (anaerobic digestion), including landfill gas	F
		Biomass gasification	F
	Ocean thermal energy conversion (OTEC)	Closed cycle	E
		Open cycle	E
Geothermal	Conventional cycle generation (high enthalpy)	Dry steam	E
		Flash steam	E
		Hot dry rock (HDR)	E
	Binary fluid cycle generation (low enthalpy)		E
	Direct heating	Low enthalpy	H
		Very low enthalpy (ground source heat pumps)	H
Tidal	Tidal barrage	Estuary	E
		Lagoon	E
	Tidal stream	Array	E
		Fence	E

Table 31 - Classification of renewable energy technologies († Key to right-most column: Form of output, E Electricity, H Heat, F Fuel)

1.3 Wave

Wave energy arises from the effect of wind blowing over long expanses of seawater. Surface effect mechanisms can be used in a variety of ways to capture energy directly from the movement of the disturbed water close to the surface, which can be communicated to a generator in a number of ways (e.g. hydraulic pumping). Oscillating water column (OWC) devices employ an open-bottomed fixed tube immersed in the water; the rise and fall of water in the tube displaces air, which then passes through a turbine (usually a 'Wells Turbine', which continues to be driven in the same direction for both directions of airflow) to generate electricity. Variable buoyancy devices (illustrated in Figure 87 below) are located well below the disturbed region of water, and rely upon differences in water pressure to compress air trapped in a 'floater', which is mounted in a fixed structure anchored to the seabed. The compression and decompression of the trapped air produces cyclic changes in the buoyancy of the floater, which then rises and falls as waves pass overhead; this motion can then be used to drive a generator.
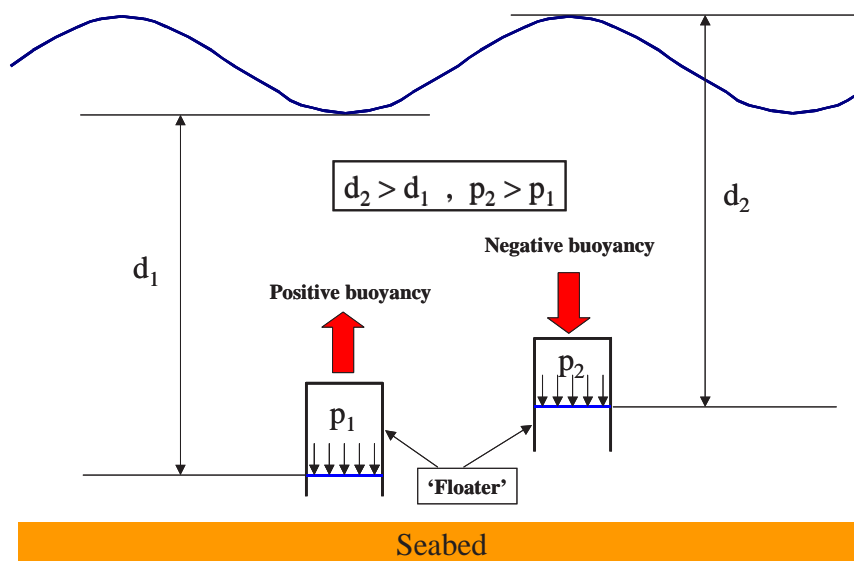
Figure 87 - Principle of variable buoyancy wave energy conversion devices

1.4 Solar thermal

Solar thermal energy can be employed in a number of ways:

→ Water heating - solar energy can be used directly (typically by circulation through a roof-mounted panel) to heat water for commercial or residential applications. This can be used directly as hot water (e.g. heated swimming pools or domestic hot water for washing), or can be used for process- or space-heating.

→ Passive solar design - commercial buildings can be designed so that solar energy is stored in the thermal mass of the building, and then exploited as part of the heating ventilation and air-conditioning (HVAC) system.

→ Solar energy can be focussed by mirrors to raise steam and drive a conventional steam turbine generator.

→ Solar chimneys - in areas where sunlight and land are plentiful, it is possible to construct a system in which air is heated in a large glazed area and forced to convect through a turbine via a tall chimney in order to generate electricity. Such systems can operate on a 24 hour basis, as the air within the glazed area continues to be warmed at night by heat stored in the ground during the day.

1.5 *Photovoltaic*

Photovoltaic systems employ semiconductor devices which generate an electric current directly from sunlight. The majority of modern photovoltaic devices use silicon semiconductors, in either monocrystalline or polycrystalline form. Monocrystalline cells suffer lower internal losses than polycrystalline cells, but are more expensive and require more energy for production. Thin film devices can be made from amorphous silicon and other materials such as cadmium telluride (CdTe) or copper indium diselenide ($CuInSe_2$), and require lower quantities of semiconductor material than crystalline devices; however, their efficiency (ratio of maximum electrical solar cell power to incident solar power) is lower than the level of 20% achieved by crystalline devices. Photovoltaic devices are rated in terms of 'maximum power point' power (i.e. power delivered at the optimum current and voltage) under standard test conditions of solar irradiance and temperature. This rated capacity is expressed in units of 'watt peak' (Wp), and is higher than the power produced under the majority of normal operating conditions. In addition to the photovoltaic components, a PV system will require a regulator (to optimise voltage and current so as to maintain maximum power delivery under varying levels of irradiance), and for AC supplies an inverter/transformer system; the cost of these 'balance-of-system' power conditioning elements can form a significant fraction of the cost of the PV system.

1.6 *Biomass*

Biomass technologies rely upon the conversion of solar energy by photosynthesis in vegetation. Vegetable matter can be used directly, or (via the food chain) in the form of animal products. Biomass materials can be used as fuels for heat, transport or the generation of electricity. A number of distinct biomass technologies exist:

→ Solid fuels such as wood or manure can be burnt directly. Such fuels can be grown specifically as 'energy crops', or waste materials (e.g. from the processing of timber) can be used as fuel. It may be noted that, as the primary source of heat in pre-industrial societies, this technology still provides the majority of the energy needs of the majority of the world population. The term 'biomass gasification' is sometimes used to refer to a form of solid fuel combustion in which a fluidised bed is used to first decompose the biomass solids by heating in the presence of oxygen; in this report, however, the term 'biomass gasification' is used to refer to the decomposition of biomass in the absence of oxygen to provide a fuel for separate use (see below).

→ Vegetable oils can be processed to produce fuels suitable for use in diesel engines – these processed fuels are known as 'trans-esterified vegetable oils' or 'biodiesels'. Such fuels can also be obtained by suitable processing of vegetable oils that have previously been used in food preparation. Biodiesel can be used in its pure form, or it can be blended in various proportions with petroleum-derived diesel fuel.

→ Alcohols can be produced by fermentation. Biomass containing sugars can be fermented directly to produce ethanol, and it is also possible to process starches or cellulosic material for fermentation. Methanol can be produced by chemical conversion of a variety of biomass materials, including forestry waste. Bioethanol and biomethanol can be used as fuels in their pure forms, or they can be blended in various proportions with petroleum products (such blends are sometimes known as 'gasohol').

→ Biogas is a mixture of methane and carbon dioxide which is produced by the anaerobic digestion of organic matter by microbes. Human or animal waste can be digested in specially designed processing vessels. Biogas is also produced by the decomposition of organic materials in municipal waste landfill sites. It is desirable to collect and burn the methane from landfill sites in any case as, in addition to presenting a potential fire/explosion hazard, methane is a more potent greenhouse gas than carbon dioxide, and in many locations this methane is now used to power electrical generators. Within the EU, Germany and the UK dominate the use of this technology.

Biomass can be broken down by heat in a restricted supply of air to produce a mixture of gases (see note above in relation to a different usage of the term 'biomass gasification'). This mixture typically includes combustible components such as hydrogen, carbon monoxide and methane. Distillates can be recovered as a mixture sometimes referred to as 'bio-oil' (which can be refined to provide liquid fuels and substitutes for petrochemical feedstocks). It is also possible to obtain charcoal as a solid fuel from such a process. By controlling the process conditions, it is possible to vary the relative proportions of solid, liquid and gaseous products.

1.7   Ocean thermal energy conversion

Ocean thermal energy conversion (OTEC) systems exploit the natural variation in seawater temperature with depth. This variation is associated with the solar energy incident on the surfaces of the oceans.

In a closed-cycle OTEC system, warm seawater from the ocean surface vaporises a working fluid, such as ammonia, flowing through a heat exchanger (evaporator). The vapour expands at moderate pressures and turns a turbine coupled to a generator that produces electricity. The vapour is then condensed in another heat exchanger (condenser) using cold seawater drawn from the ocean depths. The condensed working fluid is pumped back to the evaporator to repeat the cycle.

In an open-cycle OTEC system, warm seawater is the working fluid. The warm seawater is 'flash'-evaporated in a vacuum chamber to produce steam. The steam expands through a low-pressure turbine which drives a generator. The turbine exhaust steam is then condensed by cold seawater. If the condensed exhaust steam is kept separate from the cold seawater it can provide a supply of desalinated water.

1.8   Geothermal

Geothermal systems exploit the variation in temperature with depth below ground. Such temperature gradients can be pronounced in volcanic regions, and arise principally due to the spontaneous decay of naturally-occurring radioactive materials within the Earth's core. Existing geothermal systems use natural reservoirs of hot water, which can be tapped by wells drilled to depths of up to 2 km. High enthalpy (> 150°C) resources are suitable for conventional electrical power generation. Low enthalpy (< 150°C) resources are suitable for direct heating applications or for electricity generation using a binary cycle system.

Conventional cycle generation systems can use dry steam or wet steam. In a dry steam system, steam from the reservoir is allowed to expand through a turbine driving a generator. In a wet steam (or 'flash') system, steam and hot water from the reservoir flow into a low-pressure tank where the water flashes to steam before passing into a turbine. Dry steam fields are rarer than wet steam fields.

In binary fluid cycle generation hot water from the reservoir flows through a heat exchanger, where a working fluid evaporates. The vaporized fluid then expands through a generating turbine. Binary systems allow the use of lower temperature reservoirs for electricity generation, increasing the number of reservoirs that can be used.

In the hot dry rock (HDR) system an artificial reservoir is developed by the injection of water into impermeable rock, which fractures in a controlled manner to provide a network of channels. The creation of an HDR reservoir can involve drilling to depths of the order of 5 km. In the production phase, water is continuously circulated under pressure via an injection well, returning to the surface via one or more production wells. Hot water from the production wells can then be used to raise steam for power generation. HDR technology is currently being developed at a number of pilot plants in Europe, Japan, Australia and North America.

Direct heating systems normally employ hot water from natural geothermal reservoirs. Hot water from one or more wells is passed through a heat exchanger where a separate water system extracts the heat. In district heating systems this hot water is then piped to buildings for space- or process-heating purposes. In recent years advances have been made in the use of ground

source heat pumps, which allow the use of very low temperature geothermal resources (< 20°C) for heating and cooling purposes.

1.9 Tidal

Tidal energy conversion systems draw mechanical energy from the Earth-Moon-Sun system through variations in gravitational potential.

In tidal barrage systems the rise and fall in sea level is used to trap water behind a storage dam. Energy can be used to drive generating turbines as water flows into and out of the reservoir. In estuarial tidal barrage systems the dam is constructed across the mouth of an estuary. In tidal barrage lagoons an expanse of open sea is enclosed by the dam. Tidal barrage systems require a substantial difference in water level between high tide and low tide (i.e. a large tidal range).

Tidal stream systems draw energy from the concentrations in tidal current that occur naturally around headlands or in channels between islands, and the devices are sometimes referred to as 'underwater windmills'. A tidal stream array is analogous to a windfarm, with a number of free-standing turbines. In a tidal stream fence system a dam is constructed across a seawater channel and the tidal current is forced to flow through turbines in the dam. Tidal stream systems do not depend upon a large tidal range.

2 Selected technologies

A number of the reviewed renewable energy technologies have been highlighted for further analysis, based on a number of criteria:

→ Potential for development of substantial delivery of energy on a short- to medium-term timescale,
→ Degree of potential utilisation of steel products,
→ Potential for contribution in the context of demands and available resources within the EU market,
→ Potential for use within iron making and steelmaking processes.

On the basis of these criteria, the technologies set out in Table 32 merit attention.

Solar	Wind	Onshore turbines	E
		Offshore turbines	E
	Wave	Surface effect mechanisms	E
		OWC devices	E
		Variable buoyancy devices	E
	Biomass	Solid fuels	F
		Fuels based on vegetable oil	F
		Bioalcohols	F
		Biogas	F
		Biomass gasification	F
Tidal	Tidal stream	Array	E

Table 32 - Selected renewable energy technologies

The three 'marine' technologies (wave, tidal stream and offshore wind) are relevant to the FATHOMS project. A separate section of this report describes the distribution of these renewable energy resources, likely operating locations and environmental conditions. The following section reviews recent events involving a number of wave, tidal and offshore wind technology developments.

3 Technology developments
3.1 Ocean Power Delivery Ltd.

Ocean Power Delivery Ltd. have completed towed trials with the Pelamis P-750 wave energy device (rated at 750 kW), and installed the device at a fixed mooring at the EMEC test centre in Orkney in the summer of 2004. The Pelamis is a 150 m long semi-submerged, articulated structure composed of 3.5 m diameter cylindrical sections linked by hinged joints(see Figure 88). The wave induced motion of these joints is resisted by hydraulic rams which pump high pressure oil through hydraulic motors via smoothing accumulators. The hydraulic motors drive electrical generators. Power from all the joints is fed down a single umbilical cable to a junction on the sea bed. Several devices can be connected together and linked to shore through a single seabed cable. To date, these tubes have been manufactured from S355 EM/EMZ plate – welded using SAW (Tandem). A design life of ~15 years is envisaged for these machines, however, their fatigue performance has been highlighted for concern. Again the use of a higher strength steel could reduce fabrication and installation costs.

Figure 88 - Pelamis P1A at Peniche shipyard, Portugal

Although originally conceived as a technology demonstrator for a proposed 1.5 MW device, production examples of the Pelamis P-750 (incorporating some improvements, such as a rapid mooring detachment system, and marketed under the commercial designation "P1A") have now been ordered. Three units manufactured in Scotland were delivered in summer 2006 to the Peniche shipyard 80 km north of Lisbon (see Figure 88 above) and will be installed at an operating location 5 km off the Portuguese coast, near Póvoa de Varim. A letter of intent has also been issued by the Portuguese wave farm developer to order a further thirty Pelamis machines (20 MW) before the end of 2006 subject to satisfactory performance of the initial phase [28].

In February 2006 the UK South West of England Regional Development Agency (SWRDA) announced [29] that the Pelamis device had been selected as one of three wave energy technologies for connection to a planned "Wave Hub" 16 km off the coast of Cornwall. This project would use 10 Pelamis P1A machines. The UK Government recently announced a £4.5 million funding package for this device – it is envisaged that it will be operational by the end of 2008. If successful, the "Wave Hub" could be provide three per cent of Cornwall's electricity needs, i.e. up to 20 MW of renewable and secure emission free energy powering 7,500 homes.

3.2 AWS Ocean Energy Ltd.

The Archimedes Wave Swing (AWS) is a wave energy device that embodies the variable buoyancy principle. A demonstrator device, rated at 2 MW, was installed off the Portuguese coast in May 2004 and grid-connected trials were undertaken. Although the device succeeded in generating electricity a number of serious difficulties were encountered, and the conduct of the trials has been the subject of severe technical criticism [30] In April 2006 the company announced [31] that it had secured £2M in equity funding to finance the development of a "Mark Two" device for fabrication in 2007 and commissioning in 2008.

The major structural component (and sole moving part) is the 'floater', which is essentially a large (10 m diameter) open-base steel pressure vessel subject to cyclic pressurisation loads. For the 2 MW demonstrator this was fabricated at the Damen shipyard at Galati, Romania (see Figure 89 below). AWS Ocean Energy is now partnered with Isleburn Mackay & Macleod, which has extensive fabrication facilities around the Cromarty Firth in Scotland.

Figure 89 - The AWS 2 MW demonstrator in the building dock at Galati. The domed cap of the floater is resting on the deck of the submersible pontoon prior to fitting of the linear generator

3.3   *Wave Dragon*

The 'Wave Dragon' unit is an offshore floating wave energy device that works by channeling waves into a reservoir which is above sea level. The water is then released through a number of turbines to generate electricity. The technology has been developed and tested over the past eight years in tanks in Denmark and Ireland. The Danish prototype (a 237 tonne unit deployed off the Danish coast between 2003 and 2006) is believed to be the first offshore wave energy device in the world to deliver power to a national electricity grid.

The developers of the device have announced plans for a two-stage project. The first stage involves the deployment of a 7 MW Wave Dragon unit (see Figure 90 below) off the coast of West Wales, near Milford Haven, by spring 2007. If the first unit deployed proves successful, the second stage will feature up to 11 Wave Dragon units at a deeper-water, more energetic site, with a total capacity of 77 MW. These units are expected to be deployed during 2008 and 2009.
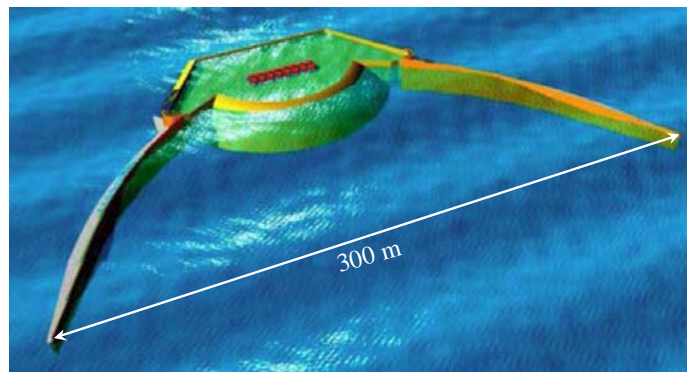
Figure 90 - Dimensioned artist's impression of the Milford Haven Wave Dragon pre-commercial demonstrator

In March 2006 it was announced via co-investor KP Renewables plc that an award of £5M had been made as an "Objective 1" grant from the Welsh European Funding Office to support the initial phase of the Milford Haven project.

3.4   Marine Current Turbines Ltd.

The monopile-mounted tidal stream turbine concept developed by Marine Current Turbines Ltd. (MCT) is suitable for water depths up to 30 m. The 'SeaFlow' tidal turbine demonstrator (see Figure 91(a) below) at Lynmouth was supported by Corus and has now operated for three years. The operators have reported that the hydrodynamic efficiency of the turbine blades has exceeded expectations, and that the 'SeaFlow' device has operated above its nominal 300 kW rating. They are now proceeding with the next stage in development - the twin-rotor 2x500 kW 'SeaGen' turbine (see Figure 91(b)), which will be installed at Strangford Lough in Northern Ireland. In February 2006 MCT announced [32] that, with financial support from the EU "Objective 1" programme, it would undertake surveys of potential tidal farm locations off the coast of Wales. Subsequently the company announced [33] that it was investigating the feasibility of constructing a 7 unit commercial tidal farm off the coast of the island of Anglesey in North Wales. The company had also announced in January 2006 that it was investigating the feasibility of building a 12 unit tidal energy farm in waters 2 km north-west of Lynmouth, off Foreland Point on the north Devon coast in the south west of England. The 10 MW tidal farm, to be known as the Lynmouth SeaGen Array, would be connected to the local electricity network.
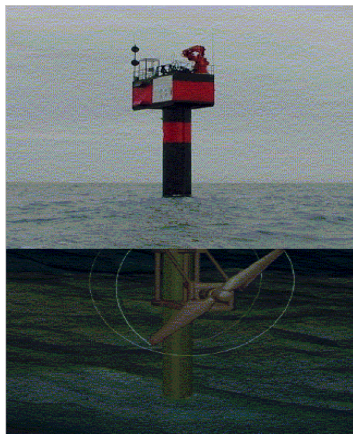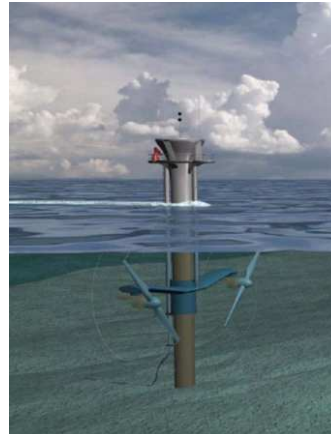
(a)   (b)

Figure 91 - (a and b): (a) SeaFlow 300 kW demonstrator; and (b) The SeaGen 2 x 500 kW tidal turbine

3.5   Tidal Stream

The 'TidalStream' device consists of four 20 m diameter rotors mounted on a semi-submersible spar bouy tethered to a seabed anchor by a swing-arm which allows the turbines to follow the flow direction as the tides change. The units can be floated into place before ballast tanks are flooded to submerge the device, removing the need for the use of cranes and barges. This operation can be reversed to bring the turbines to the surface for maintenance. The device is designed to enable economic access to tidal resources in water depths greater than 40 m. The developers of the device are particularly interested in the 60 m deep Pentland Firth off the northern tip of Scotland, and believe that this single location could meet 5% of the UK's electricity demands. The TidalStream Partnership is understood to have applied, in a consortium led by a major UK engineering company, for funding under the UK government DTI Technology Programme for a project to mitigate technical risks in the design of a pre-commercial demonstrator device.

3.6   Pulse generation

In contrast to the TidalStream proposal for a device suitable for much deeper waters than the MCT devices, Pulse Generation has proposed a device suited for much shallower waters. The proposed concept involves a pair of horizontal hydrofoils, which oscillate vertically, out-of-phase with each other, to drive a generator. Such a mechanism can operate in water much shallower than the minimum depth required for a turbine-based system, enabling devices to be placed very close to the shore and so minimising the capital costs of electrical connection.

Pulse Generation has secured funding for the development of a 100 kW proof-of-concept installation at North Killingholme in the Humber estuary in the north of England.

4   EU renewable energy targets

In January 2008 the European Commission issued a draft proposal for an EU directive on the promotion of the use of energy from renewable sources. In contrast to previous renewable energy directives (covering electricity generation from renewable energy sources and the use of biofuel for transport), this proposed directive covers total energy consumption, including heating. Targets are defined for each Member State in terms of the fraction of final energy use that must be derived from renewable energy sources. Targets from the January 2008 draft are illustrated in Figure 92 below, where Member States are listed in order of the relative magnitude of the required increase (between 2005 and 2020) of energy fraction.
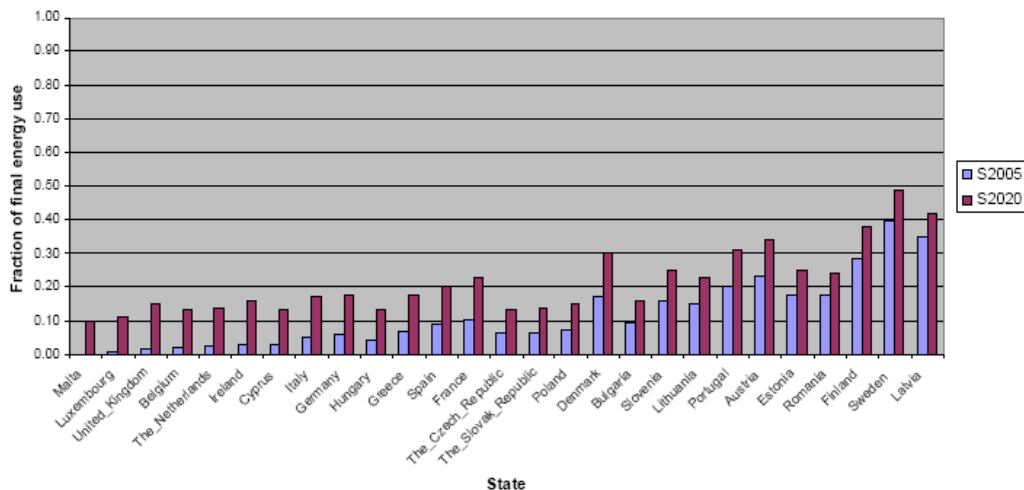
Figure 92 - Member State renewable energy source targets

It can be noted that the UK is a large energy user which, under the draft proposal, must achieve a large increase in the fraction of final energy derived from renewables. Under proposals issued for consultation in June 2008, the UK government has set out scenarios for attainment of the required use of renewables. These scenarios envisage compliance with the overall target principally through increases in the proportion of electricity generated from renewable energy sources. A large fraction of the required increase in renewable energy source electricity generation is envisaged as offshore wind energy, with scenarios ranging from 56 to 125 TWh/year from this source by 2020 (implying a range of 16 GW to 36 GW installed capacity for a load factor of 0.4).

5 Renewable applications - location and operating environment
5.1 *Offshore wind*

As shown in Figure 93 below, the European offshore wind resource is heavily concentrated in the north-west, with high energy densities extensively available in the eastern Atlantic Ocean, the Irish Sea, the English Channel, the North Sea and the Baltic Sea. Resources are generally lower in the Mediterranean apart from a small area to the south of France. Moderately large resources exist in the Aegean Sea.

Wind resources over open sea (more than 10 km offshore) for five standard heights									
10 m		25 m		50 m		100 m		200 m	
m s^{-1}	Wm^{-2}	m s^{-1}	Wm^{-2}	m s^{-1}	Wm^{-2}	m s^{-1}	Wm^{-2}	m s^{-1}	Wm^{-2}
> 8.0	> 600	> 8.5	> 700	> 9.0	> 800	> 10.0	> 1100	> 11.0	> 1500
7.0-8.0	350-600	7.5-8.5	450-700	8.0-9.0	600-800	8.5-10.0	650-1100	9.5-11.0	900-1500
6.0-7.0	250-300	6.5-7.5	300-450	7.0-8.0	400-600	7.5- 8.5	450- 650	8.0- 9.5	600- 900
4.5-6.0	100-250	5.0-6.5	150-300	5.5-7.0	200-400	6.0- 7.5	250- 450	6.5- 8.0	300- 600
< 4.5	< 100	< 5.0	< 150	< 5.5	< 200	< 6.0	< 250	< 6.5	< 300

Figure 93 - European offshore wind resource [34]

As shown in Figure 94 below, the total installed capacity of offshore windfarms has continued to grow, with particularly strong activity in The Netherlands and the UK. The world-wide installed capacity (so far all in the EU) passed the 1 GW milestone during the period of the FATHOMS project.

80
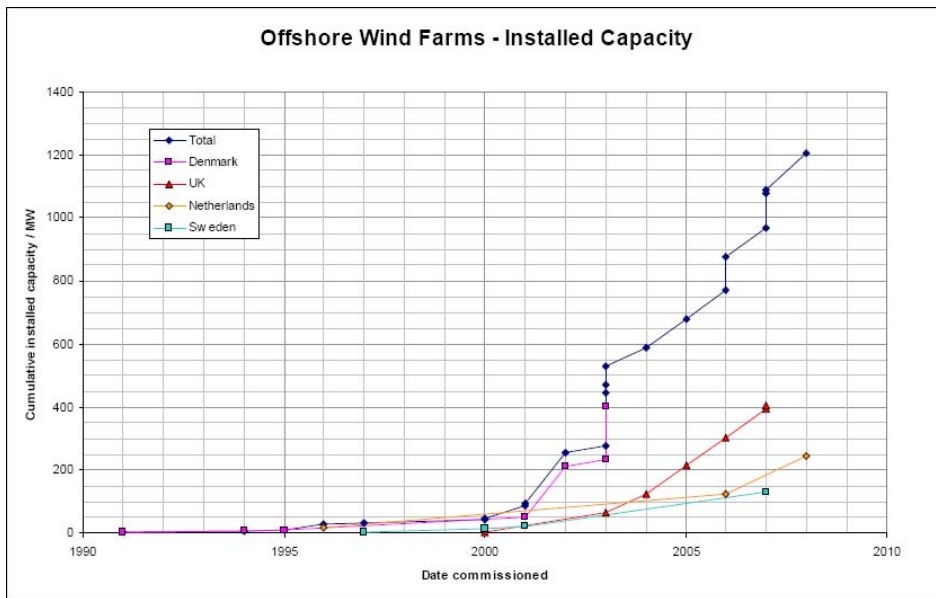
Figure 94 - Cumulative installed capacity in offshore wind farms

The majority of offshore wind turbines currently in operation employ a monopile foundation, which is considered to be a viable solution for water depths up to 30 m. At depths greater than 20 m a jacket or tripod design becomes increasingly more suitable.

The Talisman Beatrice development in the Moray Firth (north east Scotland) is being constructed in waters 40 – 50 m deep, and this project is widely regarded as representing the current technical/economic limit in terms of water depth for offshore wind farms.

A substantial increase in total installed capacity will occur in the period 2008-2009 with construction at a number of UK sites listed in Table 33 below.

Site	Number turbines	Total capacity/MW	Comments
Lynn	27	97	Completion summer 2008
Inner Dowsing	27	97	Completion summer 2008
Robin Rigg (A+B)	60	180	Under construction 2008
Rhyl Flats	25	90	Under construction 2008. Completion expected July 2009.
Gunfleet Sands	30	108	Construction start October 2008
Totals	**169**	**572**	

Table 33 - Current UK offshore wind farm construction activity

5.2   *Wave*

Concentrations of wave energy occur generally off west-facing coasts between latitudes 40 and 60 in both northern and southern hemispheres. The worldwide distribution of wave energy resources is indicated in Figure 95 below.
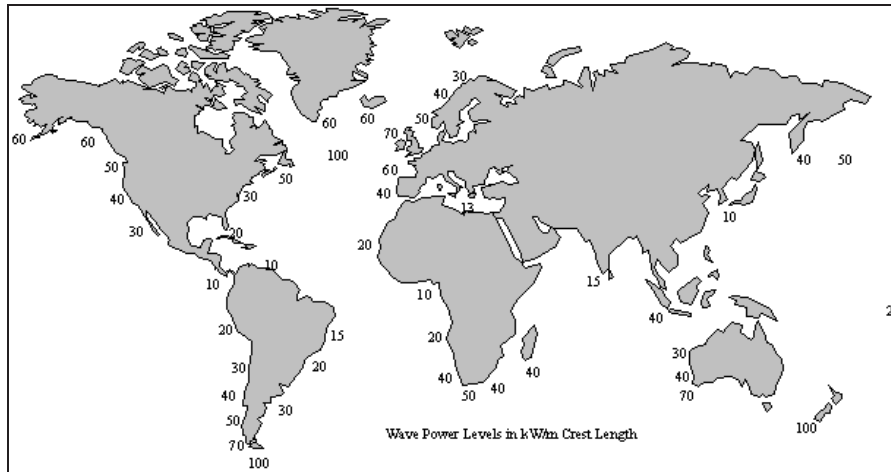
Figure 95 - Worldwide wave resources: average wave power levels in kW/m crest length [35]

The European resource is highly concentrated to the west of the British Isles and Iceland, as shown in Figure 96 below. It should be noted that significantly richer resources are found off the western coasts of UK and Ireland than off the coast of Portugal (where the first commercial wave farms have recently been demonstrated).

Although some wave energy devices have been constructed on the shoreline, most proposed concepts involve offshore arrays of machines. In deep water virtually all of the kinetic energy of the waves is concentrated in a surface layer of depth equal to half the wavelength. The propagation behavior of waves is influenced by the presence of the seabed when the water depth decreases to less than half the wavelength. Installation costs will obviously increase with increasing water depth and distance to shore. Consideration of these factors will influence the design of, and site selection for, offshore wave energy devices. Devices such as the Pelamis are designed for installation in water depths between 50 and 70 m and 5 – 10 km from shore.
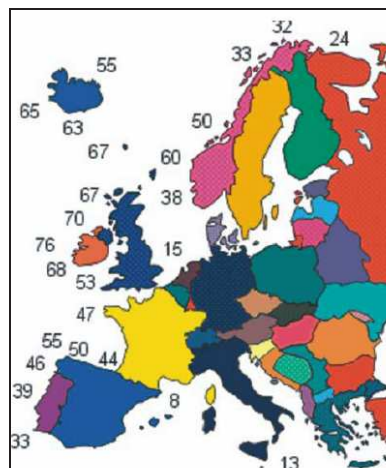
Figure 96 - European wave energy resource (average wave power, kW/m crest length) [36]

5.3 *Tidal stream*

Surveys have indicated that western Europe has substantial resources in terms of tidal streams. Significant concentrations occur around the British Isles. Assessments of the size of the practically available resource are varied, since these depend upon assumptions of the water depths and types of seabed conditions that could be accommodated. Furthermore, the results of surveys can be profoundly influenced by the modelling approach chosen. A recent study [37] of UK tidal stream resources (see Figure 97 below), concluded that the European technically

82

extractable resource was approximately 39 TWh/year, of which more than 50% (22 TWh/year) lay in UK waters, while the worldwide technically extractable resource was estimated at 160 TWh/year. The UK resource is thus approximately 14% of the worldwide resource. The UK survey also found that 80% of the UK resource is contained in just 10 of the 57 specific sites that were studied, with over 70% of the resource located at 8 sites in the Pentland Firth and the Channel Islands.

Approximately 20% of the UK resource is located in sites with water depths in the range 30-40 m. At least part of this resource could be exploited using devices similar to those, which have already been demonstrated at pre-commercial scale. Approximately 50% of the UK resource lies in waters deeper than 40 m. Exploitation of this resource will depend upon the development of new technologies, such as that proposed by TidalStream for deployment at 60 metres depth in the Pentland Firth. Some 30% of the UK resource therefore lies in waters shallower than 30 m. At depths shallower than 15 m it may be difficult to effectively employ rotor devices, and instead it may be more appropriate to exploit this resource using reciprocating hydrofoil devices such as that proposed by Pulse Generation.
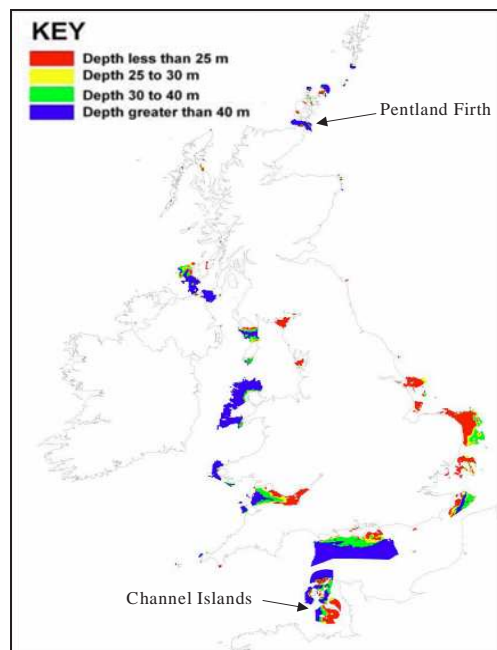
Figure 97 - Water depths for surveyed UK tidal stream sites with mean spring peak velocity > 1.5 m/s [37]

6   Environmental conditions relevant to marine renewable energy

From the overview of wind, wave and tidal resources it appears that the operating environments of interest for marine renewable energy installations will be those representing conditions in the north east Atlantic, and particularly those in relatively shallow waters around the western coasts of UK and Ireland.

Conditions in these areas (in terms of seawater composition, aeration, temperature and biological activity) can be expected be closely similar to those represented in experimental programmes of the 1970s/80s in support of the North Sea oil and gas industry.

A variety of standard synthetic seawater compositions were used in corrosion fatigue test programmes for the North Sea oil and gas industry. Two commonly quoted standard compositions are compared in Table 34 against analysis results for a sample of natural seawater from the North Sea [38].

In some programmes of work, seawater has been represented by a simple 3.5 wt. % NaCl solution. However, it is known [39] that the corrosion fatigue behaviour of cathodically protected steel in seawater is affected by the precipitation on the crack faces of calcareous deposits, mainly comprising $CaCO_3$ and Mg $(OH)_2$. Hence synthetic seawater (ASTM D1141) was used for the corrosion fatigue tests in this programme..

Standard	Composition (g/litre)								
	Na^+	Ca^{2+}	Mg^{2+}	K^+	Cl^-	SO_4^{2-}	Br^-	HCO3$^-$	Total solids
BS3900	10.50	0.49	1.29	0.39	18.9	2.72	0.07	0.15	34.7
ASTM D11451	11.02	0.42	1.33	0.39	19.84	2.77	0.04	0.15	35.96
Natural	10.56	0.40	1.27	0.38	19.0	2.65	0.07	0.14	34.5

Table 34 - Compositions of natural and synthetic seawater

Appendix B: In service loading for renewable applications

Calculations of the stress history in a wind turbine support structure need to take account of the dynamic behaviour of the wind turbine. A static analysis is appropriate only when the applied load varies over timescales much greater than the natural period of oscillation of the structure. For onshore wind turbines a system of loads will arise from loading on the rotor and from a distributed direct wind load on the tower. It is also necessary to take account of the loads introduced into the structure by torque of the generator, which depends on the way in which the generated electrical power is regulated. In the case of an offshore wind turbine it is necessary also to consider hydrodynamic (wave) loading and, in some cases, loads from winter sea ice. The analysis of combined wind and wave loading is particularly complex, as the two will generally vary (in magnitude and direction) with different frequencies. In all cases it is also necessary to take account of the fact that the rotor constitutes an aero-elastic system. Furthermore, deflection of the tower will introduce gyroscopic effects from the rotor.

The general practice for fatigue assessment of wind turbine support structures is to derive stresses from a dynamic analysis of the structure using site-specific meteorological and oceanographic data together with information provided by the manufacturers of the turbine and generator.

Similar considerations will apply in relation to wave energy devices and tidal stream generators.

Appendix C: Steel Catenary Riser Loading

1   Fatigue damage sources

A Steel Catenary Riser (SCR) is a long steel pipe suspended between a production floater and the seabed. In Figure 98 a scheme of SCR is shown. The top of a SCR is jointed to the floater in the Hang Off (HO) point, then the pipe goes into depth until it curves and lies down on the seabed starting from the Touch Down Point (TDP).
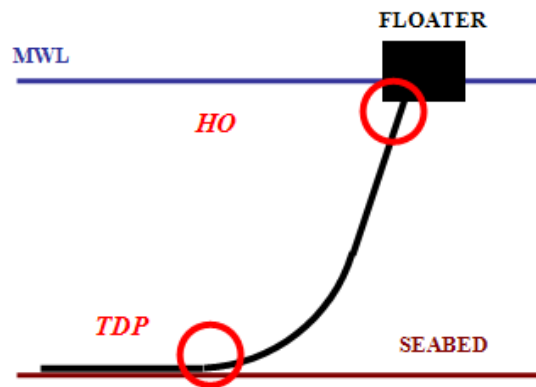
Figure 98 - Schematic representation of a SCR

Fatigue is usually the main design challenge for Steel Catenary Risers. Main sources of fatigue loading are:

→ First order wave frequency (WF) and second order low frequency (LF) vessel motions, due to waves and wind;
→ Vortex Induced Vibration (VIV) of the riser, due to currents;
→ Vortex Induced Vibration of the riser, due to vessel heave (HVIV);
→ Vortex Induced Motion (VIM) of the vessel, due to currents;
→ Installation.

WF damage is governed by direct wave loading on the riser system and WF floater motions generated by first order waves. LF damage is governed by second order floater motions due to fluctuating wind forces and second order wave excitation [40] [41] [42]. WF loads have frequency between 0.05 Hz to 0.5 Hz while LF loads have frequency content less than 0.05 Hz. In most cases high frequency loads dominate fatigue damage [43]. First and second order wave damage is strictly dependent on vessel motion characteristics. Due to their nature, SCRs are very sensitive to vessel motion, therefore their fatigue behaviour is influenced by the type of floater employed.

The damage depends also on waves direction, being the worst case in the plane of SCR [44] [45].

VIV damage is mainly due to vortex shedding induced by currents. Deepwater risers are particularly susceptible to VIV because currents are typically higher in deepwater areas; moreover the great length of the riser lowers its natural frequency thereby lowering the magnitude of current required to excite VIV. VIV can have an in-line or cross-flow direction, having the cross-flow VIV a response more significant than the in-line VIV [41]. The fatigue damage induced by VIV increases with increasing perpendicular flow velocity. Equipments like strakes or fairings are commonly used to suppress VIV.

VIM fatigue affect deepwater floater with deep draft cylinder hull, e.g. SPAR, and deep draft Semi, that vibrate under current action due to vortex shedding, transferring the additional motion to the riser.

HVIV fatigue is generated by floater vertical motions (heave), that may cause riser intermittent VIV.

Installation operation can induce additional fatigue cycles.

The relative importance of these loading components is strongly dependent on the system, environmental conditions and design solutions adopted to reduce fatigue damage.

The relative importance of fatigue sources varies considerably also with the section considered along the riser. The main critical areas are the Hang Off point, where fatigue is mainly due to stress cycles induced by WF motions, and the Touch Down Zone (TDZ), where fatigue is due to the continual lift off and set down of the riser on the seabed which produces significant bending stress cycling [40] [44].

WF and LF motions have different results in the TDZ. WF motions, which have generally relatively smaller amplitude, generate a fatigue damage concentrated mostly at one location, typically at the mean Touch Down Point (TDP). LF motions cause an additional fatigue damage with relatively small number of large stress cycles, but the large motions induced in the riser tend to spread the fatigue damage over a longer section of riser around the mean TDP. At the Hang Off point all the fatigue damages from WF and LF motions are accumulated at the same location without any spreading and mitigating effect [44] [46] [47]. The spreading effect can be beneficial also for VIV fatigue damage [40]. Is to be considered that the importance of vessel motion behaviour change with the water depth. While in relatively shallow water the motion of the floating support structure has a pronounced interaction with the behaviour of the TDZ, in deeper water the vessel motion is dampened through the SCR length and is not totally felt in the TDZ with beneficial effects [47]. Seabed properties and the possible presence of a trench dug by the riser itself have a great influence on the fatigue behaviour [40] [44] [49].

In fatigue analysis shall be taken into account all the contributes from cycling loading imposed during the service life which have magnitude and corresponding number of cycles large enough to cause fatigue damage. The combined WF and LF fatigue damage is normally evaluated using tailor made Finite Element (FE) computer programs that perform global dynamic analysis. Several software are in use by the industry and verification activities indicate that the different tools provide similar results when applied consistently.

VIV is a completely different physical phenomenon, so requires specialised dedicated computer tools. In this case state-of-practice tools often provide very different fatigue results even for well defined laboratory benchmark cases [42] [5] [50] [51].

After separate analyses, it is standard industry practise to sum up combined WF and LF fatigue damage and VIV fatigue damage [44].

2   Fatigue damage calculation

According to DNV-OS-F201 [52] and DNV-RP-F204 [40], the stress to be considered for fatigue damage accumulation in a riser is the time-dependent principal stress. The governing cyclic nominal stress component for pipes is normally a linear combination of the axial and bending stress given by

$$\sigma(t) = \sigma_a(t) + \sigma_M(\theta, t)$$

where $\sigma_a(t)$ is the axial stress and $\sigma_M(\theta, t)$ is the bending stress.

θ is the angular co-ordinate that gives the location of the hotspot along the circumference of the riser pipe.

The axial stress can be written as:

$$\sigma_a(t) = \frac{T_e}{\pi(D - t_{fat})t_{fat}}$$

where T_e is the effective tension (axial force), D is the outer diameter of the riser and t_{fag} is the fatigue thickness.

The effective tension T_e is given by

$$T_e = T_W - p_i A_i + p_e A_e$$

where

T_W is the true wall tension

p_i is the internal pressure

p_e is the external pressure

A_i is the internal cross-sectional area

A_i is the external cross-sectional area

The effective tension accounts for loading due to external and internal pressure acting on the pipe section. Effective tension is the sum of the "tensions" in the pipe wall and the internal fluid column less the "tension" in the displaced fluid column [53].

The fatigue thickness is an average representative pipe wall thickness, that accounts for variations in pipe wall thickness over the design life of the riser, in long-term fatigue damage calculations. For a stationary corrosive environment can be calculated as:

$$t_{fat} = t_{nom} - 0.5 \cdot t_{corr}$$

where t_{nom} is the nominal pipe wall thickness and t_{corr} is the corrosion allowance.

For fatigue damage calculations prior to permanent operation (e.g. during the installation) the fatigue thickness should be taken as:

$$t_{fat} = t_{nom}$$

The bending stress is a combination of the bending moments about the local y e z axes, M_y and M_z. For the mid-wall of the riser pipe, with reference to Figure 99, the bending stress can be written as:

$$\sigma_M(\theta,t) = \left(M_y(t)\sin(\theta) + M_z(t)\cos(\theta)\right)\left(\frac{D - t_{fat}}{2I}\right)$$

where I is the second moment of inertia, assumed equal about y and z axes.

This combined stress varies along the circumference of the pipe. When the waves are incident from several different directions, the fatigue damage must be calculated at a number of hotspot, at least 8, to identify the most critical location.
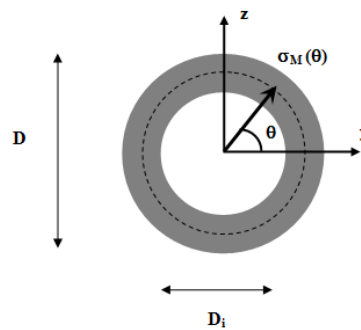
Figure 99 - Cross section of the riser

The fatigue assessment is based on the S-N curve approach. When appropriate, the fatigue analysis may be based on fracture mechanics [40] [53]. The stress range to be applied in fatigue

damage calculations is found from the nominal stress range multiplied by a stress concentration factor as well as a thickness correction factor:

$$S = S_0 \cdot SCF \cdot \left(\frac{t_{fat}}{t_{ref}} \right)^k$$

where

S_0 is the nominal stress range

SCF is the stress concentration factor

$\left(\dfrac{t_{fat}}{t_{ref}} \right)^k$ is the thickness correction factor that applies for pipes with a wall thickness t greater than a reference wall thickness, $t_{ref} = 25mm$. k is the thickness exponent, function of the actual structural design and of the related S-N curve, as reported in DNV RP-C203 [54].

The accumulated fatigue damage from stress cycles with variable range is found by using the Miner-Palmgren rule

$$D = \sum_i \frac{n(S_i)}{N(S_i)}$$

where

$n(S_i)$ is the number of stress cycles with range S_i and $N(S_i)$ is the number of stress cycles to failure as obtained from the S-N curve.

The total damage obtained using the cumulative damage summation is not affected by the sequence in which the loads are applied [44].

Random sea state wave fatigue is based on a series of dynamic simulations of sea states from a scatter wave diagram including sea state probability of occurrence. Statistical method, usually rainflow counting technique, is applied to stress time histories to provide an estimate of the stress probability density function associated with each sea state. Miner's rule should then be used to calculate the overall fatigue damage along the SCR. The weighted fatigue damage accumulation from all sea states can be expressed as:

$$D_{fat} = \sum_{i=1}^{N_s} D_i P_i$$

where

D_{fat} is the long-term fatigue damage

N_s is the number of sea states in the wave scatter diagram

P_i is the sea state probability

D_i is the short term fatigue damage

Normally the main contribution to the total fatigue damage comes from low to moderate sea states with high probability of occurrence rather than a few extreme sea states [40]

A similar approach can be adopted for calculation in VIV analyses using scatter diagram to represent the current environment [51] [55] .

Then the fatigue criterion which shall be satisfied is

$$D_{fat} \cdot DFF \leq 1.0$$

where

D_{fat} is the accumulated fatigue damage which includes the contributes from WF, LF and VIV damage

DFF is the Design Fatigue Factor, the fatigue safety factor

3   Random waves loading

Within fatigue sources, sea waves generate loading that translates into variable amplitude stress on the riser. This load originates from vessel motions due to waves that are transferred to the entire riser through the connecting section.

Sea waves are oscillating motions of the superficial water layer, due principally to wind action. They are the sum of many individual waves with different wavelengths, amplitudes and directions, as shown in Figure 100, giving to the sea an irregular configuration, with great height variation from wave to wave.
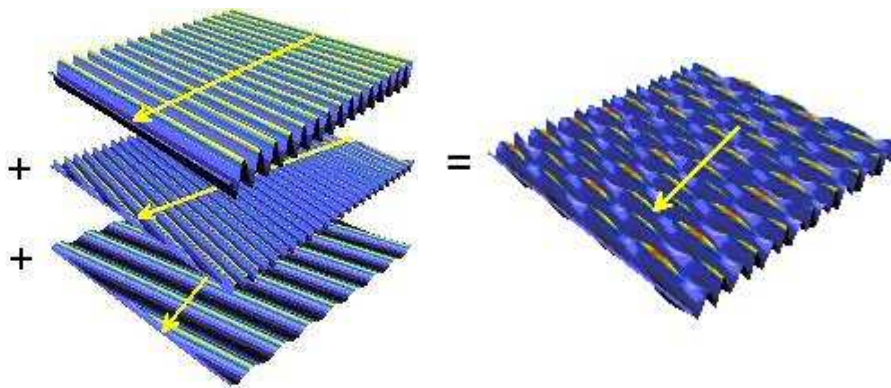
Figure 100 - Result of sum of wave components with different amplitudes, wavelengths and directions [56]

Due to the variable wave height, statistical parameters are usually used to describe sea conditions. The parameter used to represent wave height in a time interval is the *significant wave height Hs*, shown in Figure 101, approximately equal to the average height of the highest one-third of the waves. The actual definition is four times the root mean square of the water levels relative to the mean water level, where the mean water level is the level the sea would be at if it was still.
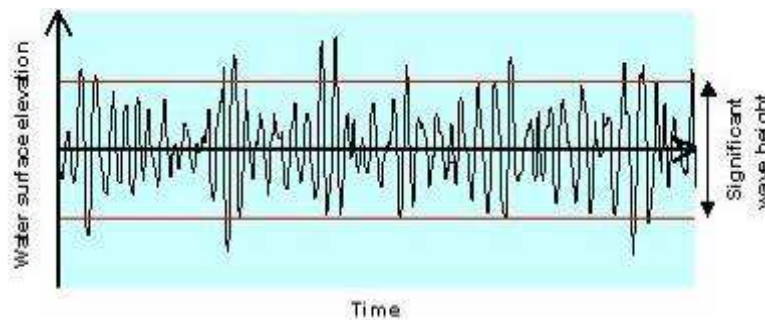
Figure 101 - Example of water surface elevations history[56]

The *zero up-crossing period Tz* is the average time between successive crossings of the mean water level in an upward direction.

When the statistical properties of the sea are assumed to be constant and can be represented by a couple of parameters *Hs* and *Tz*, we talk about a *sea state*.

Usually the *sea states* are represented by a graph of power spectral density in the frequency domain, also known as the *wave spectrum*. In a *sea state* with random distribution of wave energy over all wave frequencies, the spectrum indicates the energy carried by each frequency. Wave energy is proportional to the square of wave height.

An example of wave spectrum is shown in Figure 102. Further parameters are here introduced. *Peak frequency* (or *Peak period Tp*), is the frequency (or period) with the highest energy content. It coincides with the point of highest spectral density. *Energy frequency* (or *Energy period Te*), is the frequency (or period) of a simple sinusoidal wave that would carry the same energy as the sea. In Figure 102, the *Energy frequency* lies in the middle of the power spectral density.

From experimental data, has been found that *wave spectra* have similar shapes for sites with similar characteristics. Therefore it is possible to generalize the spectrum shape through wave spectral density functions**.**

The most used wave spectral density functions, shown in Figure 103, are the JONSWAP and Pierson Moskowitz spectra.
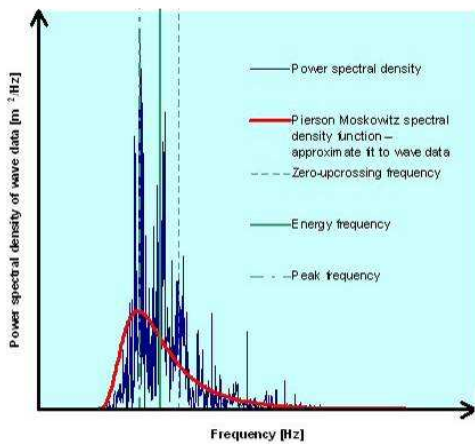
Figure 102 - Wave spectrum (power spectral density) [56]
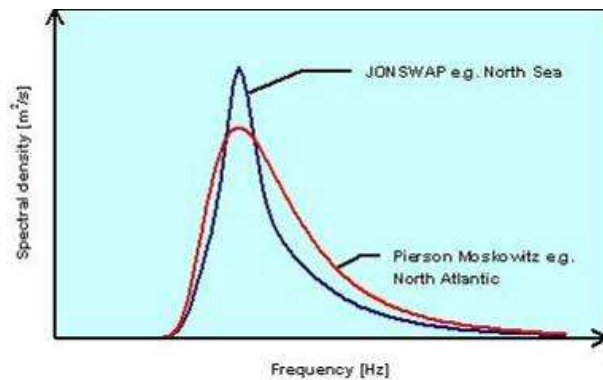
Figure 103- JONSWAP and Pierson-Moskowitz spectra [56]

In a long period, the sea is characterized by a series of different *sea states*, with different Hs and Tz (or equivalent) parameters. The couples of parameters may be subdivided into classes and the probability of occurrence of each class may be indicated in a *scatter diagram*, as in Figure 104.

Wave loading has in this way a double variability, as waves are random inside each sea state as well as different sea states occur in the long period. This variable behaviour translates into a very variable loading all over the life of the riser, characterized by different stress levels and often by the presence of peaks of load.
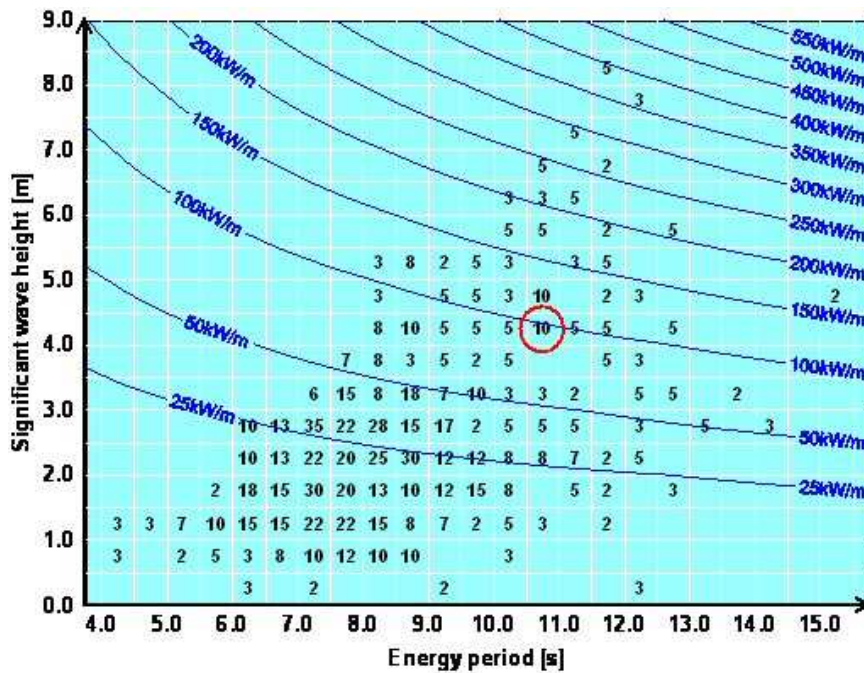
Figure 104 - Example of scatter diagram showing how often each sea state (combination of significant wave height Hs and energy period Te) occurs in parts per thousand. The blue lines are contours of constant wave power [56]

Appendix D: Offshore pipelines.

The construction of offshore pipelines has been motivated mainly by the need of exploring underwater oil and gas reserves. The first offshore pipelines were constructed in California in the early 1900's. Since then, the increased need for offshore oil & gas exploration and the need for long – distance oil & gas transportation has motivated the construction of many marine pipelines. Offshore pipelines may be classified as follows:

→ Flowlines transporting oil and/or gas from satellite subsea wells to subsea manifolds.
→ Flowlines transporting oil and/or gas from subsea manifolds to production facility platforms.
→ In-field flowlines transporting oil and/or gas between production facility platforms.
→ Export pipelines transporting oil and/or gas from production facility platforms to shore.
→ Flowlines transporting water or chemicals from production facility platforms, through subsea injection manifolds, to injection wellheads.

The main design requirement of underwater pipelines is the resistance to pressure, which can be internal (operation) or external (due to the water depth). In typical offshore applications, steel pipeline wall thickness ranges between 3/8 inch and 1⅔ inch. Installation is also a critical issue, where bending and axial loading conditions occur. Finally, repeated loads during both the operational stage and the construction (installation) stage may cause fatigue cracks and threaten their structural integrity.

Fatigue of offshore steel pipelines occurs mainly in the weld area, connecting two adjacent pipeline segments. Fatigue cracks may also appear, not so often, in pipeline areas where a major defect or damage exists (local dent, local buckle, corrosion etc.).

The three main methods of constructing a pipeline are shown in Figure 105, Figure 106 and Figure 107. They are referred to as S-lay method, J-lay method and reeling method. In all three case, the pipeline is layed from a special lay-barge to the sea bottom and has the shape of a flexible catenary, subjected to wave and current forces. In such a case, it behaves as a catenary riser. Pipeline damage (in the form of excessive stress near the yield stress and/or fatigue) may

91

also occur in pipeline spans, i.e. non-supported parts of a pipeline on the seabed. These spans may occur when contact of the pipeline with the seabed is lost or when the pipeline is on a rough seabed. The flow and wave around the pipeline may cause oscillations, which can lead to fatigue damage. In particular, in offshore pipelines, the main cause of oscillations is the current velocity, and the oscillations are in a direction parallel or normal to the current direction, referred to as "vortex shedding".
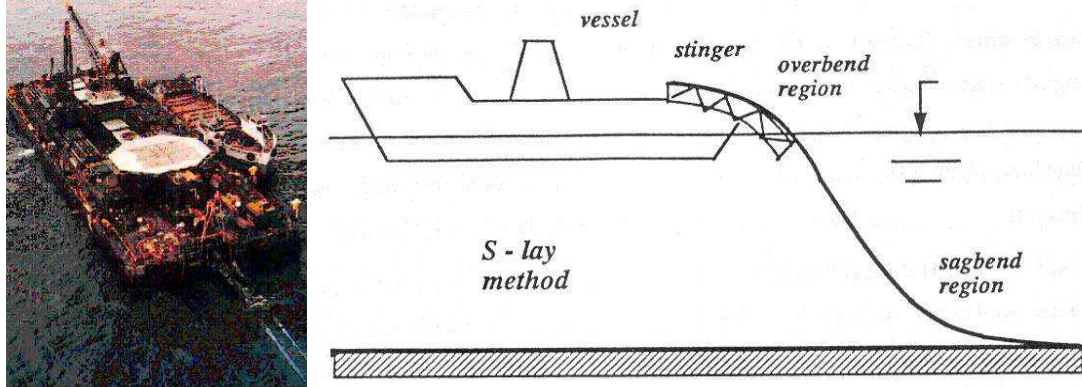
Figure 105 - Pipelaying with the S-lay method - The stinger on the lay-barge is in a quasi-horizontal position, so that the pipe shape has a double curvature. Initially it was used for relatively shallow water depths, but nowadays it has been used with modern lay-vessels for water depths greater than 2500 ft.
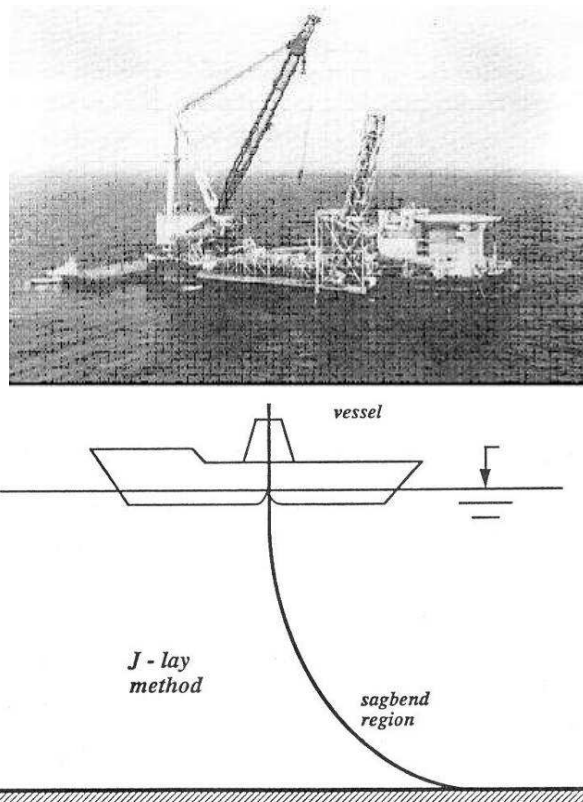
Figure 106 - Pipelaying with the J-lay method. The stinger is vertical, so that the pipe shape has a single curvature. It was developed and is currently used for deep water applications.
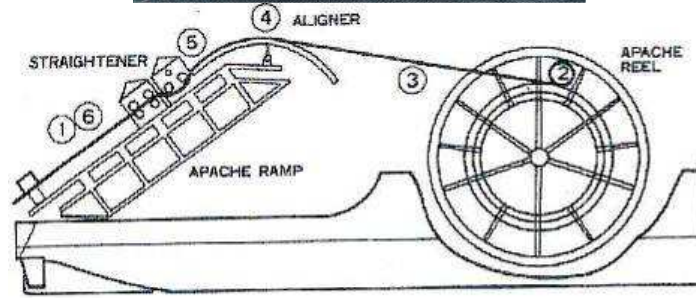
Figure 107 - Pipelaying with the reeling method. The pipe is reeled and straightened with an appropriate machine before entering the water. The size of the pipeline diameter is the most important limitation for the reeling method.

A simplified analysis of fatigue of pipeline spans, see Figure 108, under bottom currents is outlined in the following methodology:
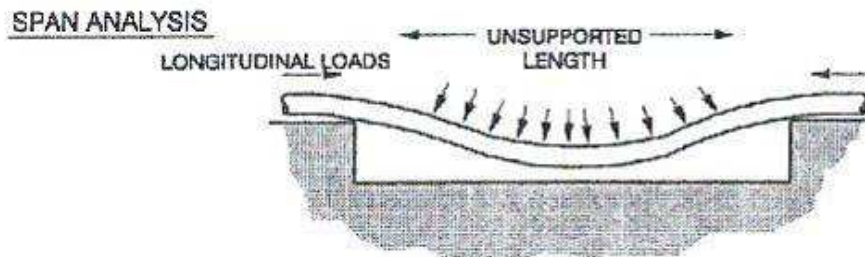
Figure 108 - Schematic representation of a pipeline free span

→ Step 1: Calculate the natural frequency according to the formula below reported.

$$f_n = \frac{C_e}{2\pi} \sqrt{\frac{EI}{M_e L_s^4}}$$

→ Step 2: Determine the near bottom current velocity occurrence distribution in histogram from using current duration blocks.

→ Step 3: Determine the frequency ratio f/f_n for each current segment based on U_c/Df_n and the diagram shown in Figure 109.

93
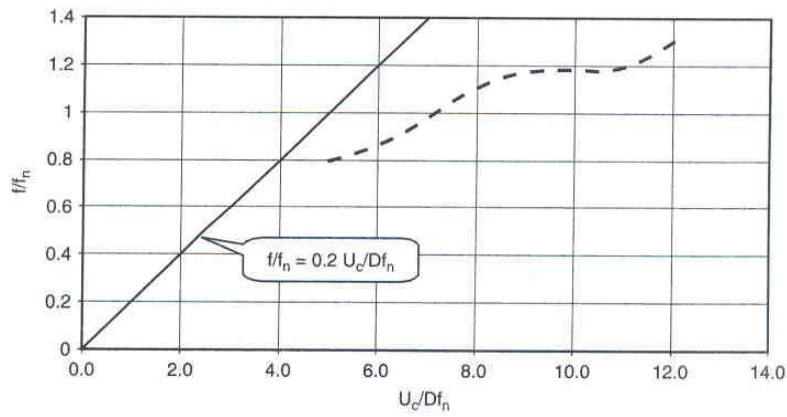
Figure 109 - f/fn *vs* Uc/Dfn

→ Step 4: Determine the amplitude ratio A/D for each current segment based on the stability
parameter K_s and the diagram reported in Figure 110.
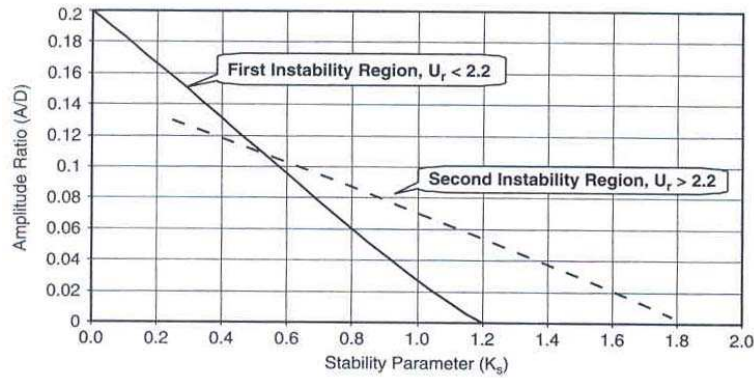
Figure 110 - Amplitude ratio *vs* Stability Parameter

→ Step 5: Calculate the fatigue life.
This calculation can be conducted through the fatigue life equation based on the
Palmgren – Miner Fatigue Model, which uses an S- N model based on the AWS-X
modified curve of the form:

$$N = \frac{6.48 \times 10^{-8}}{\Delta \varepsilon^4}$$

where N is number of cycles to failure and $\Delta \varepsilon$ is the strain range in each cycle. This
extremely simplified fatigue life equation is expanded as follows:

$$L_f = \left[\frac{5.133 \times 10^{-18\left(\frac{L_s}{D}\right)^8}}{\left(\frac{D_s}{D}\right)^4 f_n} \right] \times \left[\frac{1}{\sum_i \left(\frac{f}{f_n}\right)_i \left(\frac{A}{D}\right)_i^4 T_i} \right]$$

Where:

L_f = Fatigue life (years)

L_s = span length

D_s = outside diameter of steel

f_n = pipe frequency (H_z)

$$\dfrac{f}{f_n} \quad = \text{frequency ratio (Step 3)}$$

$$\dfrac{A}{D} \quad = \text{amplitude ratio (Step 4)}$$

$$T_i \quad = \text{current duration (hrs/day)}$$

Appendix E: Offshore standards.

1   Standards Overview

1.1   EN 1993-1-9

Standard EN 1993, often referred to as Eurocode 3, is a general code the design of steel structures, which adopts the limit state approach. In particular, Part 1-9 covers fatigue design. Partial safety factors are applied separately to loads and resistances to obtain the required safety level. Being essentially an onshore code for Civil Engineering structures, the necessity for fatigue assessment does not include fluid-induced oscillations. Moreover, the code limits the fatigue strengths specified as applicable to structures with suitable corrosion protection and subjected only to a mildly corrosive environment (such as normal atmospheric conditions). S-N curves are referred to as "fatigue strength curves" and partial safety factors are applied to these according to accessibility of the component during periodic inspection and maintenance, and the consequence of failure.

Fatigue design is based on a set of classified constructional details. Different routes through the process are taken if the detail under consideration falls within the classification, or differs from any standard detail classified, and/or is unclassified. The routes prescribe the types of fatigue stress range that can be used in the assessment (nominal or geometric) along with the fatigue strength curve to be applied. Constant amplitude and variable amplitude loading are addressed. In the case of variable amplitude loading (the more general), fatigue assessment may be based on cumulative damage (Palmgren-Miner rule) or equivalent constant amplitude. Normal stresses (to the weld) and shear stresses, individually applied or in combination, can be dealt with. Fatigue strength curves are bi-linear, or linear, on log-log plots of fatigue strength (stress range) versus endurance, with some endurance limits, referred to as "cut off levels". Provisions for weld improvement techniques and for member thickness effects are also proposed as modifications to the basic fatigue strength.

1.2   BS 7608 (1993))

BS 7608 is a general specification for fatigue design and assessment of parts of steel structures that are subject to repeated fluctuations of stress. It is restricted to structural steel with specified minimum yield strength less than 700 MPa. The document should be used together with other specific structure-related design codes, accounting for either "limit state" or "working stress" philosophy is inherent in the citing structure-specific code. T BS 7608 has four main sections dealing with: general aspects, classification of details, stress calculations and allowable fatigue stresses. The main document is supported by a number of annexes dealing with specific technical items. These include Annex A, which covers fatigue design philosophy.

Fatigue design is based on the combination of stress ranges (nominal or geometric), , S-N curves for standard details, and the Palmgren-Miner linear cumulative damage rule for joints subjected to a stress spectrum. The joint is considered safe if the cumulative damage is less than unity. S-N curves are provided for a variety of classified structural details, referred to as "basic" S-N curves, which are mean fits through experimental data. For design purposes, "standard basic" curves are derived from these by taking two standard deviations below the mean values (see below). S-N curves are linear on log-log plots of stress range versus endurance, and are made bi-linear in the standard manner to deal with spectra that contain a range of low stress cycles. The curves given are applicable to joints in air, or in contact with seawater but having adequate corrosion protection. Provision for joints in seawater under free corrosion is made by a simple factor applied to the design curve. No endurance limits are specified on these curves, but conditions are given that lead to situations where a detailed fatigue analysis can be omitted.

Modifications to the design S-N curves must be made to allow for thickness effects. The effects of weld improvement techniques on fatigue life enhancements are also taken into account.

1.3 IIW Recommendations

The IIW XIII-1965r14-03 / XV-1127r14-03, 2006, document is not a code of practice or a standard but presents recommendations for the fatigue design of welded joints and components. No recommendations are given for the fatigue load (action), nor for the partial safety factor on fatigue actions. The document focuses on the fatigue resistance of welded details in non-corrosive environments, with normal protection against atmospheric corrosion assumed. No specific recommendations are given in the document for corrosion fatigue.

The document considers different approaches for the fatigue assessment of welded joints and components: nominal stress, geometric stress (hot spot stress), effective notch stress, fracture mechanics method and component testing. The approaches of most relevance in the document are those based on nominal stress and geometric stress. The overall design approach for fatigue assessment has similarities to that in EN 1993-1-9, discussed above. The process starts with defining the constructional detail under consideration. Different routes through the process are taken if the detail falls within the set of standard classified types given, differs from those classified, or is unclassified. If the joint corresponds to a classified detail, assessment is based on nominal stress. Alternatively, assessment uses the geometric stress. For the particular case of nodal tubular joints this would involve the use of the nominal stress and appropriate SCFs is specified. Constant amplitude and variable amplitude loading are dealt with using different fatigue strength (S-N) curves. In the case of variable amplitude loading (the more general case), assessment is based on cumulative damage (Palmgren-Miner). The document recommends that for load spectra which are sensitive to the position on the S-N curve of fatigue limits or cut-off limits, additional assessment using a nonlinear damage calculation method should be performed. It is also recommended that, in cases where no test data or service experience exist and the stress spectrum is not close to constant amplitude, only half of the calculated life should be assumed. The fatigue strength curves to be used in variable amplitude loading assessment are bi-linear on log-log plots of stress range versus endurance, with endurance limits.

1.4 DNV RP C203

DNV RP C203 contains general rules covering the fatigue design of offshore structures, pipelines and risers, based on fatigue tests and fracture mechanics. The Recommended Practice is valid for steel members in air with yield stress less than 700 MPa. For steel materials in seawater with cathodic protection or steel with free corrosion the Recommended Practice is valid up to yield stress up to 500 MPa. Miner's rule, presented above, is the basis for calculating fatigue damage of a welded detail in .

Stresses to be considered in fatigue design, (for both plates and tubes), should include stress concentration factors (SCFs), and are denoted as "local" stresses in plated structures and "hot spot" stresses in welded tubular connections. The S-N curves proposed by the Recommended Practice are in the following general form

$$\log N = \log \overline{a} - m \log \left[\Delta \sigma \left(\frac{t}{t_{ref}} \right)^{k} \right]$$

The last term in brackets accounts for thickness correction, where t_{ref} is a reference thickness, equal to 25 mm for welded plated connections, and equal to 32 mm, for welded tubular connections. Various S-N curves are proposed for welded details in air and in sea water with cathodic protection. Thickness correction exponent k is given for each fatigue curve in relevant tables of the Recommended Practice.

The influence of the mean stress on the fatigue behavior of plated connections is consider in the Recommended Practice, using an appropriate reduction factor, for the fatigue behavior of the base metal, as well as in cases where residual stress influence is not significant. DnV RP-203

proposes the use of a simple diagram. The diagram is not to be used in welded tubular connections.

The values of Stress Concentration Factors can be obtained as follows

- SCFs for welded plated connections are proposed in section 2.6 considering for both misalignment and different thickness between the connected plates.

- SCFs for pipeline butt-welded connections, a formula for misalignment is also given.

1.5 *API RP2A*

API RP2A has been a very popular specification for planning, designing and constructing fixed offshore platforms. There exist two versions of this specification (a) a load and resistance factor approach LRFD, and (b) a working stress type approach WSD. In the LRFD version, that follows the philosophy of the AISC-LRFD design methodology, whilst not a limit state code, partial safety factors are applied separately to loads and resistances. Chapter F deals with fatigue and makes reference to Chapter L, which covers fabrication, including weld profiling.

In API RP2A fatigue design is conducted by means of S-N curves and the Palmgren-Miner linear cumulative damage accumulation rule. Nominal stresses (e.g. from a space frame analysis) are used in the computation of stress ranges, along with suitable stress concentration factors to give hot spot stresses. The microscopic effects, occurring at the toe of a weld under consideration, are reflected in the choice of an appropriate S-N curve. The only S-N curves provided in the document relate to tubular joints in steel structures and modifications are to be applied to these to account for operating environment and thickness effects.

According to API RP2A, the wave climate should consider all seastates to be expected in the long term. Using this wave data, an appropriate structural analysis is conducted to obtain the nominal stress at the members and the joints. A spectral analysis technique should be used to determine the stress response for each seastate. Following the structural analysis of the platform, and using appropriate stress concentration factors (SCFs) for welded tubular joints, the local stress at the weld toe of the welded connections should be computed. The micro-scale effects (often referred to as "notch effects") may not be considered, since they are included in the S-N fatigue curve. Local stresses should be considered in all possible critical locations of a weld, and for each seastate, the corresponding fatigue life should be computed. The fatigue lives from all the seastates should be combined in an appropriate manner, to compute the accumulated damage factor, considering the well-known Miner's rule is employed. Furthermore, a factor of safety equal to 2 is specified for the design fatigue life of each joint, so that it is at least twice the intended service life of the offshore structure.

For non-tubular connection details, the classification method, discussed in an earlier section, is followed. In general, the ANSI/AWS D1.1 standard (Structural Welding Code) should be used, with the appropriate S-N fatigue curves. The nominal stress range should be used in this design procedure. Geometric stress concentrations and notch effects are included in the corresponding S-N curve of each class.

On the other hand, tubular connections should be design through the design using the hot spot method. The method, described in a previous section, is based on the calculation of the maximum geometric stress in the vicinity of the weld, excluding the notch effect (which is incorporated in the fatigue curve), but including the "geometric" effects through appropriate SCFs. Upon calculation of the hot spot stress, the fatigue life is computed though an appropriate S-N fatigue curve. In API RP2A-LRFD, two curves are used, namely X and X′. For welds without profile control, but conforming to a basic standard profile according to ANSI/AWS D.1.1 and a branch thickness less than 16 mm, the X′ curve should be used. For thicknesses greater than 16 mm, a thickness correction factor should be used as follows

$$S = S_0 \left(\frac{t}{t_0} \right)^{-0.25}$$

where S is the allowable stress that includes the thickness correction, S_0 is the allowable stress from the S-N curve, t in the actual branch member thickness ($t \leq t_0$) and t_0 is the limiting branch thickness, herein equal to 16 mm. For welds with profile control and having a branch thickness less than 25 mm, curve X should be used. If the thickness is greater than 25 mm, the thickness correction t_0 should be considered, with the limiting reference thickness equal to 25 mm.

Finally, API RP2A-LRFD proposes a simplified approach, described in the Commentary of the specification, to be used for water depth less than 122 m (400 ft) and for natural frequencies less than 3 seconds, the target is that the peak hot spot stress at the tubular connections does not exceed the allowable peak hot spot stress. First, the fatigue design wave is calculated from a nomograph in terms of the water depth, and should be applied to the structure including the effects of tide, but without any other loading. In this analysis, a load factor of 1 should be used. Subsequently, the peak hot spot stress S_c at a specific weld should be determined, using the nominal stresses due to axial load, in-plane bending and out-of-plane bending, and appropriate Stress Concentration Factors (SCFs). Finally, the allowable peak hot spot stress is derived as a function of the parameter, g which defines how a structure responds to different wave heights. There are three basic assumptions to this approach:

(a) The stress range, S is related to the wave height H in a simple equation $S = C H^g$, where C is a calibrated constant and g is a calibrated exponent.

(b) The $S - N$ Curve can be written $N S^m = K$ where K, m are constants.

(c) The long-term wave height distribution can be represented by the sum of two Weibull distributions.

2 General fatigue design procedure

The approach followed by the Standards/Recommendations for fatigue assessment is quite similar. The first step is the determination of the long term distribution of stress range applied to the component/structure considered, followed by the selection of the suitable S-N design curves depending on the joint class selected.

Subsequently, after replacing the long term distribution of stress range with a stress histogram consisting of a number of constant amplitude stress range blocks (σ_i) and the corresponding number of cycles (n_i), the accumulated damage (D) should be determined.

In all the Standards mentioned in the main text, the accumulated damage evaluation follows the well-known Miner Rule:

$$D = \sum_{i=1}^{k} \frac{n_i}{N_i}$$

where:

n_i = number of occurrences at a fixed stress range drawn from the load spectrum;

N_i = number of cycles to failure at a fixed stress range drawn from the S-N curve;

Theoretically, fatigue damage occurs when the accumulated damage factor is equal to 1. In design, a critical value of this factor is specified (less than unity). Different critical values of D are recommended in various Standards. For instance both British Standards and API RP2A-LRFD recommend just $D = 1$. On the other hand, DNV Standards consider different limit damage values(see Table 35), according to the safety class, meaning with safety class "the significance of the pipeline system with respect to the consequence of failure".

Safety class	Low	Normal	High
D critical	1/3	1/5	1/10

Table 35 - Cumulative damage allowable for DNV 2000

The ISO/DIS 13628-7 gives two different values, referring to components which can be inspected and components which cannot be inspected (see Table 36).

Component acceptable for inspection	1/3
Components not acceptable fro inspection	1/10

Table 36 - Cumulative Damage allowable for ISO/DIS 13628-7

It should be noted that above striking differences in critical D values do not necessarily represent such significant differences in fatigue design. To compare fatigue design procedures from different specifications/recommendations, the entire procedure has to be examined, including load factors and load spectra, as well as the application range of the specification/recommendation under consideration.

API and DNV Standards are typically used in the common international off-shore practice. In the following, a more detailed description of the fatigue design methodologies offered in API RP2A-LRFD and DNV Recommended Practice RP – C203 is presented.

3 DNV RP C203 Fatigue Recommendations for Offshore Structures

DNV RP C203 contains general rules covering the fatigue design of offshore structures, pipelines and risers, based on fatigue tests and fracture mechanics. The Recommended Practice is valid for steel members in air with yield stress less than 700 MPa. For steel materials in seawater with cathodic protection or steel with free corrosion the Recommended Practice is valid up to yield stress up to 500 MPa.

Miner's rule, presented above, is the basis for calculating fatigue damage of a welded detail.

Stresses to be considered in fatigue design, (for both plates and tubes), should include stress concentration factors (SCFs). More specifically, in plated structures, local stress should be considered

$$\sigma_{local} = SCF \cdot \sigma_{nominal}$$

where *SCF* is an appropriate stress concentration factor.

On the other hand, in welded tubular connections, one should consider hot spot stress, computed as follows

$$\sigma_{hot-spot} = SCF \cdot \sigma_{nominal}$$

where *SCF* is an appropriate stress concentration factor.

3.1 S-N Fatigue curves
The S-N curves proposed by the Recommended Practice is in the following general form

$$\log N = \log \overline{a} - m \log \left[\Delta \sigma \left(\frac{t}{t_{ref}} \right)^k \right]$$

A thickness correction is included, where t_{ref} is a reference thickness, equal to 25 mm for welded plated connections, and equal to 32 mm, for welded tubular connections. The various S-N curves are shown in Figure 111 and Figure 112 for welded details in air and in sea water with cathodic protection. Thickness correction exponent *k* is given for each fatigue curve in relevant tables of the Recommended Practice. Figure 113 shows the S-N curves to be used in the fatigue design of welded tubular connections.
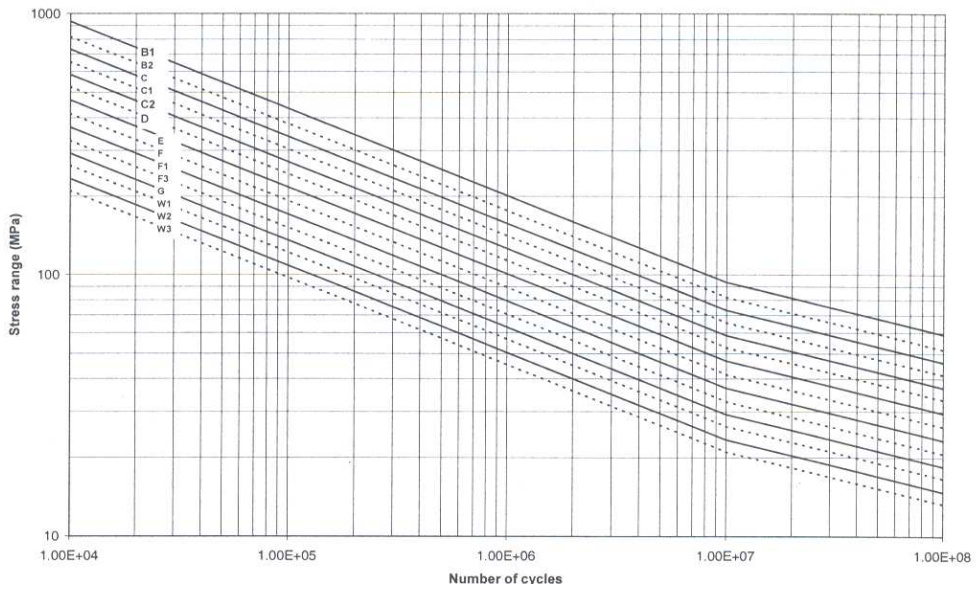
Figure 111 - S-N curves in air
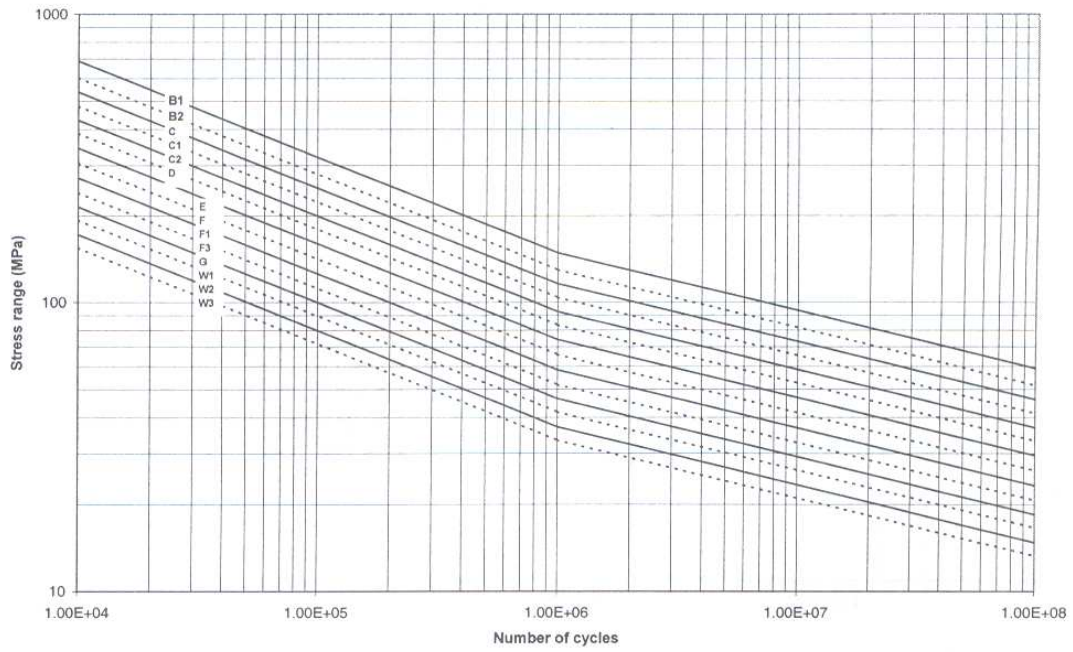
Figure 112 - S-N curves in sea water with cathodic protection

100
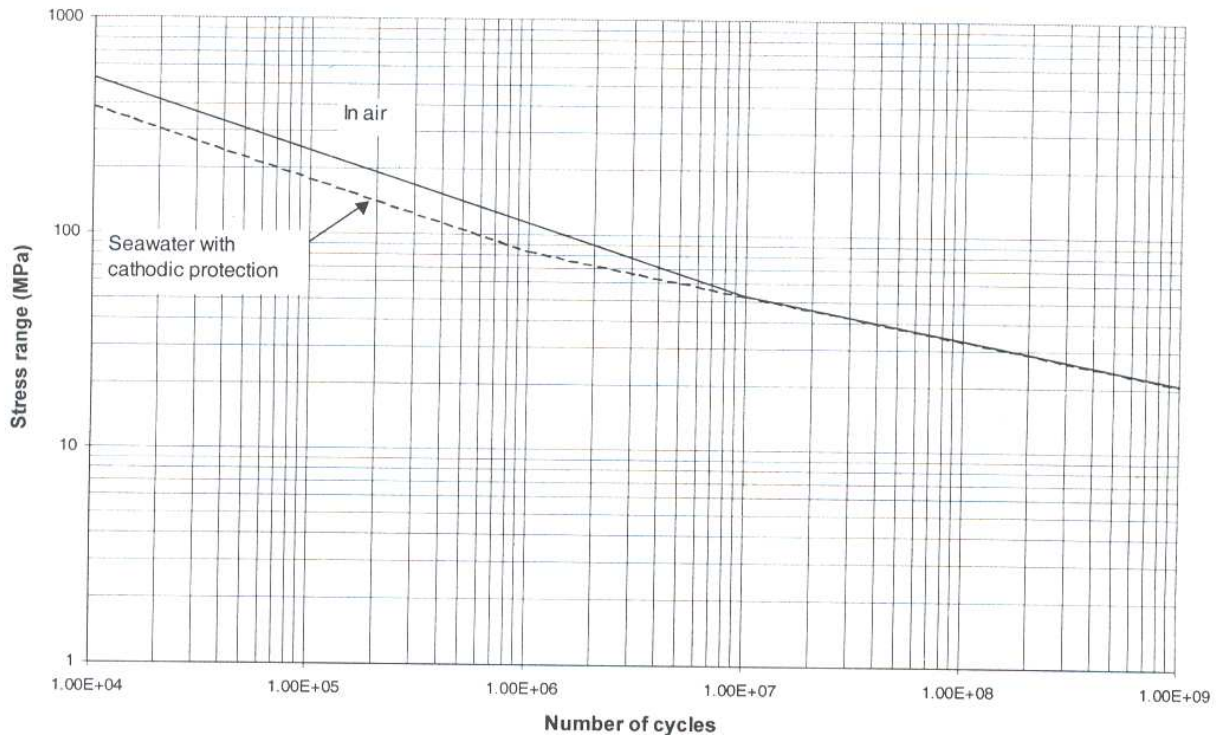
Figure 113 - S-N curves in air and in sea water with cathodic protection for welded tubular connections

The influence of the mean stress on the fatigue behaviour is considered in the Recommended Practice, using an appropriate reduction factor f_m. This reduction factor is used for the fatigue behaviour of the base metal, as well as in cases where residual stress influence is not significant. DNV RP-203 proposes the use of a simple diagram, shown in Figure 114. The diagram is not to be used in welded tubular connections.
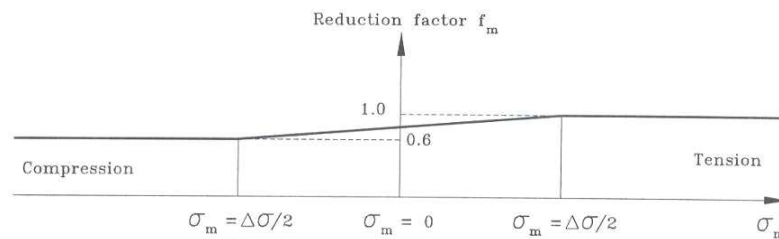
Figure 114 - Stress range reduction factor to be used with the S-N curve for base material

Stress Concentration Factors

The values of Stress Concentration Factors can be obtained as follows:

→ SCFs for welded plated connections are proposed in section 2.6; two main issues refer to misalignment and different thickness between the connected plates.
→ SCFs for pipeline butt-welded connections, Table 37 and following equation is proposed, where δ is the tolerance requirement, also given in the Table.

$$SCF = 1 + \frac{3\delta}{t} \exp\left(-\left[\frac{D}{t}\right]^{-0.5}\right)$$
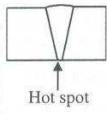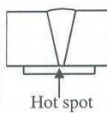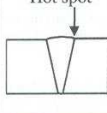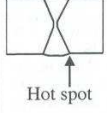
101

Table 37 – SCF proposed for welds in pipelines

→ SCFs for tubular connections are presented in section 2.8 and Appendix 2); the SCFs parametric equations proposed by Efthymiou (1988) [57] are adopted for standard connection geometry. For more complex geometries, a finite element analysis (linear elastic, usually with a unit load) should be used. Given the fact that, theoretically, the stress at the weld tow is equal to infinity, an appropriate extrapolation should be considered (DNV CN 30.7, IIW guidelines).

Appendix F: Approach for the identification of a load sequence for renewable applications.

For the variable amplitude fatigue loading tests in the FATHOMS fatigue test program, connected to the renewable application field, a pre-existing spectrum was modified on purpose. This spectrum comprised 63 pairs of values of stress range and cycle number and is illustrated in Figure 115 below. The spectrum was based on a constant value of the fatigue load ratio, R = 0.
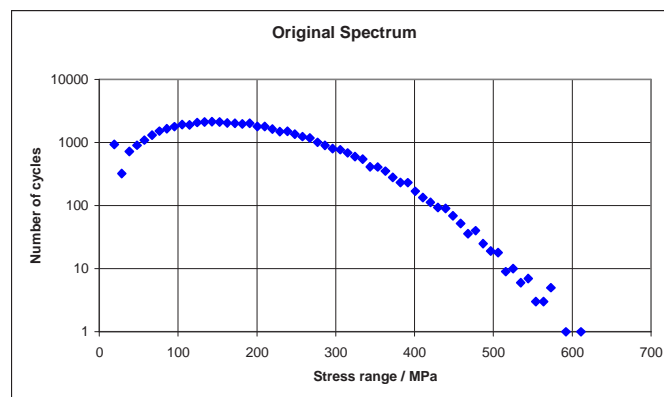
Figure 115 - Original fatigue spectrum supplied to Corus by CSM

For fatigue testing, and the generation of a randomised sequence loading history, it is convenient to simplify the spectrum by reducing the numbers of pairs of stress range and cycle values.

A fatigue loading spectrum comprises a set of pairs of values of stress range ($\Delta\sigma_i$) and number (n_i) of cycles at that stress range.

Fatigue design SN curves are of the form:

$$N_i = \frac{K}{\Delta\sigma_i^m}$$

where

N_i is the number of cycles of stress range $\Delta\sigma_i$ for failure

K, m are constants for a given detail class

Fatigue damage, D, is calculated using Miner's summation:

$$D = \sum \frac{n_i}{N_i} = \frac{1}{K} \sum n_i \cdot \Delta\sigma_i^m$$

The fatigue damage D_i for the *i*-th pair of stress range and cycle number is:

$$D_i = \frac{n_i}{N_i} = n_i \cdot \frac{\Delta\sigma_i^m}{K}$$

The proportion of the total fatigue damage due to the *i*-th pair is therefore given by:

$$\frac{D_i}{D} = n_i \cdot \frac{\Delta\sigma_i^m}{K} \cdot \frac{K}{\sum n_i \cdot \Delta\sigma_i^m} = \frac{n_i \cdot \Delta\sigma_i^m}{\sum n_i \cdot \Delta\sigma_i^m}$$

In this way the original spectrum was reduced to 16 pairs by replacing successive sets of 4 pairs from the original spectrum by a single pair, in which the number of cycles was equal to the sum of the numbers of cycles in the 4 replaced pairs and in which the stress range was set at a value such that the fatigue damage was equal to that in the 4 replaced pairs. The procedure is presented in algebraic form as follows:

The *j*-th pair in the simplified spectrum corresponds to 4 pairs, numbered *i* to (*i*+3), in the original spectrum. By definition, the fatigue damage due to the *j*-th pair in the simplified spectrum is equal to the summed damage from the 4 corresponding pairs in the original spectrum,

$$D_j = D_i + D_{i+1} + D_{i+2} + D_{i+3} = \frac{1}{K} \cdot \sum_i^{i+3} n_i \cdot \Delta\sigma_i^m$$

From the equation for the design SN curve,

$$`D_j = n_j \cdot \frac{\Delta\sigma_j^m}{K}$$

Hence,

$$n_j \cdot \Delta\sigma_j^m = \sum_i^{i+3} n_i \cdot \Delta\sigma_i^m$$

By definition,

$$n_j = n_i + n_{i+1} + n_{i+2} + n_{i+3}$$

Combining the two previous results,

$$\Delta\sigma_j^m = \frac{\sum\limits_{i}^{i+3} n_i \cdot \Delta\sigma_i^m}{\sum\limits_{i}^{i+3} n_i}$$

And so:

$$\Delta\sigma_j = \left[\frac{\sum\limits_{i}^{i+3} n_i \cdot \Delta\sigma_i^m}{\sum\limits_{i}^{i+3} n_i}\right]^{\frac{1}{m}}$$

Following this procedure a simplified spectrum was obtained, illustrated in Figure 116 below, using the value m=3 (appropriate for fatigue design of welded steel structures).
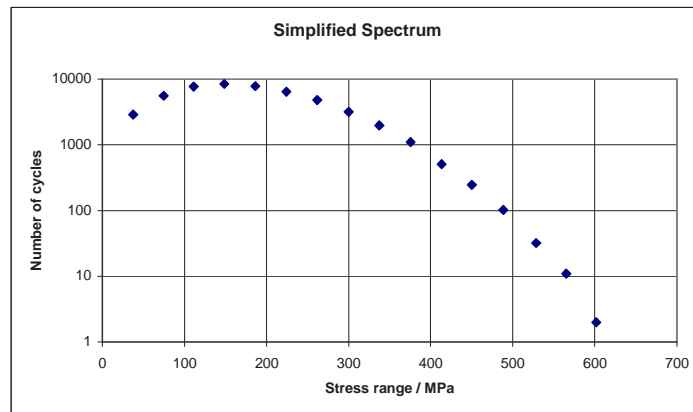
Figure 116 – Simplified spectrum

The two spectra are compared in Figure 117 below in terms of the cumulative fraction of the total number of cycles and the cumulative fraction of the total fatigue damage.
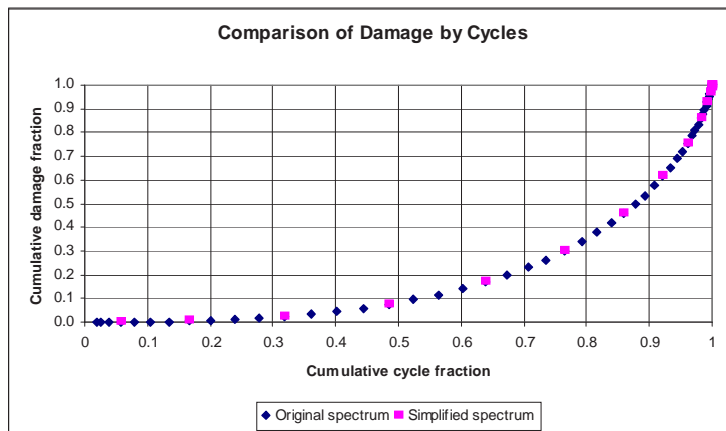
Figure 117 – Comparison of the original and simplified spectra

The contributions of the stress ranges in the simplified spectrum to fatigue damage and to the cycle count are illustrated in Figure 118 below.
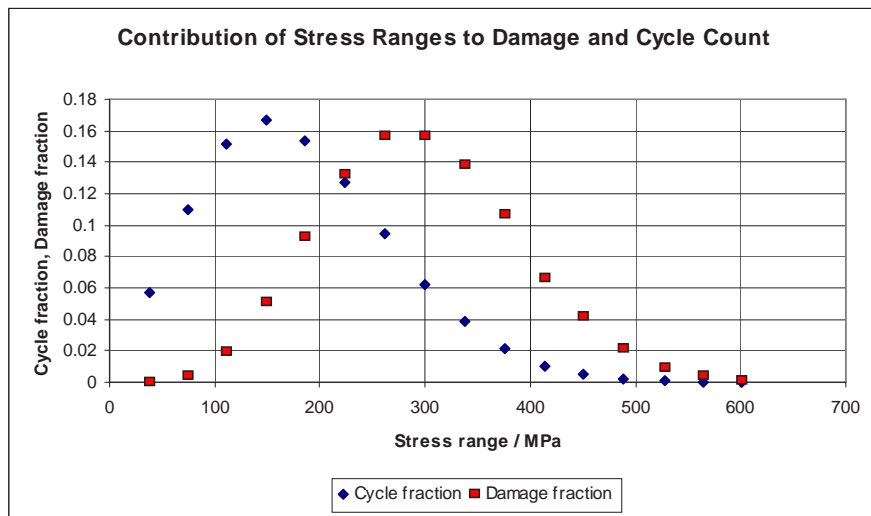
Figure 118 – Contributions to fatigue damage and cycle count in the simplified spectrum

It can be seen that the three smallest stress ranges contribute a very small proportion of the total fatigue damage while accounting for a substantial proportion of the total number of cycles. In order to reduce the time required for fatigue tests, it was decided to delete these three stress ranges from the spectrum. The small number of cycles at the highest stress ranges were, however, retained. The resulting spectrum is referred to as the abridged simplified spectrum.

In the original spectrum a fatigue load ratio R=0 was used. For the specimen design and loading arrangement to be used in the FATHOMS fatigue tests, on welded plates, it is desirable to employ a positive minimum load. It can readily be shown that the application of a constant positive value of R produces spurious cycles when a randomized loading sequence is generated from the spectrum. It was therefore considered to be more appropriate to apply a constant mean stress. The presence of the large amplitude cycles, however, implies that very large peak stresses will occur when a sufficiently large mean stress is applied to ensure a positive minimum load. It was therefore decided to impose a cut-off value for minimum stress. An example of the application of this to a portion of a random sequence loading history is illustrated in Figure 119 below.

The selection of appropriate values for the mean stress and the minimum stress cut-off involves a compromise. The selection of a large value for the mean stress would allow the large amplitude cycles to be retained, but would result in a history containing a very high value of peak stress. A lower value for the mean stress limits the value of the peak stress, but results in a larger proportion of the cycles being affected by the cut-off. A high value for the cut-off stress would distort the large amplitude cycles, but a low value could lead to practical difficulties in accurately controlling the required load value. The mean stress and cut-off stress values were arbitrarily selected as 300 MPa and 40 MPa, respectively. The modified spectrum, produced by the application of this mean stress and cut-off stress to the abridged spectrum, is referred to as the truncated spectrum.

mean_stress		200	MPa		trough_cut_off		50	MPa
R	mean	0.303						
	min	0.100						
	max	0.458						
	std_dev	0.118						
highest_peak		500.8	MPa					
deepest_trough		50	MPa					
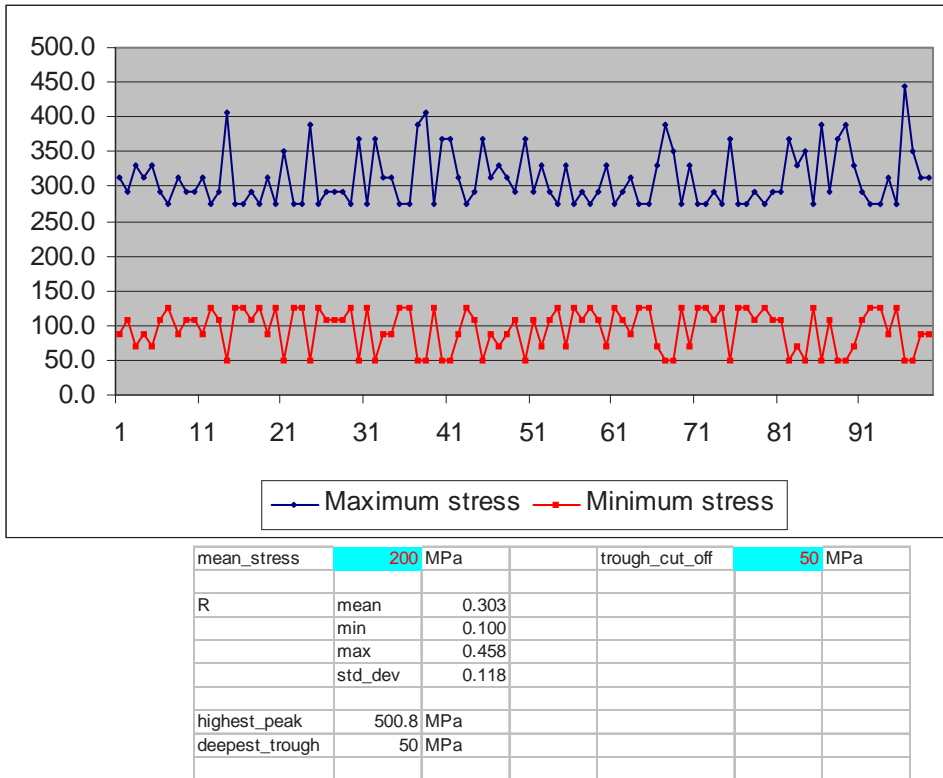
Figure 119 – Application of mean stress and minimum stress cut-off

The truncated spectrum and the abridged spectrum are compared in Figure 120 and Figure 121 below. For practical use in fatigue testing, it is desired to scale the spectrum. The truncated spectrum was therefore converted to a loading history with turning points expressed as fractions of the peak stress (i.e. as fractions of the maximum value of maximum stress). The resulting loading history is referred to as the basic load sequence; for each individual fatigue test these turning point values will be multiplied by the appropriate scaling factor. The characteristics of the four stress spectra, and of the basic load sequence, are summarized in Table 38 below.
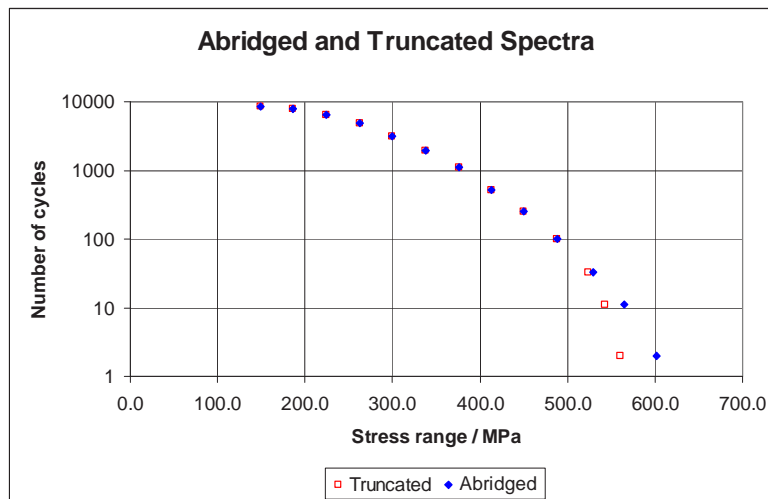
Figure 120 – Composition of truncated and abridged spectra

106
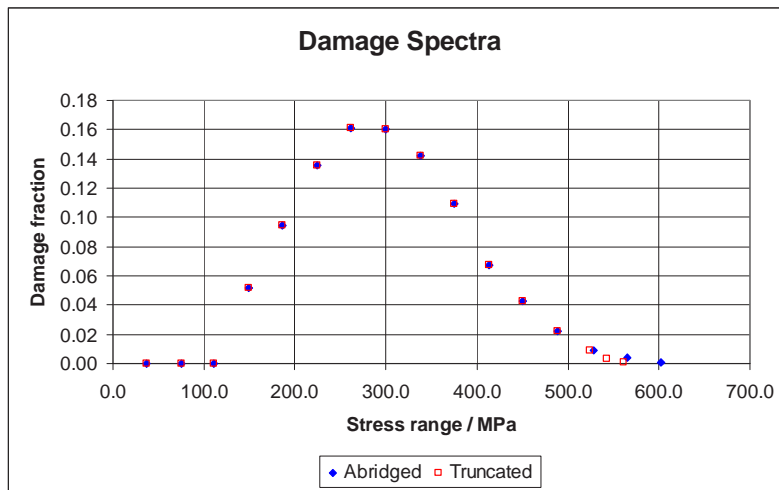
Figure 121 – Damage contributions in the truncated and abridged spectra

Spectrum	Length	Min. stress occurrence	Max. stress occurrence	Equivalent constant amplitude stress range	Damage relative to CSM spectrum
	Cycles	MPa	MPa	MPa	
CSM	50674	0.0	611.0	220.8	1.000
Simplified	50674	0.0	601.6	220.8	1.000
Abridged	34541	0.0	601.6	248.9	0.976
Truncated	34541	40.0	600.8	248.8	0.975
Basic load sequence	34541	(6.66%)	(100%)	(41.41%)	------

Table 38 - Summarized characteristics of spectra

Appendix G: Approach for the identification of a load sequence representative of real in service conditions of Steel Catenary Risers.

Steel Catenary Risers stress originated from environmental loading and are determined by vessel and riser dynamics. Therefore the resultant stress histories are strongly dependent on the field location, on the vessel employed and on characteristics and configuration of the riser. Stresses vary also along riser length.

A way to know these stresses is the collection of data from real measurements, but this could be expensive and difficult in deepwater locations.

An easier way is simulating and analyzing riser behaviour through Finite Element Analysis.

At the present time sophisticated codes with a Finite Element approach are available and are used for riser simulation. They are generally employed by oil companies, contractors and consultants, for design and analysis of dynamic risers. They allow to make static and dynamic analyses of offshore systems under environmental loading like waves and currents. DNV-OS-F201 (Appendix A) [52] and DNV-OSS-302 (Appendix B) [51] give general requirements and basic features for this type of software, and gives an overview of some of the commercial software currently used.

The offshore system is basically defined by the vessel and the risers. Vessel is described by its motion characteristic, the Response Amplitude Operator (RAO). Risers are defined through parameters like length, section geometry, material, internal fluid and configuration. Environmental conditions applied could be water depth, soil characteristics, current profiles and waves. In particular random waves are set through wave spectra like JONSWAP and Pierson-Moskowitz, defined by couples of Hs and Tz parameters.

From input data, first a static analysis is performed, giving riser disposition, curvature, static tension and bending. After, a time domain dynamic analysis is performed, giving time dependant results. The most significant ones are axial tension, bending moment and stresses (with variable amplitude). The results could be available in the form of time histories, spectra and statistics. Often an animation file is available, allowing to have a general understanding of the environment and of the vessel/riser motions.

Additional tools may be added to the basic software. One category in particular is aimed to perform fatigue analysis. Generally damage is calculated by Rainflow counting of variable amplitude stress ranges occurring during each sea state. The contributes of each sea state are summed up according to the probability of occurrence given by the scatter diagram. In such way the fatigue life along the riser is determined allowing to identify the most critical sections.

This type of software are useful to determine real stress histories of different sections along the riser, including the critical areas. Such histories can be elaborated through cycle counting to obtain the distribution of the stress range over the entire life of a riser. These distributions can be the starting point for the definition of a loading sequence for fatigue testing.

The following approach for the determination of a variable amplitude sequence has been developed:

1. Simulation of an offshore system under real environmental conditions.

2. Tracing of the time histories of stress in a selected riser section (preferably a critical section, in the Hang Off or in the Touch Down Point).

3. Composition of the time histories of stress into a global sequence representative of riser stress in a long period.

4. Testing on a machine suitable for variable amplitude loading.

As regards the first point, it has to be underlined that a representative offshore system, have to be selected, together with a specific environment, related to a geographical area. In this way the sequence could not be considered as a generic offshore sequence, but is related with the system and location selected. In this case a simplified riser-platform system has been selected, with one riser hanging from a Semisubmersible platform, as the one shown in Figure 122. Environmental conditions representative of Gulf of Mexico have been chosen, together with 1524 m water depth, representative of the state of art in deepwater platforms. Seastates representative of Gulf of Mexico conditions are listed in Table 39.

Figure 122 – Semisubmersible vessel with one free hanging Steel Catenary Riser

Seastate No.	Sig. wave Height Hs [m]	Wave Peak Period Tp [s]	Frequency [h/year]
1	0.61	2.8	367
2	0.61	4.2	1932
3	0.61	5.6	893
4	1.22	4.2	712
5	1.22	5.6	1668
6	1.22	7.0	466
7	1.83	5.6	774
8	1.83	7.0	638
9	1.83	8.5	121
10	2.44	7.0	366
11	2.44	8.5	143
12	3.05	8.5	116
13	3.66	8.5	45
14	4.27	9.2	29
15	4.88	10.6	4.5
16	5.49	10.9	3.1
17	6.10	11.1	2.2
18	6.71	11.4	1.4
19	7.32	11.7	0.9
20	7.92	12.1	0.6
21	8.53	12.4	0.45
22	9.14	12.7	0.265
23	9.75	13.0	0.2
24	10.36	13.3	0.12
25	10.97	13.7	0.085
26	11.58	14.0	0.057
27	12.50	14.5	0.038

Table 39 - Gulf of Mexico Seastates

About riser section, the geometry of one of the two pipe to be tested in the FATHOMS programme has been chosen:

→ Outer Diameter = 273.1 mm
→ Wall Thickness = 14.2 mm

In order to identify the critical section, a fatigue analysis is to be performed, as it allows to find where fatigue life is lower, as shown in Figure 123.
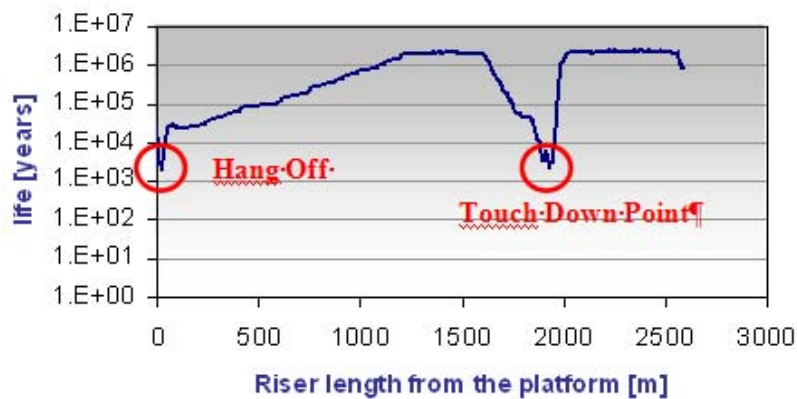
Figure 123 - Fatigue life along riser length

Time histories of stress for the selected riser section are obtained from every sea state dynamic analysis.

The stress histories from each seastate have to be combined in a single block representative of the global stress history of the riser section in one year. Every stress history should repeated proportionally to the probability of occurrence of the relative seastate in a long period, typically one year. As regards the testing phase, the software of a standard servo-hydraulic machine has been modified in order to make it suitable to apply variable amplitude loading sequences. Its interface is shown in Figure 124.
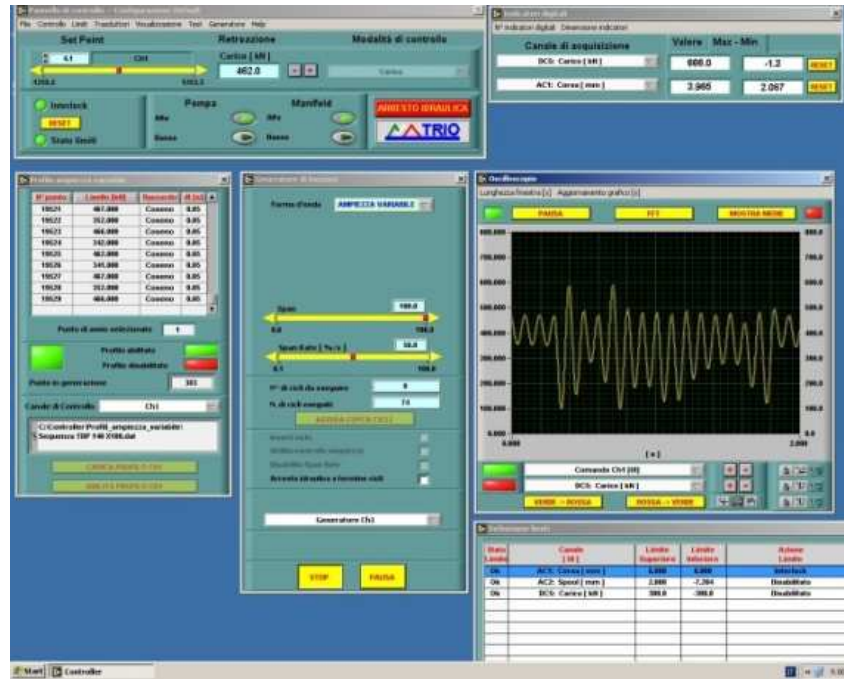
Figure 124 – Interface of the machine properly modified for variable amplitude testing

The global stress history have to be in a form suitable for the testing machine, in particular have to be filtered in order to obtain a sequence of maximum and minimum load points (peaks and valleys).

Moreover, in order to reduce the number of cycles and hence the testing time, a criterion for truncation have to be adopted. Considering the le recommendations of the International Institute of Welding [58] for variable amplitude loading, all the cycles below the cut off limit of the SN curve considered, at 10^8 cycles, are excluded (see Figure 125).
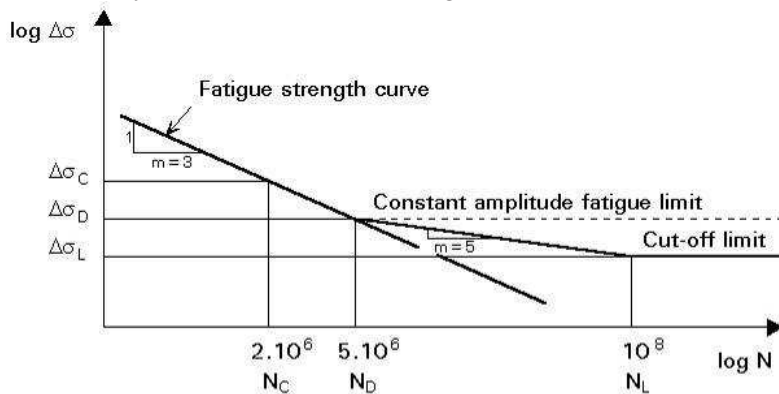
Figure 125 – Cut Off for Variable amplitude fatigue

For the curve considered, DNV-RP-C203 F1, evidenced in Figure 126, the level of cut off is 23.25 MPa.
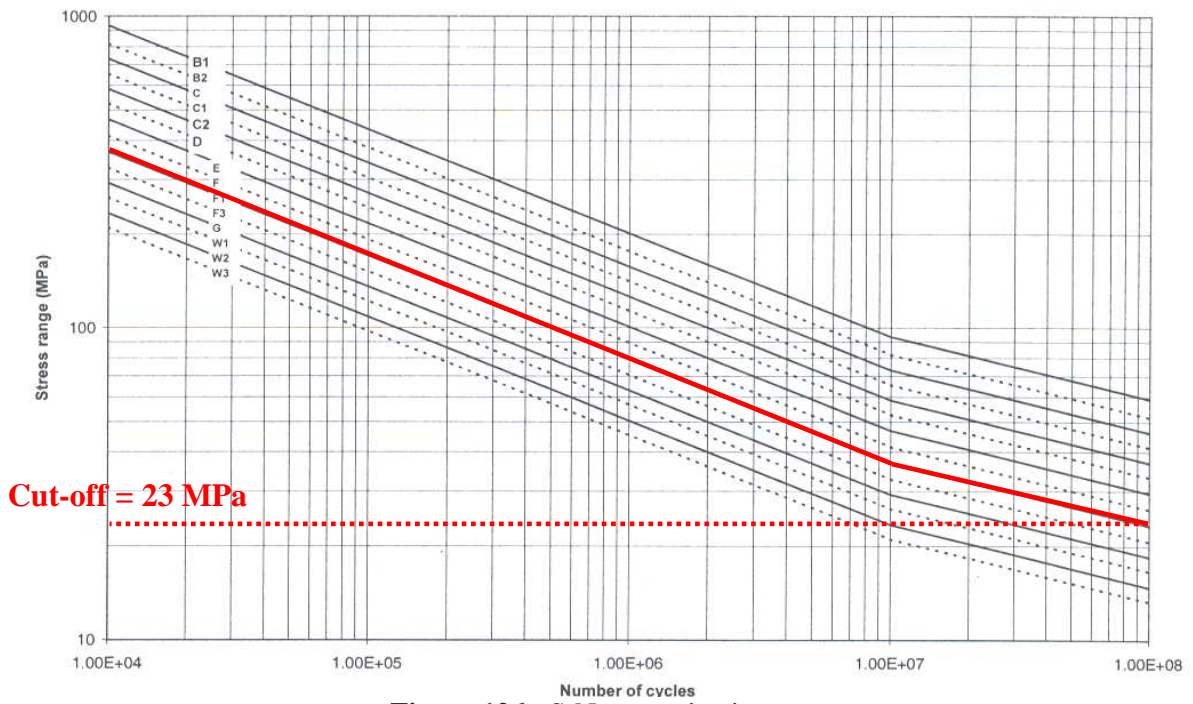
Figure 126 - S-N curves in air

The final result is a sequence made up of 19529 points (maxima and minima), giving 9764 cycles.

In Figure 127 the Stress Distribution for the final sequence is shown, where:

      S/Smax   is the ratio between Stress Range and the maximum value of Stress
                           Range found in the sequence

      N Cycles   is the Number of Cycles of each class of S/Smax value
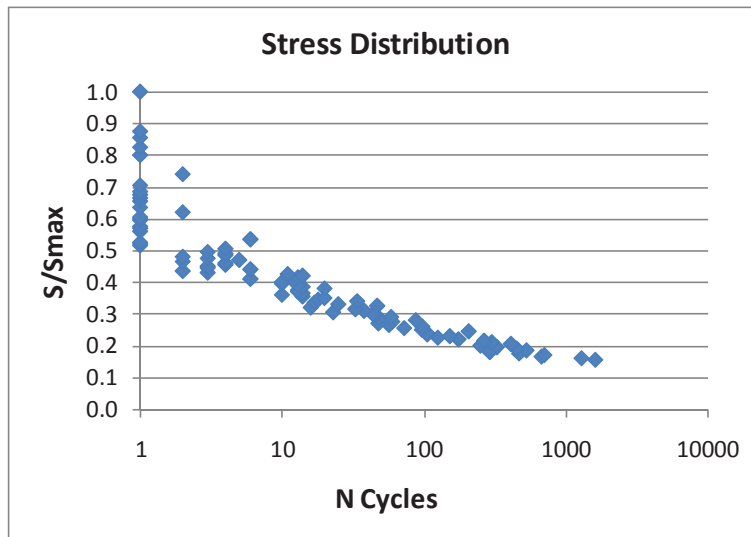
Figure 127 – Stress Distribution for the sequence representative of Steel Catenary Riser loading

Appendix H: Post-welding treatments

1. Reduction in stress concentration

1.1 Surface finish

The fatigue limit tends to increase with strength. Steels of similar strength have similar fatigue limits regardless of manufacturing processes such as casting, forging, rolling or welding [59]. However the manufacturing processes may have inherent flaws such as inclusions, shrinkage cavities and cracks which may have a bearing on the fatigue limit. The critical surface roughness a_c, below which the fatigue limit for a plain specimen cannot be reduced was obtained from experimental results (Figure 128) [59]. The predictive equation relating a_c and yield strength was derived by Usami using short crack fracture mechanics, assuming $\Delta K_{TH} = 6.2$ MPa $\sqrt{m}$:

$$a_c = 1700 \, \sigma_y^{-2}$$
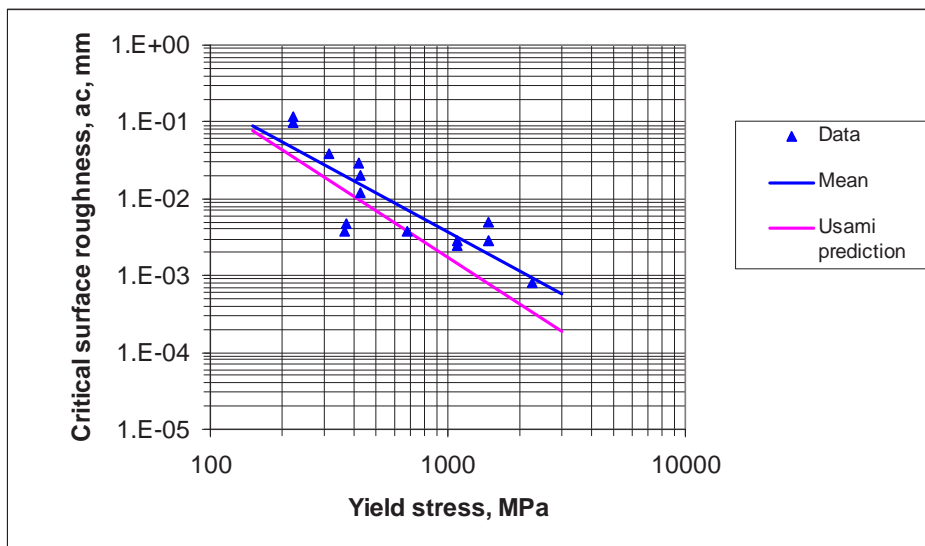
Figure 128 - Relationship between yield stress and critical surface roughness for steel

This suggests that surface finish is absolutely critical for UHS steels, such as those used in aerospace, with finishes ~ 1 m required. In contrast, for structural steels, the values appear to be ~20-50 m and as-rolled surface finishes are usually within this range. For high strength steels such as turbine blades (~700 MPa), it is possible to obtain a small increase in fatigue endurance by improving the surface finish to a mirror finish, and this has been tried by Rolls Royce on turbine blades used in generators at Redcar Power Station.

1.2 Weld geometry improvement methods

Weld geometry improvement methods seek to improve the weld shape and/or remove weld defects. Machining methods are generally applied to weld toes and are devised to remove or reduce size of the weld toe flaws from which fatigue cracks propagate. At the same time, they aim to reduce the local stress concentration effect of the weld profile by smoothly blending the transition between the plate and the weld face.

Remelting methods remove weld defects by remelting weld metal and parent metal in the weld toe, and similarly result in a smoother transition between the weld and the parent plate. IIW recommendations [24] provide extensive guidance on the effective performance of the burr grinding and TIG dressing methods, together with rules on the extent to which the improved performance can be relied upon in design calculations. Special welding techniques seek to achieve a low stress concentration by controlling the overall shape of the weld to obtain a

concave profile and requiring a gradual transition at the weld toe, or use specially developed electrodes with coatings that have good wetting and flow characteristics.

1.3 Weld toe grinding

In weld toe grinding a disk grinder or rotary burr grinder (see Figure 129) is used to remove metal from the weld toe. The technique of weld toe grinding was established in the 1960s and although widely applied in offshore oil rigs, it was only formally recognized as a recommended practice in 1990 [25] [60]. The latest recommendations for weld toe grinding are contained in the International Institute of Welding (IIW) draft recommendations [24]. The equipment used is usually a high-speed pneumatic, hydraulic or electric grinder with a rotation speed of 1500 – 4000 rpm. The tool bit is normally a tungsten carbide burr with a hemispherical end. To avoid notch effects the diameter of the burr should be scaled to the thickness of the parent metal and is typically 10 to 25 mm for 10 – 50 mm thick sections.

Figure 129 - Pneumatic grinder and burrs [24]

Weld toe grinding has 2 effects:

(a) The removal or reduction any local sharp imperfections introduced by welding, notably undercut, cold laps, large slag inclusions and crack-like flaws, all of which form initiation sites for fatigue cracks.

(b) It reduces the local stress concentration effect of the weld profile by smoothly blending the transition between parent metal and weld.

The procedure requires the removal of material at the weld toe to a sufficient depth, usually of 0.5 – 1 mm, to remove all traces of undercut or other weld toe discontinuities (see Figure 130 [24]). The final surface must be smooth with any grinding marks oriented normal to the weld toe. There are slightly different recommendations depending on the source. Bignonnet [61] recommended a radius no less than 0.25 x thickness, and 4 x grinding depth. The last two conditions are to reduce the stress concentrations due to the groove produced by grinding, to ensure that it does not act as a notch. BS 7608 [23] and the DEn recommendations [25] require that grinding should be 0.5 mm below the bottom of any visible undercut, with a maximum depth of grinding into parent plate of 2 mm or 0.05 t, whichever is less.
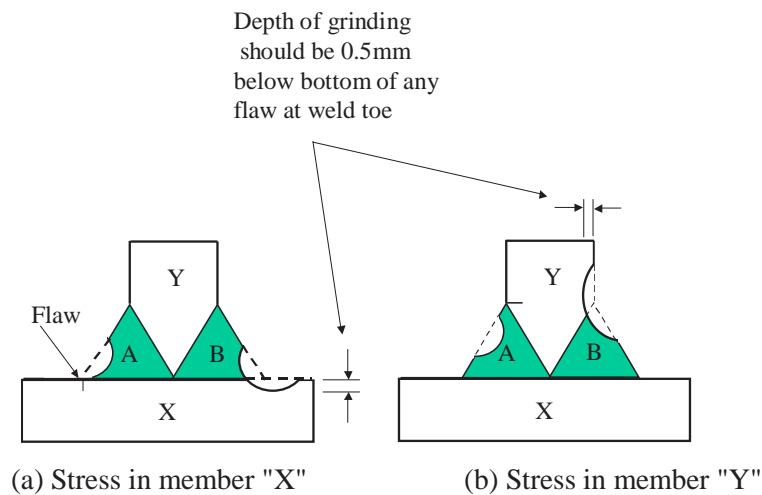
Figure 130 - (a and b): Toe grinding to improve fatigue [24]

It should be noted that grinding a weld toe tangentially to the plate surface as in example "A" in Figure 130, will produce little improvement in fatigue strength. Grinding should extend below the surface as in "B", in order to remove the weld toe flaws.

The results obtained using this technique depend greatly on the amount of care taken when performing the operation. In the case of disk grinding, the grinder leaves scratches parallel to the weld bead. These score marks favour crack initiation, and should be eliminated using a small burr tool [61].

Weld toe dressing has been reported to produce an improvement of 2.2 in fatigue life of welded joints [23],[25],[60],[61]. This is equivalent to a 30% increase in stress. This improvement can be claimed for joints in air and those exposed to seawater with adequate protection against corrosion. In the IIW draft [24] the allowable improvement is x1.5 on stress, for steels >300 MPa yield, corresponding to x3.4 on life for details in FAT 90 class or lower. Higher classes are either not welded or already improved. However, the maximum improved class, which can be claimed is the closest category below the new value. For example, when a FAT63 class is toe ground the new value will be 63 x1.5 = 94.5, which gives a FAT 90 class[*].

In austenitic and duplex stainless steels Maddox has recently shown weld toe grinding to produce a minimum 30% improvement in fatigue strength [62]. This benefit was shown to increase with a decrease in applied stress to the extent that the fatigue limit was increased by more than 60%. Thus the maximum benefit of this improvement technique was in the high cycle low stress regime, which confirms the behaviour previously observed for carbon steels.

Maddox [62] also showed that for thin material (3 mm) toe grinding was less successful due to small radii and the loss of wall thickness (up to 20%). This indicates the limited scope for using toe grinding in such thin material. Indeed the draft IIW recommendation is for a thickness limit of 6 mm [24].

1.4 Weld dressing
Tungsten Inert Gas (TIG) dressing is a relatively standard process for weld improvement, with plasma dressing also available. The aim is relatively similar to weld toe dressing i.e. to remove weld toe imperfections and reduce the stress concentration effect of the local weld toe profile by

---

[*] In the IIW draft, fatigue design curves have the same relationship as in BS 7608 i.e. log N = log K_2 – m log S. However all the curves have a slope of 3. The class of the curve is defined by the stress at 2 x 10^6 cycles i.e. FAT90 has S= 90 MPa at 2 x10^6 cycles. Because m = 3, this one definition (FAT90) uniquely describes the equation of the curve.

providing a smooth transition between the plate and the weld. These aims are achieved by re-melting the weld toe region using a TIG or plasma welding torch, without the addition of any filler metal.

For sensitive steels such as austenitic and duplex stainless steels, control of microstuctures can be achieved by the addition of varied amounts of nitrogen in the shielding gas [59].

A typical TIG dressing is shown in Figure 131 (a), together with a micrograph showing improvement in weld profile (Figure 131 (b)).

For an optimum result the re-melted line has to be positioned carefully with respect to the weld toe. Normally, the best result is obtained when the arc is located a small distance from the weld toe, at an appropriate angle and with a small backward tilt. (Figure 132 (a)).

If the arc is positioned too close to the weld bead it may result in the formation of a new toe. According to Kado et al [63], the optimum position 0.5-1.5 mm results in a smooth blend as shown in Figure 132 (b).
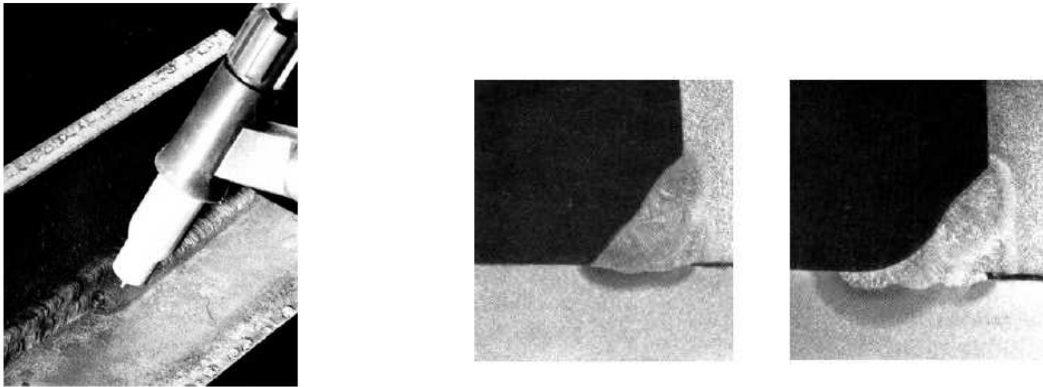
(a) TIG dressing(b) before and after TIG dressing

Figure 131 - (a and b): TIG dressing and improvement in profile
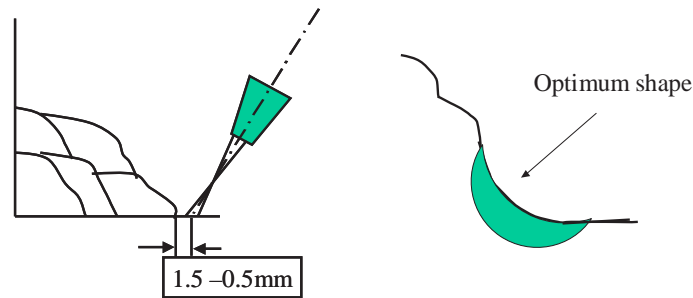
(a) Typical position   (b) Optimum profile

Figure 132 - (a and b): Position of welding torch to produce optimum weld bead shape for good fatigue properties from Kado et al [63]

For IIW FAT 90 or lower class the benefit of TIG dressing is to increase the allowable stress range by a factor of 1.5, corresponding to a factor of 3.4 on life.

2. Residual stress methods

Residual stress methods involve local plastic deformation to either reduce the level of residual tensile stresses from welding or to create a region of beneficial compressive residual stresses. Mechanical peening methods involve substantial plastic deformation at the weld toe, and in some cases this can be sufficient to effectively obliterate some forms of weld toe defect. Hammer peening and needle peening are covered in the IIW recommendations [24]. The proprietary 'UIT' ultrasonic impact peening technique has recently been the subject of extensive fatigue test programmes [64] [65] [66]. Overloading methods involve the use of quasi-static forces (rather than the impulsive forces used in peening).

An initial overload of a structural member can produce tensile plastic strain at stress concentrations such as welds; upon removal of the initial overload the elastic relaxation of the structure results in the creation of residual tensile stresses in the yielded regions. The local compression method uses a pair of dies to cause yielding in the through-thickness direction; due to constraint by surrounding material, this results in the generation of residual compressive stresses acting parallel to the plate surface. Appropriate selection of locations for local compression allows protection of localised notches such as the ends of longitudinal fillet welds. Thermal methods include stress relief heat treatment (to reduce the residual stresses from welding) and the use of differential thermal expansion/contraction to generate compressive residual stresses. Spot heating and Gunnert's method involve localised thermal treatments. Low temperature transformation electrodes are used to generate compressive residual stresses from the volume changes associated with a low temperature martensite transformation of weld metal.

3. Applications considerations

It has been shown in laboratory tests that it is sometimes possible to improve the performance of welds to the extent that fatigue failure eventually occurs in parent metal away from the weld detail, as illustrated in Figure 133 below.

Figure 133 - Examples of laboratory fatigue tests in which weld improvement has led to eventual failure away from the weld detail [64] [67].

However, a number of concerns must be addressed when using weld improvement techniques to achieve increased fatigue life:

→ Complete coverage must be ensured,
→ In processes involving modification of residual stresses, only indirect methods are generally available for verification that the required effect has been achieved,
→ Improvement in one area (e.g. weld toe) may result in little overall benefit if another area (e.g. weld root) then becomes the governing fatigue detail,
→ Where weld improvement is achieved through modifications to residual stresses, the effect may be lost as a result of service loads (e.g. vibratory stress relief or overloads).

These concerns contribute to a generally cautious approach by design and regulatory authorities (for example, IIW [68]), according to which:

→ Weld improvement is recognised only in connection with repair or upgrading of existing structures, and not for general use in design in order to obtain a longer fatigue life than the use of standard design S-N curves would give;
→ Fatigue tests for the verification of the procedure in the endurance range of interest are recommended.

Results from tests on welded assemblies employing ultrasonic impact treatment have shown a marked change in the inverse slope of the log-log S-N curve [64], as indicated in Figure 134 below. This observation would be consistent with a substantial increase in the proportion of the fatigue life occupied by fatigue crack initiation. Attempts have been made to describe the fatigue life of such welds using a two-stage model combining a propagation life derived from the behaviour of as-welded joints and an initiation life derived from a strain-life approach [69].

In the context of the FATHOMS project, two particularly significant points would follow if it could be confirmed that a dominant portion of the life of such improved welds was governed by the process of initiating an engineering-sized crack:

→ While fatigue crack propagation behaviour is insensitive to the tensile properties of the material, fatigue crack initiation properties are related to strength and ductility. It may therefore be possible to obtain enhanced improvements for higher strength steels.
→ Existing fatigue design approaches for corrosive conditions such as seawater are effectively based on the increase in fatigue crack growth rates observed in aggressive environments. The influence of the environment might be considerably reduced if the fatigue life was dominated by initiation rather than propagation, provided that corrosion damage (such as pitting) did not create initiation sites.
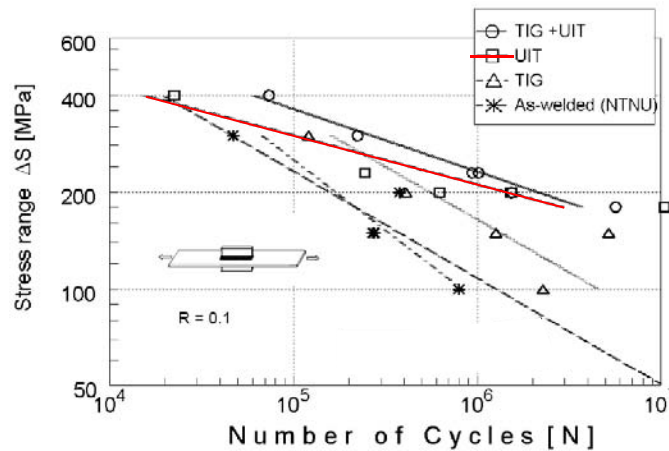
Figure 134 - Reduced slope of S-N curve for welds improved by ultrasonic impact treatment (adapted from [64])

4.   Post welding treatment
4.1 Ultrasonic peening – Technique description

Ultrasonic peening was selected as a promising technique to increase the general fatigue strength of the structure. This technique consists in the application of ultrasonic- and mechanical-impulses to the high stressed locations in the weld; as a result of these ultrasonic- and mechanical-impulses the welded metal is modified at the atomic- and/or metallurgical-level. Ultrasonic peening contributes in reducing the local stress concentration at the weld toe and in relaxing residual stresses and creating a compressive stress field (down to three mm) beneficial for the fatigue resistance of the weld. Furthermore this treatment assures that crack – like flaws possibly present at the weld toe are removed; this introduces a fatigue crack initiation phase in the fatigue crack grow process so that for a treated weld the total fatigue life is extended by the number of cycles that it takes for the fatigue crack initiation.

The ultrasonic peening equipment consists of the ultrasonic frequency generator and the ultrasonic peening tool. The ultrasonic generator produces frequencies 20-25 kHz and has a Peak Output or max pulsed power of 3kW with an average continuous output power of 600W. The ultrasonic peening tool is air cooled to ensure continuous max output for demanding treatments in terms of power demand and/or time requirement. The device is shown in Figure 135.

Figure 135 - Ultrasonic generator and peening tool

The ultrasonic peening tool comprises a piezoelectric converter and a booster. The piezoelectric converter transform electrical energy into mechanical pulses and it frequency is defined by the frequency produced by the ultrasonic generator.

The working head of the ultrasonic peening tool can vary according to the needs and the type of weld to be treated. In the case of the treated weld we used solely working heads at 90° angle relative to the tip of the converter (booster). For other applications we have developed working head at 45° working angle to the tip of the converter (booster), for example.

The working head can be single striker or multi striker (see Figure 136).The single striker can have either 3 mm diameter or 4 mm diameter giving a tip radius of 1.5 mm alternatively 2.0 mm. The smallest diameter is used to clean the weld toe of weld imperfections whereas the pin with tip radius 2 is used to decrease the local stress concentration at the weld. That is to produce a smooth transition between the weld metal and the parent plate. The multi-striker is used to clean the weld and the adjacent areas from weld spatter and induces a general relaxation of tensile residual stresses produced during the weld process. As a result the use of the multi-striker is beneficial for the removal of weld spatter and for the redistribution of weld induced residual stresses.

Figure 136 – Single and multi striker working heads

4.2 Ultrasonic peening on fatigue samples from FCAW girth welded pipes

The contractor selected to perform ultrasonic peening on the joints of interest was Lets Global, an engineering and consulting company based in the Netherlands, which main field of business is the life extension of welded structures and components. Lets Global specializes in the application of ultrasonic peening treatment on customer's installation in the offshore field.

Ultrasonic peening was applied on FCAW welded strips both X70 and X100 destined to the fatigue program (see Figure 137). It was stated to apply the treatment only on FCAW welds as for LH welds the weld geometry at the root pass was sensibly of good quality. The treated locations are shown in Figure 138.

Figure 137 – Fatigue specimens destined to the fatigue program
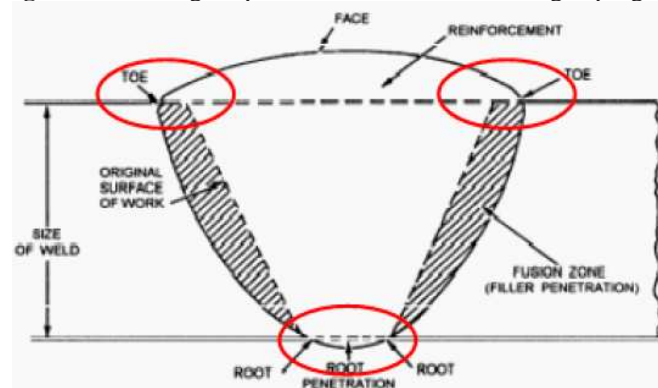
Figure 138 – Treated locations in fatigue specimens

The first step was to clean out the weld toe region of crack-like imperfections adopting a single peen diameter 3 mm with tip radius 1.5 mm. After the weld toe is free from imperfections the next step was to obtain a smooth transition between the weld material and the parent plate. It was done with a single pin diameter of 4 mm. After this the welded strips were treated by multi striker giving the positive effect as relaxes the tensile residual stresses produced by the welding procedure. Furthermore the introduction of compressive stresses up to certain depth produced by

119

the ultrasonic peening treatment has also a positive effect on the fatigue life extension of the treated welds.

Both sides of the weld were treated. Fatigue specimens after treatment by ultrasonic peening are shown in Figure 139.
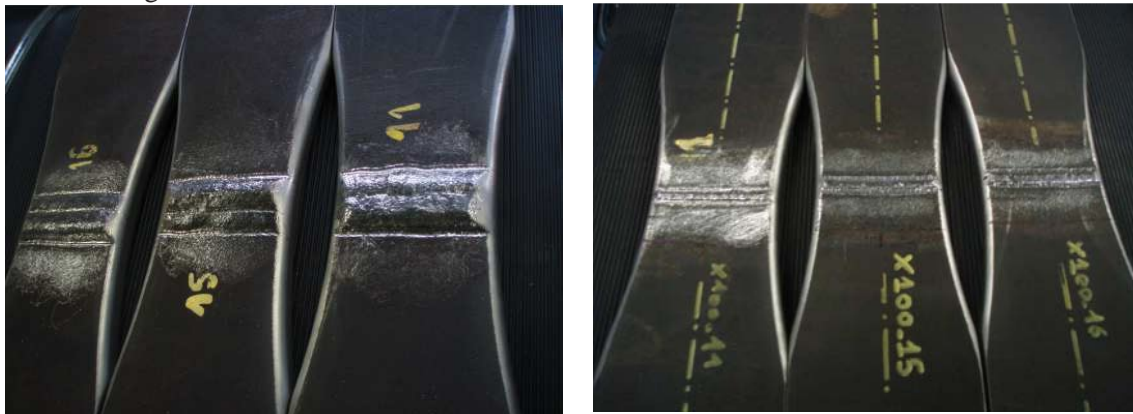
Weld cap   Weld root
Figure 139 – X100 – FCAW - UP treated specimens

Residual stresses on treated samples were measured by X-ray diffraction method. In Figure 140, as an example, the comparison between the residual stresses measured before and after UP on the inner surface of a X100 FCAW welds, is reported. As evident after the treatment residual stress field is strongly compressive.

The same situation is noticeable on X70 FCAW welds in Figure 141 where the residual stress field after applying ultrasonic peening is shown.
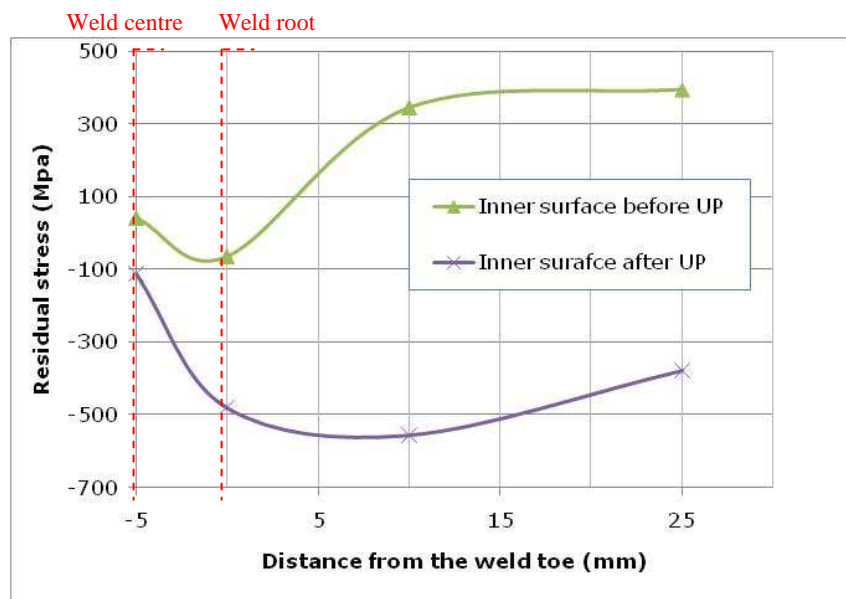
Figure 140 – X100 FCAW – Residual stresses before and after UP

120
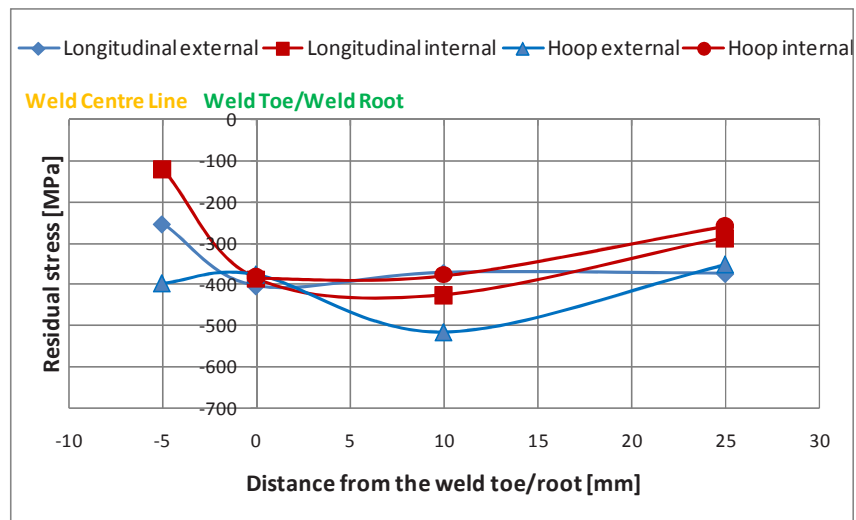
Figure 141 – X70 FCAW – Residual stresses after UP

Appendix I: WPS and weld mechanical characterization

1. SAW welds on T plates – WPS and mechanical characterization

In order to produce a number of submerged arc full penetration fillet welded 'T' joint specimens for fatigue studies, the RQT 701 plates were laser cut and beveled and fillet welded using the following welding specification, as developed by Corus.

Welding was carried out using low hydrogen practice - for Submerged Arc Welding (SAW) a scale D hydrogen level (between 5 and 10 ml/100 g) was targeted. The actual welding preparation is shown in Figure 142. The consumable utilized here was a 3.2 mm diameter wire (SD3 2.5Ni, 0.5Cr, 0.5Mo) with flux OP121.
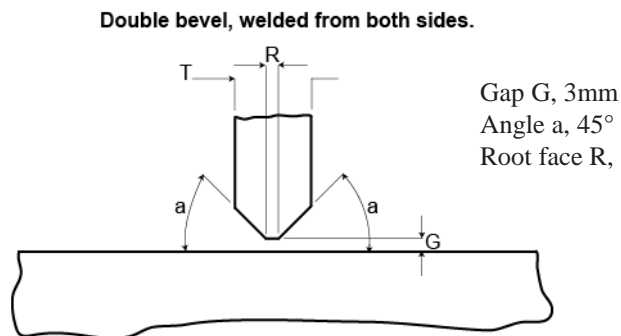
Figure 142 - Weld preparation for the RQT 701 Fillet welded T joint

The equipment used for the RQT701 welding trials is illustrated in Figure 143 below. The welding power source was a commercial ESAB "LAD 1400" welding rectifier unit rated at 44 V / 1400 A. The electrode feed unit employed a commercial ESAB "PEF" control box. The carriage and beam assembly employed a Corus RD&T in-house design rack-and-pinion system and a commercial ESAB "A6-PTF" speed controller.

Figure 143 - Equipment used for RQT701 welds

The amount of preheat required is dependent upon factors such as hydrogen levels, welding heat input as well as the fixed factors of plate CEV and thickness. In this case, a preheat of 75° C was used, for both welding and for tacking the plates together - based on an assumed hydrogen level of approximately 5 ml/100 g and a welding heat input of approximately 1.5 kJ/mm.

In order to determine whether the level of preheat was sufficient, trial welds were made to ensure that weld defects were kept to a minimum (i.e. hydrogen cracking or solidification cracking).

Examination of macro sections from Trial 1 revealed that full penetration had not consistently been achieved. In an attempt to correct this deficiency, Trial 2 used a higher arc current for the first pass on the first side, in conjunction with a higher travel speed to maintain the same value of arc energy. Examination of macro sections from Trial 2 revealed that this had led to blow-through. In order to avoid these identified problems the strategy adopted for Trial 3 concentrated on achieving a sound deposit of weld metal in the first pass on the first side, and relying upon the first pass on the second side to attain full penetration. Accordingly, arc current for the first pass on the first side was reduced to a value below that used in Trial 1; travel speed was increased to the highest controllable level consistent with an arc energy greater than 1.5 kJ mm-1. The arc current for the first pass on the second side was increased while retaining an arc energy of 1.98 kJ mm-1. Trial 3 led to satisfactory welds giving repeatable welds, in terms of geometry, penetration and hardness levels.

This procedure was then used for the manufacture of all further samples. Details of the trial welding parameters are given in Table 40.

Basic metallography and hardness tests were performed on the weld details obtained from each trial. Figure 144 shows the results from tests performed on sample 3 (from trial 3).

Traverse A suggests that the hardness in the HAZ, around the weld toe region is quite high approaching 350 HV - much higher than that exhibited throughout the rest of the weld. This is probably due to the fact that subsequent weld passes have refined most of the weld, apart from the weld toe region.

Trial	Side	Pass	Arc voltage	Arc current	Travel speed	Arc energy (heat input)
			V	A	mm min⁻¹	kJ mm⁻¹
1	1	1	33	650	650	1.98
		2	33	600	600	1.98
	2	1	33	700	700	1.98
		2	33	600	600	1.98
2	1	1	33	700	700	1.98
		2	33	600	600	1.98
	2	1	33	700	700	1.98
		2	33	600	600	1.98
3	1	1	33	600	750	1.58
		2	33	600	600	1.98
	2	1	33	750	750	1.98
		2	33	600	600	1.98

Table 40 – Parameters for RQT701 welding trials
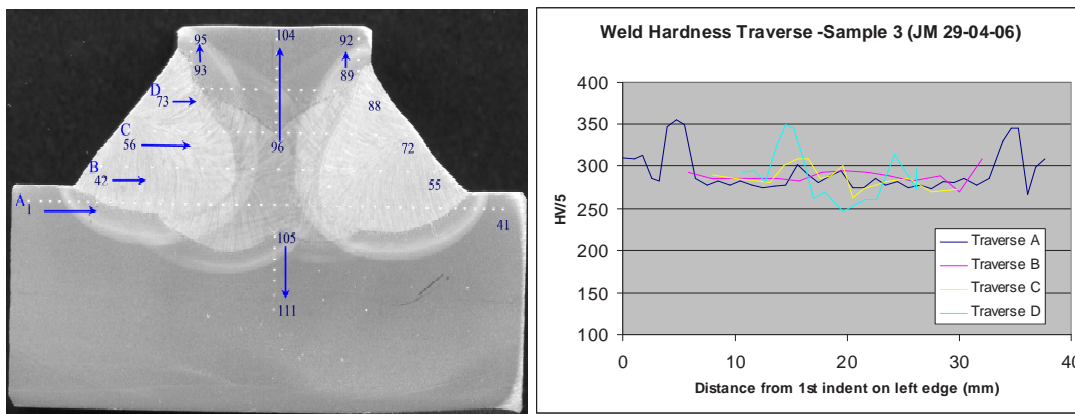
Figure 144 - Macrograph and hardness traverse for trial 3

The nominal dimensions of the SAW full penetration fillet welded 'T' joint fatigue specimens are shown in Figure 145.
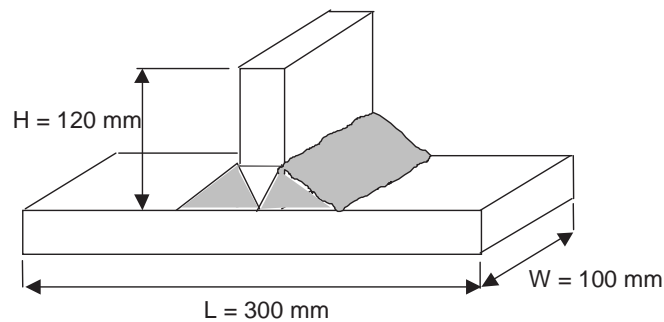
Figure 145 - SAW full penetration fillet welded 'T' joint - fatigue specimen dimensions

The characterisation performed included the following activities:

→ Macro-etching along the joint in order to highlight both the weld metal and the HAZ extension and documentation of microstructure.

→ Mechanical characterization including micro-hardness measurements along the joint, tensile tests, Charpy V tests, CTOD tests and Fatigue crack growth rate (FCGR) tests.

→ Residual stresses measurements

As regards the mechanical characterization, it should be noted that all fatigue crack growth rate, CTOD and Charpy tests were performed on parent plate material, as any cracks initiating and growing from the full penetration fillet weld toe in a welded 'T' joint in service, will, for the most part sample parent plate. (see the macrograph in Figure 144). The results are reported in detail in the following.

1.1 Macro-etching and documentation of microstructure

Stereo-Optical microscopy was performed on the transverse section of the "T" joint specimen etched with a solution of 30% HNO_3 in H_2O. Results are shown in Figure 146 where the weld metal, as well as the HAZ is clearly highlighted.
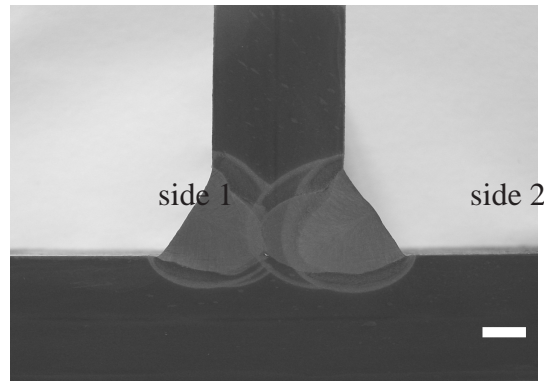
Figure 146 - Macro structure of the SAW fillet weld

Full metallographic analysis was performed on the cross section by etching with Nital 2%. The base plate exhibited a fine microstructure, which consists of tempered lath martensite and carbides (Figure 147). From Figure 148, to Figure 150 the microstructure at various positions within the HAZ is presented. The microstructure near the boundary with the base plate consists of aggregated carbides and ferrite (Figure 148), while towards the weld metal contains plate martensite and ferrite (Figure 149). At the interface with the weld metal a mixture of martensite, acicular ferrite and small quantities of Widmanstatten ferrite can be found (Figure 150). The weld metal exhibits a fine microstructure which consists of acicular ferrite and carbides (Figure 151).
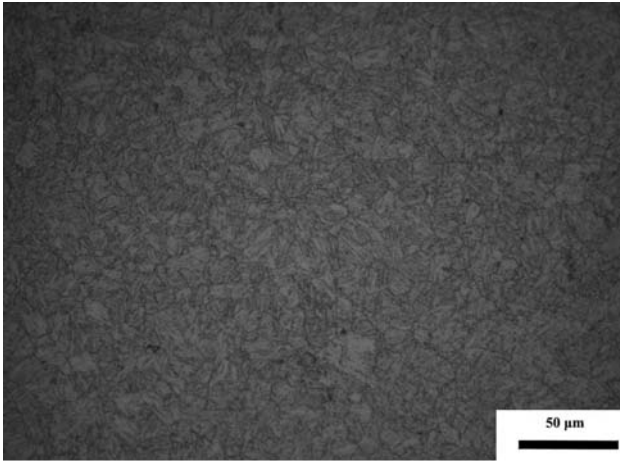
Figure 147 – Base Metal- Lath martensite and carbides
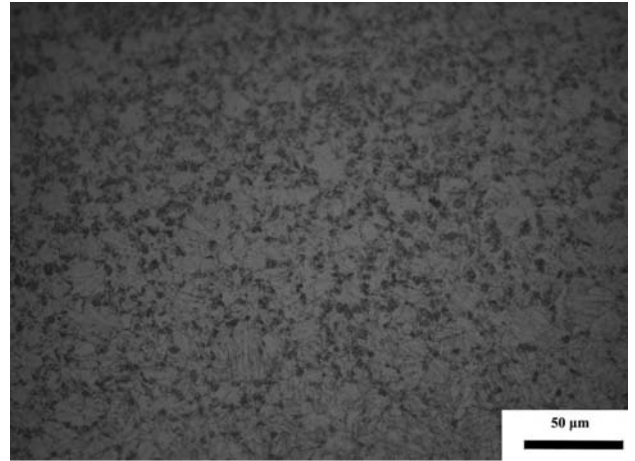
Figure 148 - HAZ at the interface with the base metal- aggregated carbides and ferrite
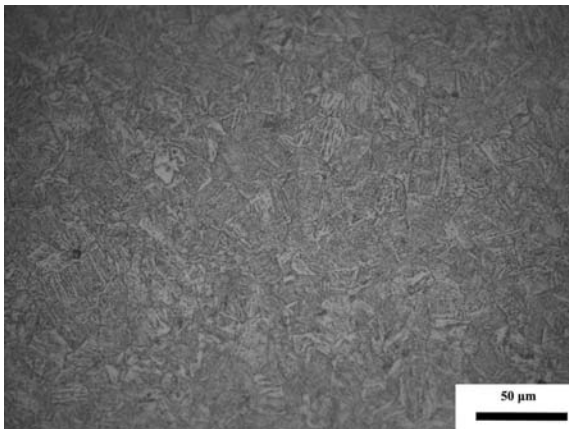
Figure 149 - Center of the HAZ- Plate martensite and ferrite
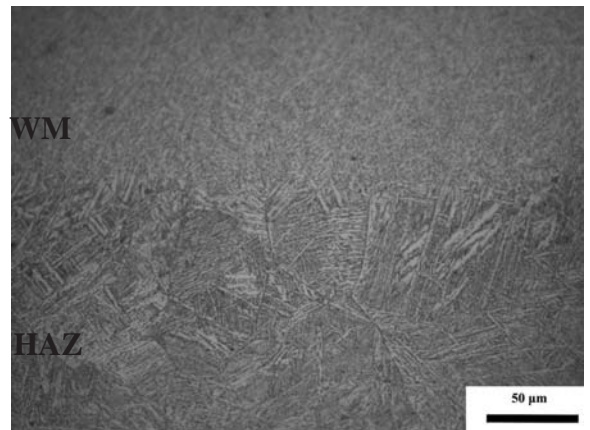
Figure 150 - HAZ /weld metal interface- Ferrite and martensite
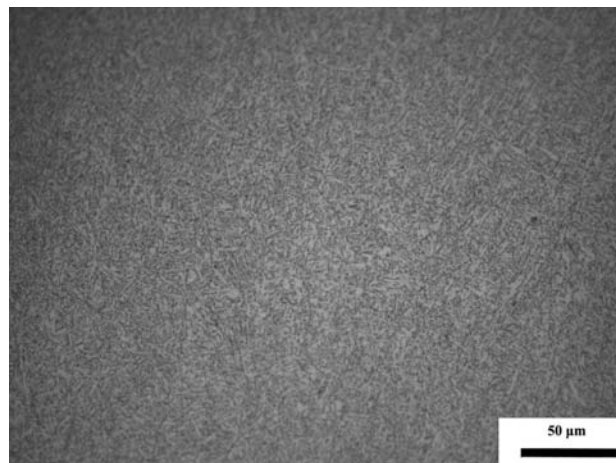
Figure 151 – Weld metal- Acicular ferrite and carbides

1.2 Mechanical characterization

Microhardness measurements were performed according to the profiles shown in Figure 152, with a load of 2kgr on Vickers scale. The results in detail are presented in Figure 152. All measurements are within the range of 220-335 HV_2.
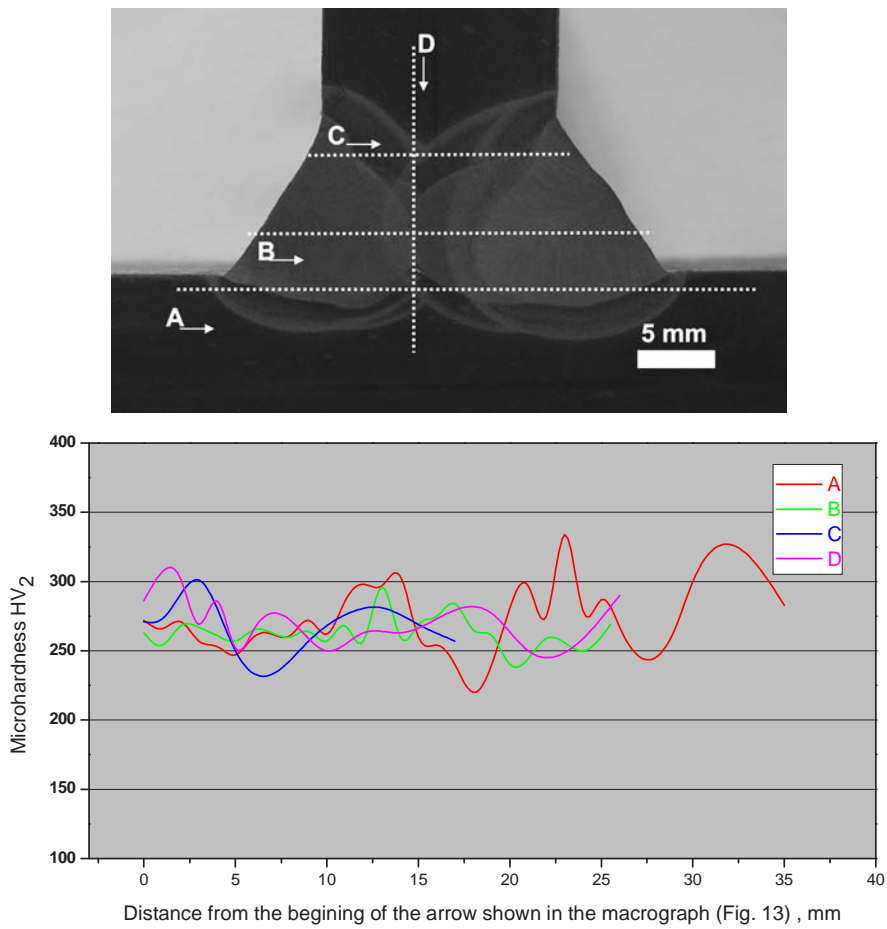
Figure 152 - Microhardness measurements

Tensile tests were carried out according to BS EN 10002 - part1 [70] on round specimens taken in both longitudinal and transverse (in terms of the rolling direction) at RT and at T=-10°C. The results are shown in Figure 153.

It is clear that for the longitudinal specimens, the yield strength of the material remains largely unaffected by changes in the test temperature – however, for the transverse specimens, yield strength is increased by approximately 10% as the test temperature is reduced. For both specimen orientations, the tensile strength of the material increases by approx. 20% as the test temperature reduces. In terms of '%' elongation and reduction of area, no significant effects from reducing the test temperature were apparent.
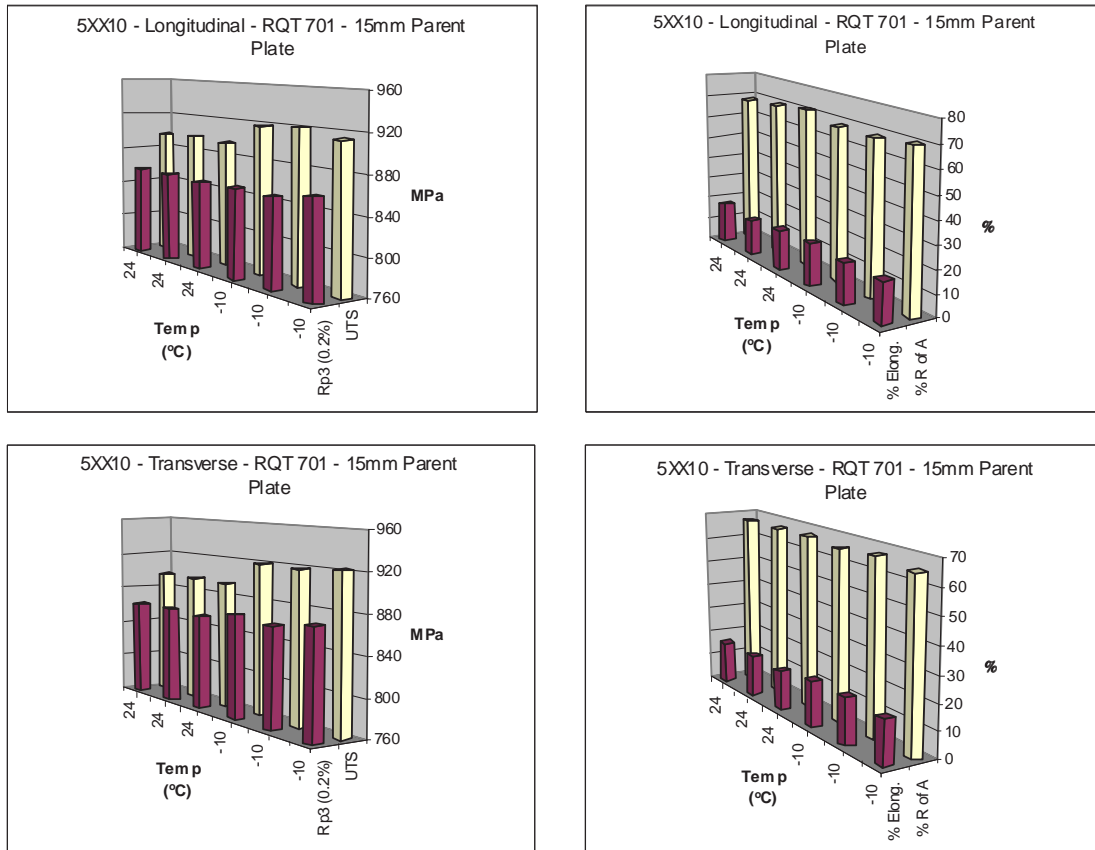
Figure 153 - Results of tensile tests on RQT 701 Parent Plate

Charpy impact tests to BS EN 10045 Part 1 [14] were conducted on specimens taken from the parent plate material and machined with the notch parallel to the plate rolling direction. A Ductile-Brittle Transition Temperature (DBTT) curve was generated as shown in Figure 154 giving a $T_{27J} = -62$°C.
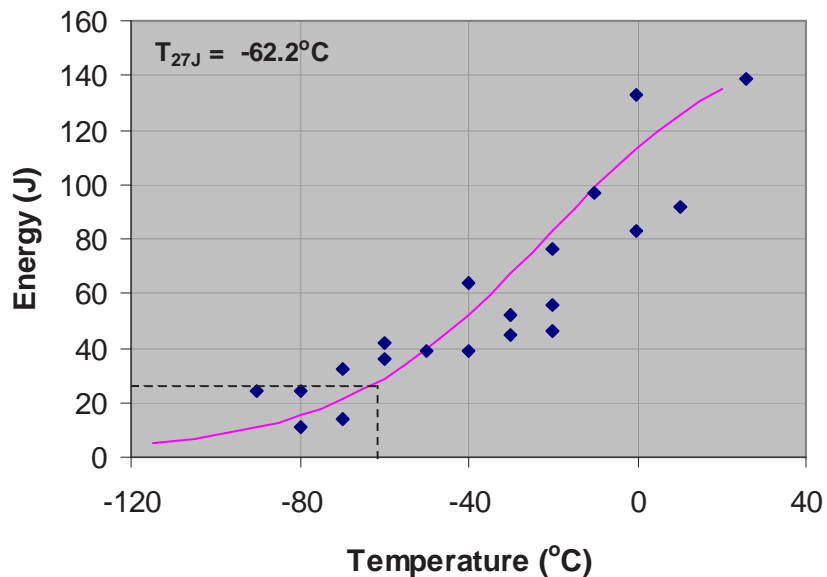
Figure 154 - Ductile-Brittle Transition Temperature Curve for Parent RQT 701 Plate Material

127

Fracture toughness (CTOD) tests were performed by SENB specimens machined from the parent plate with notch perpendicular (T) and parallel (L) to the plate rolling direction according to [15]. Tests were performed at RT and at T=-10°C and the results are reported in Table 41.

The results are typical of that obtained for Q&T steels having a yield strength of the order of 700 MPa [73]. The results suggest that the fracture toughness values obtained from the specimens notched perpendicular to the RD are, on average, approximately 25% greater than those obtained for specimens notched parallel with the RD - not unexpected as the cracks in the former specimens will be growing across the direction of grain flow.

Specimen ID	Orientation	Test Temp. (°C)	Notch Position	CTOD, δ (mm)	CTOD Fracture Type [1]
5XX10 -12	T	RT	Parent	0.176	m
5XX10 -13	T			0.187	m
5XX10 -14	T			0.160	m
5XX10 -21	L			0.128	m
5XX10 -22	L			0.146	m
5XX10 -23	L			0.141	m
5XX10 -24	L			0.126	m
5XX10 1a	T	-10		0.164	m
5XX10 1b	T			0.239	m
5XX10 1c	T			0.177	m
5XX10 1d	T			0.150	m
5XX10 2a	L			0.144	m
5XX10 2b	L			0.136	m
5XX10 2c	L			0.159	m
5XX10 2d	L			0.133	m

Notes: (1) m = maximum load

Table 41 – Fracture toughness test results

Fatigue crack growth rate tests were carried out in accordance with ASTM E647-05 [74]. Tests were performed at RT on CT specimens with notches machined in longitudinal (L) and transverse (T) direction, at stress ratios R=0.1 and R=0.7. The results of the fatigue crack growth rate tests in terms of da/dN versus ΔK are shown in Figure 155.

Best fits to the straight-line regions of both the longitudinal and transverse fatigue crack growth data yield the Paris Law constants, C and m, outlined in Table 42. These constants, C and m govern the speed of fatigue crack growth and are thus critical inputs when, for example, defining safe inspection intervals for structures and components which are subjected to cyclic loading conditions in service. It is clear that the slopes (m values) obtained here for the transverse specimens are slightly higher than those obtained for the longitudinal specimens – however, these small differences are well within the bounds of experimental error and would not greatly influence any subsequent fatigue life calculations.

(a) Longitudinal   (b) Transverse
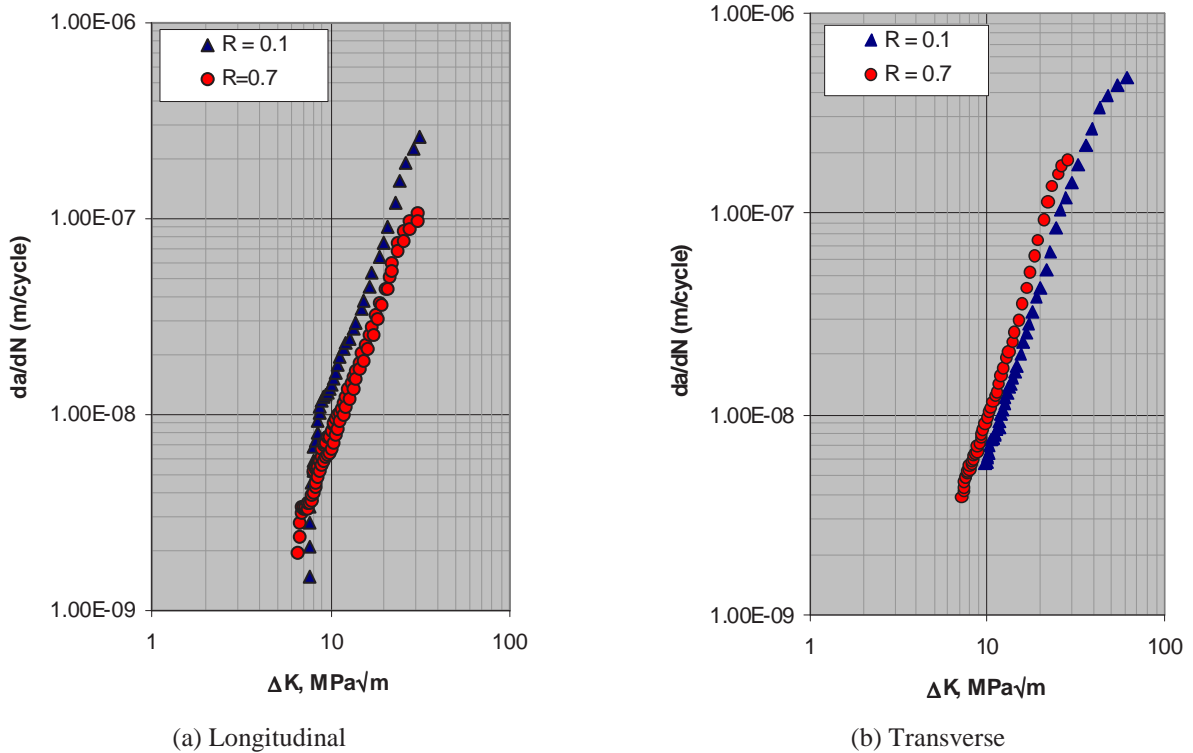
Figure 155 - FCGR data obtained for RQT 701 parent plate material tested in air at RT at R-ratios of 0.1 and 0.7

Material	R-Ratio	C	m
Longitudinal	0.1	4.08×10^{-11}	2.539
	0.7	2.45×10^{-11}	2.462
Transverse	0.1	8.32×10^{-12}	2.863
	0.7	1.29×10^{-11}	2.892

Note: The Paris Law coefficients (C) and exponents (m) were determined from regression analyses of log(da/dN) - log (ΔK) data, where da/dN in m/cycle and ΔK in MPa $\sqrt{m}$

Table 42 – Summary of Paris Law constants obtained from FCGR experiments conducted in air

1.3 Residual stress measurements

X-ray diffraction measurements were performed on a T-Joint plate of RQT 701 SAW welded by X-Ray diffraction (RIGAKU Strainflex MSF-2M)

Residual stresses were measured in longitudinal and transverse directions, in the centre of weld seam, at the weld toe and at 10 mm and 100 mm away from the weld toe (see blue areas in Figure 156).
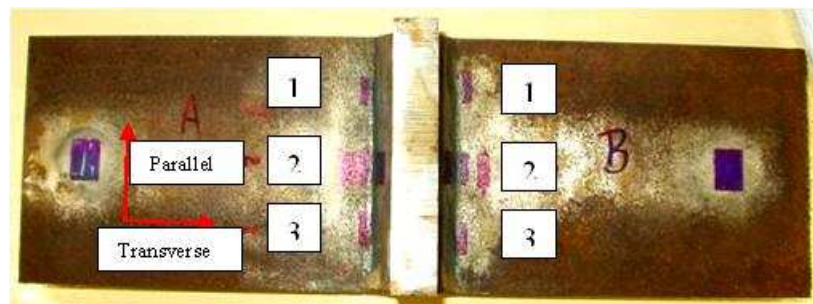
Figure 156 - Locations of residual stress measurements (Blue areas)

The measured stress values are presented in Figure 157 and Figure 158.

129
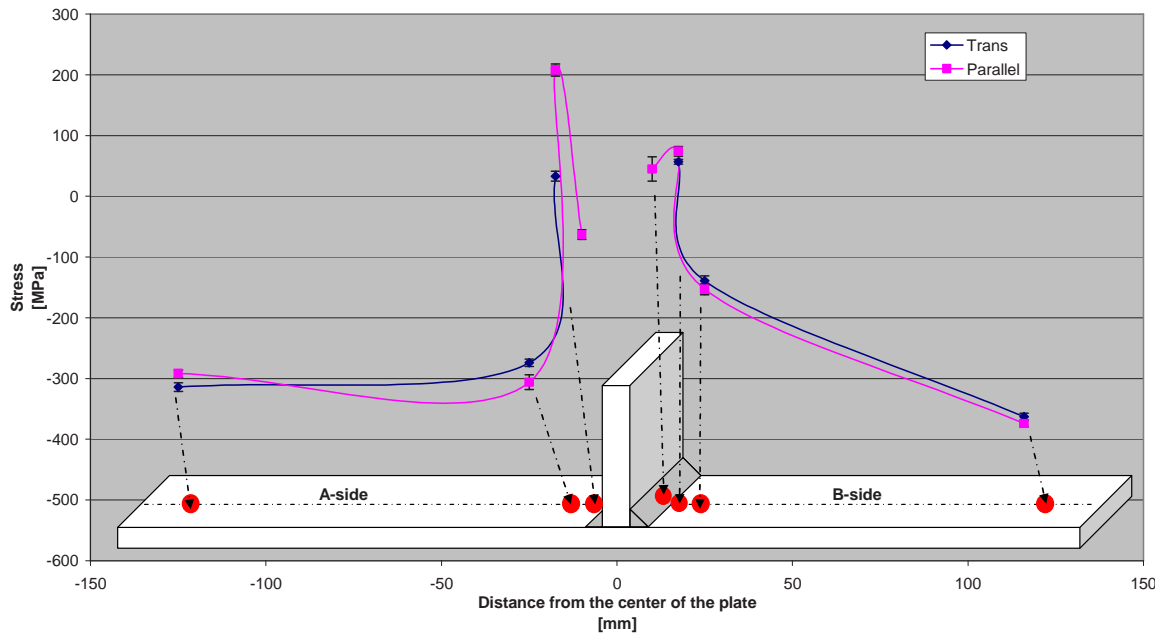
Figure 157 - Parallel and transverse stress profile along a line at the middle of the plate
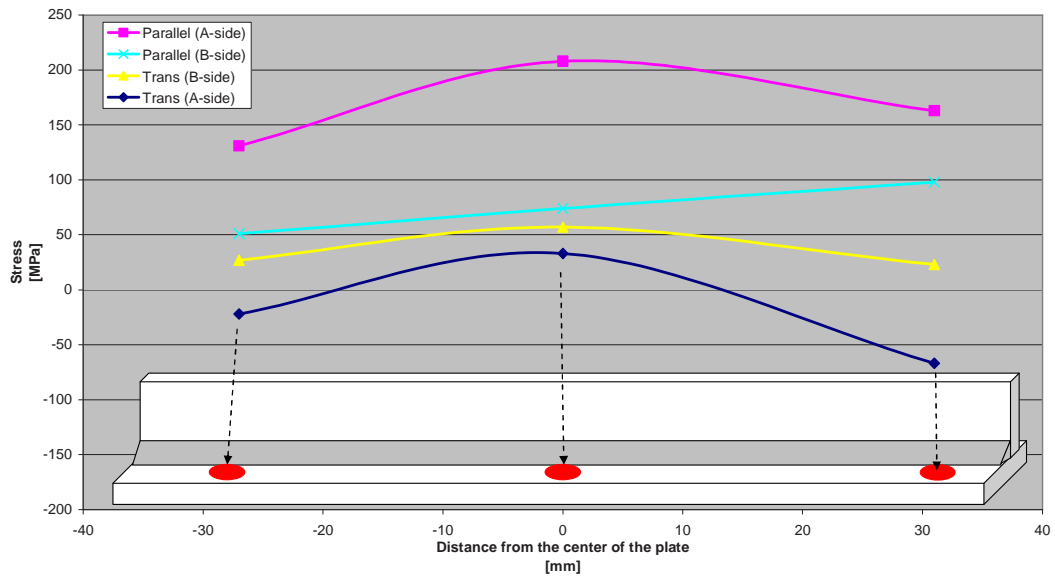
Figure 158 - Parallel and transverse stress profile at the weld toe in both sides of the plate

The following conclusions can be drawn (see Figure 157 and Figure 158):

– Residual stresses are mainly tensile in both transverse and parallel directions at the weld toe and weld seam.

– Residual stresses are mainly compressive in both transverse and parallel directions at 10 mm and 110 mm away from the weld toe.

2 FCAW welds - WPS

2.1 X100 FCAW welded pipes

Details of WPS and welding parameters for X100 FCAW butt joints are reported in Figure 159, in Table 43 and in Table 44.
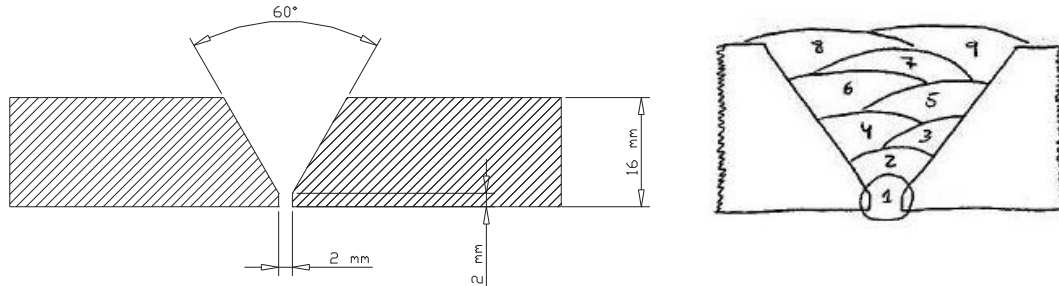
Figure 159 - Weld preparation and welding sequence for the X100 FCAW butt joints

Welding process	Size of filler material	Current (A)	Voltage (V)	Type of current/polarity	Filler material	Preheat T (°C)	Interpass T (°C)
FCAW	1-2	150-350	27-35	DC+	OK1509	130	165

Table 43 – Welding specifications for X100 FCAW butt joints

Run	Welding process	Size of filler metal (mm)	Current (A)	Voltage (V)	Type of current/polarity	Wire feed speed (m/min)	Welding speed (mm/s)	Heat Input (kJ/mm)
1			236.50	29.00		13.00	3.40	2.00
2			265.00	29.90		13.00	4.80	1.65
3			257.00	28.95		13.00	6.20	1.20
4			271.50	29.85		14.00	7.10	1.10
5	FCAW	1.2	271.50	29.90	DC+	14.00	7.40	1.10
6			273.50	29.90		14.00	6.80	1.20
7			264.00	29.90		14.00	9.00	0.90
8			287.50	29.90		14.00	5.80	1.50
9			300.00	29.90		14.00	4.00	2.20

Table 44 – Welding parameters for X100 FCAW butt joints

2.2 X70 FCAW welded pipes

Details of WPS and welding parameters for X70 FCAW butt joints are reported in Figure 160 and in Table 45 and Table 46.
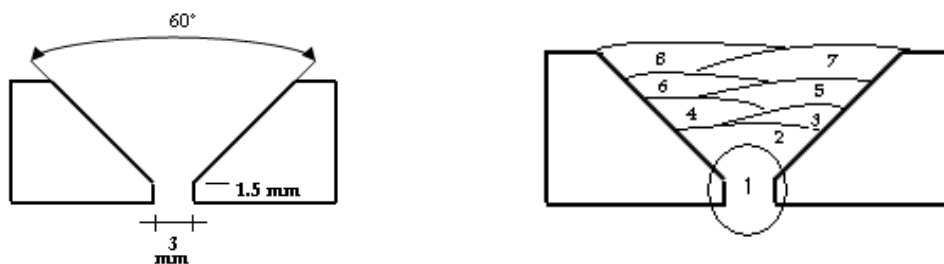
Figure 160 - Weld preparation and weld sequence for the X70 FCAW butt joints

131

Filler material designation and make	EN 758 T 46 5 1Ni P M 1 H5 (EN 758) Filarc PZ6138 (ESAB)
Any Special Baking or Drying	None
DesignationGas/Flux: -Shielding	M21 (EN 439) – Ar 80% / CO$_2$ 20%
Gas Flow Rate -Shielding	18 L/min
Distance contact tube/work piece	15 mm
Welding position	PA (down hand)
Preheat Temperature	100ºC (EN1011-1)
Interpass Temperature	250ªC
Other information	Run 1 – Semi – automatic
	Runs 2 to 8 – Mechanized
	Ceramic support in the root side

Table 45 – General preliminary welding specifications (pre-WPS)

Run	Welding Process	Size of Filler metal (mm)	Current (A)	Voltage (V)	Type of current/Polarity	Wire Feed Speed (m/min)	Welding Speed (mm/min)	Heat input (KJ/mm)
1	FCAW	1.2	180	23	DC (+)	≈ 11	≈ 292	0.9
2 to 8	FCAW	1.2	250 to 270	32.9 to 33.3	DC (+)	≈ 11	≈ 342	1.4 to 1.6

Table 46 – Welding parameters for X70 FCAW butt joints

A welding post was prepared with positioners for rotating the pipes under a fixed welding torch as shown in Figure 161.
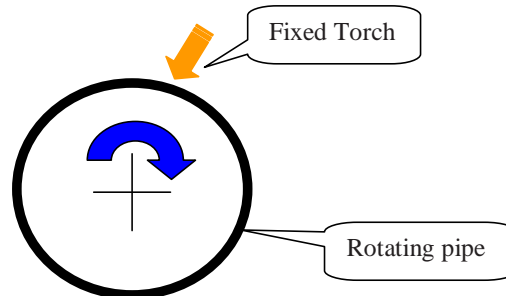
Figure 161 - Scheme for mechanized welding

After welding, the pipes passed a radiographic examination and the films were evaluated according to API 1104/2005: "Welding of pipelines and related facilities".

3   FCAW welds –Mechanical characterization

The characterization performed included the following activities:

→ Macro-etching along the joint in order to highlight both the weld metal and the HAZ extension and documentation of microstructure.

→ Mechanical characterization including micro-hardness measurements along the joint, tensile tests, Charpy V tests, CTOD tests.

→ Residual stresses measurements

3.1 X100 FCAW – X70 FCAW pipes - Macro-etching and documentation of microstructure

The macrostructure of the X100 weld is given in Figure 162, where the weld metal, as well as the HAZ is clearly highlighted. A detail of both the weld face and the weld root is presented at higher magnification in Figure 163. The weld is free of macro-defects, and there is a smooth transition from the weld metal to the HAZ and the base metal.
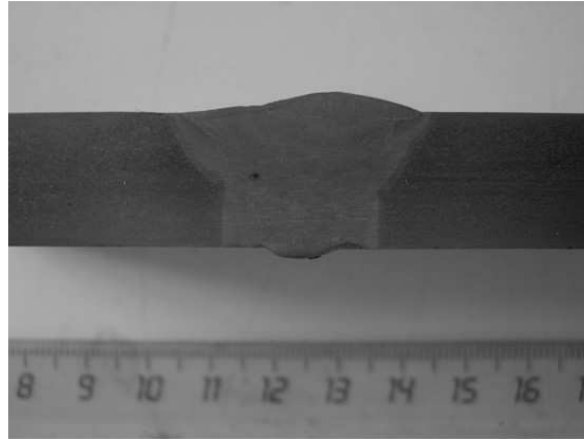
Figure 162 - Macro structure of the X100 weld

| Weld cap | Weld root |
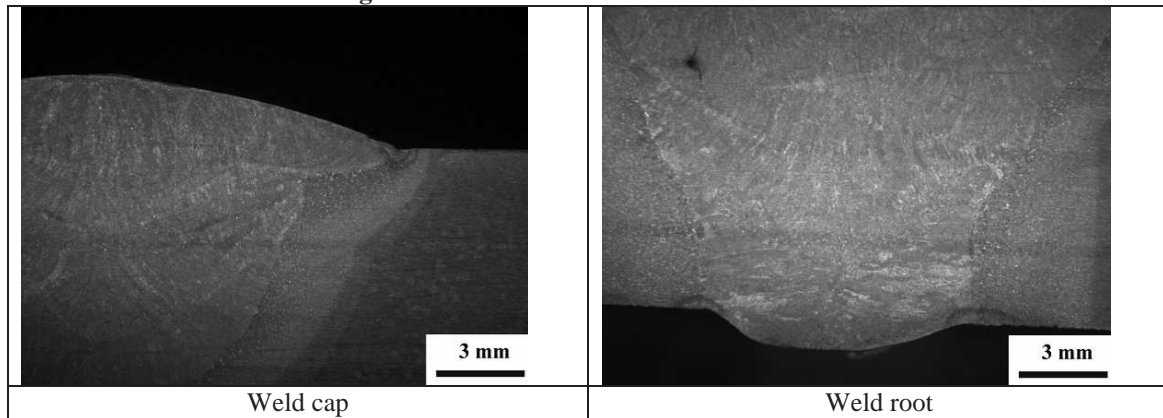
Figure 163 – X100 FCAW **-** Macro of the weld cap and root

Metallographic analysis was conducted on the cross sections of the welds. Specimens were polished and etched by Nital 2% and then examined by Optical Metallographic Microscope.

In the base metal microstructure mainly consists in bainite as reported in Figure 164. The weld metal exhibits a fine microstructure consisting in acicular ferrite and carbides (Figure 165).

In the HAZ the microstructure near the fusion boundary consists of coarse bainite (Figure 166 a). Next to this area fine grained ferrite associated carbides was found (Figure 166 b).

133
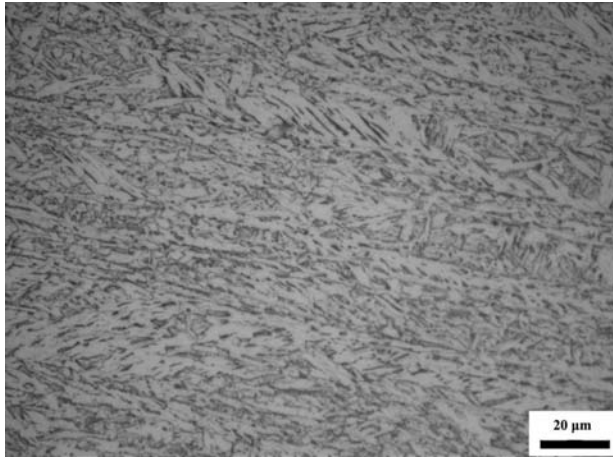
Figure 164 - Microstructure of X100 base metal consists of bainite.
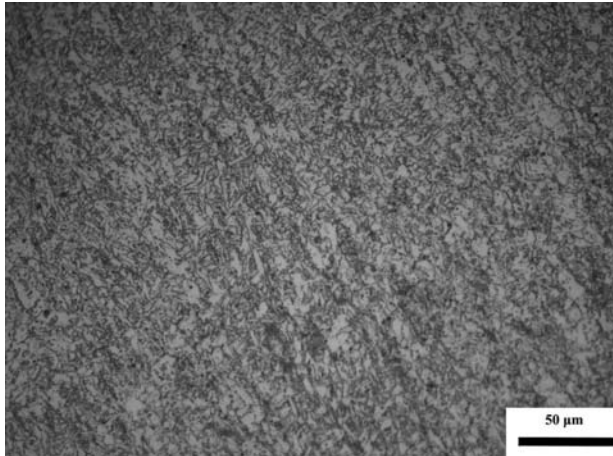
Figure 165 - Weld metal microstructure of X100. Ferrite and carbides

Coarse bainite

(a)

50 μm
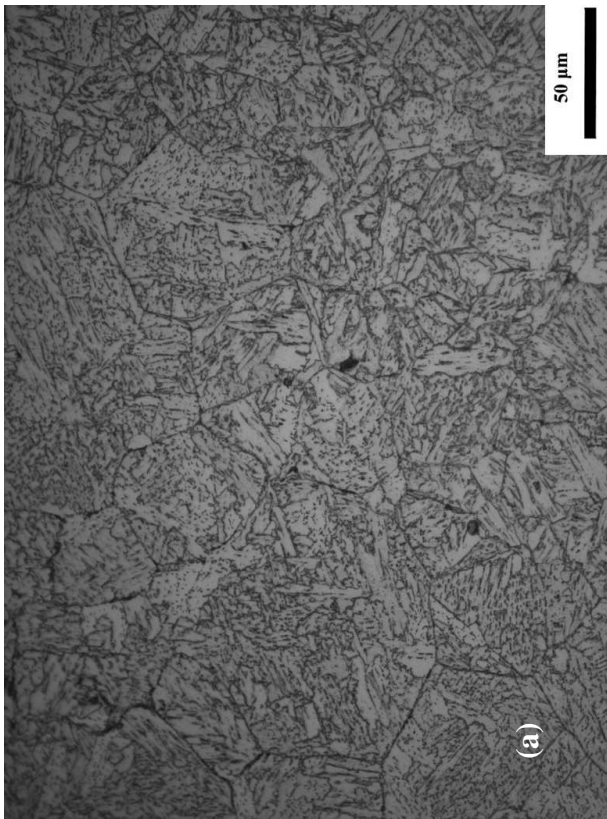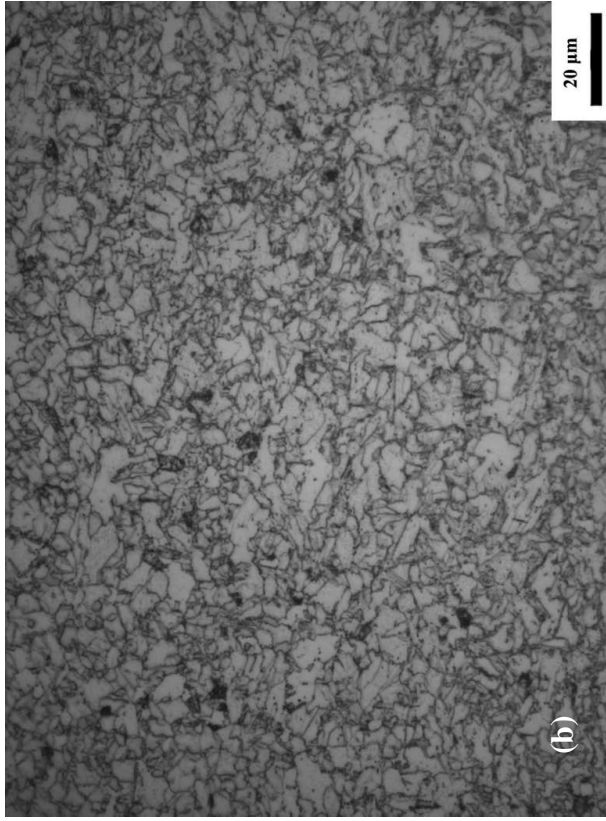
Equiaxed fine ferrite+carbides

(b)

20 μm

0.3mm
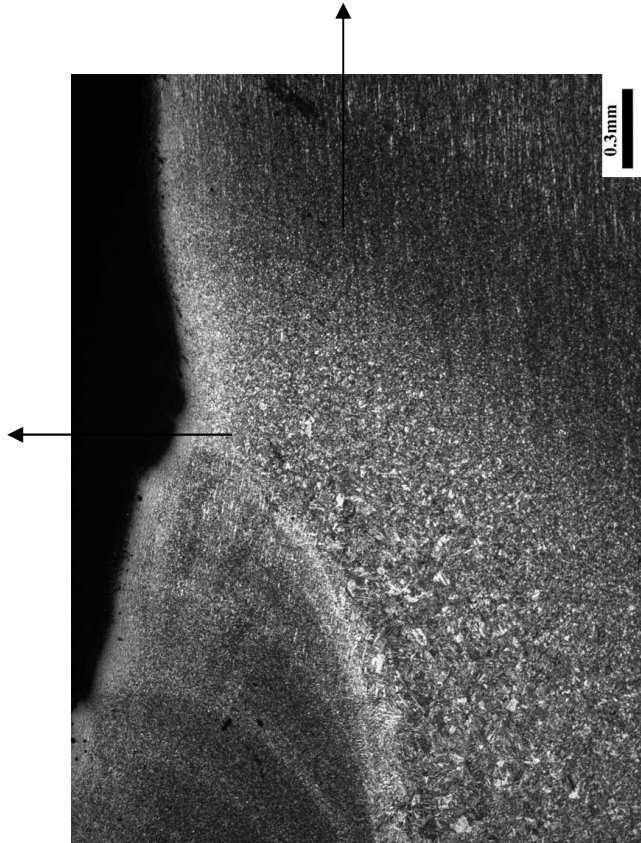
Figure 166 - X 100 HAZ microstructure

135

The macrostructure of the X70 weld is shown in Figure 167 where the weld metal, as well as the HAZ is clearly highlighted. A detail of both the weld face and the weld root is presented at higher magnification in Figure 168.

The weld is free of macro-defects, and there is a smooth transition from the weld metal to the HAZ and the base metal.
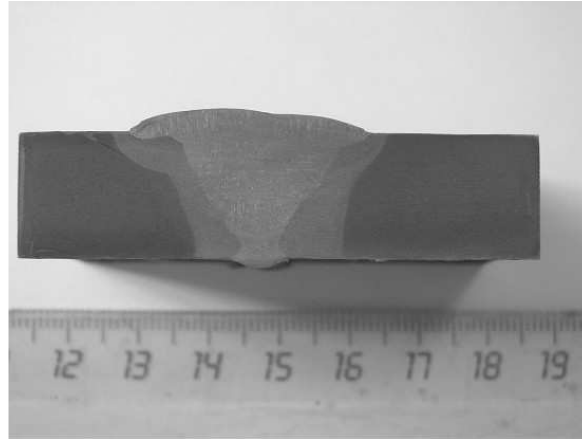
Figure 167 - Macro structure of the X70 weld

| Weld cap | Weld root |
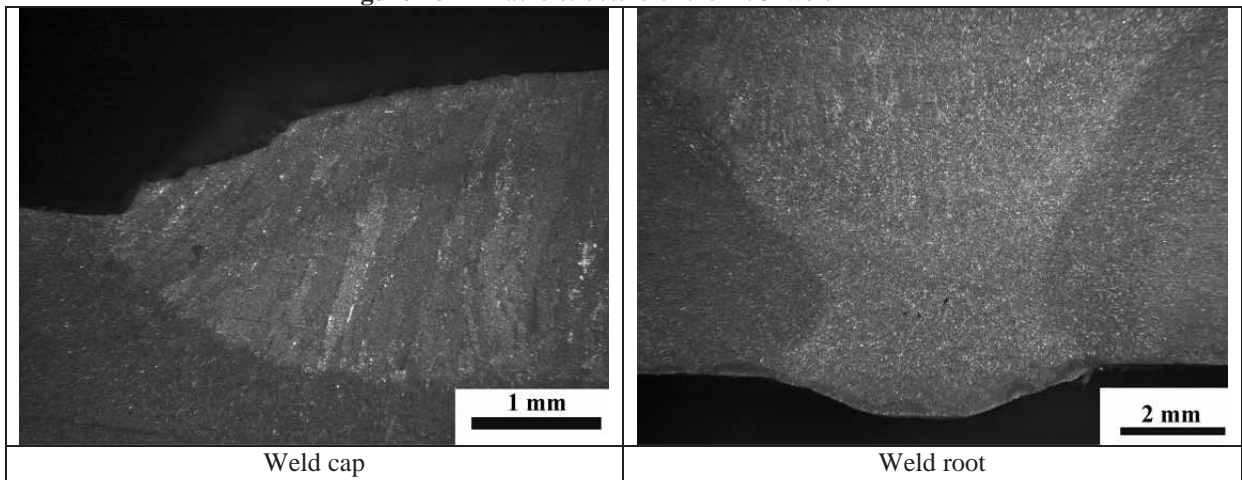
Figure 168 – X70 FCAW **-** Macro of the weld cap and root

Metallographic analysis was conducted on the cross sections of the welds. Specimens were polished and etched by Nital 2% and then examined by Optical Metallographic Microscope.
As reported in Figure 169 the base metal consists mainly in acicular ferrite and bainite.
The weld metal exhibits a fine microstructure which consists of acicular ferrite and carbides , as shown in Figure 170.

In the region near to the weld metal microstructure showed coarse bainite associated with small amounts of ferrite (Figure 171 a). Away from the fusion boundary fine grained ferrite plus carbides can be observed (Figure 171 b). A region with banded structure consisted of ferrite and carbides is found at the mid thickness of the specimen in the HAZ (Figure 171 c).

136
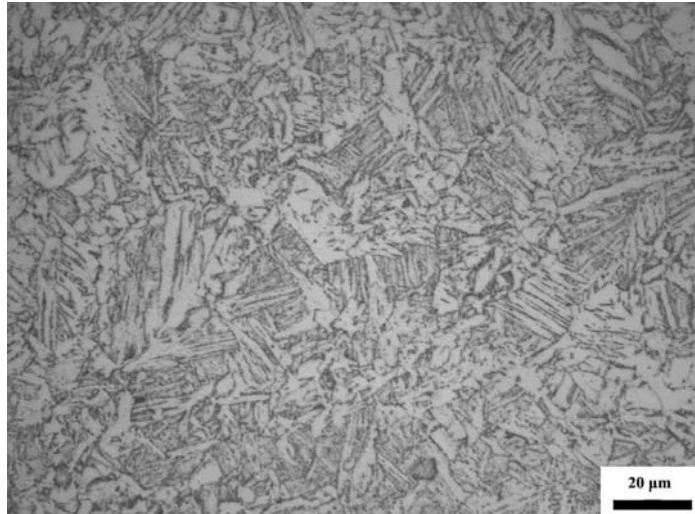
Figure 169 - X70FCAW - Base metal . Bainite and acicular ferrite.
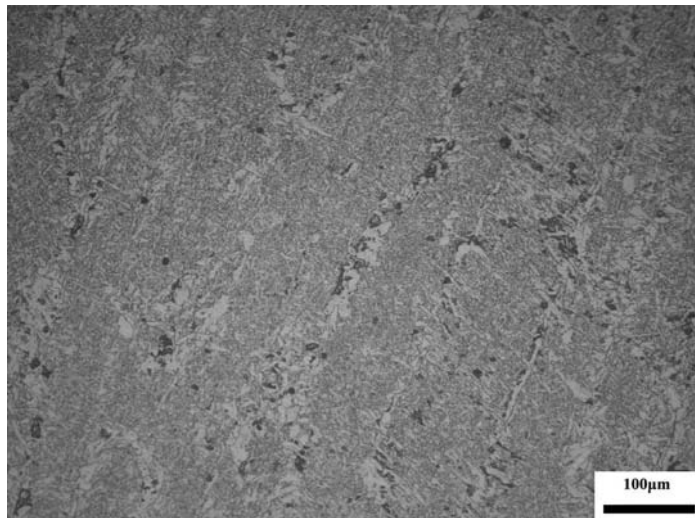
Figure 170 - X70 FCAW - Weld metal microstructure. Ferrite and carbides

137

(b)

HAZ Away from the fusion boundary: Fine grained ferrite+carbides

(c)
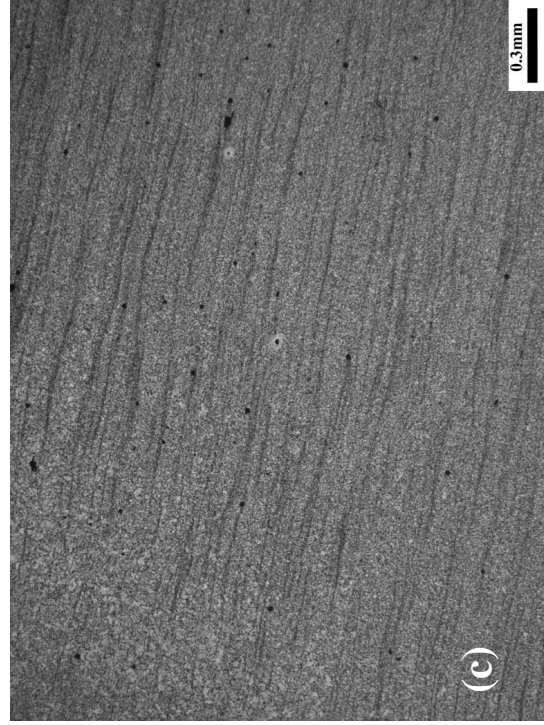
Banded structure (ferrite+ carbides)

(a)

HAZ adjacent to WM: Coarse bainite + small amounts of ferrite
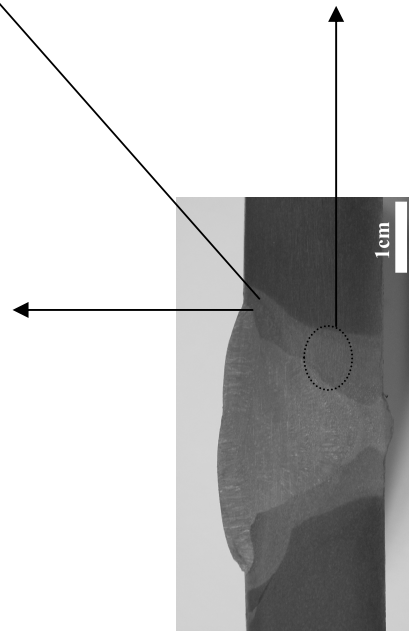
Figure 171 - X70FCAW - HAZ microstructure

138

3.2 X100 FCAW – X70 FCAW pipes - Mechanical characterization

For X100 FCAW joints micro-hardness measurements were performed with a load of 2kgr on Vickers scale, according to the profiles shown in Figure 172 where the results are presented in detail.
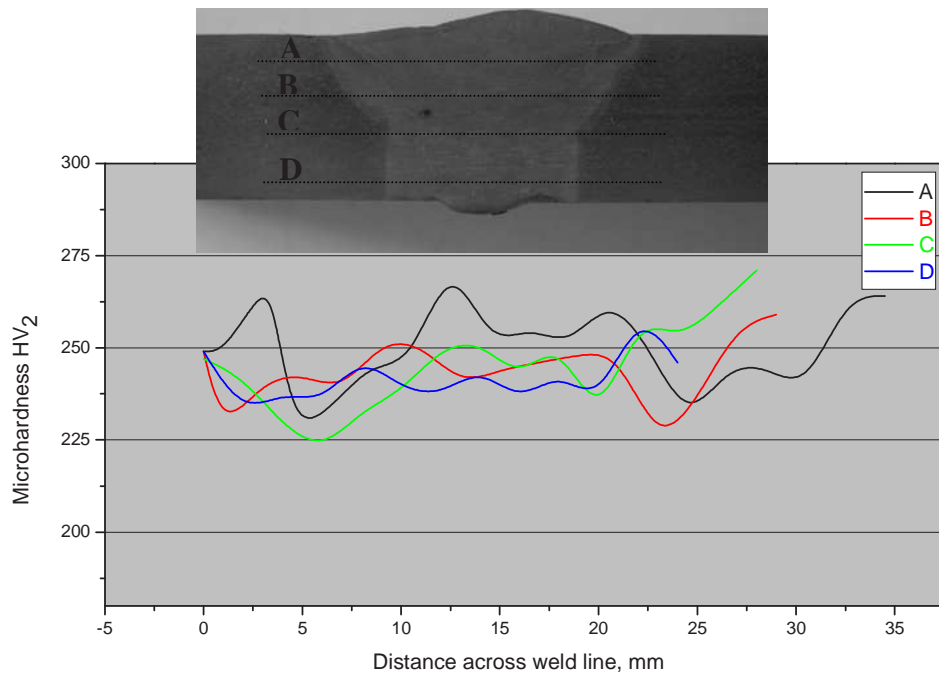
Figure 172 – X100 FCAW - Microhardness profile across the weld. - Measurements performed across the lines A,B,C,D shown in the embedded macrograph

For X70 FCAW joints microhardness measurements were performed with a load of 2kgr on Vickers scale, according to the profiles shown in Figure 173 where the results are presented in detail.
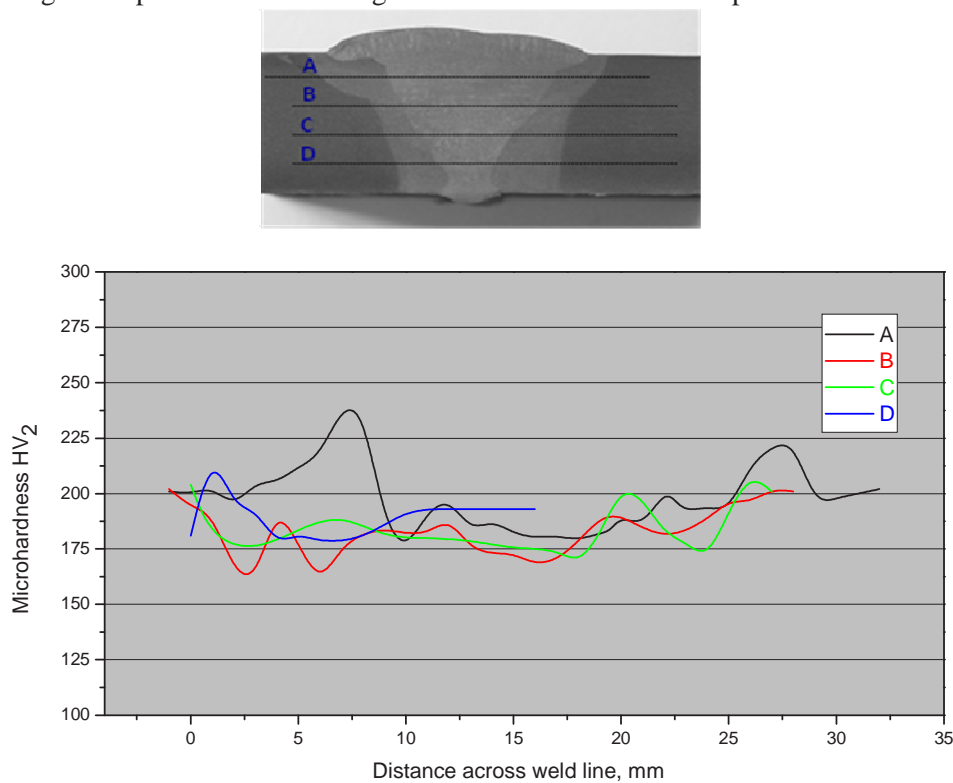
Figure 173 – X70 FCAW - Microhardness profile across the weld. - Measurements performed across the lines A,B,C,D shown in the embedded macrograph

Tensile tests have been performed at room temperature (RT) on prismatic specimens taken transverse to the weld, and the results are reported in Table 47 for X 100 pipe and in Table 48 for X 70 pipe.

Specimen label	Test temperature (°C)	Rm (MPa)	Notes
T1	23	775	Failure in base metal
T2	23	769	Failure in base metal

Table 47 – X100 FCAW pipes **-** Tensile tests results

Specimen label	Test temperature (°C)	Rm (MPa)	Notes
T1	23	613	Failure in weld metal
T2	23	602	Failure in weld metal

Table 48 – X70 FCAW pipes - Tensile tests results

Lateral bend tests were performed according to EN 910 using specimens taken transverse to the weld, giving good results. The requirement that the test specimens shall not reveal any one single flaw > 3mm in any direction was fulfilled. The results are in agreement with the Standard as for X100 failure occurs in the base metal and for X70 the tensile strength of the specimens is higher than the specified minimum value for the parent metal (i.e 565 MPa according to API 5L).

Impact tests have been performed using Charpy V samples with notch located in the the Weld Metal (WM), Heat Affected Zone (HAZ) and base metal (BM), according to EN 875, as shown in Figure 174.
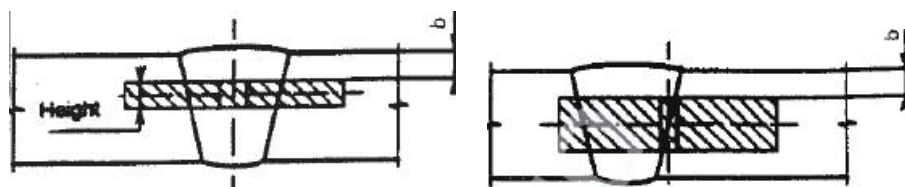
Figure 174 - Impact specimens in WM and HAZ

Tests have been performed both for X100 and X70, at T=-10° C on Charpy V samples with notch located both in the weld metal (WM), in the heat affected zone (HAZ). The results are reported in Table 49. and in Table 50.

Specimen label	Test temperature (°C)	Notch location	Absorbed Energy (J)	Average Absorbed Energy (J)
R1	-10	WM	69	68
R2	-10		68	
R3	-10		68	
R4	-10	HAZ	129	134
R5	-10		134	
R6	-10		139	
TL-2	-10	BM	246	246

Table 49 – X100 FCAW pipes **-** Impact tests results

Specimen label	Test Temperature (°C)	Notch location	Absorbed Energy (J)	Average Absorbed Energy (J)
R1	-10	WM	124	128
R2	-10		124	
R3	-10		136	
R1	-10	HAZ	243	239
R2	-10		235	
R3	-10		240	
R1	-10	BM	266	267
R2	-10		268	
R3	-10		268	

Table 50 –X70 FCAW pipes - Impact tests results

140

CTOD tests were carried out following the BS 7448 standard, with specimens B x 2B type, loaded in bending, with the maximum thickness allowed by the pipe wall. Test were performed at RT and at T=-10°C with specimens taken with transverse notch located in the Base Metal (BM), in the weld metal (WM) and in the Fusion Line (FL).

CTOD tests results shown in Table 51 and in Table 52 are in agreement with the standard requirements (0.15 mm) for all notch locations.

Weld	Notch position	T [°C]	CTOD (mean) [mm]	CTOD (range) [mm]	CTOD type
X100 FCAW	WM	RT	0.24	0.18 – 0.30	δ_m
	FL	RT	0.31	0.27 – 0.34	δ_m
	BM	-10	0.39	0.27 – 0.50	δ_m
	WM	-10	0.21	0.19 – 0.22	δ_m
	FL	-10	0.155	0.153 – 0.158	δ_u

Table 51 – X100 FCAW **-** CTOD testing results

Weld	Notch position	T [°C]	CTOD (mean) [mm]	CTOD (range) [mm]	CTOD type
X70 FCAW	WM	RT	0.61	0.59 – 0.65	δ_m
	FL	RT	0.72	0.66 – 0.77	δ_m
	BM	-10	0.99	0.99 – 1.00	δ_m
	WM	-10	0.55	0.45 – 0.62	δ_m
	FL	-10	0.75	0.52 – 0.86	δ_m

Table 52 – X70 FCAW **-** CTOD testing results

3.3 X100 FCAW – X70 FCAW pipes - Residual stress measurements

Residual stress measurements were performed by X-Ray diffraction method.

At first, as case study measurements were performed on X100 FCAW welded pipes on the whole pipe (before cutting) and on strips cut from the pipe (after cutting) with the aim to investigate the eventual release of residual stresses from entire weld to test specimen. Such measurements were performed on the external surface as the measurements on the inner surface was not feasible.

The results highlighted that for the stresses of interest for our case, considering the in service loading condition of the selected components (i.e. longitudinal stresses) the residual stresses release was not remarkable.

Therefore residual stresses measurements were performed both for X100 FCAW and X70 FCAW on the inner surface of the pipes, focusing the attention on the most critical site where usually failure occurs.

Results are shown in detail in the following.

3.3.1 Residual stresses measurements on X100 FCAW

Residual stresses were measured on the external surface in the center of the weld seam, at the weld toe and 10 and 300 mm away from the weld toe, with steps of 90º as shown in Figure 175.
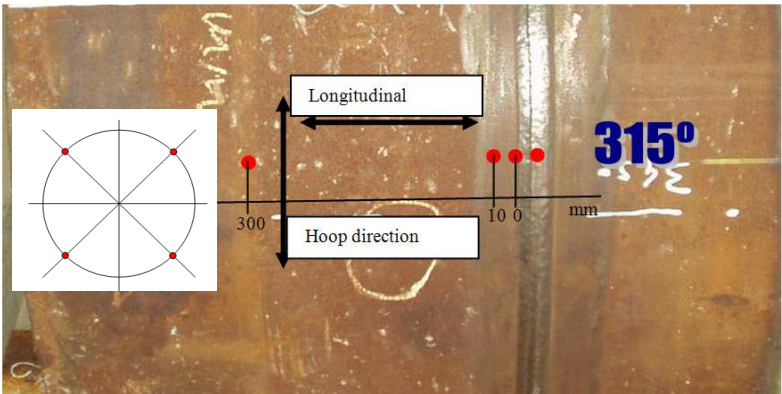
Figure 175 – X100 FCAW - Locations of residual stress measurements (red dots)

From Figure 176 to Figure 183 is shown the comparison between residual stresses measured on the external surface both in hoop and longitudinal direction, before and after pipe cutting.
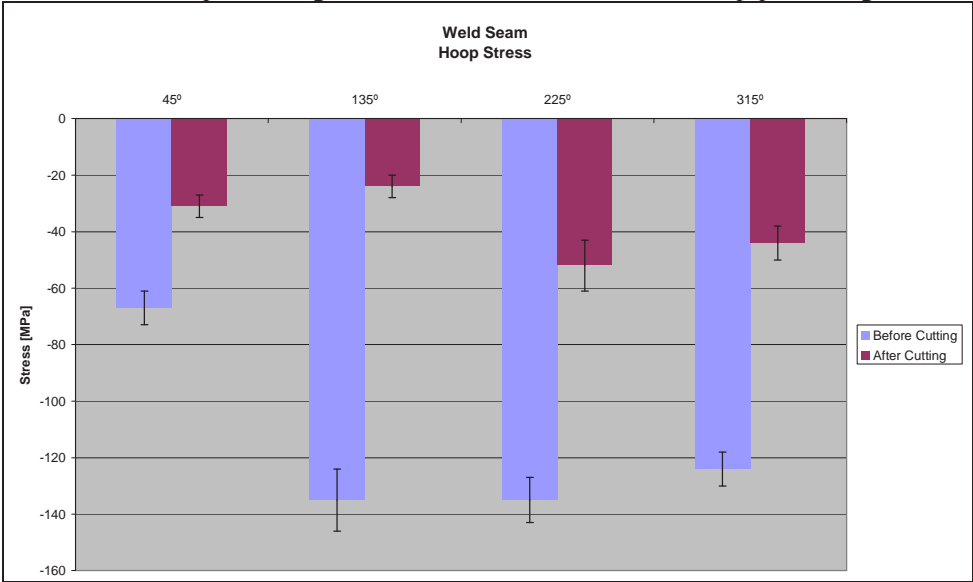
Figure 176 – Weld seam **-** Hoop residual stresses before and after pipe cutting
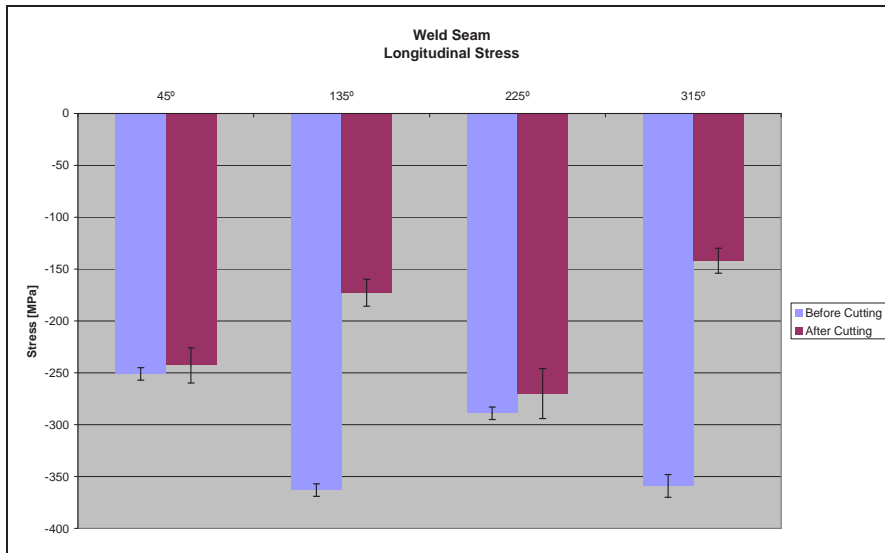
Figure 177 – Weld seam - Longitudinal residual stresses before and after pipe cutting
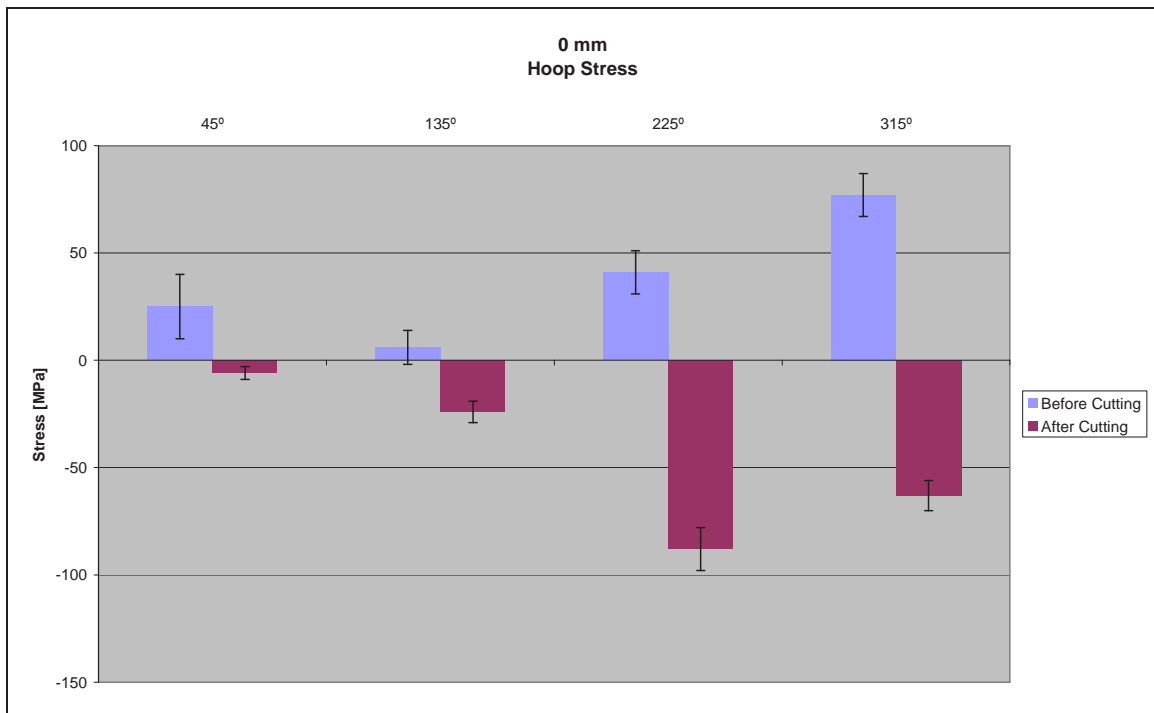
Figure 178 – Weld toe - Hoop residual stresses before and after pipe cutting

143
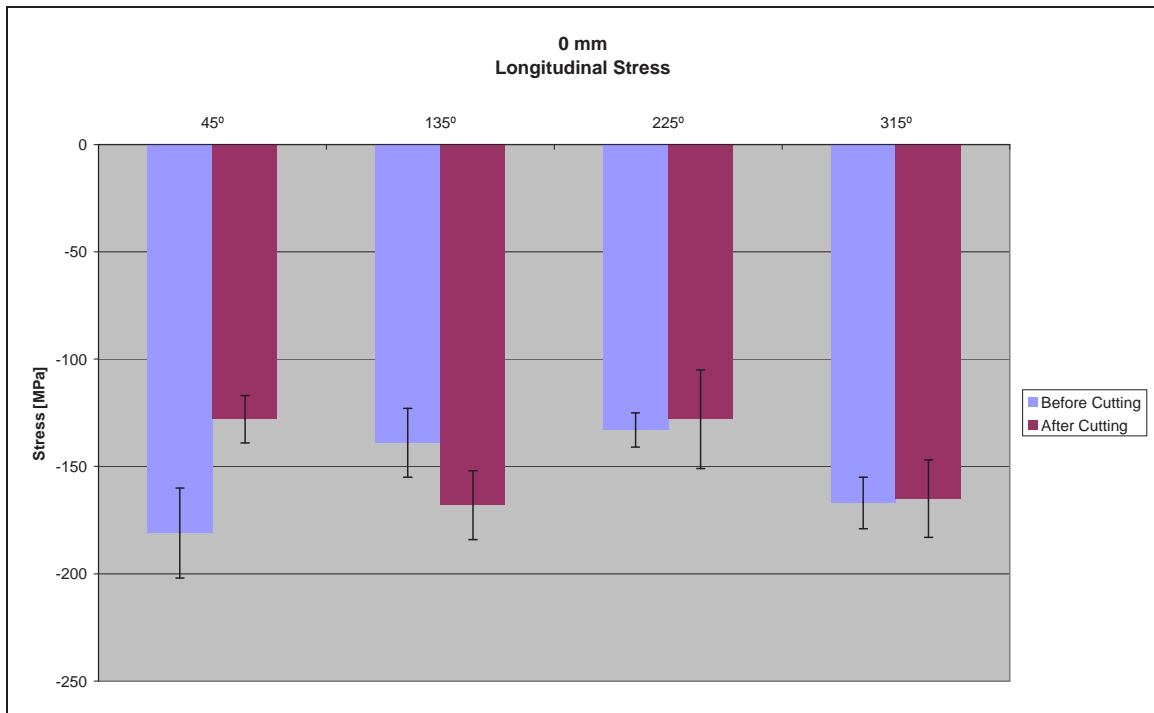
Figure 179 – Weld toe - Longitudinal residual stresses before and after pipe cutting
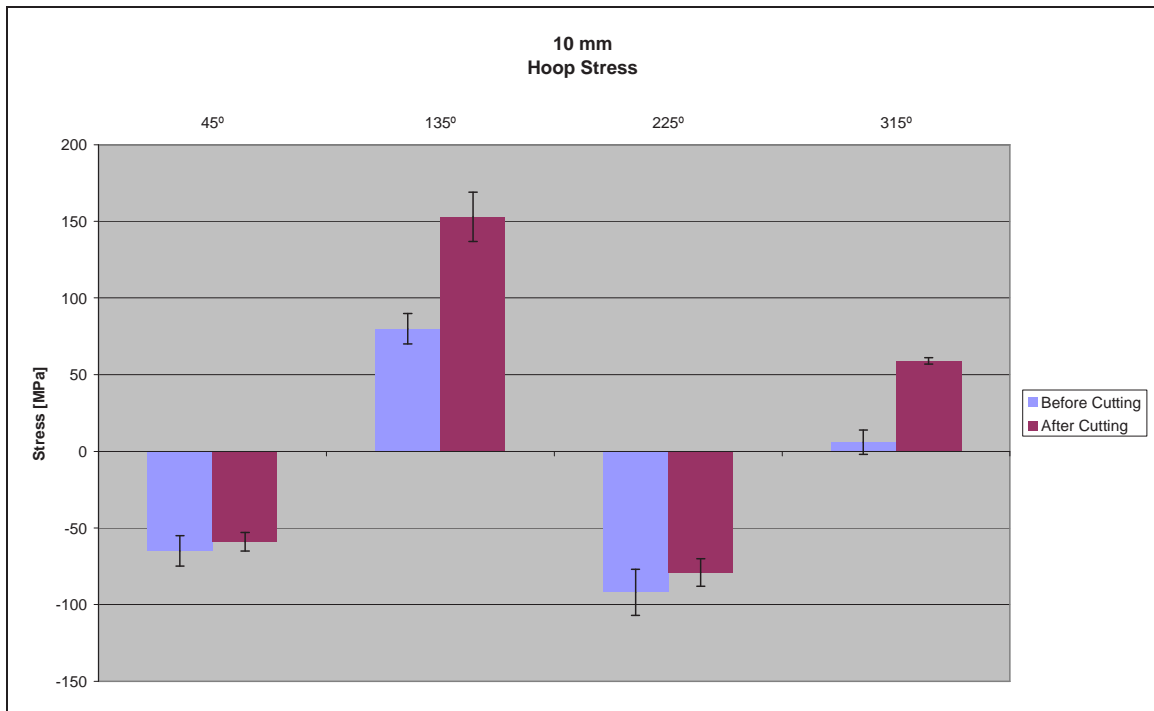
Figure 180 – 10 mm from the weld toe - Hoop residual stresses before and after pipe cutting
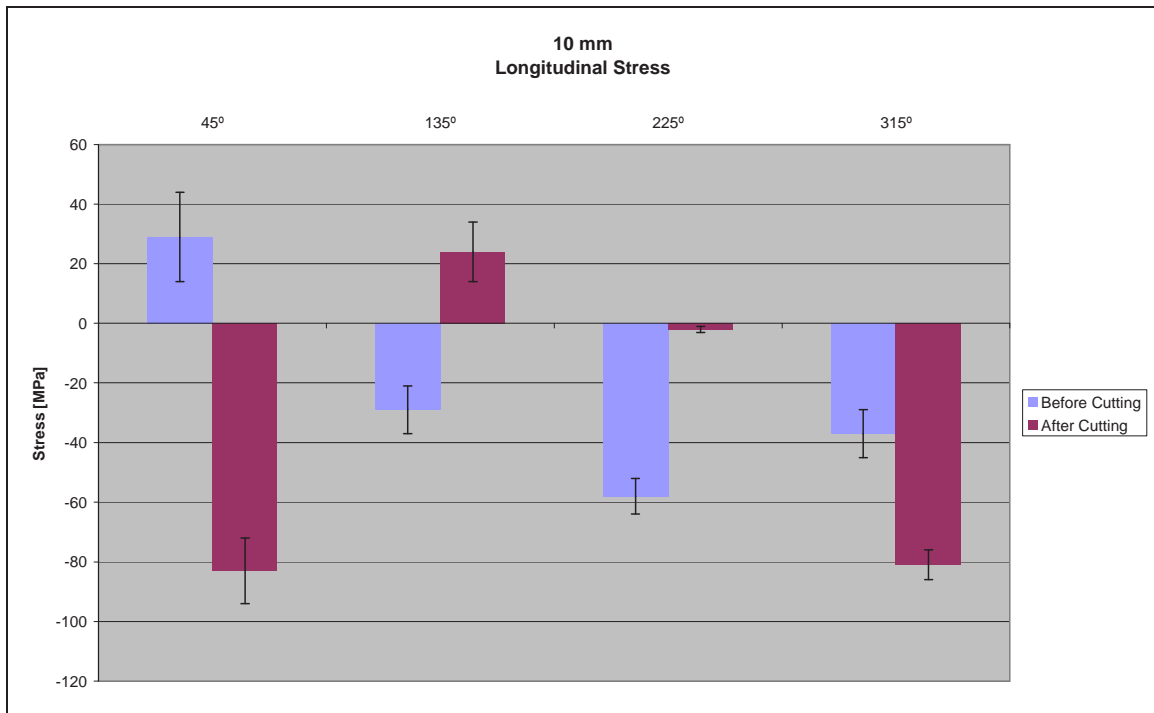
Figure 181 – 10 mm from the weld toe - Longitudinal residual stresses before and after pipe cutting
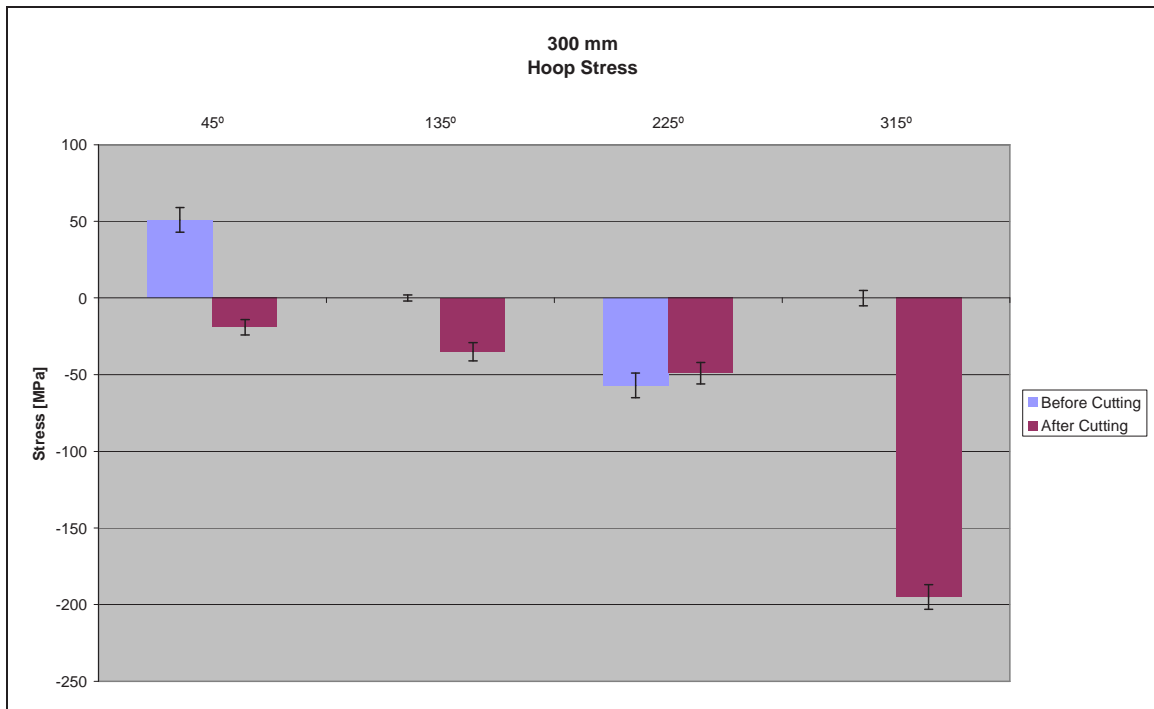
Figure 182 – 300 mm from the weld toe - Hoop residual stresses before and after pipe cutting
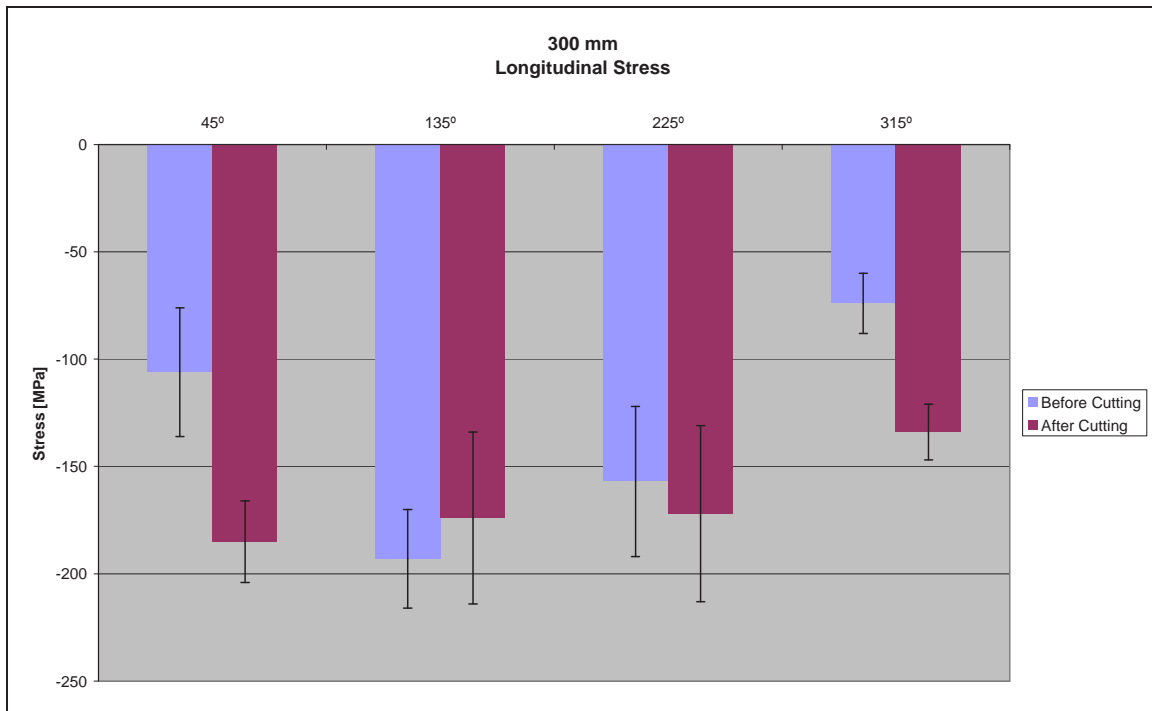
Figure 183 – 300 mm from the weld toe - Longitudinal residual stresses before and after pipe cutting

Finally in Table 53 a summary of the results obtained is reported.

Measurement location	Longitudinal stress before cut [MPa]	Longitudinal stress after cut [MPa]	Hoop stress before cut [MPa]	Hoop stress after cut [MPa]
Weld	-177 to -363	-142 to -270	0 to -173	-24 to -52
Toe	-133 to -311	-128 to -168	77 to -45	-6 to -88
10mm from toe	84 to -58	24 to -83	119 to -92	153 to -79
300mm from toe	-74 to -193	-134 to -185	51 to -234	-19 to -195

Table 53 – X100 FCAW –Residual stresses measurements results

According to the results above shown the following conclusions can be drawn:

→   Residual stresses are mainly compressive.

→   No remarkable release due to the cut of the strips was noticed as concerns the longitudinal residual stresses, that is the most relevant stress when considering the in service loading conditions of our components.

The attention was then focused on the inner surface of the pipes that is expected to be the most critical location were usually failure occurs. Residual stresses were measured in longitudinal and hoop direction, on the inner surface of the pipe on strip specimens devoted to the testing program (see Figure 184).

146
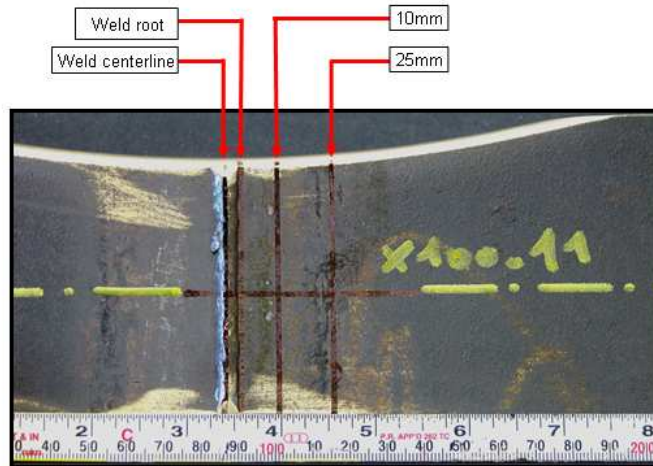
Figure 184 – X100 FCAW – Residual stresses measurement points on inner surface

The results are reported in Figure 185 and Figure 186.
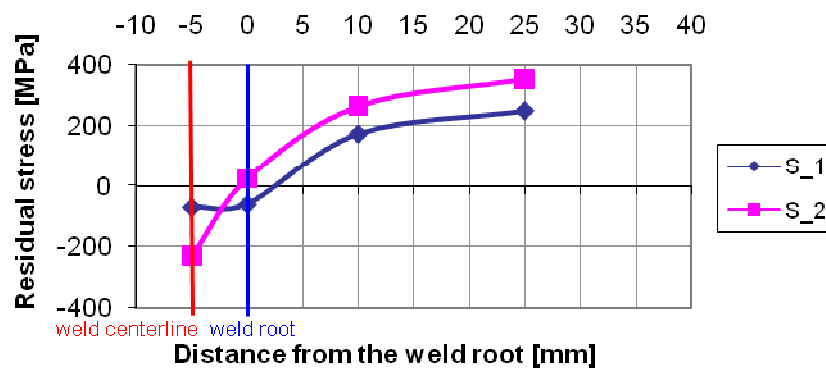
Figure 185 – X100 FCAW - Residual stresses on internal surface in longitudinal direction
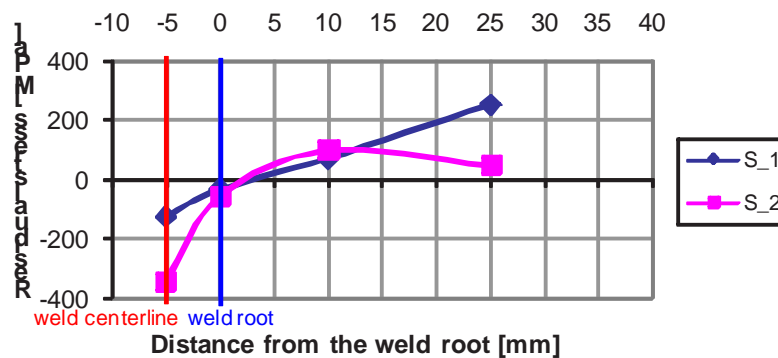
Figure 186 – X100 FCAW - Residual stresses on internal surface in hoop direction

For both longitudinal and hoop residual stresses, compressive values in the weld centreline and near zero values in the weld toe have been found. The residual stresses tend to become tensile and increase moving away from the weld.

3.3.2 Residual stresses measurements – X70 FCAW

Residual stress measurements were carried out through an X-Ray diffraction on the inner surface of samples destined to fatigue program in longitudinal and hoop direction. The measurements points are the same of Figure 184. The results are reported in Figure 187 and Figure 188.

147
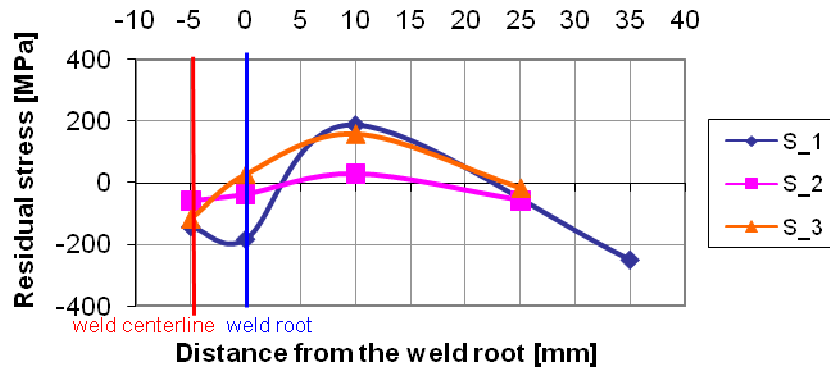
Figure 187 – X70 FCAW - Residual stresses on internal surface in longitudinal direction
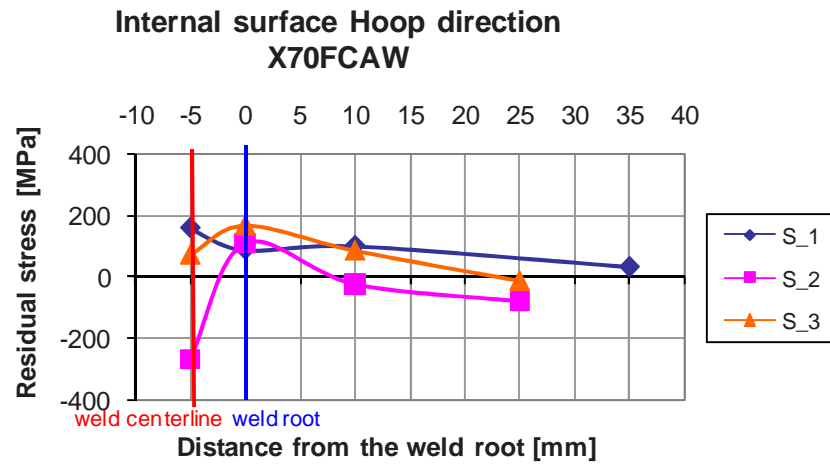
Figure 188 – Residual stresses on internal surface in hoop direction

As regards longitudinal residual stresses, compressive values have been found in the weld centreline and in the weld toe. In the area near the weld toe the residual stresses are tensile but tend to become compressive far away from the weld.

Hoop residual stresses are mostly tensile in the weld centreline and in the weld toe. The residual stress values tend to decrease moving away from the weld.

4   Laser -GMA welds - WPS

The welds were performed in several passes the first one only performed by Laser-GMAW. For the root pass (often the most critical and welded with less productivity in offshore girth welding), were set two main productivity targets, to have realistic convenience figures compared to standard arc welding techniques:

– welding travel speed far more better than current automatic orbital GMAW systems;
– root pass thickness larger than the comparable pass performed by orbital GMAW systems.

A Nd:YAG laser system was employed, as the fibre transmission of the beam makes this type of laser much more attractive as manufacturing tool for orbital welding. Operational choices were made for the experiments to be as close as possible to real offshore welding activity; this was done also for consumables and equipments.

In particular for the two pipe materials included in the project, welding was aimed to simulate real activity in offshore linepipe fabrication:

– for X70 pipes: linepipe/riser fabrication at the lay barge (J-lay) – 2G/PC position;
– for X100 pipes: prefabrication of double joints at barge/land base – 1G/PA position.

Evaluation and testing of welded joints was done accordingly to recognized offshore fabrication standards (DNV-OS-F101 "Submarine pipeline systems"). Use of "standard" consumables wherever possible (filler wire, gas mix) was also emphasized.

148

4.1 X100 LH welded pipes

The welding session for X100 pipes was performed simulating prefabrication of double/quadruple joints at lay barge/land base, i.e. weld activity was performed in horizontal position (AWS 1G/EN PA) with the pipe rotating on a horizontal axis beneath the laser – arc energy source on roller pairs specifically designed.

The X100 pipes received a narrow – compound bevel preparation requiring low amount of filler material and fewer passes than a conventional joints. Filler metal of ER 100 class (solid wire) was mainly employed. The weld was performed in three passes, the 1st one only by Laser-GMAW and the 2nd and 3rd by single wire GWAW.

For laser – GMA root pass weld of 16.4 mm thick X100 pipe, the productivity target was initially set to 7 mm of welded root throat size, with travel speed between 1.0 and 1.5 m/min. Root opening was set to zero during all the welding trials (perfect contact of the ends). No backing support was used. A commercial ER100S-G low-alloyed solid wire was chosen as welding consumable to provide adequate mechanical properties and weld integrity in the WM. For the root pass only was chosen an ER70 grade due to the expected higher dilution with the parent metal. The diameter employed was 1.2 mm (Table 54).

Wire	C	Si	Mn	Cr	Ni	Mo	Cu	Pass
ER70 S-G	0.10	0.35	1.10	-	-	-	-	Root
ER100 S-G	0.08	0.72	1.45	0.52	0.54	0.23	0.25	Fill

*mass %, Fe % remaining.

Table 54 – Consumables for Laser – GMA welding of X100 pipes

The gas flow was provided from the GMA torch nozzle only, as external protection. Mill scale was removed from the surfaces near the weld zone. Edges of weld preparation were restored at bright metal condition just before coupling of pipes in pairs for tacking. The material chemistry was reviewed in sight on the faster cooling rates expected as consequence of the faster welding speed and the limited WM size. Laser – GMAW was performed with a solid wire, then a very low hydrogen content for the WM was expected. Nevertheless, though the pipe chemistry was quite lean, due to the relatively more alloyed wire and the high restraint of the joint made by X100 pipes, it was assumed that cold cracking could be a concern for WM. Therefore, it was chosen that the welding activity was to be carried out with preheating.

Laser – GMA butt welds were performed using equipment available in the CSM Welding Laboratory already described. Welding was performed in flat position (1G/PA), being the welding head kept fixed (except for joint line tracking) and the tube rotating on a motorised roller pairs (with horizontal axis). In Figure 189 the weld setup is shown. Trial, as well prototype pipes, had total length of about 500 mm.
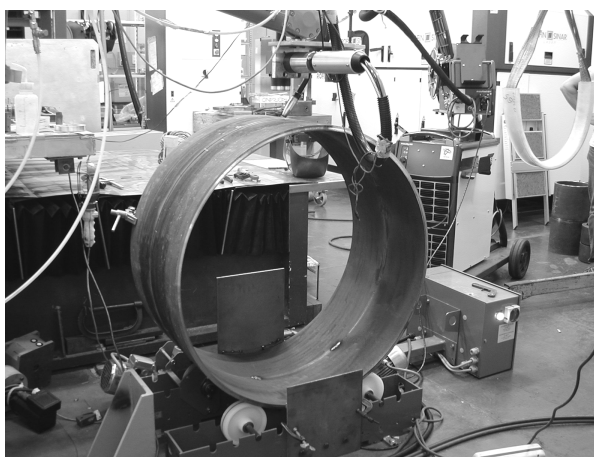
Figure 189 – Weld setup for X100 pipes (1G position)

A suitable welding procedure specification was developed at CSM Welding Laboratory after extensive trials, for exploring the maximum productivity figures while keeping adequate weld integrity and soundness. Test weld were whole circumferences or partial ones (e.g. 60° ÷ 120° arcs). The quality of the joints has been assessed at first by visual testing, while radiographic inspections, PT and

metallographic sections taken through the thickness of the welds were performed later on selected samples in which VT gave promising quality.

In Table 55 and Table 56 are reported details on the tuned welding procedure for X100 pipes.

Steel Grade and Standard	X100
Product	longitudinal welded pipe
Joint type	Butt weld
Welding position and direction	1G (AWS), rolling pipe
Nominal thickness [mm]	16.4
Nominal outer diameter [mm]/[inches]	914
Weld preparation	as sketched, machined surfaces
Backing	-
Root opening (g) [mm]	0
Cleaning	grinding of mill scale from weld area
Clamping	Turning table (from inner surface)
Welding process	Laser – GMA welding (single arc)/GMAW
Passes	3 (1st (root)/hot & fill)
Laser Nd:YAG Rofin Sinar	DY044
Operating mode	CW
Optical fibre diameter [μm]	600
Collimator length [mm]	200
Focal length [mm]	120
Workpiece laser power [W]	4200
Gas flow [l/min]	25
Laser – GMA torch lay-out	GMA torch leading (tilted 35° with respect to a diameter in horizontal), laser following
Welding consumable and classification	see detail
Polarity	DC+
Interpass/PWHT	max 180 °C/-

Table 55 – Common Laser – GMAW conditions for root pass

150

Pass	1st	2nd	3rd
Position	root	hot	cap
Welding process	Laser - GMAW	GMAW	GMAW
Travel speed [m/min]	1.25	0.55	0.45
Focal position [mm] (above inner surface)	3	-	-
Mode of metal transfer (current type)	smooth	smooth	smooth
Wire diameter [mm]	1.2	1.2	1.2
Laser spot – wire tip distance [mm]	0 - 1	-	-
Gas protection	$Ar+20\%CO_2$	$Ar+20\%CO_2$	$Ar+20\%CO_2$
Measured current [A]	310	370	370
Measured voltage [V]	26	26	31
Electrode wire feed rate [m/min]	8	10	12
Preheating [°C]	130	-	-
Gross heat input [kJ/mm]	~0.6	~0.85	~1.20

Table 56 - Laser – GMA conditions for welding X100 pipe 16.4 mm thick

Both weld cap and root reinforcements merged quite smoothly with the parent wall in most of welded circumferences. No spatter was pointed out at the root. (Figure 190 and Figure 191). The WM thickness welded in the root pass was about 7 mm.

Figure 190 – Laser – GMA weld root appearance on X100 pipes 16.4 mm thick

Figure 191 – Weld cap appearance on X100 pipes 16.4 mm thick.

4.2 X70 LH welded pipes

As for X100 pipes also for X70 ones it was planned to weld the joint in three passes, the 1st one only performed by Laser-GMAW and the 2nd and 3rd by single wire GWAW, following the same productivity targets for the root pass.

X70 pipes received a narrow – compound bevel preparation requiring low amount of filler material and fewer passes than a conventional joints. The intention was to use three passes only to complete the joint (1st with Laser-GMAW, 2nd and 3rd with GMAW). Welding was to be performed in frontal position (2G in AWS standard) with the pipe rotating on a vertical axis beside the laser – arc energy source.

For laser – GMA root pass weld of 14.2 mm thick X70 pipe, the productivity target was initially set to 7 mm of welded root throat size, with travel speed between 1.5 and 2.0 m/min. Bevelling of pipes was performed by machining. In Figure 192 (left side) is reported a sketch of the preparation with the main dimensions at first adopted. Some minor adjustments were made during the trials. In the same figure (right side) is shown the preparation machined on some pipe ends. Root opening was set to zero during all the welding trials (perfect contact of the ends). No backing support was used.

Narrow groove slope: 3°

Vee slope: 25°

1st pass total height: until 9 mm

Root face: 3 or 4 mm
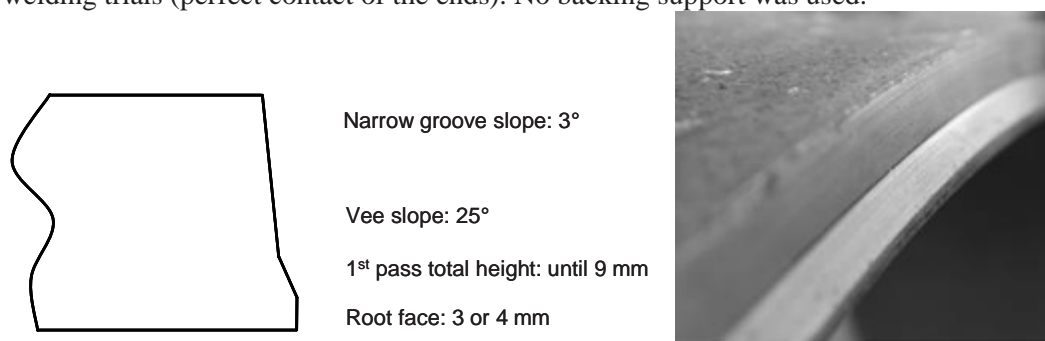
Figure 192 – Joint preparation for root Laser – GMAW of X70 pipes 14.2 mm thick (left) and appearance of the bevel preparation machined (right).

A commercial ER70S-6 low-alloyed solid wire was chosen as welding consumable to provide adequate mechanical properties and weld integrity in the root WM. The diameter employed was 1.2 mm. The gas flow was provided by the GMA torch nozzle only, as external protection. Mill scale was removed from the surfaces near the weld zone. Edges of weld preparation were restored at bright metal condition just before coupling of pipes in pairs for tacking.

The material chemistry was reviewed in sight on the faster cooling rates expected as consequence of the faster welding speed and the limited WM size. Laser – GMAW was performed with a solid wire, therefore a very low hydrogen content for the WM was expected. From this point of view, and looked at the relatively low thickness of the X70 pipes, it was assumed that cold cracking would not be a concern, especially because a special procedure is followed to avoid such problem. To do this, the 2nd and 3rd passes are deposed shortly after the 1st (hot pass technique). Therefore, it was chosen that all welding activity was to be carried out at room temperature (no preheating).

Laser – GMA butt welds were performed using the equipment available at the CSM Welding Laboratory. It consisted in a solid state Nd:YAG laser source, rated 4.4 kW of maximum power, coupled with a microprocessor controlled arc welding inverter, rated 500 A of maximum current. The filler wire train drive was capable of 25 m/min of wire feed rate. The Nd:YAG laser source was diode pumped and allowed the use of smaller diameter optical fiber (ϕ=600 μm) for beam delivering. Laser beam focusing was obtained by a lens with 120 mm of focal length, after beam collimation in a lens with 200 mm focal length. Beam manipulation was performed by a 6-axis robot plus an additional axis for pipe rotation. Laser spot and welding wire tip were very close, laser welding head allowing fine adjustment of their relative position. Laser beam was always perpendicular to the tube outer surface, while the GMA torch was tilted about 35° from the laser beam axis. GMA welding alone could be performed using the same equipment simply switching off the laser source.

Welding was performed in frontal position (2G/PC), being the welding head kept fixed (except for joint line tracking) and the tube rotating on a motorised clamping table (with vertical axis). Robot, rotating unit, laser source and inverter controls were fully integrated in a CNC system for robotised welding. In Figure 193 the weld setup is shown. Trial, as well prototype pipes, had total length of about 500 mm.
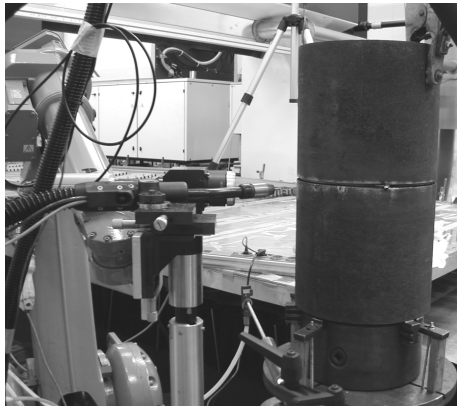
Figure 193 – Weld setup for X70 welds performed in 2G position

A suitable welding procedure specification was developed after extensive trials, for exploring the maximum productivity figures while keeping adequate weld integrity and soundness. The effect of welding travel speed, wire feed rate, arc current mode, laser - GMA torch lay out and CTWD were mainly investigated. As main philosophy for conducting the experiments, travel speed and wire fed rate were always varied accordingly to obtain the targeted root welded thickness, within the prescribed travel speed range. Laser power was always set to the maximum available, while GMA influence was controlled mainly through the CTWD and the laser – arc distance. Test weld were whole circumferences or partial ones (e.g. 60° ÷ 120° arcs). A valid overlap strategy was also implemented. The quality of the joints has been assessed at first by visual testing, while radiographic inspections, PT and metallographic sections taken through the thickness of the welds were performed later on selected samples in which VT gave promising quality. In Table 57 and Table 58 are reported details on the tuned X70 welding procedure

Steel Grade and Standard	API 5L X70
Product	Seamless pipe
Joint type	Butt weld
Welding position and direction	2G (AWS), rolling pipe
Nominal thickness [mm]	14.2
Nominal outer diameter [mm]/[inches]	273.1
Weld preparation	as sketched, machined surfaces
Backing	-
Root opening (g) [mm]	0
Cleaning	grinding of mill scale from weld area
Clamping	Turning table (from inner surface)
Tacking	3 laser seams spaced 120°
Welding process	Laser – GMA welding (single arc)/GMAW
Passes	3 (1st (root)/hot & fill)
Laser Nd:YAG Rofin Sinar	DY044
Operating mode	CW
Optical fibre diameter [μm]	600
Collimator length [mm]	200
Focal length [mm]	120
Workpiece laser power [W]	4200
Gas flow [l/min]	25
Laser – GMA torch lay-out	GMA torch leading (tilted 35° with respect to a diameter in horizontal), laser following
Welding consumable and classification	AWS A5.18 ER70 S-6
Polarity	DC+
Interpass/PWHT	max 250 °C/-

Table 57 - Common Laser – GMAW conditions for root pass on X70 pipes

Pass	1st	2nd	3rd
Position	root	hot	cap
Welding process	Laser - GMAW	GMAW	GMAW
Travel speed [m/min]	1.50	0.50	0.52
Focal position [mm] (above inner surface)	3	-	-
Mode of metal transfer (current type)	smooth	smooth	pulsed
Wire diameter [mm]	1.2	1.2	1.2
Laser – GMA torch lay-out (tilted 30° - 35°)	ML	pushing	pushing
Laser spot – wire tip distance [mm]	0 - 1	-	-
Gas protection	Ar+8%CO_2	Ar+20%CO_2	Ar+20%CO_2
Measured current [A] (mean if pulsed)	290	240	315
Measured voltage [V] (mean if pulsed)	24	26.5	32.5
Electrode wire feed rate [m/min]	9	9	12
Preheating [°C]	RT	RT	RT
Gross heat input [kJ/mm]	~0.50	~0.80	~1.10

Table 58 - Laser – GMA conditions for welding X70 pipe 14.2 mm thick

As expected, the weld root reinforcement was very narrow, merging quite smoothly with the parent wall in most of welded circumferences. Fine spatter was pointed out at the root flat. As special care was adopted in tuning the parameters for the last pass, the weld cap metal merged smoothly with the parent wall as well. This circumstance should positively influence the fatigue strength. In Figure 194 and Figure 195 the appearance of WM respectively at root and cap are shown.

Figure 194 – Laser – GMA weld root appearance on X70 pipes 14.2 mm thick
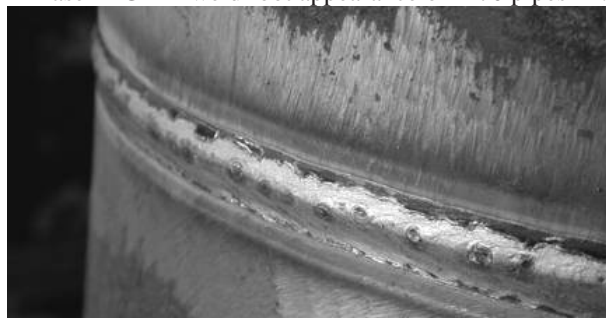
Figure 195 –Weld cap appearance on X70 pipes 14.2 mm thick

5 LH welds –Mechanical characterisation

The characterization performed included the following activities:

→ Macro-etching along the joint in order to highlight both the weld metal and the HAZ extension and documentation of microstructure.

→ Mechanical characterization including micro-hardness measurements along the joint, tensile tests, Charpy V tests, CTOD tests. Full qualification of the established WPS was undertaken according to DNV-OS-F101. For X100 LH welded joints due to some lack of material, to save up enough samples for fatigue testing purpose, static mechanical testing could not be as comprehensive as for X70.

→ Residual stresses measurements

5.1 X100 LH – X70 LH pipes – Macro-etching and documentation of microstructure

5.1.1 X100 LH welded pipes

Vickers hardness measurements (HV_{10}) were made on metallographic samples taken through the thickness of the welds (shown in Figure 196).
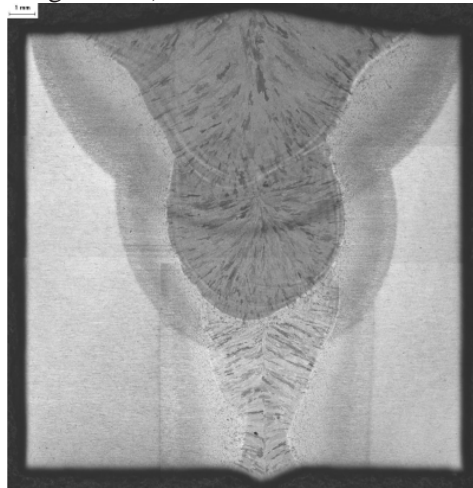
Figure 196 – Macrosection of welds on X100 pipes 16.4 mm thick

The results are shown in Table 59. No values exceed DNV general requirements (max. 325 HV in BM, FZ or HAZ).

Location	HV(mean)	HV (range)
BM (outer surface)	292	290 ÷ 295
BM (mid thickness)	290	288 ÷ 291
BM (root)	283	280 ÷ 289
CGHAZ root	255	253 ÷ 256
CGHAZ cap	247	244 ÷ 249
FZ root	242	240 ÷ 244
FZ cap	249	247 ÷ 250

Table 59 – Hardness testing results on X100 pipes welded by Laser – GMAW

Basic microstructure of welds on X100 steel was investigated by light optical microscope on metallographic samples taken through the thickness (transversal sections). Samples were mounted and polished with grinding paper and eventually with diamond paste (until 1 μm). Etching was made using standard Nital practice.

The weld metal (WM), in the pure GMAW passes (2nd + 3rd), consisted mainly of fine bainitic phase. The root pass, performed by Laser-GMA process, showed a fine microstructure as well, with again presence of bainite and considerable amount of acicular ferrite, due to the lower grade 70 consumable. In Figure 197 a typical actual WM microstructure is shown for the cap and root area respectively.
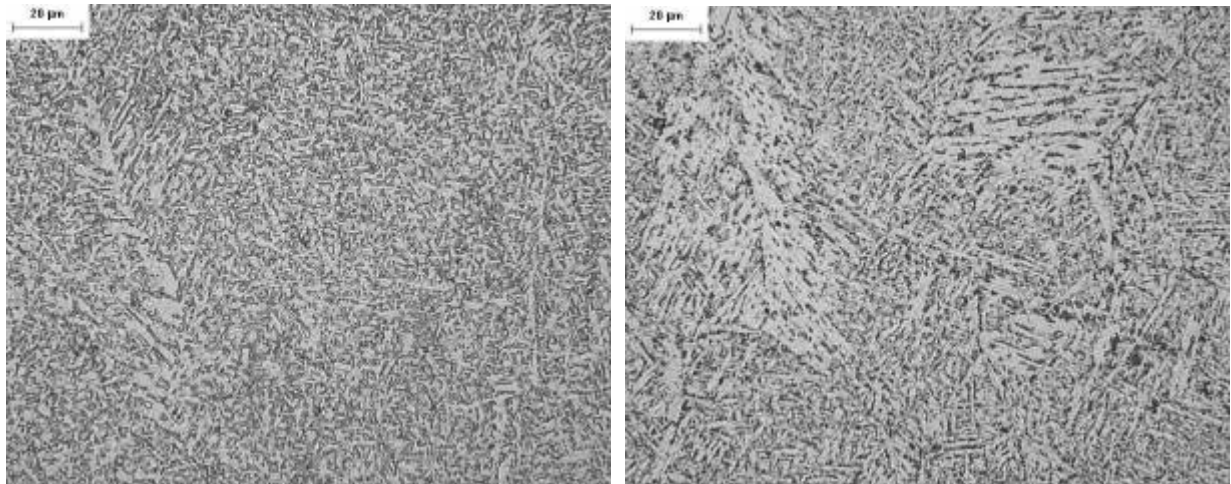
Figure 197 – Microstructure of WM for welds on X100 pipes 16.4 mm thick (left, cap area; right, root area)

The heat affected zone (HAZ) showed a more uniform behaviour between passes, with a limited grain growth in root CGHAZ pass sides. Predominant microstructure was bainite, coarser in the HAZ area beside the GMAW passes and with presence of some ferrite, possibly explanation for the not optimal toughness relevant readings. In Figure 198 typical HAZ actual microstructures are shown, for the CGHAZ cap and root area respectively.
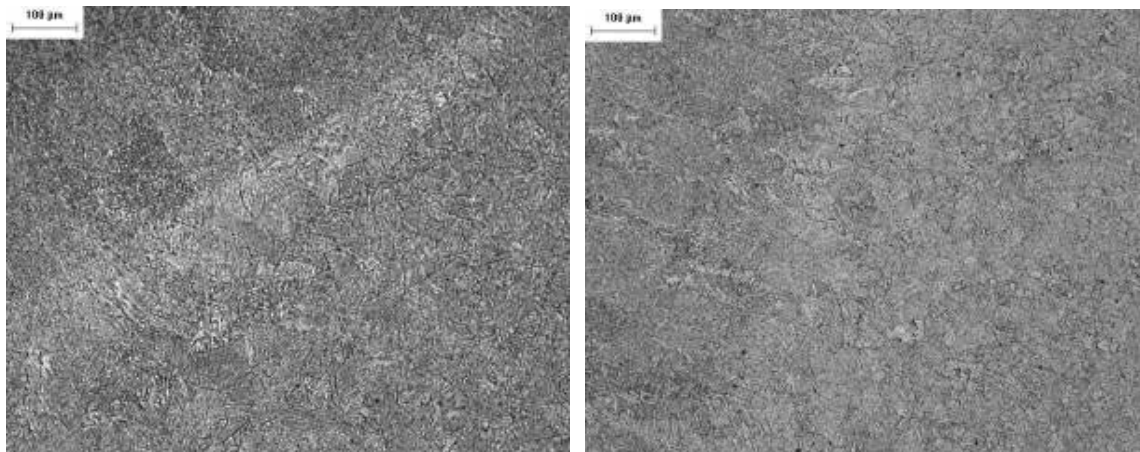
Figure 198 – Microstructure of CGHAZ for welds on X100 pipes 16.4 mm thick. The FZ is located on the upper, left portion (left, cap area; right, root area)

5.1.2   X70 LH welded pipes

Vickers hardness measurements (HV10) were taken on metallographic samples taken through the thickness of welds (shown in Figure 199).
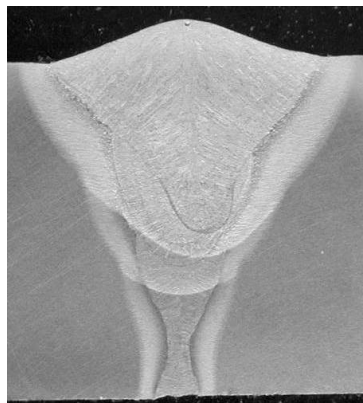
Figure 199 – Macro-section of laser – GMA welds on X70 pipes 14.2 mm thick

In Table 60 below are shown details of the result. No values exceed DNV requirements (max. 325 HV in BM, FZ or HAZ), even in the root area, despite to the hardening occurred from the severe laser thermal cycle.

Location	HV (mean)	HV (range)
BM (root)	243	241 ÷ 244
CGHAZ root	297	291 ÷ 302
CGHAZ cap	275	273 ÷ 276
FZ root	313	309 ÷ 315
FZ cap	228	225 ÷ 231

Table 60 – Hardness testing results on X70 pipes welded by Laser – GMAW

Basic microstructure of welds on X70 steel was investigated by light optical microscope on metallographic samples taken through the thickness (transversal sections). Samples were mounted and polished with grinding paper and eventually with diamond paste (until 1 µm). Etching was made using standard Nital practice.

The weld metal (WM), in the pure GMAW passes (2nd + 3rd), consisted mainly of fine acicular ferrite (AF) with minor presence of polygonal ferrite (PF) and Widmanstätten ferrite (FS-A). The root pass, performed by Laser-GMA process, showed in general a finer microstructure, with again presence of AF plus bainite and considerable amount of martensite (mostly tempered or autotempered), due to the higher cooling rate. The reported microstructure is consistent with the good notch toughness behaviour pointed out and the results of the hardness survey. In Figure 200 a typical actual WM microstructure is shown for the GMA passes.
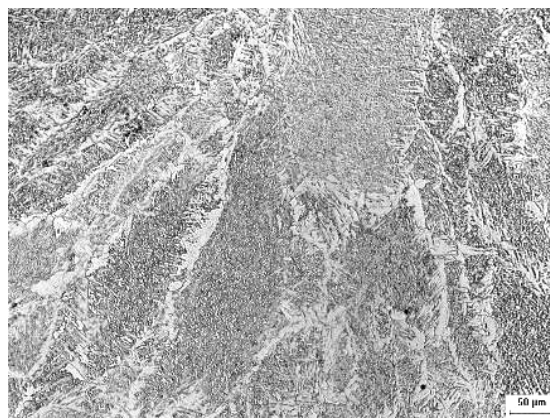
Figure 200 – Microstructure of WM for welds on X70 pipes 14.2 mm thick (GMAW alone area)

The heat affected zone (HAZ) showed a more uniform behaviour between passes, with a limited grain growth in CGHAZ, especially on root pass sides. Predominant microstructures were bainite and martensite (most pronounced at the root area), with minor presence of ferrite beside the GMA passes only. In Figure 201 and Figure 202 typical HAZ actual microstructures are shown, for the CG and the FG area respectively, taken from the GMA influence area.
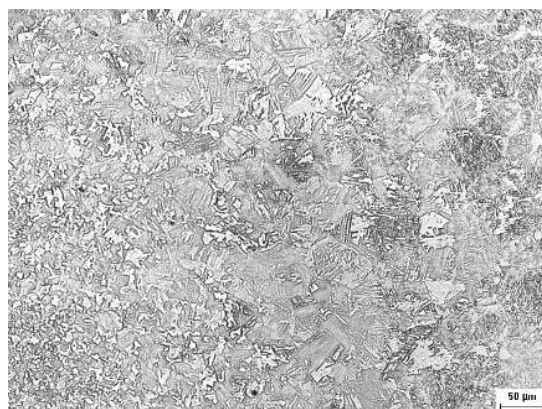
Figure 201 – Microstructure of CGHAZ for welds on X70 pipes 14.2 mm thick (WM on the right – up)

157
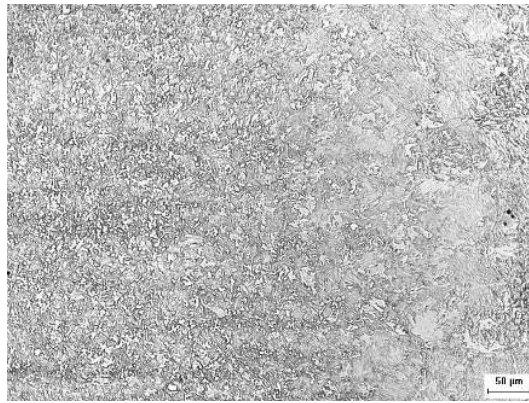
Figure 202 – Microstructure of FGHAZ for welds on X70 pipes 14.2 mm thick

5.2 X100 LH – X70 LH pipes – Mechanical characterisation

5.2.1 X100 LH welded pipes

Transverse tensile tests were carried out on two nominally identical specimens (rectangular, 25 mm wide at the gauge section) with full pipe wall thickness (see Figure 203).
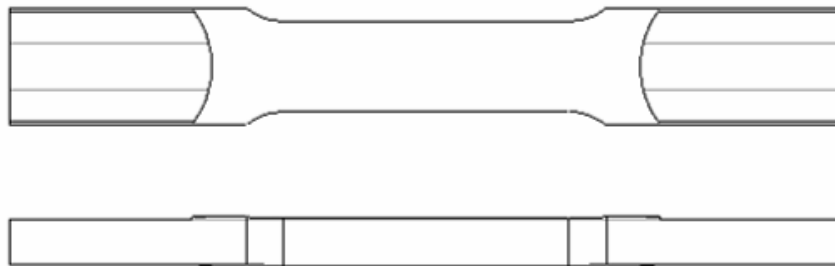
Figure 203 – Specimen geometry for transverse tensile testing of welds on X100 pipes

The results (see Table 61) are in agreement with the DNV OS F101 Standard as for X100 the tensile strength of the specimens is higher than the specified minimum value for the parent metal (i.e 760 MPa according to ISO 3183).

Specimen label	Test temperature (°C)	Rm (MPa)	Notes
T1	23	760	Failure in weld metal
T2	23	771	Failure in weld metal

Table 61 – X100 LH pipes **-** Tensile tests results

Side bending test were carried out on 2 specimens (rectangular, 10 x 15 mm) with roller bending radius of 25 mm. All passed the requirements (180° bending), with no evidence of imperfections.

Full size Charpy – V specimens were extracted from weld samples 2 mm below the surface, with notch perpendicular to the surface. Tests were performed at -20 °C (i.e. Tmin – 10 °C) and results are shown in Table 62.

Notch position	T [°C]	KVT (mean [J]	KVT (range) [J]	Specimens tested
WM	-20	104	70 ÷ 150	5
FL	-20	59	42 ÷ 79	3
FL+2 mm	-20	81	74 ÷ 91	3
FL+5 mm	-20	243	232 ÷ 253	3

Table 62 – Charpy – V testing results on X100 pipes welded by Laser – GMAW

158

CTOD testing was carried out following the well recognised BS 7448 standard, specimens being of the B x 2B type, loaded in bending, with the maximum thickness permitted by the pipe wall (actually 15 mm). CTOD specimens were extracted with notch perpendicular to the surface. CTOD toughness tests were performed at -10 °C (i.e. Tmin) and gave results shown in Table 63.

Notch position	T	COD (mean)	COD (range)	CTOD type
	[°C]	[mm]	[mm]	
WM	-10	0.205	$0.19 \div 0.22$	δ_m, δ_u
FL	-10	0.15	$0.15 \div 0.152$	δ_c

Table 63 – CTOD testing results on X100 pipes welded by Laser – GMAW

5.2.2 X70 LH welded pipes

Transverse tensile tests were carried out on rectangular specimens as for X100 LH (Figure 203). The results (see Table 64) are in agreement with the DNV OS F101 Standard as failure occurs in the base metal.

Specimen label	Test temperature (°C)	Rm (MPa)	Notes
T1	23	683	Failure in base metal
T2	23	666	Failure in base metal

Table 64 – X70 LH pipes **-** Tensile tests results

Side bending tests were carried out on 4 specimens (rectangular, 10 x 14 mm) with roller bending radius of 25 mm. All passed the requirements (180° bending), with no evidence of imperfections.
Full size Charpy – V specimens were extracted from weld samples 2 mm below the surface, with notch perpendicular to the surface. Charpy-V notch toughness test were performed at -20 °C (i.e. Tmin – 10 °C) and results are shown in Table 65.

Notch position	T	KVT (mean)	KVT (range)
	[°C]	[J]	[J]
WM	-20	158	$148 \div 164$
FL	-20	179	$163 \div 187$
FL+2 mm	-20	248	$237 \div 265$
FL+5 mm	-20	265	$265 \div 266$

Table 65 – Charpy – V testing results on X70 pipes welded by Laser – GMAW

CTOD testing was carried out following the well recognised BS 7448 standard, specimens being of the B x 2B type, loaded in bending, with the maximum thickness permitted by the pipe wall (actually 12 mm). CTOD specimens were extracted with notch perpendicular to the surface (Figure 204).
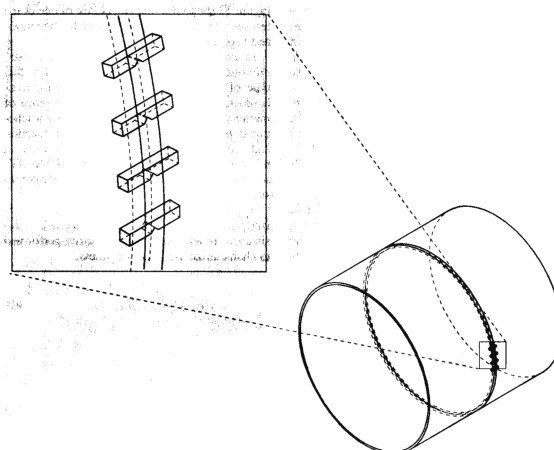
Figure 204 – CTOD specimens orientation for fracture toughness testing of welds on X70 pipes 14.2 mm thick

Results confirmed the good toughness behaviour already pointed out by mean of Charpy-V testing. CTOD toughness tests were performed at -10 °C (i.e. Tmin) and gave very encouraging results (shown in Table 66), with values largely exceeding the standard requirements (0.15 mm) for all notch locations.

Material	Notch position	T [°C]	COD (mean) [mm]	COD (range) [mm]	CTOD type
X70 Laser - GMAW	WM	-10	0.48	0.40 ÷ 0.56	δ_m
X70 Laser - GMAW	FL	-10	0.53	0.50 ÷ 0.54	δ_u, δ_m
BM	-	-10	0.97	0.95 ÷ 1.00	δ_m

Table 66 – CTOD testing results on X70 pipes welded by Laser – GMAW

5.3 X100 LH – X70 LH pipes – Residual stresses measurements

Residual stress measurements have been carried out on a number of samples destined to fatigue testing program. Measurements have been performed in longitudinal and hoop directions, on internal surface as for FCAW welds (see Figure 31), considered the critical area for fatigue failure according to the in service loading conditions. In the following the results obtained are reported.

5.3.1 X100 LH welded pipes

The results of residual stresses measurements for X100 LH welds are reported in Figure 205 and Figure 206.
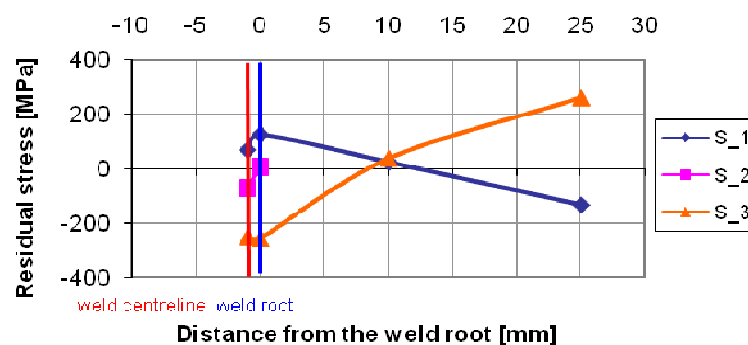
Figure 205 – Residual stresses on internal surface in longitudinal direction
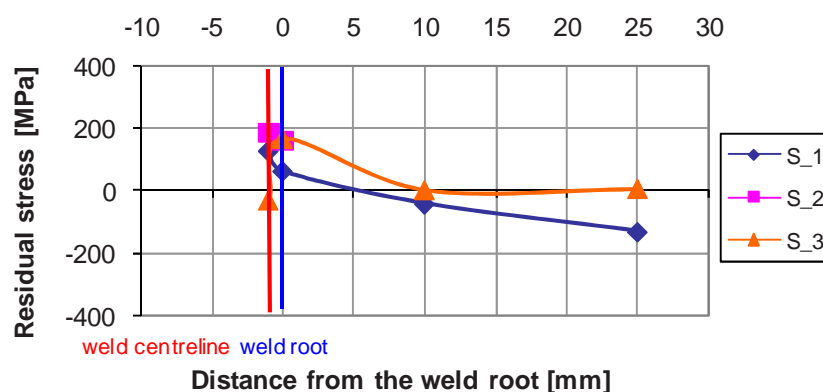
Figure 206 – Residual stresses on internal surface in hoop direction

As concerns X100 LH longitudinal residual stresses are very scattered in the weld root with compressive, near zero e tensile values.

160

5.3.2 X70 LH welded pipes

The results of residual stresses measurements for X70 LH welds are reported in Figure 207 and Figure 208.
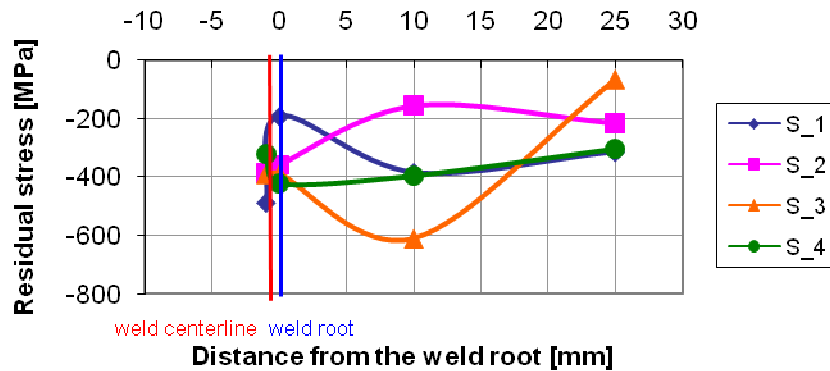
Figure 207 – Residual stresses on internal surface in longitudinal direction
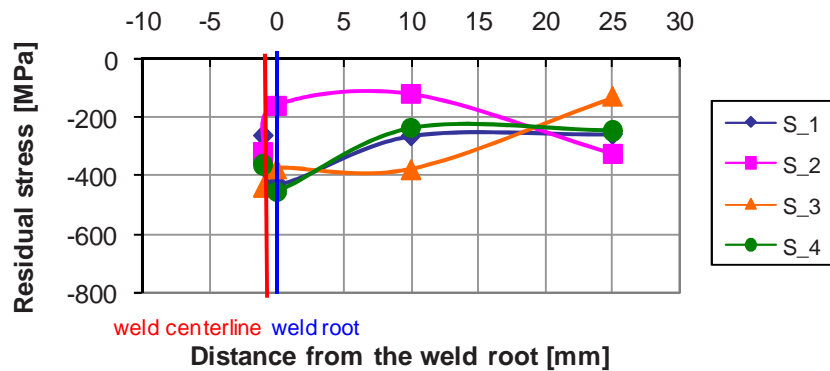
Figure 208 – Residual stresses on internal surface in hoop direction

The residual stresses are compressive in longitudinal and hoop direction. In particular the weld root has pronounced values of residual stresses, beneficial for the fatigue behaviour.

Appendix J: Elaboration of variable amplitude fatigue tests results

Different approaches have been used in the analysis and presentation of variable amplitude fatigue data.

The approach attributed to Gassner uses a modified SN diagram (Figure 209), in which lives are plotted as a function of the maximum stress in the loading history. A Gassner line is specific to a particular shape of loading spectrum and it is necessary to plot a separate Gassner line for each loading spectrum.
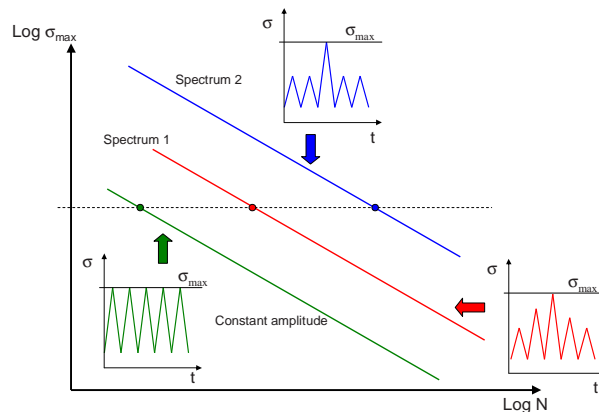
Figure 209 - Gassner lines for different loading spectra

161

Another approach is to represent results with lives plotted as a function of an equivalent constant amplitude stress range, $\Delta\sigma_e$.

Fatigue design SN curves are of the form:

$$N_i = \frac{A}{\Delta\sigma_i^m} \qquad\qquad \ldots (3)$$

Where

N_i is the number of cycles of stress range $\Delta\sigma_i$ for failure

A, m are constants for a given detail class

For a given detail class, this is equivalent to a linear relationship between $\log N$ and $\log \Delta\sigma$. Such a straight line is sometimes referred to as a Wöhler line. For welded details, design codes commonly assign a fixed value $m = 3$.

For cases where fatigue loading occurs at more than one stress range, the Palmgren-Miner Rule is used to sum the damage, D_i, at each stress range:

$$D = \sum_i D_i = \sum_i \frac{n_i}{N_i} = \sum_i \frac{n_i \cdot \Delta\sigma_i^m}{A} = \frac{1}{A}\sum_i n_i \cdot \Delta\sigma_i^m \qquad\qquad \ldots (4)$$

Where

D_i is the fatigue damage incurred at the i th stress range

n_i is the number of cycles applied at the i th stress range

By definition, fatigue failure occurs when the summed fatigue damage reaches unity.

For a loading history involving a number of cycles at j different stress ranges, it is possible to define an equivalent constant amplitude stress range, $\Delta\sigma_e$, producing the same fatigue damage in the same total number of cycles:

$$D = \frac{1}{A}\sum_{i=1}^{j} n_i \cdot \Delta\sigma_i^m$$

$$D = \frac{1}{A} n_e \cdot \Delta\sigma_e^m$$

$$n_e \cdot \Delta\sigma_e^m = \sum_{i=1}^{j} n_i \cdot \Delta\sigma_i^m$$

$$n_e = \sum_{i=1}^{j} n_i$$

$$\Delta\sigma_e = \left[\frac{\sum_{i=1}^{j} n_i \cdot \Delta\sigma_i^m}{\sum_{i=1}^{j} n_i} \right]^{\frac{1}{m}}$$

$\Delta\sigma_e$ is dependent on *m* value. As a first approach, m=3 can be used. From the Gassner plot of raw σ_{max} – N data the slope of the line m_G can be calculated and in turn used to recalculate $\Delta\sigma_e$ values as illustrated by Figure 210.
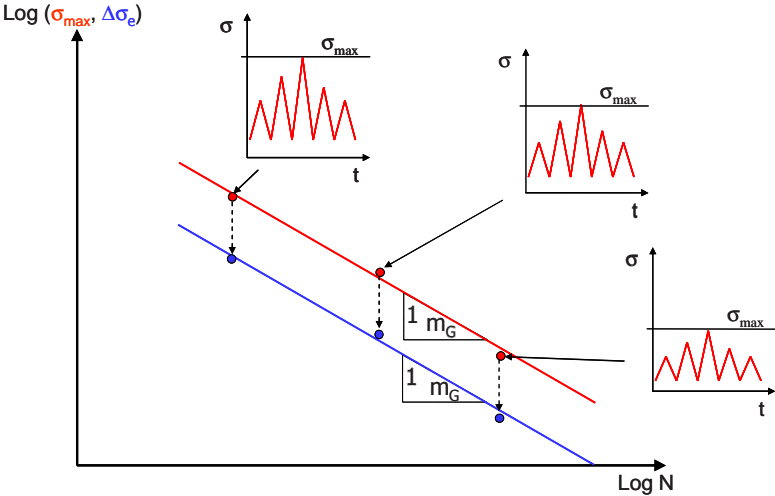
Figure 210 - Typical Gassner plot of test data

Appendix K: Fatigue Crack Growth Rate tests

The results of the fatigue crack growth rate tests in terms of da/dN versus _K are shown in Figure 211, for specimens tested in air and in Figure 212 and Figure 213, for seawater with cathodic protection.
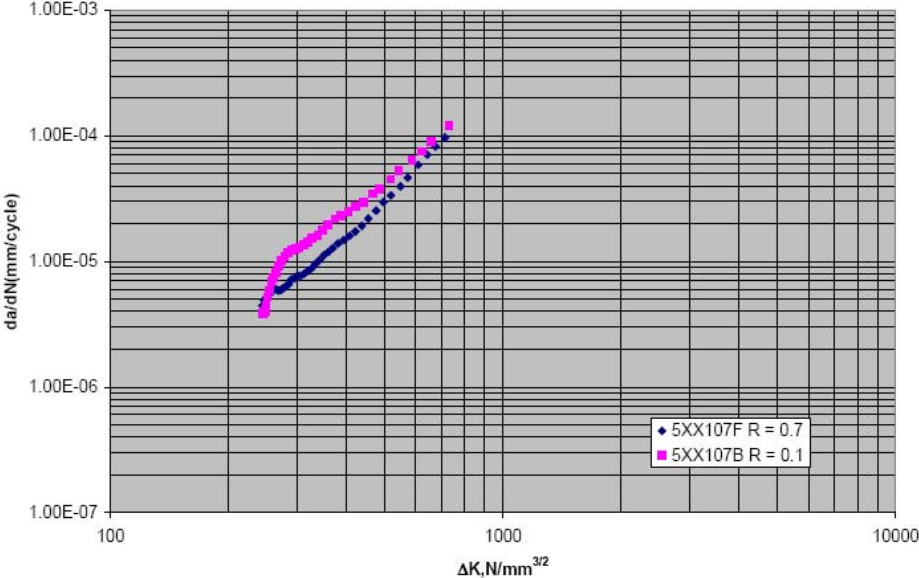
Figure 211 - FCGR data for RQT 701 parent plate material tested in air using R-ratios of 0.1 and 0.7

163
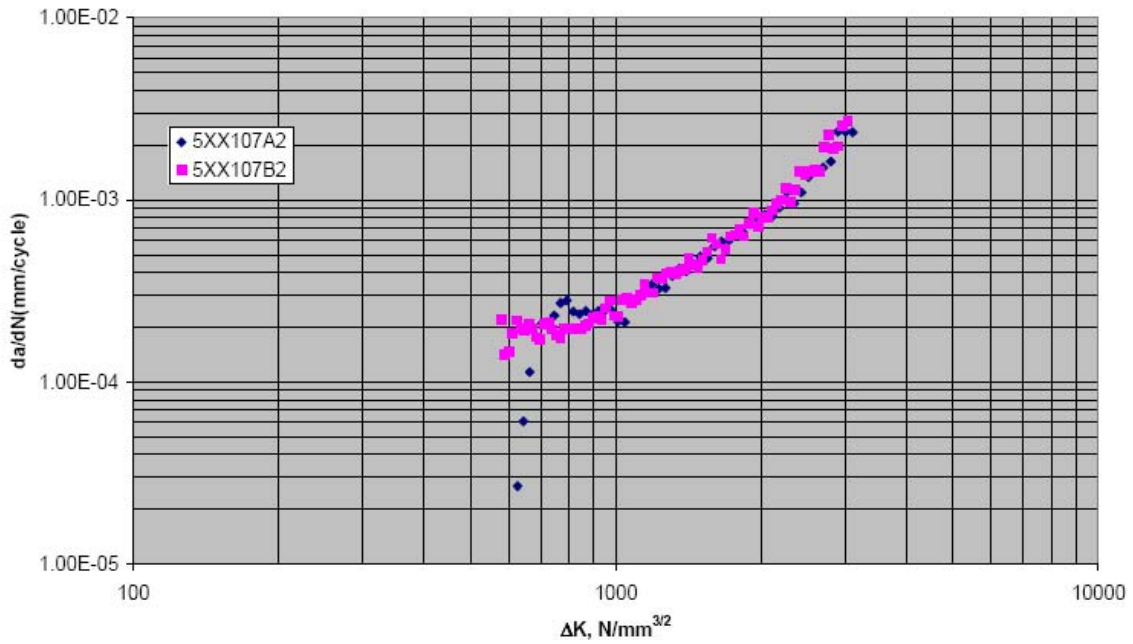
Figure 212 - FCGR data for RQT 701 parent plate material tested in seawater under cathodic protection (-900 mV) with R-ratio of 0.1
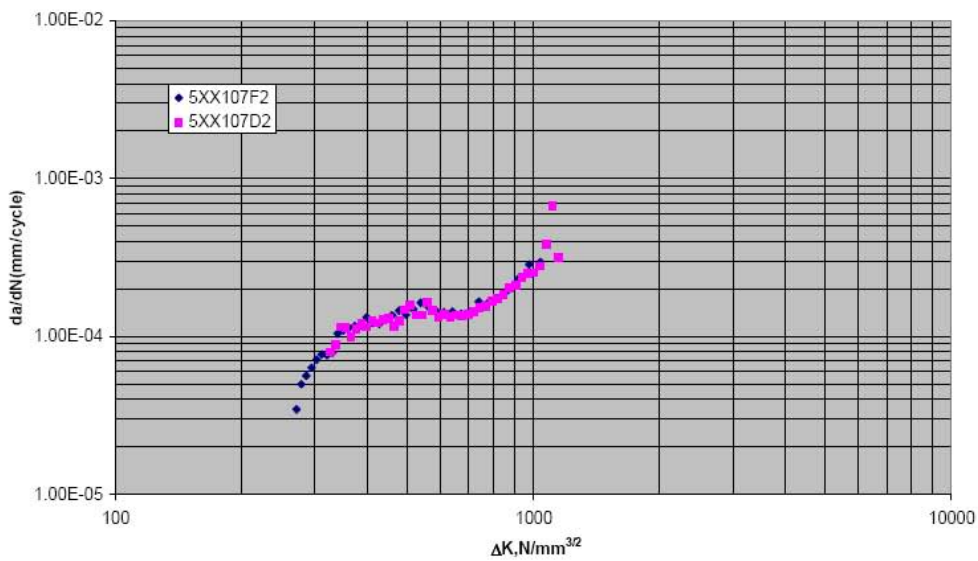
Figure 213 - FCGR data for RQT 701 parent plate material tested in seawater under cathodic protection (-900 mV) with R-ratio of 0.7

As can be seen from the above shown figures, the overall relationship between da/dN (m/cycle) and ΔK (MPa _m) is normally a sigmoidal 'S' curve in a log da/dN versus log ΔK plot. The central portion of the curve is usually assumed to be linear and may be described using the Paris Law:

$$\frac{da}{dN} = C\Delta K^m$$

164

Where C and m are constants which depend on the material and the applied conditions, including environment and cyclic frequency. (It should be noted that these parameters are also dependent on the units of K and the growth rate).

At low values of ΔK, the rate of growth falls off rapidly, such that, below a threshold stress intensity factor range, ΔK_0, crack growth is insignificant. At high values of ΔK, when the maximum stress intensity factor in the cycle, K_{max} approaches the critical stress intensity factor, K_{IC}, the rate of crack growth accelerates rapidly. That said it is often sufficient to assume that the Paris Law equation can be applied for all values of ΔK from ΔK_0 up to failure. Best fits to the straight line regions of the air and seawater fatigue crack growth data yield the Paris Law constants contained in Table 67.

Environment	R-ratio	C	m
Air	0.1	4.6×10^{-11}	2.479
Seawater CP -900 mV	0.1	4.5×10^{-10}	1.808
Seawater CP -900 mV	0.1	3.3×10^{-10}	1.886
Air	0.7	1.1×10^{-11}	2.861
Seawater CP -900 mV	0.7	8.6×10^{-11}	2.353
Seawater CP -900 mV	0.7	5.1×10^{-10}	1.816

Note: The Paris Law coefficients (C) and exponents (m) were determined from regression analyses of log (da/dN) – log (ΔK) data, with da/dN in m/cycle and ΔK in MPa m^1/2

Table 67 - Summary of Paris Law constants obtained from FCGR conducted on RQT 701 parent material

These constants, C and m govern the speed of fatigue crack growth and are thus critical inputs when, for example, defining safe inspection intervals for structures and components which are subjected to cyclic loading conditions in service. Reliable fatigue crack growth prediction is critically important for safe design and maintenance of engineering structures subjected to cyclic loading [[75][76]],. Crack closure models often used in such predictions require an appropriate relationship for crack opening stress intensity factor, Kop. Theoretically, based on an elastic material behaviour, a tension stress acting on a cracked specimen will open a crack but when the tension stress is removed, crack opening displacements return to zero. However, for an elastic-plastic material Elber [77] observed that the fatigue crack closed during unloading even before the tension stress returned to zero. This phenomenon where crack closure occurs under positive tension stresses is called plasticity induced crack closure. Elber suggested that an effective range of stress intensity factor (SIF), ΔK_{eff} can be calculated as

$$\Delta K_{eff} = K_{max} - K_{op}$$

Where Kmax is the maximum SIF during a load cycle and Kop is the SIF when the crack tip is just fully open. According to Elber's crack closure model the fatigue crack growth rate depends solely on ΔK eff. While the slopes (m values) obtained for the tests undertaken in air at the two R-ratios of 0.1 and 0.7 are higher for the latter stress ratio, the fatigue crack growth rates as shown by Figure 211 are very similar. The theory explaining similar crack growth rates in air at two different R-ratios might be that the crack is fully open at both R = 0.1 and 0.7. As RQT 701 is a high strength steel, so one could argue that the residual strains (controlling the plasticity induced closure) in the wake of the growing crack are limited and this is the reason why the crack may be fully open and consequently have the same effective crack tip driving force (delta K effective) at R = 0.1 and the higher ratio 0.7.

In Figure 214and Figure 215 the fatigue crack growth data have been compared to the recommended fatigue crack growth laws for steels in air and marine environment as stated in BS 7910.
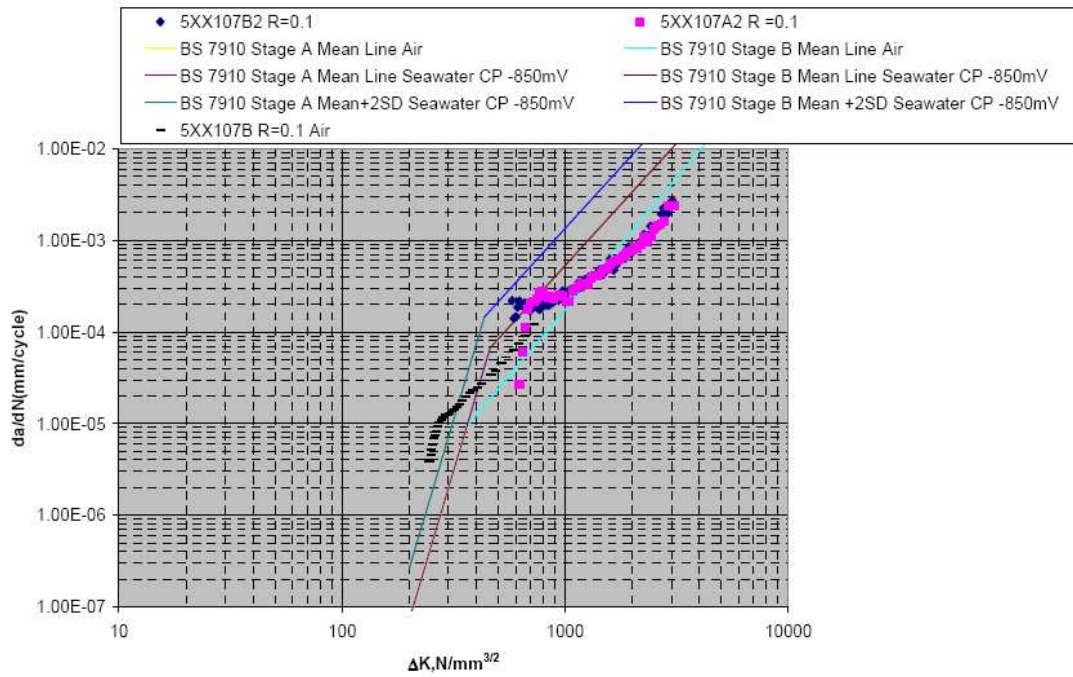
Figure 214 - Fatigue crack growth data in air and seawater at R = 0.1 compared to fatigue crack growth laws in BS 7910
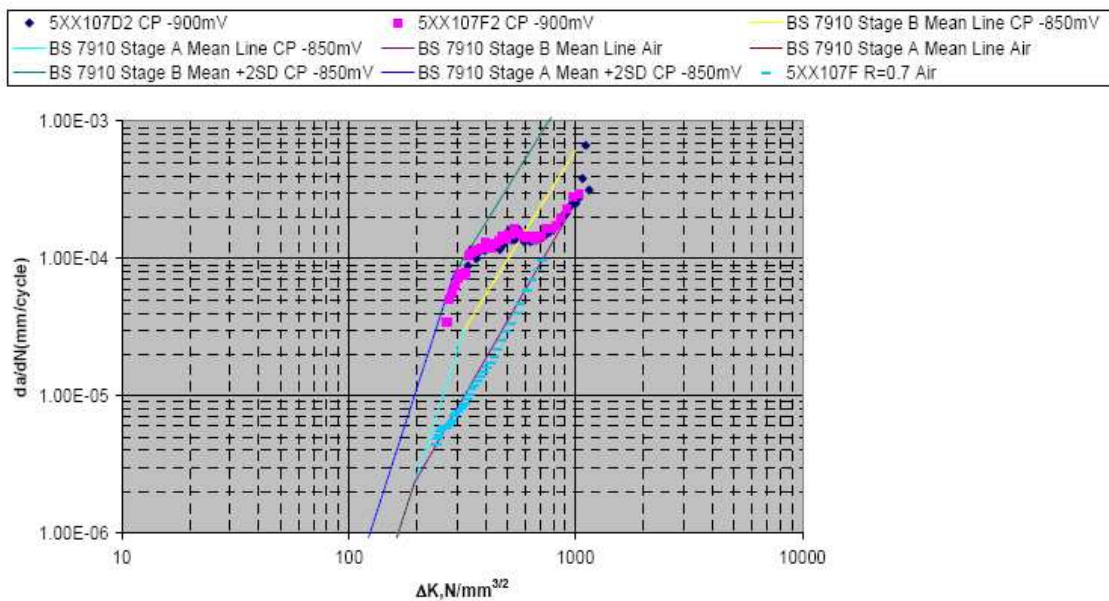
Figure 215 - Fatigue crack growth data in air and seawater at R = 0.7 compared to fatigue crack growth laws in BS 7910

While the generated FCGR data have been compared to the fatigue crack growth laws quoted in BS 7910 it should be recognised that the data in BS 7910 is for steels with yield strengths less than 700 MPa and therefore may not obey the same rules. The seawater data with R-ratio of 0.7 crosses both the mean and mean +2SD lines before tracking the mean line in air, suggesting this may well be the case. A possible explanation is that the real-time crack extension rate (da/dt) exceeds the rate at which the environment can influence the crack growth and the crack continues to grow as if it's in air, as shown in Figure 215. The environmental influence decreases with increases in the real-time rate of crack extension

(da/dt) because the faster the crack growth rate, the less time available for environmental interaction. The real-time rate of crack extension (da/dt) depends on the cyclic fatigue crack growth rate (da/dN), itself a function of the applied ΔK, stress ratio and test frequency. Finally, the environmental influence depends on the accessibility of the environment to the crack tip, which can be affected by crack length,

specimen thickness, ΔK, Kmax, and stress ratio. A similar pattern of events is highlighted by the R-ratio 0.1 seawater data, as illustrated by Figure 214. Whereas for the air data and in particular the R-ratio of 0.7 there is little deviation from the corresponding mean line for air.

1 Fatigue crack growth rate (FCGR) tests HAZ

Test results for the RQT 701, S460 Q&T and S355 EMZ materials are given in Table 68 and results are shown in Figure 216.

Material	R-Ratio	C	m
S460 parent	0.1	3.2×10^{-13}	3.9
S460 parent	0.1	6.2×10^{-13}	3.82
S460 HAZ	0.1	1.5×10^{-13}	3.671
S460 HAZ	0.1	1.3×10^{-13}	3.855
S355 parent	0.1	2.4×10^{-14}	4.944
S355 parent	0.1	3.5×10^{-14}	4.842
S355 HAZ	0.1	2.9×10^{-15}	4.989
S355 HAZ	0.1	4.2×10^{-16}	5.707
RQT 701 parent	0.1	4.6×10^{-11}	2.479
RQT 701 parent	0.1	8.32×10^{-12}	2.863
RQT 701 HAZ	0.1	5.1×10^{-12}	2.79
RQT 701 HAZ	0.1	2.5×10^{-11}	2.38

Note: The Paris Law coefficients (C) and exponents (m) were determined from regression analyses of log (da/dN) – log (ΔK) data, with da/dN in m/cycle and ΔK in MPa m^1/2

Table 68- Summary of Paris Law constants obtained from FCGR tests conducted on RQT 701 S460 and S355 parent and HAZ material
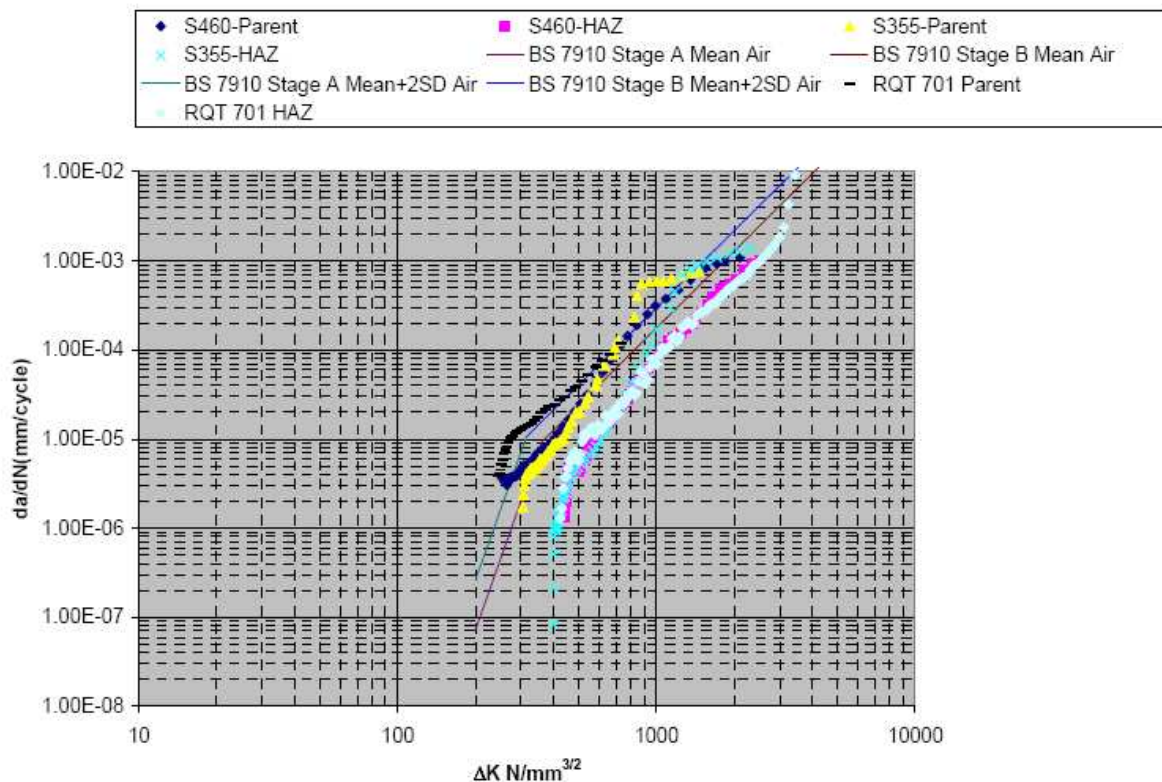
Figure 216 - Fatigue crack growth data in air at R = 0.1 for RQT 701, S460 and S355 material compared to fatigue crack growth laws in BS 7910

It is clear that the slopes (m values) obtained here for the lower strength materials (S460 and S355) are significantly higher than those obtained for the higher strength (RQT 701) parent and HAZ material. The observed trend being the lower the yield strength the greater the value of m. The lack of scatter in

individual data sets with the exception of the S355 HAZ data suggests that the data is valid. Visual analysis of the surface notched samples,

particularly the RQT 701 material shows that the advancing fatigue crack migrated towards the under-matched weld material as shown by Figure 217, suggesting that the stated Paris Law constants may be more attributable to the weld metal than the HAZ. The level of weld metal under-matching relative to parent plate is illustrated in Figure 218. However, on inputting the Paris Law constants into fatigue assessment software [78] for a 1 mm deep semi elliptical flaw in a flat plate, lower crack growth rates for all HAZ material relative to parent material were observed, as illustrated by Figure 219. Similar observations have been made by others [79], [80]. A possible explanation for the lower crack growth rates is that residual stresses in heat affected zones are considered to be compressive and may, therefore, inhibit crack growth.

Very limited fatigue data have been generated for the HAZ of high strength steel weldments.

The available data [81] show that the fatigue performance of the HAZ is similar to that observed for both the structural grade steel and the high strength parent plate data. Similarly weld metal FCGR test results [82] obtained on a 450 MPa steel were found to be comparable to higher strength weld metals. No relationship between yield stress and fatigue performance was found for the weld metals tested. It would appear that welding under controlled conditions does not significantly affect FCGR in these steels.
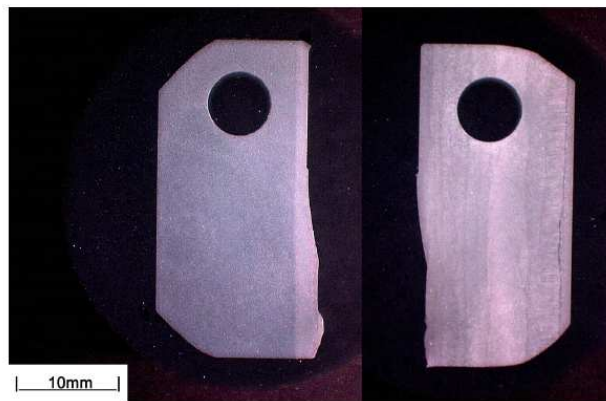
Figure 217 - RQT 701 weld profile and compact tension specimen orientation
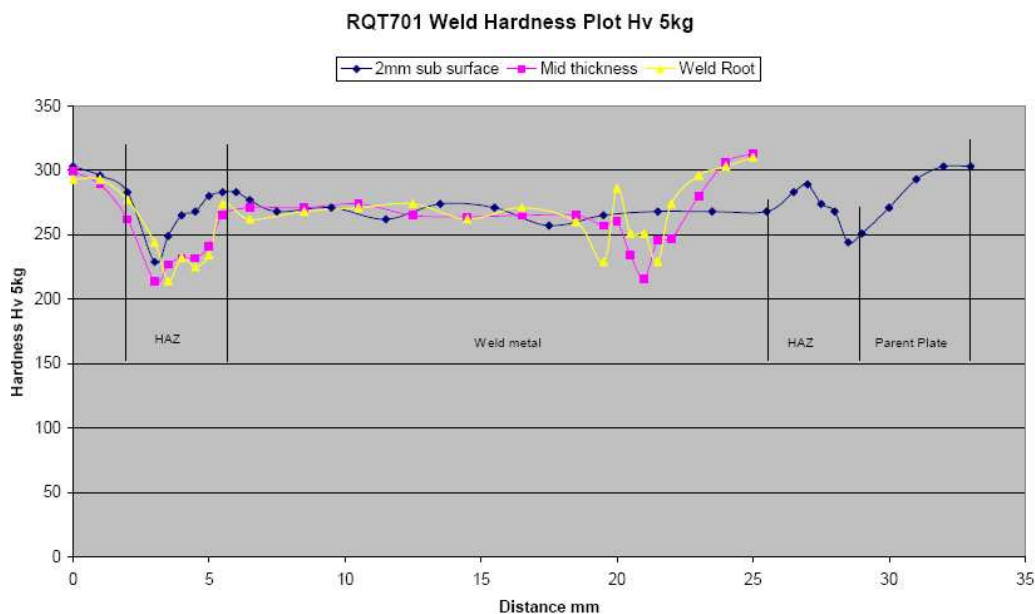
Figure 218 - Hardness traverse for RQT 701 weld used in FCGR assessment

168

Figure 219 - Comparison of FCGR data using TWI Crackwise fatigue software

4   List of figures and tables

5   List of References

[1]   Stephen J. Maddox Julian B. Speck G. Reza Razmjoo, TWI, *An Investigation of the Fatigue Performance of Riser Girth Welds,* Journal of Offshore Mechanics and Arctic Engineering FEBRUARY 2008, Vol. 130

[2]   www.rigzone.com

[3]   www.offshore-technology.com

[4]   www.shell.us

[5]   *www.offshore-mag.com*

[6]   DNV-RP-F105 "Free Spanning Pipelines", 2006

[7]   Larsen CM, Koushan K and Passano E: "Frequency and time domain analysis of vortex induced vibrations for free span pipelines" OMAE 2002, paper 28064

[8]   DNV-OS-J101 "Design Of Offshore Wind Turbine Structures", 2004

[9]   Peter Schaumann, Patric Kleineidam "Support Structures Of Owecs In A Water Depth Of About 30 m", Offshore Wind Energy, Special Topic Conference, December 2001

[10]   O.B. Sertã, M.M. Mourelle, F.W. Grealish, S.J. Harbert, L.F.A. Souza, "Steel Catenary Riser for the Marlim Field FPS P-XVIII" OTC 1996, paper 8069

[11]   A. Couch, J. Guion, D. Rieth, B. Rager, J. Bouwman, "Independence installation" OTC 2007, paper 18585

[12]   R. Song, P. Stanton, "Advances In Deepwater Steel Catenary Riser Technology State-of-the-Art: Part I — Design", OMAE2007, paper 29329

[13]   Kirkhope, K J, Bell, R, Caron, L, Basu, R I and Ma, K-T: 'Weld detail fatigue life improvement techniques, Part 1: review', Marine Structures, (1999), Vol. 12, pp447-474.

[14]   BS EN 10045 – Part 1. British Standard for Charpy impact tests on metallic materials. Part 1. Test Method ('U' and 'V' notches). British Standards Institution. 1990.

[15]   BS 7448 – Part 2. 'Fracture mechanics toughness tests – Part 2: Method for the determination of KIc, critical CTOD and critical J values of welds in metallic materials', British Standards Institution, August 1997.

[16]   BS 7910: 2005, "Guide to methods for assessing the acceptability of flaws in metallic structures", BSi 2005.

[17]   ASTM E647-05.'Standard Test Method for Measurement of Fatigue Crack Growth Rates'. American Society for Testing Materials. ASTM International, PA, USA 2005.

[18]   Anderson, T L: 'Fracture Mechanics Fundaments and Application, 1995, 2nd edition, CRC Press, Inc.

[19]   DNV OS-F201 "Dynamic risers", 2001

[20]   DNV RP-F204 "Riser fatigue" 2005

[21]   Salama, M.: Fatigue design of girth welded pipes and the validity of using strips. 18th International Conference on Offshore Mechanics and Arctic Engineering (1999) Paper OMAE 99-2003, ASME

[22]   S.J Maddox, Y-H. Zhang, TWI Comparison Of Fatigue Of Girth-Welds In Full-scale Pipes And Small-Scale Strip Specimens OMAE2008, paper 57103

[23]   British Standard, BS 7608: 1993, "Code of practice for fatigue design and assessment of steel structures".

[24]   Haagensen, P J and Maddox, S J: "IIW recommendations on post weld improvement of steel and aluminium structures", IIW document XIII – 1815-00, 2004.

[25]   Offshore Installations, Guidance on Design, Construction and Certification, UK Department of Energy, HMSO, Fourth Edition 1990.

[26]   BS 7910: 2005, "Guide to methods for assessing the acceptability of flaws in metallic structures", BSi 2005.

[27]   Kirkhope, K J, Bell, R, Caron, L, Basu, R I and Ma, K-T: 'Weld detail fatigue life improvement techniques, Part 1: review', Marine Structures, (1999), Vol. 12, pp447-474.

[28]   http://www.oceanpd.com/docs

[29]   http://www.southwestrda.org.uk/news/release

[30]   Mill, A: "Archimedes Wave Swing evaluation of test procedures and results from deployment in Portugal 2004", EMEC Report AM/EMEC/0100, 17 December 2004, (http://www.hie.co.uk/archimedes-wave-swing-evaluation-of-test-procedures-report.pdf

[31]   http://www.awsocean.com/pdf/2006-04AWSrelease.pdf

[32]   http://www.marineturbines.com/mct_text_files/New_impetus_for_tidal_energy_in Wales_embargoed_until_08FEB06.pdf

[33]   http://www.marineturbines.com/mct_text_files/MCT%20Anglesey%20scoping% 20press%20release%2024JUL06.pdf

[34]   http://www.windatlas.dk/Europe/oceanmap.html

[35]   http://www.worldenergy.org/wec-geis/publications/reports/ser/wave/wave.asp

[36]   http://ec.europa.eu/energy/res/sectors/doc/ocean/wave_energy_brochure.pdf

[37]   "PHASE II UK TIDAL STREAM ENERGY RESOURCE ASSESSMENT" (Carbon Trust/ Black & Veatch, July 2005) – see Carbon Trust Website.

[38]   Lindley, C: "Influence of the level of cathodic protection on the corrosion fatigue properties of higher strength welded joints", European Commission report EUR 18295 EN, 1998.

[39]   Grovlen, M, et al: "Effects of corrosion and cathodic protection on fatigue of welded steel structures in sea water environment – state of the art", SINTEF report STF 34 F89104, 1989.

[40]   DNV-RP-F204 "Riser Fatigue", 2005

[41]   Yong Bai, "Pipeline and Risers", Elsevier Ocean Engineering Book Series Volume 3, Series Editors R. Bhattacharyya & M. E. McCORMIC 2001

[42]   Kim J. Mørk, Luiz Souza, Nils Sødahl "Present and Future Fatigue Analysis Procedures for Dynamic Risers" OMAE 2001/OFT-1272

[43]   Gautam Chaudhury Stolt Offshore "Combined Low and High Frequency Fatigue of Platforms in Deep Waters" OMAE 2001/OFT-1252

[44]   API-RP-2RD "Design of Risers for Floating Production Systems (FPSs) and Tension-Leg Platforms (TLPs)", 1998

[45]   J. Xu, A. S. Jesudasen, J. Fang "Wave Loading Fatigue Performance of Steel Catenary Risers (Scr) in Ultradeepwater Applications" OTC 2006, paper 18180

[46]   Ghiath (Guy) Mansour "The Impact of The Second Order Vessel Motion on The Fatigue Life of Steel Catenary Risers" OMAE 2004, paper 51644

[47]   W. Ye, J. Shanks, J. Fang "Effects of Fully Coupled and Quasi-Static Semi-Submersible Vessel Motions on Steel Catenary Riser's Wave Loading Fatigue" OTC 2003, paper 15105

[48]   Basim B. Mekha "New Frontiers in The Design of Steel Catenary Risers for Floating Production Systems" Journal of Offshore Mechanics and Arctic Engineering, November 2001, vol. 123, pp. 153-158

[49]   Carl G. Langner "Fatigue Life Improvement of Steel Catenary Risers Due to Self-Trenching at the Touchdown Point" OTC 2003, paper 15104

[50]   Muthu Chezhian, Kim Mørk, Marit Ronaess, Trond Stokka Meling "Application of DNV-RP-F204 for determining riser VIV safety factors" OMAE 2005, paper 67021

[51]   DNV-OSS-302 "Offshore Riser Systems", 2003

[52]   DNV-OS-F201 "Dynamic Risers", 2001

[53]   API-RP-2RD "Design of Risers for Floating Production Systems (FPSs) and Tension-Leg Platforms (TLPs)", 1998

[54]   DNV-RP-C203 "Fatigue Design of Offshore Steel Structures", 2005

[55] Kim J. Mørk, Luiz Souza, Nils Sødahl "Present and Future Fatigue Analysis Procedures for Dynamic Risers" OMAE 2001/OFT-1272

[56] www.carbontrust.co.uk

[57] Efthymiou, M, "Development of SCF Formulae and Generalized Influence Functions for Use in Fatigue Analysis", Recent Developments in Tubular Joint Technology, OTJ'88, October 1998, London.

[58] International Institute of Welding, "Recommendations on Fatigue of Welded Components", 1995

[59] Usami, S: "Short crack fatigue properties and component life estimation" from "Current research on fatigue cracks", Eds T Tanaka, M Jono and K KomaiElsevier, 1987, pp119-147.

[60] Knight, J W: "Improving the fatigue strength of fillet welded joints by grinding and peening", Welding Institute Report 8/1976/3- Doc. IIW - XIII –851-77.

[61] Bignonnet, A: "Improving the fatigue strength of welded steel structures", Steel in Marine Structures, Proc. 3rd Int. conf. on steel in marine structures (SIMS 87), Delft, Netherlands, June 15-18, 1987, Ed C Noordhoek and J de Back, Elsevier 1987.

[62] Maddox, S J: "Improving the fatigue performance of welded stainless steels", TWI report 13631.01/2005/1257.2.

[63] Kado, S et al: "Influence of the conditions in TIG dressing on the fatigue strength in welded high tensile strength steels, IIW Doc. No. XIII –771-75, 1975.

[64] Haagensen, P J, Statnikov, E S and Lopez-Martinez, L: "Introductory fatigue tests on welded joints in high strength steel and aluminium improved by various methods including ultrasonic impact treatment (UIT)", IIW Document XII-1748-98.

[65] Statnikov, E S: "Physics and mechanism of ultrasonic impact treatment", IIW Document XIII-2004-04.

[66] Statnikov, E S, et al: "Efficiency evaluation of ultrasonic impact treatment (UIT) of welded joints in Weldox 420 steel in accordance with the IIW Program", IIW Document XIII-1817-00.

[67] Haagensen, P J: "Fatigue of high strength steels", presentation to 2nd International Symposium on High Strength Steel, Stiklestad, April 2001.

[68] Hobbacher, A: "Recommendations for fatigue design of welded joints and components", IIW Document XII-1965-03/XV-1127-03, February 2003.

[69] Lihavainen, V-M and Marquis, G: "Estimation of fatigue life improvement for ultrasonic impact treated welded joints", paper presented at the "15th European Conference on Fracture – Advanced Fracture Mechanics for Life and Safety Assessment", Stockholm, August 2004.

[70] BS EN 10002 – Part 1. British standard for tensile testing of metallic materials. Part1. Method of tests at ambient temperature. British Standards Institution. 2001.

[71] BS EN 10045 – Part 1. British Standard for Charpy impact tests on metallic materials. Part 1. Test Method ('U' and 'V' notches). British Standards Institution. 1990.

[72] BS 7448 – Part 2. 'Fracture mechanics toughness tests – Part 2: Method for the determination of KIc, critical CTOD and critical J values of welds in metallic materials', British Standards Institution, August 1997.

[73] Dixon, M J and Bateson, P H: 'The effect of extended stress relief treatments on RQT 701 Parent Plate and HAZ Fracture Toughness'. British Steel Technical Report. 1998.

[74] ASTM E647-05. 'Standard Test Method for Measurement of Fatigue Crack Growth Rates'. American Society for Testing Materials. ASTM International, PA, USA. 2005.

[75] Schijve, J: 'Fatigue of Structures and Materials', Kluwer Scademic Publishers, 2001.

[76] Anderson, T L: 'Fracture Mechanics Fundaments and Application, 1995, 2nd edition, CRC Press, Inc.

[77] Elber, W: "The significance of fatigue crack closure", Damage Tolerance in Aircraft Structures, 1971, ASTM STP 486, pp230-242.

[78] TWI Software BS7910 fracture/fatigue assessment procedures, crackwise V 4.1.

[79] Rudd W.J, Booth G.S "Near threshold fatigue crack growth in structural steels" EUR 17846. 1991-1994.

[80] Tanaka T, Jono M, Komai K "Current Research on Fatigue Cracks" Current Japanese Materials Research Vol.1 1987.

[81]   Billingham J, Sharp J V, Spurrier J, Kilgallon P J,- Review of the performance of high strength steels used offshore, Research report 105 HSE (2003).

[82]   Gunther, H. P and Kuhlmannu, "Use and application of high performance steels for steel structures" IABSE Structural engineering documents 8, 2005.